The Effects of Developed Selective Laser Melting Strategies on Titanium Hybrid Parts

by

Devon Hagedorn-Hansen

Thesis presented in fulfilment of the requirements for the degree of Master in Industrial Engineering in the Faculty of Engineering at Stellenbosch University

Supervisor: Dr G.A. Oosthuizen

March 2017

Declaration

By submitting this thesis electronically, I declare that the entirety of the work contained therein is my own, original work, that I am the authorship owner thereof (unless to the extent explicitly otherwise stated), and that I have not previously, in its entirety or in part, submitted it for obtaining any qualification.

…….. **……March 2017……..**

Signature **Date:**

Abstract

Additive manufacturing (AM) is gaining popularity in industries such as the aerospace, medical, and tool-and-die industries. One of the major challenges faced by additive manufacturing technology is the high costs involved. In the case of selective laser melting (SLM), a metal powder bed fusion technology, warping due to residual stress could lead to the part being scrapped. SLM can be compared to a repetitive laser welding process whereby hundreds of layers are welded together in a specific shape to produce a 3-dimensional geometry.

During the SLM process a thermal heat sink effect takes place between the base plate and the previously consolidated layers. This results in extremely large directional thermal gradients, which act in the direction of the scan track. These high thermal gradients cause the build-up of residual stresses, which can cause part deformation. The stress built up by the thermal shrinkage of the solidified melt pool induces a tensile stress at the top surface of the SLM part. These tensile stresses cause the part to curl upward, which is usually restrained by the base plate being anchored to the machine with screws. Sometimes the stress is so great that the base plate still warps and the screws break or get elongated past their elastic limit.

To reduce the costs involved with SLM a process chain with subtractive manufacturing (SM) and additive manufacturing processes has been suggested. Process chains can incorporate a combination of manufacturing technologies in order to produce a product in the most resource efficient manner. Components produced using a combination of SLM and conventional machining are referred to as hybrid parts if the SLM section is fused to the machined section. The problems associated with the SLM technology, such as geometric deviation (warping) and porosity, are still applicable to the production of hybrid components. The purpose of this study was to determine whether different laser scan strategies can be developed to reduce geometric deviation and porosity in titanium hybrid parts. A new method called Hatch Pattern Designing was developed to bypass the default hatch strategies used by the Concept Laser machine.

A new scan strategy was developed and compared to the patented Concept Laser Island scan strategy. Using the new scanning strategy on the experimental samples resulted in less geometric deviation and less porosity than those produced using the Concept Laser M2 Cusing machine’s default scan strategy.

Opsomming

Additive Manufacturing (AM) is besig om in gewildheid in bedrywe soos die Ruimte, mediese, en instrument-en-sterf nywerhede. Een van die groot uitdagings in die gesig gestaar deur toevoeging vervaardiging tegnologie is die hoë koste daaraan verbonde. In die geval van Selective Laser Melting (SLM), 'n metaal poeier bed fusie tegnologie, buiging as gevolg van residuele spanning kan lei tot die deel wees gesloop. SLM kan vergelyk word met 'n herhalende laser sweiswerk proses waardeur honderde lae saam in 'n spesifieke vorm van 'n 3-dimensionele meetkunde produseer gesweis.

Gedurende die SLM proses neem 'n warm heat sink effek tussen die basisplaat en die voorheen gekonsolideer lae. Dit lei tot 'n baie groot directional termiese gradiënte wat optree in die rigting van die scan spoor. Hierdie hoë termiese gradiënte veroorsaak die opbou van die oorblywende spanning wat deel vervorming veroorsaak. Die spanning opgebou deur die hitte krimping van die gestolde smelt swembad veroorsaak 'n trekspanning aan die bokant oppervlak van die SLM deel. Hierdie trek spanning veroorsaak dat die deel te krul opwaarts wat gewoonlik opgehou deur die basisplaat word geanker aan die masjien met skroewe. Soms is die spanning is so groot dat die basisplaat nog warps en die skroewe te breek of te verleng verby hul elastisiteitsgrens.

Om die betrokke met SLM koste van die gebruik van 'n hibriede proses ketting is voorgestel te verminder. Hybrid proses kettings inkorporeer 'n kombinasie van vervaardiging tegnologie om 'n produk in die mees hulpbron doeltreffende wyse te produseer. In hierdie geval is 'n kombinasie van subtraktiewe vervaardiging en toevoeging vervaardiging tegnologie gebruik sal word. Die probleme wat verband hou met die SLM tegnologie, soos geometriese afwyking (buiging) en porositeit, is steeds van toepassing op die produksie van hibriede komponente. Hierdie studie bepaal of verskillende laser scan strategieë ontwikkel kan word om meetkundige afwyking en porositeit in titanium baster dele verminder. 'N nuwe metode genoem Hatch Patroon ontwerp is ontwikkel om die verstek broei strategieë wat gebruik word deur die Concept Laser masjien te omseil.

'N Nuwe scan strategie is ontwikkel en in vergelyking met die gepatenteerde Concept Laser Island skandering strategie. Die gebruik van die nuwe skandering strategie op die eksperimentele monsters gelei tot minder geometriese afwyking en minder porositeit dan diegene wat met behulp van standaard scan strategie die Concept Laser M2 Cusing masjien se.

Acknowledgements

I would like to acknowledge the financial support received from the Department of Science and Technology. I furthermore would like to express my profound sense of gratitude to the following people who contributed in various ways to make this work possible.

I would like to thank my amazing wife, Niquelle, for putting up with me and for all of the sacrifices she made during the writing process. Without her, I would not be the man I am today. I am truly blessed to have such a loving wife.

My parents, Johny and Yolande for their unconditional love, affirmation and never-ending support and encouragement to achieve in life whatever I set my mind to.

My supervisor, Dr G.A. Oosthuizen for his help and for securing the funding.

Martin Bezuidenhout, Philip Hugo, Emad Uheida, Lourens Delport, and Xola Madyibi for engaging in constructive argument with me and for helping me iteratively develop the strategy to its current point. It has been a great journey and I couldn't imagine where I would be without all of the help and guidance I received from you all.

Mike Saxer and the team at the Stellenbosch Technology Centre (STC-LAM) for their help throughout this project and for also allowing me the use of the facilities.

My Heavenly Father: for granting me the ability and grace to pursue my dreams.

Table of Contents

List of Figures

List of Tables

Glossary

Acronyms and Abbreviations

ABS	Acrylonitrile Butadiene Styrene
AM	Additive Manufacturing
AMTS	Advanced Manufacturing Technology Strategy
ANOVA	Analysis of Variance
BCC	Body-Centred Cubic
BD	Building Direction
CAD	Computer Aided Design
CSIR	Council for Scientific and Industrial Research
CT	Computerised Tomography
CUT	Central University of Technology
DED	Directed Energy Deposition
DIY	Do it yourself
DMLS	Direct Metal Laser Sintering
EDM	Electrical Discharge Machine
FDM	Fused Deposition Modeling
FEM	Finite Element Method
HCP	Hexagonal Close Packed
HPD	Hatch Pattern Design
HRSA	Heat resistant super alloys
HE	Higher education
IP	Intellectual properties
LENS	Laser Engineered Net Shaping
LOM	Laminated Object Manufacturing
MJM	Multi-Jet Modeling
MTF	Modulation Transfer Function
PDS	Product Design Specification
PLA	Polylactic Acid
RAPDASA	Rapid Product Development Association of South Africa
RAM	Random Access Memory
RP	Rapid prototyping
SLA	Stereolithography
SLM	Selective Laser Melting
SLS	Selective Laser Sintering
SM	Subtractive manufacturing
STL	Standard Triangulation Language
TGM	Temperature Gradient Mechanism
UAM	Ultrasonic Additive Manufacturing
UV	Ultraviolet
2D	Two-dimensional
3D	Three-dimensional
3DP	Three-Dimensional Printing

Nomenclature

Symbol	Description	Units
$\boldsymbol{\alpha}$	Significance level when determining the confidence interval	-
$\boldsymbol{A}$	Area	m^2 *or* mm^2
A	Powder bed absorptivity to the laser beam	-
$\boldsymbol{C}$	Specific heat	$J/kg \cdot K$
$\frac{\boldsymbol{\partial T}}{\boldsymbol{\partial x}}$ *or* $\frac{\boldsymbol{\partial T}}{\boldsymbol{\partial y}}$	Temperature gradient in the direction of heat flow	K/m
ρ	Density	kg/m^3
$\boldsymbol{E}$	Stiffness of material	N/m
ε	Emissivity	-
ϵ	Strain	%
ϵ_{xx}	Strain in a specific direction	%
h	Convection heat transfer coefficient	$W/m^2 \cdot$ ℃
H	Volumetric Enthalpy	J/kg
$\boldsymbol{h_p}$	Height of SLM part	mm
$\boldsymbol{h_b}$	Height of base plate	mm
$\boldsymbol{k}$	Thermal conductivity	$W/m \cdot K$
λ	Thermal conductivity	$W/m \cdot K$
$\boldsymbol{P}$	Power of the laser	W
$\boldsymbol{Q_L}$	Input laser energy	W
$\boldsymbol{Q_{CD}}$	Conduction losses	W
$\boldsymbol{Q_{CD}}$	Convection losses	W
$\boldsymbol{Q_R}$	Radiation losses	W
$\boldsymbol{q_x}$	Heat transfer rate	W
$\dot{\mathbf{q}}$	Energy generated per unit volume	W/m^3
q_c	Heat loss from the surface to the atmosphere	W
q_e	Energy density of the fibre laser	J/m^3
q_g	Internal heat generation (Used by [107])	W
Φ	Internal heat generation (Used by [130])	W
$\boldsymbol{\omega}$	Equivalent radius of the laser beam	mm
$\boldsymbol{r^2}$	Distance from the powder bed to the centre of the laser beam area	mm^2
σ	Proportionality constant called the Stefan-Boltzmann constant $5.669 \times 10^{-8}\ W/m^2 \cdot K^4$	$W/m^2 \cdot K^4$
$\boldsymbol{\sigma}$	Materials yield strength	Pa
$\boldsymbol{t}$	Time	s

$\boldsymbol{t}$	Thickness of SLM layer	mm
T	Temperature	K
$\boldsymbol{T_{\omega}}$	Temperature of the surface	K
$\boldsymbol{T_{\infty}}$	Temperature of the fluid	K
T_0	Ambient Temperature	K
T^{inf}	Temperature of the environment	K
U	Heat source due to volumetric absorption of the laser radiation	W
v	Scanning velocity of the laser	mm/s
$\boldsymbol{w_p}$	Width of SLM part	mm
$\boldsymbol{w_b}$	Width of base plate	mm

Chapter 1

Background of Additive Manufacturing in South Africa

Additive manufacturing (AM) in South Africa has come a long way since it was first introduced to the country in 1994. The initial industry base was relatively small and limited to automotive components, jewellery masters, anthropological studies, medical visualisation, architectural models, and industrial design models [1]. Since then the technology has grown to become a key player in industries such as the medical, automotive, and aeronautical industries. Smaller industry sectors have also had a positive response to AM technologies such as the academic and research, sports, gaming, toy, arts and craft, and consumer goods sectors [2].

During the 1980's/1990's sanctions were imposed on South Africa, thus the initial launch of the AM technology was a missed opportunity for the country. However, once the sanctions were lifted, the government had implemented a few initiatives (Fab Lab), to help the country's manufacturing sector to a better condition. Several governmental initiatives have had a direct impact on the implementation of AM technologies in the country. The government encouraged industry and higher education (HE) facilities to closely collaborate in order to boost the manufacturing industry [1]. This strategy paid off and led to the efficient use of the country's limited economic resources.

Additive manufacturing was first introduced into South Africa in 1994 and by 1998 there were seven AM machines in the country [3]. However, only one of these AM machines were owned by a private company. This was an indication that the higher education facilities led the way for industry to follow and that the collaboration would lead to more confidence in AM technology from the private sector. Research programmes aimed at improving AM technology in South Africa were established and this led to an increase in growth of AM technology in the country [1]. The increasing number of materials available for AM technology positively influenced industry's acceptance of the technology. Due to the rise of AM technologies in the country, Computer Aided Design (CAD) vendors also reported an increase of sales of the 3D design programmes [2].

One of the initiatives responsible for the positive AM trend in South Africa was the "Fab Lab" initiative, which forms part of the governments advanced manufacturing technology strategy (AMTS). A Fab Lab provides access to modern means for invention and fabrication for a wide range of projects. The labs serve as a learning platform to educate and expose learners and industry

partners to technologies such as additive manufacturing and CAD fabrication techniques [2]. The Rapid Product Development Association of South Africa (RAPDASA) also played a crucial role in the development of AM technology in the country through organising an annual conference, which brought international and local industries together to share information and research on additive manufacturing [2].

Today additive manufacturing machines can be found throughout South Africa. The launch of the 'Maker Nation' movement was the start of the do it yourself (DIY) trend. DIY and hobby enthusiasts now build their own machines and many of them have even started businesses with their newly found skills [4]. Open source initiatives like RepRap, started by Adrian Bowyer, have also contributed to the rapid development of the AM technology. Open source initiatives share intellectual properties (IP) in order to further develop them with a network of interested parties. This innovative method allows for co-creation of technologies. Once shared over the open source platform the think tank becomes so large that the intellectual resources and available researchers are never limited, which speeds up the development of the technology.

South Africa is still yet to fully exploit the business opportunities that can be derived from AM technologies. Shapeways is a company in the United States that connects designers with consumers by producing the designer's parts using their in-house AM machines. The final product is then shipped to the consumer and the company takes a fabrication fee. i.materialise in Leuven uses a similar business model to Shapeways [5]. However, companies such as Shapeways and i.materialise do not yet exist in South Africa. This shows that there is still room for growth for AM technology in South Africa.

One of the up and coming AM technologies in South Africa is Selective Laser Melting (SLM). SLM is a powder bed fusion process whereby a three-dimensional (3D) object is built up layer by layer by melting a powdered metal with a laser. SLM can be used to produce parts with complex geometries, which cannot be produced using conventional machining and is therefore a great candidate to produce hybrid parts. A hybrid part is produced using a combination of additive and subtractive manufacturing processes [6]. A new project has been established to boost South Africa's AM industry and to gauge what South Africa's capabilities are in terms of AM technology. Collaboration between several universities was established in 2015 and is called the Collaborative Program in Additive Manufacturing (CPAM). One of the aims of this program is to do a qualification of all the university owned AM machines in South Africa, that are capable of printing with metals such as Ti-6Al-4V. Currently, at Stellenbosch University, the achievable material performance of the Concept Laser M2 Cusing machine is being studied.

Recently the Council for Scientific and Industrial Research (CSIR) and Aerosud partnered up to develop one of the largest SLM machines in the world called the Aeroswift [7]. The Aeroswift was originally designed to manufacture large titanium components for the aerospace industry. The machine boasts a 5 kW laser and a large powder bed, which is 2 m (L) x 0.6 m (W) x 0.6 m (H) and is also said to be one of the fastest SLM machines currently available [8]. The Aeroswift was manufactured in South Africa, which is a huge milestone for the country. With the development of this machine, come more applications and opportunities for AM technology in South Africa for the aerospace, medical, and tool-and-die industries.

1.1. Aerospace Applications

The prevalent strategy for aircraft manufacturing companies is to reduce costs especially for the small to middle range aircraft. The most optimal way for them to cut costs is to reduce the process times by increasing production speeds [9]. Utilising AM technology is one of the ways these companies are decreasing costs without sacrificing quality of complex components [10].

The main driving force for the aerospace industry is the need to travel long distances in the shortest possible time. One of the main factors that influences the market is costs [9]. The reduction of aircraft weight is an important factor in the aerospace industry [11]. The fuel consumption of the aircraft is mainly determined by the weight of the aircraft [12]. Therefore, by reducing the weight of the aircraft the costs will subsequently reduce as well, making the market more competitive, which will result in more customers for the competitive airlines. Studies [12], [13] suggest that AM can be used to reduce the weight of existing aircraft components by using different strategies such as topology optimisation.

Topology optimisation can be used to design load adapted parts and can then be manufactured using an AM technology [12]. The topology optimisation process makes use of a Finite Element Method (FEM) analysis tool. The part is loaded onto the software with all of the defined loads and forces and in an iterative process all of the FEM elements with low stresses are deleted until the part is at its optimum weight. An aircraft seat manufacturer has successfully used this method and SLM to reduce the weight of a kinematics seat lever by 15 % [12].

The main materials used in the aerospace industry are aluminium and titanium alloys, composites, and heat resistant super alloys (HRSA) [14]. Aluminium alloys are typically used because of their light weight and are mainly used for the airframe of most commercial aircraft [9]. Titanium alloys are typically used in the heavily loaded structures such as the wings and landing gear beams [15]. Most SLM machines are capable of producing parts out of aluminium alloys (Al-Si12 and

Al-Si10-Mg) and titanium alloys (Ti-Al6-V4). However, strategies still need to be developed to improve the material properties of SLM parts as they fall short in some cases when compared to the wrought material.

Even though there are still significant challenges for AM technologies, a lot of progress has been made. For instance the fabrication of a laser sintered alumide turbine was successful and the turbine managed to run at 12,000 revs/min without experiencing any problems [2]. This gives promise for the future of AM for the aerospace industry. Hybrid parts could be the answer to some of the problems faced by the aerospace industry. A hybrid part could be produced up to a point with conventional machining processes and the difficult to machine and intricate geometry section could be built on the machined part using an AM technology such as SLM. Using this strategy would make the part less expensive than parts developed using just AM technology and one would still have the benefit of low weight and complex components, which one couldn't get from conventional machining. The part in Figure 1.1 below is a load bearing cabinet bracket, on the Airbus A35, made from Titanium which is 3D printed on an SLM machine. The original cabinet bracket was manufactured by using subtractive machining methods. A topology optimisation was performed on the bracket and then produced with the SLM machine in order to save material and weight [16].

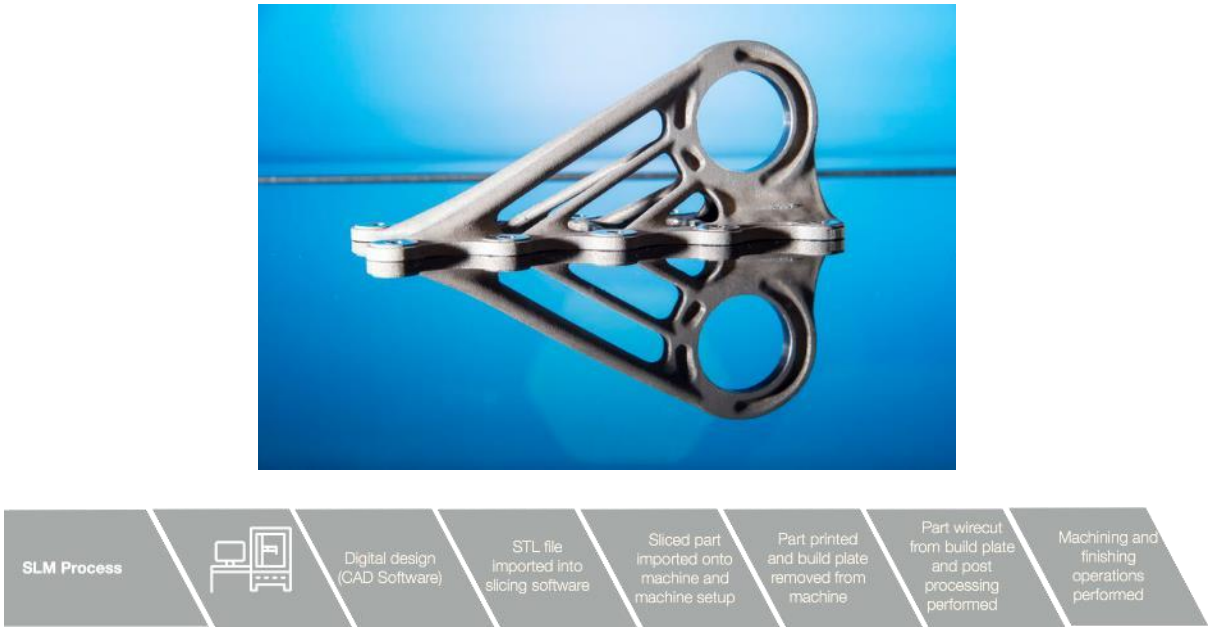

Figure 1.1: Airbus Titanium Cabinet Bracket, which has gone through a topology optimisation process and has been produced with SLM. The process chain is displayed below the part [16]

When producing the bracket in Figure 1.1 as a hybrid part, the bottom plate could be produced using conventional machining and the more complex section could be produced with the SLM process. This would save time as well as costs, as SLM powder is substantially more expensive than wrought material.

1.2. Medical Applications

Additive manufacturing has become increasingly popular in the medical industry. Studies [2], [17]–[20] have suggested different applications for AM technology in the medical industry. Applications include, but are not limited to patient-specific shielding masks [17], dental implants [18], knee and hip implants [20], [21], prosthetic fingers [22], prosthetic ears [23], prosthetic hands [24], jaw implants [25], and antibiotic delivery systems [26]. Surgeons can also utilise AM technology to prepare for surgeries. Models can be created to be used as surgical aids for dental implants, ensuring that the holes for the implants are drilled to the correct depth and orientation while performing a complex operation [27]. The patient's computerised tomography (CT) scans can be manufactured into a 3D model, which can be used for preoperative planning and rehearsal procedures to improve skills and optimise the final procedure which results in time saved and less trauma for the patient [27], [28].

Hip and knee implants are becoming more popular. In Germany alone more than 400 000 joints a year are replaced with artificial joints, most of which are made out of biomedical titanium alloys [29]. One of the problems the medical industry faces is implant infections. Implant infections are extremely resistant to antibiotics and generally persist until the implant has to be removed from the patient's body [30]. The development of patient-specific intelligent implants has been proposed [26], [29], [30]. Intelligent implants make use of drug delivery systems, which gradually deliver antibiotics and other drugs to the infected areas. The implants are also patient-specific, meaning they are customised and produced for the patient by making use of the CT scans. AM technologies such as SLM can be used because of its unique ability to produce complex metallic parts in the shortest possible lead time.

There are many different materials that can be used in the medical industry, however only some are regularly used due to their unique properties and biocompatibility. Titanium alloys are still the best metallic materials for biomedical applications. Ti-6Al-4V has been the main medical titanium alloy for many years, due to its unique material properties [31]. The Ti-6Al-4V alloy has great properties such as, high strength to weight ratio and high ductility. These properties make Ti-6Al-4V a great candidate for the production of patient-specific hip and knee implants using SLM.

A common feature of all additive manufacturing processes is the ability to control the porosity of the part that is to be manufactured. Porous materials are important for biomedical applications [32]. Research [33], [34] has been performed to prove if implants such as hip and knee replacements should contain a scale of porosity to promote biocompatibility and bone intergrowth. AM processes such as SLM would be the most suitable candidate to produce porous implants. SLM can produce

irregular structures that mimic human cancellous bone. Once chemical and thermal treatments have been performed on the SLM manufactured implants, osteoconductivity and osteoinductivity are induced, which promote bone growth within the implant structure and reduce the chance of rejection by the body [33].

Subtractive manufacturing (SM) processes are traditionally used to produce fully dense implants. However, if a mixture of AM and SM were used, the combination of these two technologies could offer a competitive advantage. The basic structure of the implant could be manufactured using SM processes such as 5-axis machining and the complex structures such as the porous microstructures could then be manufactured using an AM technology such as SLM [35]. One could also utilise SLM in the implant manufacturing process chain in order to include slow release drug delivery systems. This would shorten the process chain by removing the need for membranes in the manufacturing process.

1.3. Tool-and-Die Applications

Studies [36]–[38] have been conducted on the plausibility of utilising additive manufacturing for tool and die production and have thus far been successful. AM processes are potentially the best solution for industries that have short production runs and where tooling costs are the highest costs in the manufacturing process chain [39]. The need to manufacture a small batch of parts (less than 100) for various applications such as design validation, proof of concept, pre-production tests, and approval of production tooling occurs often in industry [36]. AM technology allows one to simply build a mould or tool directly from a CAD file with little skill and without a lengthy process chain. This ability could lead to significant cost savings and quicker lead times for manufacturers [32]. However, AM is still limited by size, surface finish, and costs.

There are still several problems with the AM technology that limit its use for tool and die production and as a result, conventional machining still takes preference over AM. In order to successfully manufacture moulds and dies, it is crucial that residual stresses in AM parts are reduced [40]. Most machines have a small build volume because the build-up of residual stresses during the process causes large parts to warp. The part size that can be produced using AM technology is limited by the build space of the machine. A typical SLM machine is equipped with a build space of 250 x 250 x 300 mm^3 [12]. This limits the machines applications in industry to small parts only. However, new machines are being launched with a bigger build space in order to become more productive and competitive in industry. The new X-Line 1000R by Concept Laser GmbH boasts a big build space of 630 x 400 x 500 mm^3 and two process chambers so that one chamber can be prepared while the SLM process takes place in the other [41].

Due to the nature of AM being a layer by layer building process the resolution or layer thickness of the machine limits the surface finish. The surface finish produced by AM techniques is not adequate for tool and die production, thus further post processing procedures, such as finish machining, are required to achieve a better surface finish for the tool. Post processing operations can be a costly and time consuming activity. The additional process also extends the process chain, which increases the lead time and thus an advantage AM holds over conventional machining is lost. The costs of AM machines and material are also substantially high in comparison to conventional machining costs.

The accuracy of the mould production process is very important in the tool-and-die industry because any deformation in the mould will be transferred to the final moulded part. When using the SLM process to manufacture tools and dies, deformation of the part could occur due to thermal stress induced by the laser. This phenomenon is a characteristic of most AM processes and it directly affects the accuracy of the process and the final part. However, strategies are being developed to reduce the residual stresses in the SLM parts [42], [43].

The greatest advantage that AM technologies possess over conventional machining for tool and die production, is the ability to produce parts with complex geometries and hollow structures. Studies [21], [44], [45] have shown the advantages of introducing conformal cooling channels into the mould and dies by utilising an AM technology. These cooling channels allow the moulded parts to be rapidly cooled during production, which reduces the cycle time and improves the part quality. These advantages directly result in a massive cost saving despite the initial high costs to produce the moulds with AM [46].

In order to introduce conformal cooling channels into a mould, without producing the entire mould with an AM technology, a hybrid part can be produced [47]. Hybrid parts are parts that have been manufactured using the best combination of machines and technologies. The most cost effective way to produce a mould with conformal cooling channels is to use a combination of subtractive and additive manufacturing processes. A project for a plastic conversion company, USABCO, Cape Town, South Africa, was undertaken by the RPD Lab at Stellenbosch University to increase efficiency of a Cutlery Drainer mould. The cycle time with the conventionally cooled mould was reduced by 30.78% with the new hybrid mould with surface cooling channels. This led to major cost savings for the company in available free capacity [47]. The CAD model and actual finished mould can be observed in Figure 1.2 below with the process chain below it.

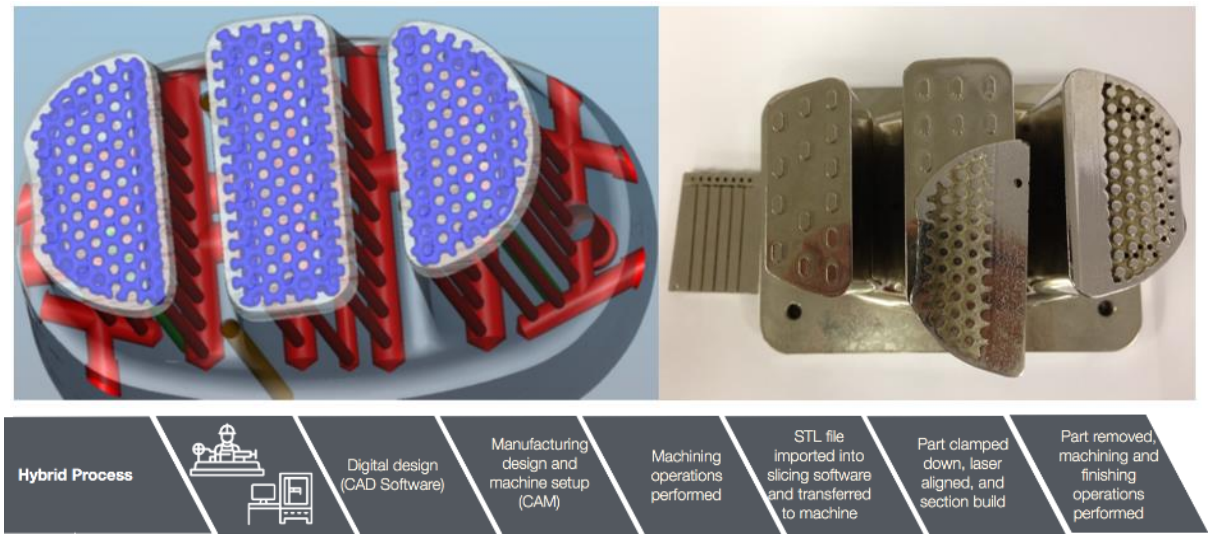

Figure 1.2: Cutlery Drainer mould with surface cooling channels manufactured using SLM and machining. (Left) CAD model showing the surface cooling channels. (Right) Manufactured hybrid mould showing surface cooling channels. (Bottom) the production process chain [47]

1.4. Challenges in Additive Manufacturing

Regardless of all the advantages that AM holds over other technologies, several challenges still exist and aspects of the AM process chain need to be improved on. A major disadvantage of AM is that the part production is time consuming. The reputation AM has as a fast production process comes from the time gained in pre-processing, where the user can simply create the part with a CAD file. The time saved is significant in comparison to conventional manufacturing methods such as machining, where an entire production process chain needs to be designed by skilled workers to produce a part. Other aspects that require improvement in the metal AM department are [48]:

- The limited amount of metal alloys that are commercially available for AM is one of the factors that require improvement to make AM more appealing for industry.

- AM lacks in-process quality control and feedback control. To have good repeatability and to produce AM parts for critical applications, the technology needs to be commercialised to control the quality of parts during the building process. This would save time and money and make some post-processing inspections redundant.

- High cooling rates during the process need to be controlled. The high cooling rates result in unique, metastable microstructures, which could have positive or detrimental effects on the part's mechanical properties. Metallic parts produced with an AM technology respond to heat treatment in a different manner to that of forged or cast material.

- Residual stress induction in the parts caused by high cooling rates and other mechanisms needs to be reduced. The stress limits the build size of the part and determines the required size of the base plate. The bigger the part is, the thicker the base plate needs to be, to restrict the warping of the part during production. This then also limits the height that one can build as the thicker base plate takes up some of the build volume.

- Parameter optimisation is very important with AM technologies. Each machine and material requires different parameters. Non-optimal process parameters lead to porosity in the part and can also have a detrimental effect on mechanical properties of the part. More research needs to be conducted to determine the influence, microstructure or residual stress have on the mechanical properties of a part produced with metal AM technologies.

1.5. Problem Statement and Research Objectives

In order to determine the achievable material performance of the Concept Laser M2 Cusing machine at Stellenbosch University, several samples for different testing methods had to be constructed using the M2 Cusing machine. During production of the fatigue test samples, using default building parameters, some problems were observed and are displayed in Figure 1.3 and Figure 1.4.

Figure 1.3: Delamination of Ti-6Al-4V fatigue testing sample produced on the Concept Laser M2 Cusing machine with default parameters

Figure 1.3 displays delamination of some of the build layers. The cracks and delamination result from the residual thermal stress, built up in the part during the building process [49]. Slight deviations due to warping can also be observed on the right-hand side of the part. Figure 1.4 shows the cross section of another fatigue testing sample. The section was wire-cut with an electrical discharge machine (EDM).

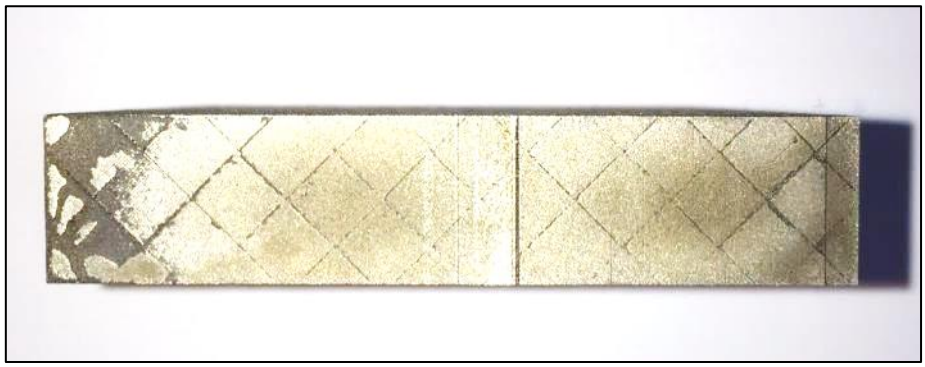

Figure 1.4: Visible Islands on Ti-6Al-4V fatigue testing sample produced on the Concept Laser M2 Cusing machine with default parameters

One could observe in Figure 1.4 that the islands are clearly visible. This is because the first 17 layers were scanned as Slice 1. Aligned porosity is the result of rescanning the same island without shifting it and it is caused by a local overheating effect [50]. This is an indication that the bond between the islands is not adequate and this island scanning strategy relies on the fact that the islands shift by 1 mm in the x and y directions to reduce porosity in parts. One should note that the terms SLM and LaserCusing or Cusing are used interchangeably in this paper. The term LaserCusing is coined by Concept Laser GmbH and the word is made up from the letter C from Concept Laser and the word Fusing. The process that LaserCusing is classed under is Selective Laser Melting (SLM).

1.5.1. Problem Statement

Additive manufacturing technologies such as SLM are simple to use and users don't need years of experience in order to create a 3D object. One would only need knowledge of the machine and CAD software to produce a product [51]. However, unlike subtractive manufacturing (SM) methods, SLM still has a large amount of problems and unknowns. A vast amount of research has been done on SLM and the challenges that the technology faces [46], [52]–[55]. One major problem with the SLM technology, which is displayed in Figure 1.3 above, is warping or deformation due to residual stresses. Stresses are induced during the SLM process through large thermal gradients and temperature fluctuations. Due to these phenomenon, parts are often scrapped which requires an expensive rework. Often post processing operations need to be performed for the SLM part to be up to standard, thus the advantages SLM holds over subtractive manufacturing processes are often lost to additional time and costs not associated with the SLM process.

To reduce the costs involved with SLM a process chain with subtractive manufacturing (SM) and additive manufacturing processes has been suggested. Process chains can incorporate a combination of manufacturing technologies in order to produce a product in the most resource efficient manner. Components produced using a combination of SLM and conventional machining are referred to as

hybrid parts if the SLM section is fused to the machined section. The problems associated with the SLM technology, such as geometric deviation (warping) and porosity, are still applicable to the production of hybrid components. The aim of this study is to determine whether different laser scan strategies can be developed to reduce geometric deviation and porosity in titanium SLM parts and consequently hybrid parts.

1.5.2. Research Questions

The problem statement is investigated by answering the following research questions:

1. Does the number of layers influence the geometric deviation of hybrid parts?
2. Is the current SLM process chain sufficient for the production of hybrid parts?
3. Can one change the scan strategies on the Concept Laser M2 Cusing machine to a user defined scan strategy?
4. Is the default scan strategy, patented by Concept Laser GmbH, the optimal strategy in terms of porosity and geometric deviation?
5. Does changing the scan strategy have a significant effect on the porosity of an SLM part?
6. Does changing the scan strategy have a significant effect on the geometric deviation of a hybrid part in terms of deviation in the z direction?

1.5.3. Research Objectives

The focus of this study is not to optimise the process parameters like [56]–[61] but to study and discover better SLM strategies. By answering the above research questions, the objectives of this study are to

- Determine the effects of Selective Laser Melting on the geometry of hybrid parts.
- Study the current SLM process chain and identify the main factors that would be detrimental to hybrid parts during production.
- Create a method to change the scan strategy on the Concept Laser M2 Cusing machine to a user defined strategy.
- Investigate the effects of SLM strategies on the porosity and geometric deviation of SLM parts and consequently hybrid parts.
- Develop a scanning strategy to improve the porosity and geometric deviation of SLM parts and consequently hybrid parts.

Chapter 2
Additive Manufacturing and Hybrid Part Manufacturing

2.1. Introduction

Additive manufacturing (AM) technology was initially developed in the late 1980's to be used to manufacture prototypes and parts in a shorter time than conventional subtractive manufacturing (SM) methods [62]. However, depending on the AM technology, AM could be more expensive than conventional subtractive manufacturing. Additive Manufacturing has been gaining popularity in the aerospace, medical, and tool-and-die industries [51].

Moulds for injection moulding can now be manufactured with complex cooling channels, which allows for a significant increase in the production efficiency of moulded parts. These moulds are produced using a combination of additive manufacturing and subtractive manufacturing processes. Parts that are manufactured using a combination of these processes are called hybrid parts.

2.2. Hybrid Part Manufacturing

Hybrid manufacturing is the integration of various manufacturing technologies into a single system in order to manufacture complex components in the most resource efficient way [63], [64]. A hybrid manufacturing platform is made up of two or more combined additive, subtractive, joining, or transformative processes. Hybrid manufacturing platforms offer new capabilities and opportunities for product design. However, high levels of expertise are required to effectively design and manufacture products using hybrid platforms. In order to effectively design for hybrid manufacturing, the designer requires a vast knowledge of a number of manufacturing technologies, which might be highly varied in their methods [65]. Karunakaran et al. [66] describes how one can use an additive manufacturing process followed by a subtractive manufacturing process in order to eliminate the times and costs of NC programing and rough machining for complex parts. This study suggests that the subtractive process be performed first to a point. The additive process would then build the remainder of the part on top of the machined section. This process can save time and costs with regards to SLM, as the SLM process is considerably more expensive than conventional machining, but is this application is also part dependent.

2.3. Subtractive Manufacturing

Subtractive manufacturing is the process of removing material from a piece of raw material to form a specific shape or part. Subtractive manufacturing is generally performed with a cutting tool and is performed by either rotating the tool or the workpiece at high speeds [67]. There are several types of subtractive manufacturing processes, but the main three types are milling, turning, and drilling. The first machine tools that were used to perform material removal processes were developed in the late 1760's around the same time the first steam engine was developed by James Watt. The steam engine's commercial success could be attributed to the timely aid of the first successful boring machine [68].

Additive manufacturing is becoming increasingly popular, due to the rapid manufacturing advantages it holds. However, high speed cutting (HSC) technology is often compared to AM technologies and also holds certain advantages over the AM technology [69]. One of the advantages is the vast amount of materials that can be used for production. Multi-axis high speed cutting allows for the complete machining of a component in a single set-up [69]. This feature drastically improves lead time and shortens the process chain.

Some of the problems faced by conventional machining though, is the amount of material that needs to be removed in order to produce a specific component. In some cases, up to 95% of the original material needs to be removed and ends up as formed chips. The time, machining costs, and raw material all contribute to the costs incurred during the machining process [55]. Similarly, SLM also has its cost downfalls in terms of powder material, machine time, and post processing costs. To manufacture hybrid components a combination of additive manufacturing and machining is used to utilise the benefits of the respective technologies and to improve the costs. As illustrated in Figure 2.1 the costs linked to additive manufacturing increase at a faster rate when the volume is increased when compared to subtractive processes [55].

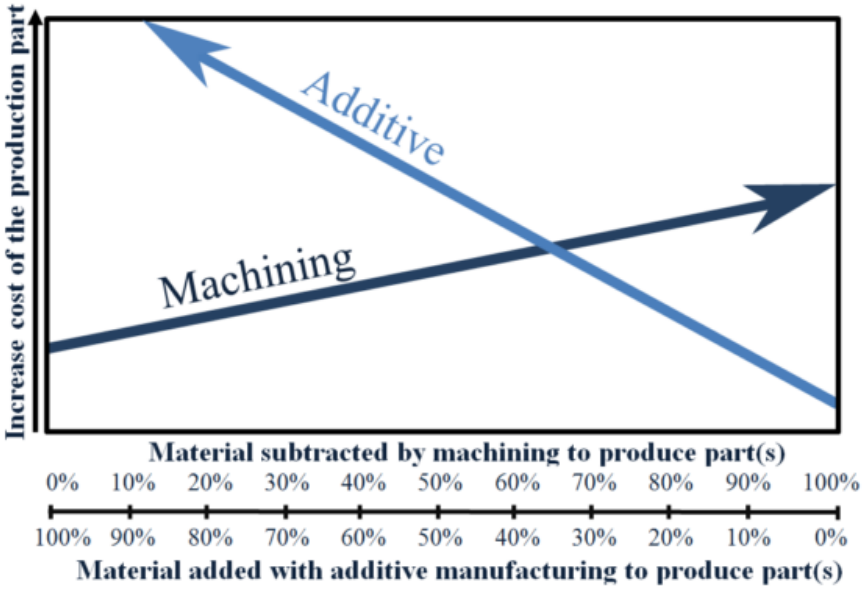

Figure 2.1: Illustration of the relation between increasing costs associated with the amount of added or subtracted material [55]

The optimal balance between the material removal and material addition needs to be determined when it comes to hybrid parts. Doing this would exploit the advantages of both the additive and subtractive manufacturing processes. The hybrid part should be produced in a more cost and resource efficient manner than if either AM or SM manufacturing technologies were solely utilised.

2.4. Additive Manufacturing Technologies

Additive manufacturing has evolved over the years and has assisted designers and manufacturers to create and develop physical models at a fraction of the time and costs in comparison to conventional methods. The AM development timeline can be observed in Figure 2.2. One should take note of the expiration of patents, which has had a positive effect on the growth of AM technologies.

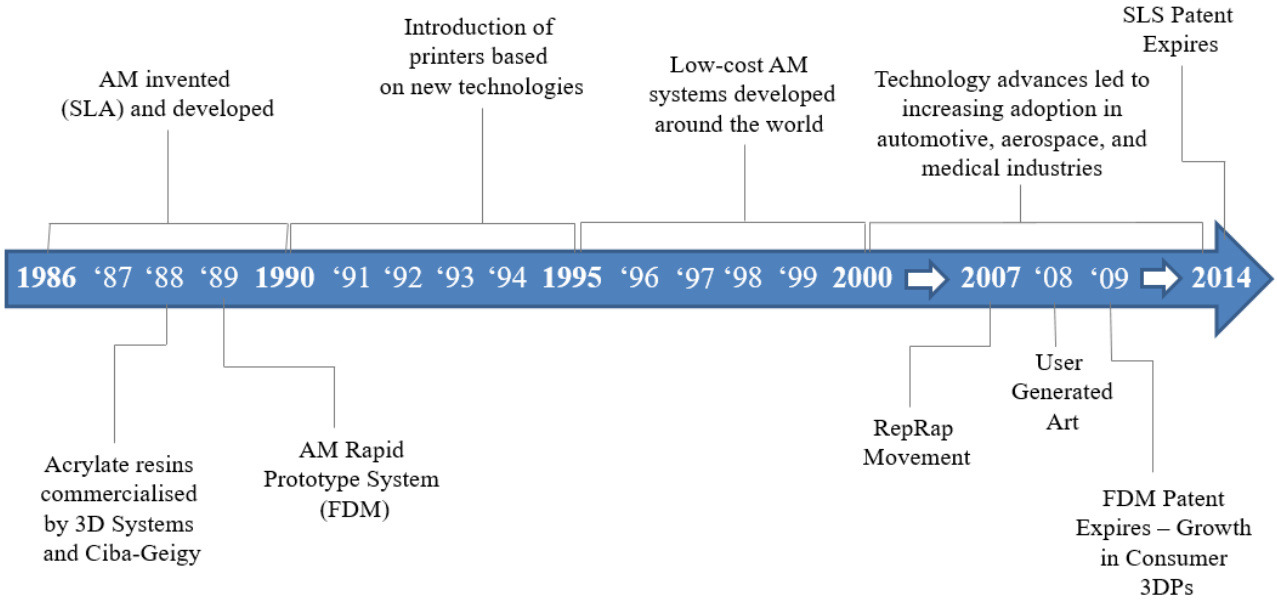

Figure 2.2: Additive manufacturing evolution timeline adapted from [70], [71]

The ASTM F42 Committee created the term Additive Manufacturing (AM) as the standard term for a model or part that has been initially generated using three-dimensional model data and fabricated layer upon layer without extensive process planning [51].

AM is an essential part of the product development stage and the prototyping aspect of AM allows products to be assessed in terms of the form, fit, and functionality before the final investment in the tooling is made [72]. Prototyping also plays a large role in the marketing stage as consumers can now interact with the design and modify it before any significant costs are incurred. The generic process chain used for most AM technologies can be observed in Figure 2.3 below.

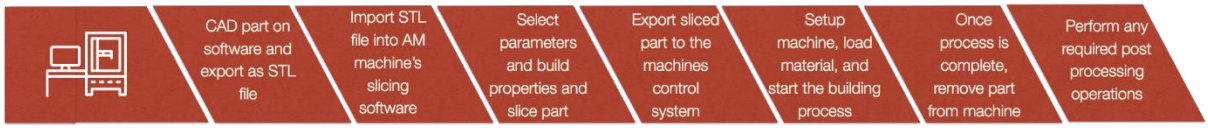

Figure 2.3: Generic Additive Manufacturing Process Chain that can be applied to most AM technologies

Before the introduction of AM technologies into industry, new concept models and prototypes had to be manufactured using standard subtractive machining operations with two dimensional (2D) engineering drawings. Skilled artisans were needed in order to manufacture these prototypes and the processes were excessively time consuming and costly [73]. AM is a simpler process to produce 3D objects where very little skill is required, compared to other manufacturing processes. With other manufacturing processes a detailed analysis of the object geometry is required in order to determine the different features that can be fabricated and the different machines and tools needed to do so [51]. An extensive process chain needs to be developed in order to produce just one part. With AM the process chain is considerably shorter and less complex than other traditional manufacturing methods. Most AM technologies all have the same processes but they tend to vary with material and binding mechanisms. There are several systems that are used to classify and categorise AM technologies. The one proposed by the ASTM F42 Committee [74] classifies AM technologies into seven areas. These seven areas are:

1. Vat Photo-Polymerisation,
2. Material Jetting,
3. Binder Jetting,
4. Material Extrusion,
5. Directed Energy Deposition,
6. Sheet Lamination, and
7. Powder Bed Fusion.

According to Guo and Leu [53], AM processes can also be divided into four broad categories, which relies on the initial state of the build material. The four categories are [62]:

1. Liquid,
2. filament/paste,
3. powder, and
4. solid sheet.

There are many different systems used to class AM technologies [53], [74]–[77] but in order to keep to a standard, the ASTM standard was used for this study. Some of the different AM technologies have been classed into the categories described by the ASTM F42 Committee in Table 2.1 below.

Table 2.1: Different Types of AM Technologies, which are classed into the categories described by the ASTM F42 Committee [39], [51]

Name	Acronym	Area of Classification	Material	Commercial Machine
Stereolithography	SLA	Vat photo-polymerisation	Photopolymer	ProJet 6000 – 3D Systems
Multi-Jet Modeling	MJM	Material Jetting	UV Curable Polymer	ProJet 300 SD – 3D Systems
3D Printing	3DP	Binder Jetting	Specialised Powder and Binder Materials	ProJet 260 - 3D Systems
Fused Deposition Modelling	FDM	Material Extrusion	Thermoplastics, Metals	Dimension Elite - Stratasys
Selective Laser Melting	SLM	Powder Bed Fusion	Metal Powders	Concept Laser M2 Cusing
Selective Laser Sintering	SLS	Powder Bed Fusion	Thermoplastics, Metal Powders	P110 - EOS
Electron Beam Melting	EBM	Powder Bed Fusion	Titanium Alloys	S12 - ARCAM
Laminated Object Manufacturing	LOM	Sheet Lamination	Adhesive Coated Sheets	

Each of the AM technologies are discussed briefly in the following sections under each of the respective categories. However, due to SLM being the focus of this study, the technology was thoroughly discussed.

2.4.1. Vat Photo-Polymerisation processes

Additive manufacturing processes that utilise a material that is initially in a liquid state in a vat would be classed under the vat photo-polymerisation category. There are several types of liquid materials available, namely, photo-curable resin, wax, thermoset resin, and polyamide. Stereolithography (SLA) was the first AM technology that was commercially available. The technology makes use of a liquid photosensitive resin, which is transformed to a solid state through the selective exposure of an ultraviolet (UV) light. The CAD part is sliced into layers using slicing software. The slices are then loaded onto the machine and the UV light then traces out each layer, strategically solidifying the resin in the vat. Once the layer is complete the build vat drops by one layer thickness and the blade coats the build area with a fresh layer of resin to start the process over again [51], [53].

2.4.2. Material Jetting processes

Material jetting makes use of similar technology that is utilised in an inkjet printer. Material is released onto a build platform using jets. Multi-Jet Modeling (MJM) is a technology that is classed as a material jetting process. The print head has multiple nozzles that can be moved along the x and y planes in order to dispense UV curable polymer on demand. The layer of polymer is deposited and the UV light then flashes to cure the polymer, the platform is then descended one layer, and the process repeats until the part is complete [51], [78]. Jetted Photopolymer is similar to MJM but uses wide inkjets to deposit layers of photo-polymers. An example of a jetted photopolymer machine is an Objet 500 Connex 3.

2.4.3. Binder Jetting processes

The binder jetting process makes use of two different materials. The powder based material is usually bonded with a liquid binder. The binder acts as an adhesive and solidifies the powder in a layer wise manor. Once a slice is completed, the build platform is lowered by one layer and a new layer of powder is rolled over the platform. This process is repeated until the part is complete. The AM technology that falls under this category is 3D Printing (3DP).

2.4.4. Material Extrusion processes

The Fused Deposition Modelling (FDM) process is the most common material extrusion process. The concept makes use of a filament and a hot end that is located on three (3) different axes namely the x-, y-, and z-axes, also commonly known as the Cartesian coordinates [79]. The filament is fed into the hot end where it is melted down and fed out the nozzle at a certain rate depending on the rate of movement of the three axes [79]. The filament is deposited onto the build platform in a layer

wise manner until the part is complete. The temperature of the hot end is usually kept around 170 ºC to 250 ºC depending on the type of material that is used as a filament. The most common filaments that are used are Polylactic Acid (PLA) and Acrylonitrile Butadiene Styrene (ABS).

2.4.5. Direct Energy Disposition processes

Several technologies fall under the Directed Energy Deposition (DED) class, such as: Laser Engineered Net Shaping (LENS), directed light fabrication, direct metal deposition, and 3D laser cladding. These processes are more commonly used to repair or to add material to an existing component. A typical DED process utilises a nozzle mounted on a multi axis arm to deposit melted material onto a specific surface. The material is deposited through the nozzle onto the workpiece and is rapidly melted with a laser or electron beam. Different materials such as polymers, ceramics, and metals can be used with DED processes [51].

2.4.6. Sheet Lamination processes

Sheet lamination technologies include Ultrasonic Additive Manufacturing (UAM) and Laminated Object Manufacturing (LOM). UAM is an additive manufacturing technique that utilises ultrasonic vibrations in order to weld thin metal plates into near net shaped parts [80]. UAM can be used to process materials such as aluminium, copper, stainless steel, and titanium. UAM is similar to LOM, however, LOM uses paper instead of metal and an adhesive instead of welding.

2.4.7. Powder Bed Fusion processes

Powder bed fusion (PBF) processes utilise either a laser beam or an electron beam to melt (sinter) and fuse powder together. Selective Laser Sintering (SLS), Direct Metal Laser Sintering (DMLS), Electron Beam Melting (EBM), Selective Heat Sintering (SHS), and Selective Laser Melting (SLM) all fall under the powder bed fusion process category. Some of these technologies are discussed in more detail in the following sections.

2.4.7.1. Selective Laser Sintering

Selected laser sintering utilises a laser to sinter and fuse the powder together. A counter-rotating roller is used to distribute the powder across the build platform. The manufacturing process occurs inside an enclosed compartment, which is filled with nitrogen or argon gas such that oxidation and degradation of the powdered material is minimised [39].

2.4.7.2. Electron Beam Melting

The fundamental difference between SLM and EBM is the energy source used to melt the powdered material. However, studies show that the energy source used to melt the powder plays a role in

other aspects such as the material and mechanical properties [81]. In the case of EBM an electron beam is used to melt a fine powder layer in order to create a 3D object once all the layers are melted and fused together. Due to the scope of the study only the SLM technology will be reviewed.

2.4.7.3. Selective Laser Melting

Since Selective Laser Melting is the focus of this study it is discussed in greater detail in the following section.

2.5. Selective Laser Melting

The Selective Laser Melting process makes use of a laser to melt fine layers of metallic powder together to create a 3D object. The powder is distributed from the powder bed across to the build platform using a metal or rubber scraper. The SLM process occurs inside an airtight compartment, which is filled with either nitrogen or argon gas so that oxidation and degradation of the powdered material is minimised during the process. In some machines the temperature of the build chamber is maintained below the melting point (Roughly 600ºC) of the metal by means of infrared heaters. The elevated temperature also serves to prevent non-uniform expansion and contraction of the build platform, which can cause the part to deform during the building process [39], [51], [82]. A graphical representation of the SLM machine can be observed in Figure 2.4.

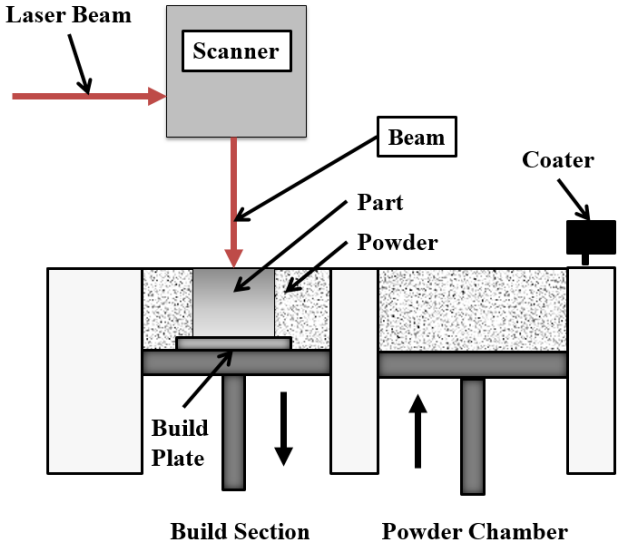

Figure 2.4: Graphical representation of a selective laser melting machine, which demonstrates how the building process is performed

A common trait of all SLM machines is the rigid attachment of the parts to a build plate located at the bottom of the build platform. The reason this is done, is to reduce movement of the part as well as distortion in the part caused by residual stresses. The part tends to bend upward towards the laser as the material is rapidly heated and cooled [51], [83]. Other limitations to SLM processes include

inadequate surface quality, remnant porosity, and a layer step effect, which is a feature of all layer manufacturing [84].

Titanium and titanium alloys have a high reactivity and the melting process needs to be conducted in an inert argon atmosphere. A better understanding of the SLM process is required to deal with the deviation and warping problems. SLM is a complicated process that features a wide range of non-equilibrium phenomena that rely on a vast number of parameters. These parameters are discussed further in the following sections. External parameters that also apply to the process are surface tension and thermal conductivity of the material [83].

2.5.1. SLM Process Parameters

There are many parameters that have an influence on the quality of the final produced parts. As an example, the SLM Solutions SLM280HL machine has more than 150 parameter settings that can be changed by the user. Machine parameters are generally categorised as in-process scan parameters, atmosphere related parameters, and laser related parameters.

2.5.1.1. Scan parameters

The most important in-process parameters are the laser power P [W], scan speed v [mm/s], hatch spacing h [µm], scan strategy or exposure strategy, and layer thickness t [µm] [48]. These parameters are the most important when it comes to porosity optimisation. The power, scan speed, hatch spacing, and layer thickness can be combined to determine a single parameter called energy density. The energy density E (in J/m³) is a measure for the averaged applied energy per volume of material during the scanning of one layer and the equation for energy density is given by Equation 2.1

$$\boldsymbol{E = \frac{P}{v \cdot h \cdot t}} \tag{2.1}$$

where P is the laser power (in W), v is the scanning velocity (in mm/s), h is the hatch spacing (in mm) and t is the layer thickness (in mm) [83]. The laser hardware limits the maximum laser power. The laser scan speed is limited by the inertia of the mirrors in the galvanoscanner. The laser power and scan speed should not be varied independently as the melt pool properties and the final part quality rely on these parameters [85], [86]. In order to fully understand the SLM process and some of the laser and scanning parameters, Figure 2.5 was sketched.

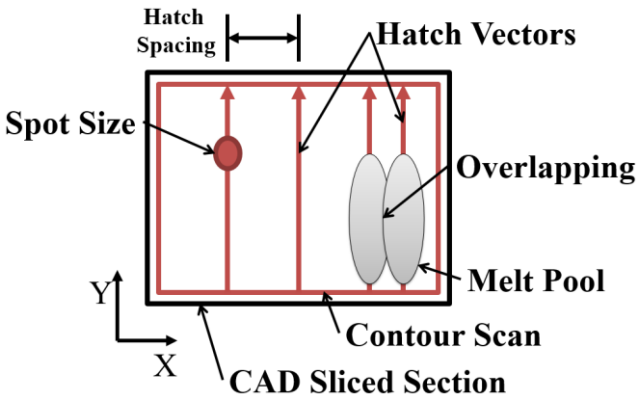

Figure 2.5: The SLM melting process being performed on a slice of a rectangular part and the terminology used for the laser and scanning parameters

In Figure 2.5 above the spot size is the laser focus/spot diameter, which is a laser parameter. The spot diameter of the laser is one of the factors that determine the size of the melt pool, and the hatch spacing needs to be taken into consideration when changing the spot diameter. The hatch vectors in Figure 2.5 are the fill vectors that the laser follows in order to melt the powder. The software used to create the slice vectors (Magics) does not show the direction of the vectors but rather the path for the laser to follow. The machine software (Concept Laser) also does not allow the user to select custom hatch vectors but rather allows the user to select from 6 fixed scan strategies and a contour scan, which are shown in Section 3.2.4. The contour scan is usually a set of vectors that outline the contour/perimeter of the part.

The hatch spacing (which is designated as a1 on the M2 Cusing machine) is the perpendicular distance between two hatch vectors. The hatch spacing affects the overlapping of the melt pools, which in turn, affects the density (porosity) of the part. The hatch spacing should always be significantly less than the width of the melt pool [48]. The width of the melt pool is mostly determined by the laser spot size, but also the laser power and scan speed play a significant role [87], [88].

Two factors limit the lower limit of the layer thickness of the machine, one being the motor step size and the other being the particle size of the powder. The upper limit is restricted by the need for complete penetration of the melt pool into the subsequent layers. If the powder layer is too thick, a layer of un-melted powder will be present between the exposed layers, causing the part to fall apart when removed. While a larger layer thickness results in a higher productivity rate, the geometrical resolution is sacrificed, which enhances the staircase effect. This could be of a benefit to hybrid parts as the final surface finish relies on the machining parameters and not the layer thickness.

A very important scanning aspect is the scan strategy that is used to solidify the layers of the part. There are several characteristics to a scan strategy and these characteristics are listed below:

- Scan vector pattern
- Vector direction
- Length of the vectors
- Orientation of the vector patterns with regards to the part axes
- Time between exposure of vectors
- Layer offset
- Layer orientation
- Layer remelt
- Layer melting distribution

Different machine manufacturers all use different scan strategies. There are many different strategies used but some are not adequately documented. The vector and layer scan strategies are thoroughly discussed in Section 3.2.4 as well as the effects they have on the final parts.

2.5.1.2. Atmosphere related parameters

The atmospheric parameters are important, as many problems could arise if the parameters are not correct. With regards to titanium powder, the system needs to be filled with an inert gas such as argon (Ar). The build chamber is supplied with argon gas from the ventilator at a slight overpressure to avoid any leakage of oxygen into the chamber, which could lead to oxidation of the part and powder, fire, or even an explosion.

The atmospheric pressure has also been documented to have a great effect on the melt pool stability [48]. Another aspect that needs to be considered is the temperature and flow rate of the gas inside the chamber. These two parameters could have a huge effect on the thermal gradients induced in the part. Dadbakhsh et al. [86] found that the gas flow can have an effect on the thermal stress and bonding strength between particles, which consequently influences the mechanical properties of the final parts. It was found to be beneficial to manufacture the parts perpendicular to the gas flow rather than parallel. Several mechanisms that cause warping and deviation are discussed in detail in Section 3.1.

2.5.1.3. Laser related parameters

Certain laser parameters cannot be varied through the software and require the hardware to be changed and calibrated in order to make a change. The scan mode of the laser, wavelength, intensity distribution, laser spot geometry, laser spot size, and offset of the focal point with the powder are

several parameters that all rely on the laser hardware and software capabilities [48]. Many of these parameters cannot be varied on the Concept Laser M2 Cusing machine as the user's control over the laser parameters is very limited. The Concept Laser M2 Cusing machine has a Rofin Starfiber 200 laser.

Since the laser is the crucial element of an SLM system. An understanding of how the laser system works is beneficial. The scanning system of the Rofin Starfiber 200 laser operates by utilising a galvanometric system, which consists of two mirrors driven by limited-rotation motors. These mirrors rotate in order to focus the laser beam to a specific point on the Cartesian plane. The rotation of these mirrors however does not rely on input of x and y coordinates, but rather the reflection angles of the laser. The first mirror (X-Scanner) controls the laser beam along the x coordinates and the second mirror (Y-Scanner) controls the laser beam along the y coordinates [89]. The galvanometric laser scanning system can be observed in Figure 2.6.

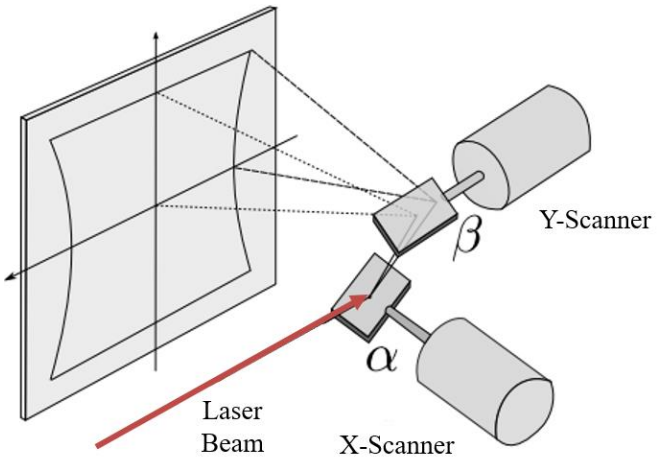

Figure 2.6: A galvanometric scanning system of a laser system, which is directed onto a two-dimensional plane that represents the SLM powder bed adapted from [89]

Errors in scanning can result, when the scanning mirror is too large and has a large moment of inertia. The fast movement of the mirror and the large moment of inertia could cause the mirror to over rotate due to the motors not being able to stop the mirror instantaneously. This would be detrimental to the SLM process, so mirror size and weight are some of the limiting factors of laser scan speed in order to avoid this error.

2.5.2. SLM Process Chain

In this section the SLM process chain for the M2 Cusing machine is discussed. Process chains differ for different AM technologies as well as for different machine manufacturers. The process chain for the M2 Cusing machine from Concept Laser GmbH is displayed in Figure 2.7.

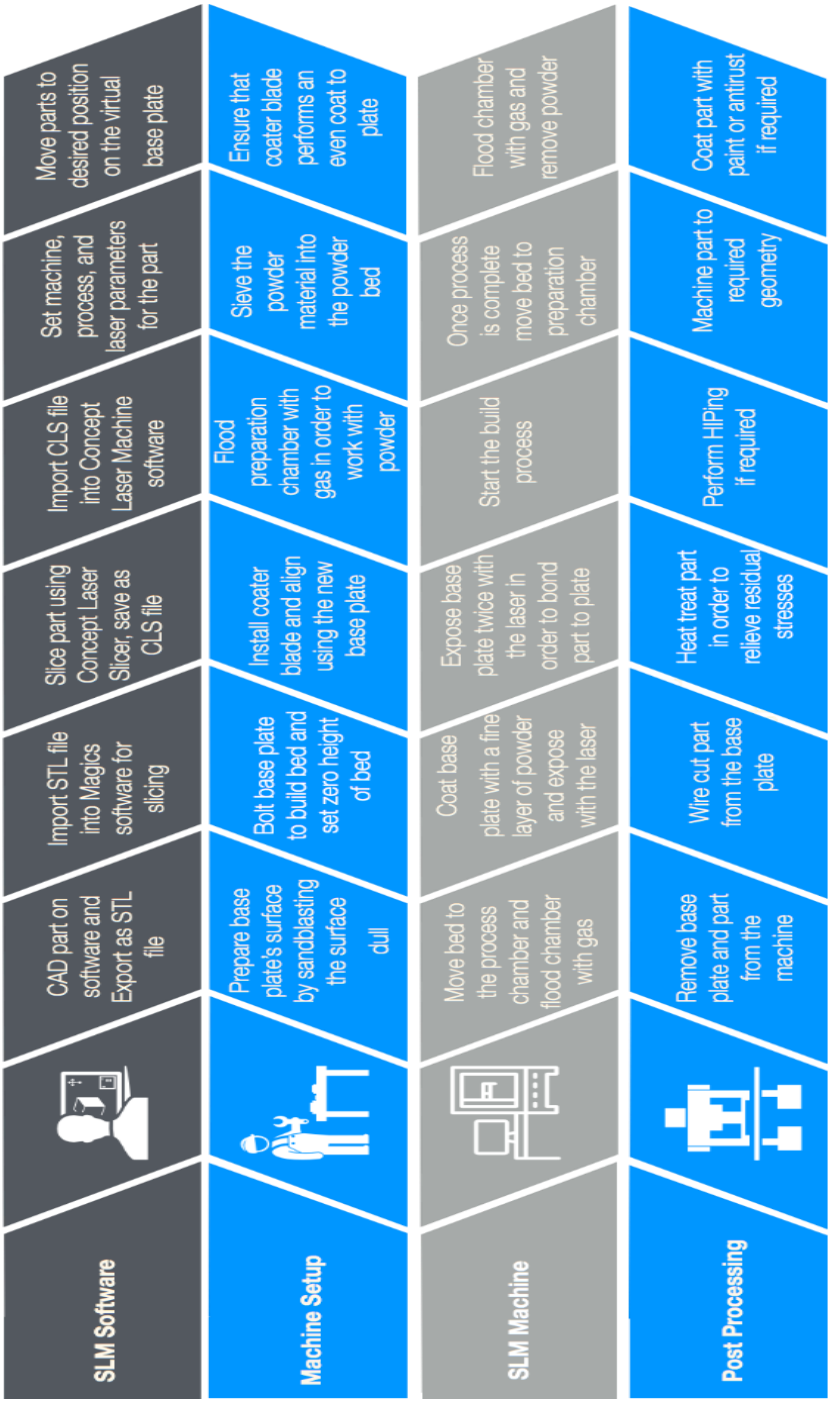

Figure 2.7: Entire SLM process chain to create a part on the M2 Cusing machine from Concept Laser GmbH.

The process chain has been divided into four sections. Each section is a process chain in itself and the four sections make up the entire SLM process. These four sections are SLM software, machine setup, SLM machine, and post processing. Each of the process chains in these sections are discussed in detail in the following sections.

2.5.2.1. SLM software

Any CAD program can be used to design a part and export it as an STL file. Most AM technologies can utilise any 3-dimensional solid model data if it is converted into the Standard Triangulation

Language (STL) file format before being loaded onto the machines slicing software. Before the digital model can be loaded onto the M2 Cusing machine, the CAD data needs to be prepared on Magics 3D software and sliced with the Concept Laser Slicer.

Magics 3D software is a data processing program that is used to construct supports and repair STL files. The CAD models are imported as a STL file into Magics. The file is imported onto the machines virtual bed so that the user can place the parts with reference to the actual build plate of the machine. Once the user is satisfied with the part's positioning and supports, the user then inputs the required parameters and uses the Concept Laser Slicer to slice the model into layers. Each part is then converted into a Concept Laser Slice (CLS) file, which can be imported directly onto the machines software.

Once the CLS files are imported onto the machine's software, the user must set the process parameters for the machine. The M2 Cusing machine has several parameters that the user can change and others that cannot be changed. These parameters are classed into three groups, namely, Machine Parameters, Cusing Process Parameters, and Laser Parameters. Each of these parameter sets and the variable parameters are displayed in the following sections.

Machine Parameters:

The variable machine parameters on the Concept Laser machine's software can be observed in Table 2.2.

Table 2.2: : M2 Cusing Machine parameters that can be varied by the user [90]

Parameter	**Variable Values**
Coater blade type	Flexible rubber blade or Steel blade
Layer thickness	20 – 50 µm
Speed	
Coater in process	1-1000 mm/s
Coater manual	1-1000 mm/s
Extra coating	1-1000 mm/s
Fan	
Revolution Process	0-100%
Filter Clean blow	
Time interval for blow	0 - 300 min
Number of cleans	0 - 10
Break between	5000 ms
Pressure in Glovebox	
Overpressure	0.01 – 0.1 Bar

Cusing Process Parameters:

The variable Cusing process parameters on the Concept Laser machine software can be observed in Table 2.3.

Table 2.3: M2 Cusing process parameters that can be varied by the user [90]

Parameter	Variable Values
Exposure sequence	Vectors then Contours or Contours then Vectors
Powder Delivering Height	
Correction Factor	100 – 1000%
Start Slices	1-10 [Slices]
Factor	100 – 1000%
Additional Slices	
Number of additional slices	0 – 100 [Slices]
Scanning System	
Waiting time for beam off	0.0 - 100.0 ms
Waiting time for beam on	0.0 - 100.0 ms
Waiting time at edges	0.0 - 100.0 ms
Waiting time after laser jump max	0.0 - 100.0 ms
Waiting time after laser jump min	0.0 - 100.0 ms
Saturation after in mm	0.0 - 100.0 mm

Laser Parameters:

The variable laser parameters on the Concept Laser machine software can be observed in Table 2.4.

Table 2.4: M2 Cusing laser parameters that can be varied by the user [90]

Parameter	Units	Core	Skin	Contours	Support
Power	Watts	20-200	20-200	20-200	20-200
Scan Speed	mm/s	1-7000	1-7000	1-7000	1-7000
Focus/Spot Diameter (d)	µm	70 - 200	70 - 200	70 - 200	70 - 200
Operation Mode	-	CW/Pulse	CW/Pulse	CW/Pulse	CW/Pulse
Hatching	-	5 Hatch Patterns	6 Hatch Patterns	Contour Scan	-
Hatch Spacing (a1)	-	0 - 10	0 - 10	-	-
Beam Compensation (a2)	-	0 - 10	0 - 10	-	-
Exposure	-	Expose every n slice	Expose every n slice	Expose every n slice	Expose every n slice

One could observe that the machine has many different parameters that the user can vary. It is best that the user not change too many parameters, as it could have a detrimental effect on the part quality. Some of the main parameters are the laser parameters (Power, Scan speed, Hatch Spacing) as well as the coater parameters (Correction Factor, Speed). The fan's speed could also have an effect on warping of the parts, if the gas flow over the part is changed significantly [86]. Once the

parameters have been set the user can move and rotate parts to the desired position on the machine's virtual bed.

2.5.2.2. Machine setup

Firstly, the base plate's surface needs to be dulled to limit the reflection of the laser during the SLM process. The base plate is sandblasted and then demagnetised. Once this process is completed the base plate is ready to be inserted into the machine. The base plate needs to be screwed to the machine's build plate. The base plate will be the reference for the coater so it is very important that the base plate be placed on the build plate with no obstructions. It is also important that the base plate be skimmed as flat as possible. Any errors with the base plate will be carried through to the SLM parts.

Once the base plate has been correctly fastened to the build plate, the base plate then needs to be referenced to 0. There is no machine tool to reference the base plate to exactly 0, so this needs to be performed by the operator's eye. This process is not accurate and could lead to errors with the first layer of the part. After the plate has been correctly referenced, the coater blade can be aligned. The blade is aligned by placing it on top of the zeroed base plate and tightening it to the coater.

The powdered material then needs to be sieved into the powder bed. However, before this can take place the preparation chamber or glove box needs to be flooded with an inert gas. Once the oxygen level is less than 1% the powder can be sieved into the powder bed. The powder is sieved with a 105 µm rated sieve. Once the powder bed is filled to the required height the coater blade can then evenly distribute the powder in the powder bed and build bed.

2.5.2.3. SLM machine

Once the machine is set up, the build platform needs to be moved to the build or process chamber. The process chamber needs to be flooded with an inert gas during the Cusing process. Since titanium is volatile and reacts with nitrogen, argon gas is used to flood the chamber. Once the level of oxygen is less than 0.1 % the exposure process can begin.

The user needs to ensure that there is a thin layer of powder over the base plate before the exposure of the layers can begin. Once the user is satisfied the next step can begin. In order to sufficiently bond the first layer of the part to the base plate, the starting exposure slices need to be performed. This process utilizes the laser to expose slice 1 of the part, a user defined number of times. This process is usually done 2 to 3 times before starting the Cusing process. The laser Cusing process can then begin.

Once the process is complete, the platform can be moved to the preparation chamber and the chamber must be filled again with the inert gas, in order to remove the powder from the build bed. Once the part and the powder have been removed the post processing steps can take place.

2.5.2.4. Post-Processing operations

Post processing operations are a very important step in the SLM process. Since SLM technology makes use of a base plate, the part needs additional post processing operations to remove it from the base plate. The current solution is to remove the part with an EDM wire-cut machine. The base plate is placed on a clamping jig in the EDM machine and the wire is aligned with the base plate. Since the M2 Cusing machine exposes slice 1 of the part, a user defined amount of times, provisions in the part have been made for the removal of the part. Once the part is removed the base plate needs to be skimmed in a milling machine. It is important to note that the order in which the part is removed may differ depending on the other post processing operations. There are several other methods for post-processing SLM parts. To achieve a better surface finish, mechanical post-processing methods such as abrasive sandblasting, machining, and ultrasonic filing are utilised [19], [84]. Chemical methods include acid etching and oxidation. To relieve the residual stress in the parts, heat treatment and annealing are recommended by manufacturers [91]. Laser Surface Re-melting (LSR) is a method that is used during the building process. LSR is a technique where the laser re-melts the surface layer after the layer has been built. This re-melting is used to reduce the effects of residual porosity and improve surface finish [84].

Mechanical Post-Processing Methods

For the purpose of this study only machining, as a mechanical pre-and-post processing operation will be discussed.

Machining processes

In order for a part to be classified as a hybrid part, a machining process needs to take place before, in between, or after the SLM process takes place. Performing an SLM process in order to reduce material waste could reduce costs when using costly materials like Ti-6Al-4V. Conradie et al. [55] concludes that a material saving of 87% can be achieved when using a combination of SLM and machining technologies, over using just SM technologies. Parts produced by the SLM process have a poor surface finish and the finish cannot compare to parts produced with conventional machining. Various studies suggest using a machining operation as a post process to improve a components surface finish and accuracy [51], [55], [92], [93]. This is only required if the product design specifications require a certain accuracy or finish.

Thermal Post-Processing Methods

Heat treatment

The SLM process is generally characterised by high scan speeds and high thermal gradients, which result in high cooling rates of the scanned part. High cooling rates lead to non-equilibrium microstructures, which often require post operation heat treatment for certain applications [81]. The primary aim of the heat treatment process is to reduce internal stresses in parts produced by the SLM process [94]. Heat treatment can also be utilised to produce an optimum combination of ductility, machinability, and structural stability (annealing), or it can be used to improve the mechanical properties of the part such as fatigue strength, breaking elongation, and tensile strength [40], [95], [96]. Different forms of heat treatments result in different effects on the part. The heat treatment of SLM parts is different to that of conventionally produced parts and therefore is a science on its own. The heat treatment method needs to be optimised for the SLM build parameters that were used to produce the part [94].

Hot Isostatic Pressing (HIP)

Hot isostatic pressing is a well-recognised process that is used to reduce the porosity of either metal or non-metal parts. The process involves the application of a high pressure gas (usually inert) at an elevated temperature to a part in a specially constructed vessel. The isostatic pressure ensures the part's initial geometry is retained through the process while the simultaneous application of heat and pressure collapse and weld the part's internal pores or defects [97]. The HIP process makes the density of the model near 100% and gives a greater density than that achievable with SLM, which results in less defects that impair the part's mechanical properties [40]. Defects and pores result in reduced tensile strength, elongation, fatigue life, etc. [97]. The HIP process can be utilised to remove porosity imperfections such as hot tears, micropores, and shrinkage cavities. HIP can be utilised as a post-processing operation in order to reduce the inherent porosity and defects of SLM parts. In order to produce reliable load bearing parts, a HIP process should be added to end of the SLM process chain [98]. HIPing is usually performed on parts for the aerospace industry in order to remove any pores which could cause cracks in parts that are cyclic loaded.

2.5.3. Challenges with the SLM technology and the SLM process

Although the SLM process is an innovative manufacturing method. The technology still faces many challenges such as inferior mechanical properties of fabricated parts [52]. Some of these challenges are:

- Efficiency in terms of Time and Cost [99]
- Crack formation [49], [59], [100], [101]

- Poor repeatability and consistency of parts [53]
- Delamination of layers and delamination from build plate [49], [86], [101], [102]
- Porosity [20], [57], [59], [60], [100], [103]
- Geometric deviation [55], [104]–[106]
- High Residual Stress [44], [54], [59], [86], [107]–[109]
- Poor Surface finish [55], [110], [111]
- Dimensional Inaccuracies [53], [55], [111], [112]

The aim of this study is to develop a scan strategy that can be used to solve some of these challenges. The focus will be on SLM challenges that relate to hybrid parts. From the process chain displayed in Figure 2.7 several problems were identified that apply to this study and the manufacturing of hybrid parts on the Concept Laser M2 Cusing machine. These problems are discussed and a solution for each challenge is proposed in the sections below.

2.5.3.1. SLM software challenges

- The machine software does not allow users to make their own scan strategies and the users must use the contour scan or the 6 standard fill strategies. A solution to this problem was developed and is discussed in Section 6.1.
- When printing hybrid parts, the AM part needs to be printed on an existing part. However, the AM part only exists in the virtual wold in the form of a digital model. A challenge exists to line up the digital AM model on the machine software, with the physical part clamped to the build plate. Accurately moving parts on the machine software is challenging as there isn't a grid system on the physical machine or a system in place to move the part to the correct position. A possible solution for this challenge, is to manufacture a base plate with a grid coordinate system that matches with the machine software's coordinate system. Physical parts can then be lined up on the base plate and the coordinates on the plate can be used with the software to line up the digital part. In order to check if the part is correctly lined up on the software and the base plate before the build is started, a touch probe and arm should be installed on the machine. However as this is a costly endeavour a trail and error approach can be taken and an exposure strategy should be performed. An exposure slice should be performed with low set laser parameters. The laser power should be set to the lowest possible setting in order to not alter the surface properties of the part or melt any powder. The laser speed should also be set to a low value to see where the laser is at all times. Once these laser parameters are changed, an exposure slice can be performed. The laser will then outline where the digital part is positioned with respect to the physical part. If the laser does not outline where the operator wants the physical part to be,

then the part should be moved on the software again and the exposure process should be restarted.

2.5.3.2. Machine setup challenges

- In order to minimise the chances of the laser reflecting off the part surface, the surface needs to be dulled with sandblasting operations. The sandblasting operation turns a potentially reflective surface into a non-reflective, dull surface. However, the problem with sandblasting is there could be inclusions of the erosive particles in the hybrid part. A possible solution is to clean the sandblasted parts with acetone, ethanol, and distilled water before placing the part in the machine.
- The sieving of the powder is an important operation. All powder needs to be sieved into the powder chamber during the machine preparation, in order to remove any inclusions or unwanted particles. To effectively remove most of the inclusions, the sieve needs to be rated to just above the particle size of the powder. So, if the powder particle size distribution is 25 – 55 µm then the sieve should be a 55 µm rated sieve.
- The machines coater blade is not set up by any electronic levelling method but rather by placing the coater blade on the base plate and then tightening several screws along the length of the coater blade. This is a very inaccurate method of levelling the coater blade, as there is a large possibility of human error. The average layer thickness is supposed to be 30 µm, however it is not possible to accurately level the coater blade to that tolerance with the current machine setup.

2.5.3.3. SLM machine challenges

- The first layer of powder that is distributed onto the base plate could be any thickness and not the chosen layer thickness of 30 µm, as the levelling process is done by the eye, which introduces the chance of human error. This could lead to the first layer of powder being too thick to properly melt and adhere to the base plate. A starting strategy to ensure adequate melting should be used. It is proposed by the author to use scan strategy 5 when performing the starting process, which makes use of double hatch vectors in order to melt the powder. This theory is investigated in Section 5.2.

2.5.3.4. Post-Processing challenges

- Since hybrid parts are not separated once the SLM process is complete, there is no need for the EDM wirecut process. The hybrid parts still need to be heat treated in order to remove any residual stresses built up during the SLM process. If there is any residual porosity left in the part during the SLM process, a Hot Isostatic Pressing operation is often performed. A problem arises

as there is no HIPing facility in South Africa. This could make a component very costly if it needs to be transported to another country for the process. Therefore, there should be a focus on porosity optimisation with the scan strategy and process parameters for components that require near 100% density.

2.6. Materials Processed by Selective Laser Melting

Currently commercial SLM machine manufacturers offer between 10 to 15 different materials that can be utilised in the SLM process. These materials include pure Ti and Ti-6Al-4V, CoCr, AlSi10Mg, AlSi12, stainless steel, tool steel, bronze alloys and nickel alloys [113]. The materials that are available from Concept Laser GmbH can be observed in Table 2.5. Apart from these materials, numerous research groups are looking into other materials such as North West University (NWU) looking at Platinum and the STC at the University of Stellenbosch looking at Tungsten Carbide [75], [114]. Since the focus of this study is only on Titanium hybrid parts, the other materials will not be covered in depth.

Table 2.5: M2 Laser Cusing material types adapted from [91]

Material Type	Designation
Stainless Steel	CL 20ES (1.4404)
Hot-Work Steel	CL 50WS (1.2709)
	CL 60DG (1.2709)
	CL 90RW (comparable 1.2083)
Aluminium	CL 30AL (Al Si12)
	CL 31AL (Al Si10 Mg)
Titanium	CL 40TI (Ti-6Al-4V)
Nickel-based alloy	CL 100NB (Inconel 718)

2.6.1. Titanium Alloys

Titanium was first discovered in 1791 by a British mineralogist, William Gregor. However, it was only much later, in 1932 that Wilhelm Justin Kroll from Luxembourg developed a method to extract Titanium by using magnesium as a reducing agent [115]. Today, workable mineral deposits can be found in several countries across the globe, including South Africa, and the Kroll process is still used today to extract the titanium. Titanium is generally alloyed to achieve the best material properties. Titanium alloys generally have high specific strength and excellent corrosion resistance. These properties, along with others, make titanium alloys the material of choice in the aerospace, chemical, medical, and leisure industries [115].

2.6.1.1. Material properties of Ti-6Al-4V

The material chosen for this study is an extra low interstitial (ELI) grade of Ti-6Al-4V alloy. The powder is supplied by Concept Laser GmbH and it is produced by using a plasma atomisation process. The powder particles are spherical in shape and have a particle size distribution of 5-50 µm [83]. The Ti-6Al-4V powder which has been designated the name CL 41TI ELI, is the only titanium powder available from Concept Laser GmbH at the moment. Currently more than 100 titanium alloys are known but only a fraction of them have reached commercial status. Ti-6Al-4V was first discovered in 1954 and now covers more than 50 % of commercial usage [115]. Ti-6Al-4V is also biocompatible, which makes it a great candidate for the production of medical implants using SLM.

The Microstructure of Ti-6Al-4V

It is very important to study the microstructure of parts that have been produced using SLM. One can determine some of the mechanical properties and material behaviour from the microstructure. Various microstructures have a strong effect on the mechanical properties of titanium alloys. The influence of various microstructural features on the different mechanical properties are displayed in Table 2.6. The table shows whether certain microstructural features have a positive or negative effect on properties such as strength, ductility, fracture toughness, crack initiation, and crack propagation.

Table 2.6: Influence of the various microstructural features on different mechanical properties of Ti-6Al-4V [48]

Microstructure Feature	Strength (UTS)	Ductility (єfrac)	Fracture Toughness (KIC)	Crack Initiation (HCF)	Crack Propagation (HCF+LCF)
Fine	+	+	-	+	-
Course	-	-	+	-	+
Lamellar	-	-	+	-	+
Equiaxed	+	+	-	+	-
Widmanstatten α	-	-	+	-	+
Colony α	-	-	+	-	+
Secondary α	+	+	-	+	-
GBα		-	+	-	+

Depending on the application of the part, the design requirements could vary a lot and certain mechanical properties could be vitally important and others not. The product design specification (PDS) is an important aspect of any design and should be used to determine what strategies, parameters, and post processing should be utilised to achieve the required mechanical properties.

It is important for researchers to know what the microstructures look like in order to evaluate the microstructures and determine the properties that could be expected from the part. An example of the three main microstructures for Ti-6Al-4V can be observed in Figure 2.8 below:

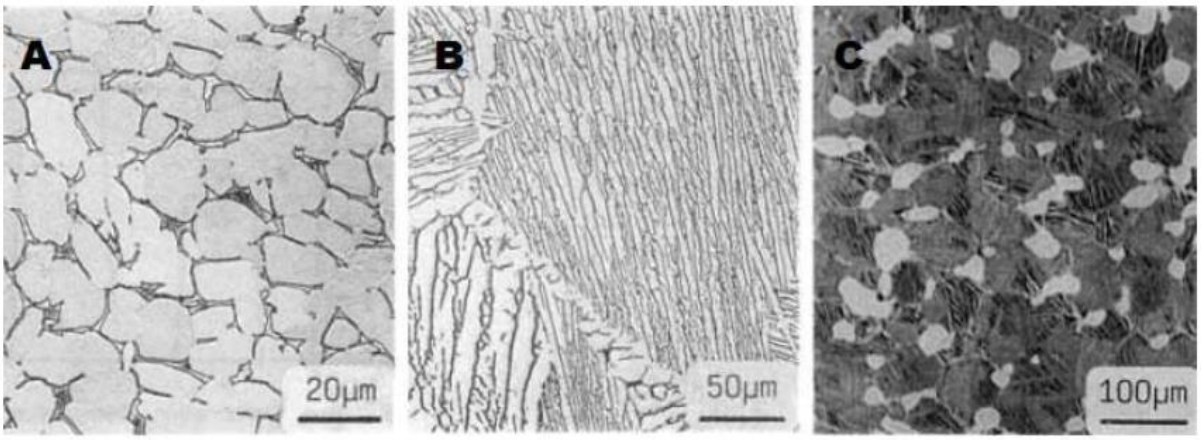

Figure 2.8: Example of (a) Equiaxed (b) lamellar and (c) bimodal Ti-6Al-4V microstructures [116]

Researchers [83], [117] agree that during the SLM processing of Ti-6Al-4V a columnar microstructure forms. The elongated grains are orientated in the direction of the build or building direction (BD). The orientation of the elongated grains is dependent on the scan strategy and the rotation of the layers [83], [118]. So, one could note that the scan strategy can play a major role in the residual stress, and mechanical properties of a part.

Properties of Titanium alloy: Ti-6Al-4V

Titanium is known for its great mechanical properties and resistance to corrosion. The physical and mechanical properties of the α+β titanium alloy, Ti-6Al-4V are displayed in Table 2.7 below:

Table 2.7: Physical and Mechanical Propeties of Titanium Alloy: Ti-6Al-4V [115], [119]–[122]

Property	Metric Value	Range
Density	4.43 g/cc	-
Hardness, Vickers	349 HV	300-400 HV
Young's Modulus (E) Stiffness	113.8 GPa	110-140 GPa
Yield Strength (YS)	880 MPa	800-1100 MPa
Ultimate Tensile Strength (TS)	950 MPa	900-1200 MPa
% Elongation (%El)	14%	13-16 %
Fracture Toughness (K_{IC})	75 MPa m½	33-110 MPa m½
Poisson's Ratio	0.342	-
Shear Strength	550 MPa	-

The thermal properties of Ti-6Al-4V are the most important material properties for this study due to the fact that SLM is a thermal process. The thermal properties of Ti-6Al-4V can be observed in Table 2.8.

Table 2.8: Thermal properties of Titanium Alloy: Ti-6Al-4V [119]–[122]

Thermal Properties	Metric Value
Annealing Temperature	700-785 °C
Coefficient of Thermal Expansion, Linear 20°C	8.6 µm/m °C
Coefficient of Thermal Expansion, Linear 250°C	9.2 µm/m °C
Coefficient of Thermal Expansion, Linear 500°C	9.7 µm/m °C
Specific Heat Capacity	0.5263 J/g °C
Thermal Conductivity	6.7 W/m K
Melting Point	1604-1660 °C
Solidus	1604 °C
Liquidus	1660 °C
Transus Temperature T_β	980 °C

Properties of Ti-6Al-4V ELI Powder

The powder that was used was supplied by Concept Laser GmbH. The powder particles are spherical in shape and have a particle size distribution of 25 – 55 µm. The material properties of the powder can be observed in Table 2.9.

Table 2.9: Material properties of Ti-6Al-4V ELI powder [91]

Material Property	Range/Value
Yield Strength (YS)	900 - 1200 MPa
Tensile Strength (TS)	1100 – 1300 MPa
%Elongation (%El)	5 – 10%
Young's Modulus (E) Stiffness	110 GPa
Thermal Conductivity (λ)	7 W/m K
Coefficient of Thermal Expansion	9 µ/K

One could observe that the properties for wrought Ti-6Al-4V are very similar, if not the same as, the material properties of the powder. However, one must note that the mechanical properties of a wrought Ti-6Al-4V part are different from a part produced with SLM. The production process is crucial and has a significant effect on the microstructure of the part.

Chapter 3

Factors Influencing Integrity

3.1. Residual Stress and Warping Mechanisms

As early as 1993, residual stresses in additive manufacturing was identified as a major problem faced by the technologies [123]. Residual stress is defined in the following sections as well as some of the mechanisms that cause warping/deviation during the SLM process.

3.1.1. Residual Stress

There are different ways to classify residual stresses. A commonly used method is to define the residual stresses based on the length scale over which they come to equilibrium by themselves. ***Type I*** residual stresses act on the whole body. Type I stresses are macroscopic and can cause deformation of the part if the boundary conditions are altered. ***Type II*** residual stresses originate from local, intergranular phenomena and are averaged out over the grain scale. ***Type III*** residual stresses vary over the atomic scale and are caused by intergranular defects in the crystal structure [48], [124].

Residual stress has many origins, which all result in inhomogeneous plastic deformations. Thermal residual stresses are induced through temperature gradients and can even be induced during equilibrium cooling because of local differences in thermal expansion. This form of induction is common with SLM and welding processes as the melt pool does not cool equally. This can cause contraction of the cold zone in the material, which results in the hot zone yielding [48]. This process can cause the part to warp and deform if it is free to move as illustrated in Section 3.1.3.2 below.

3.1.1.1. Effects of residual stress on mechanical behaviour

Residual stress can have negative effects on the mechanical behaviour of a part during production. The effects of residual stress on mechanical behaviour can be summarised into these three phenomena [48]:

- Unwanted deformation of a component. During the SLM process, thermal gradients can induce residual stress in the part.
- Unexpected failure of a part due to superposition of residual stresses onto applied stresses.
- Stress-corrosion cracking can occur if Type I or Type II tensile stresses are present at the exposed surfaces [125].

3.1.2. Residual Stress in SLM

One of the detrimental consequences of residual stress in SLM parts is deformation of the parts. Bending moment created by the distribution of the stresses can cause the part to curl or warp upwards. This phenomenon occurs regardless of the part shape and is dependent on the size and orientation of the part [48]. The tendency of parts to warp is often exploited as a method to study the residual stress in a part [126]. Thermal residual stresses originate from temperature gradients, which are discussed in detail in the following sections.

3.1.3. Warping/Deformation Mechanisms and Thermal Gradients

When the laser beam comes into contact with the surface of the powder bed, most of the energy concentration is absorbed by the powder particles, which leads to localised melting. Once the Gaussian laser heat source moves over the melt region, the molten metal powders rapidly consolidate to form a solid scan track. The main heat transfer mechanisms that occur during the SLM process are; heat radiation from the laser beam to the powder bed, heat conduction between the powder particles and the previous layers, and heat convection between the inert ambient atmosphere and consolidated layer. These three heat transfer mechanisms make the thermal behaviour during the SLM process complex [127]. A physical model of the thermal behaviour during the SLM process can be observed in Figure 3.1.

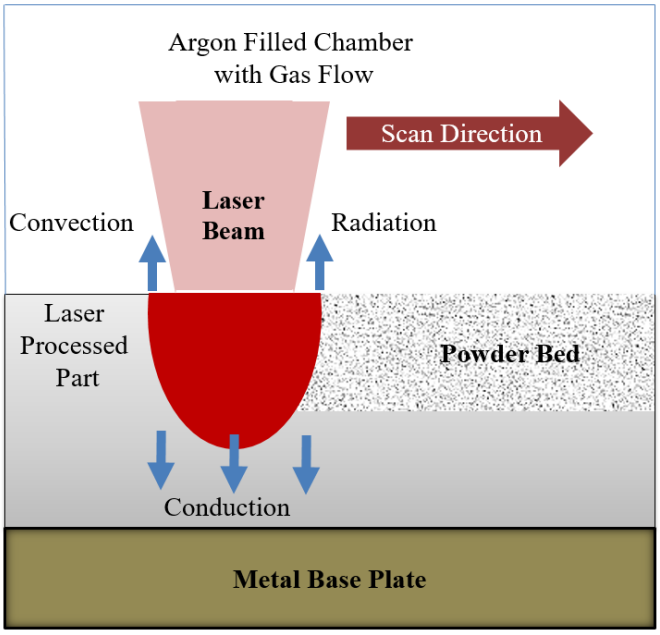

Figure 3.1: Schematic of the SLM physical model adapted from [127]

One of the mechanisms that contribute to the warping of parts is the heat transfer mechanisms that occur during the SLM process. Research shows that there are many different methods employed to calculate the heat transfer mechanisms [61], [105], [127]–[133]. Many researchers use different symbols to denote certain variables so each symbol has been defined below each equation.

Firstly, the SLM system needs to be defined, as well as all the modes of energy transfer in the system. Using the first law of thermodynamics, the general energy balance equation in the closed SLM system can be written as

$$\boldsymbol{Q_L = Q_{CD} + Q_{CV} + Q_R} \tag{3.1}$$

where Q_L is the input laser energy, Q_{CD} is the conduction losses, Q_{CV} is the convection losses, and Q_R is the radiation losses [127], [132].

Heat conduction losses can be described by Fourier's law, which satisfies the second principle of thermodynamics. This equation is [134]

$$\boldsymbol{q_x = -kA\frac{\partial T}{\partial x}} \tag{3.2}$$

where q_x is the heat transfer rate, $\frac{\partial T}{\partial x}$ is the temperature gradient in the direction of heat flow, k is thermal conductivity, and A is the area of the surface. The general three-dimensional heat conduction equation is [134]

$$\boldsymbol{\rho C\frac{\partial T}{\partial t} = k\left(\frac{\partial^2 T}{\partial x^2} + \frac{\partial^2 T}{\partial y^2} + \frac{\partial^2 T}{\partial z^2}\right) + \dot{q}} \tag{3.3}$$

where q̇ is the energy generated per unit volume, C is the specific heat, ρ is density, and T is the temperature. Losses due to convection can be described by Newton's law of cooling [134]

$$\boldsymbol{q = hA(T_\omega - T_\infty)} \tag{3.4}$$

where q is the heat transfer rate, h is the convection heat transfer coefficient, T_ω is the temperature of the surface, and T_∞ is the temperature of the fluid.

Radiation heat transfer can be derived by using the Stefan-Boltzmann law of thermal radiation, which is described by the following equation [134]

$$\boldsymbol{q_{emitted} = \sigma AT^4} \tag{3.5}$$

where σ is the proportionality constant called the Stefan-Boltzmann constant and has the value $5.669 \times 10^{-8}\ W/m^2 \cdot K^4$.

3.1.3.1. Thermodynamic model timeline

The following is a timeline of the AM research that has been conducted using thermodynamic models. Each set of authors use different methods and equations to model the heat exchange mechanisms that occur during the SLM process.

2002: Matsumoto et al. [105] uses the governing equation of two-dimensional heat conduction within the material. The equation is expressed with density ρ, specific heat C, and thermal conductivity λ, as

$$\boldsymbol{\rho C \frac{\partial T}{\partial t} = \lambda \left(\frac{\partial^2 T}{\partial x^2} + \frac{\partial^2 T}{\partial y^2} \right) + q_g + q_c} \quad \textbf{(3.6)}$$

where T is the temperature, t is the time, x and y are the coordinates, q_g is the internal heat generation and q_c is the heat loss from the surface to the atmosphere.

2004 - 2005: Dai and Shaw [133], [135] developed a simulation model, which encompassed the following major material and process parameters:

- The incoming laser beam power with a Gaussian distribution.
- Optical pyrometer simulation as well as closed loop temperature control.
- Powder to solid transition.
- Temperature dependent thermal convection.
- Temperature and porosity dependent thermal conduction and radiation.

Dai and Shaw then studied the effects of volume shrinkage due to the transformation from a compact powder to a dense liquid [133]. A three-dimensional finite element model was produced and their governing equations for conduction, convection, and radiation were

$$\boldsymbol{\rho \frac{\partial (CT)}{\partial t} = \frac{\partial}{\partial x}\left(k \frac{\partial T}{\partial x} \right) + \frac{\partial}{\partial y}\left(k \frac{\partial T}{\partial y} \right) + \frac{\partial}{\partial z}\left(k \frac{\partial T}{\partial z} \right)} \quad \textbf{(3.7)}$$

and

$$\boldsymbol{K \frac{\partial T}{\partial n} + h(T - T_0) + \sigma \varepsilon \left(T^4 - T_0^4 \right) = q} \quad \textbf{(3.8)}$$

where T_0 is the ambient temperature, n is the normal vector of the surface, h is the heat transfer coefficient, ε is the emissivity, and σ is the Stefan-Boltzmann constant.

2006: Ma and Bin [128] use a similar equation to Matsumoto [105], however, Ma and Bin have included the third dimension, z, and do not have the heat loss to the atmosphere due to convection. However, they have included the convection heat transfer in their model. The equation is

$$\boldsymbol{\rho C \frac{\partial T}{\partial t} = \lambda \left(\frac{\partial^2 T}{\partial x^2} + \frac{\partial^2 T}{\partial y^2} + \frac{\partial^2 T}{\partial z^2} \right) + \Phi} \quad \textbf{(3.9)}$$

where T is the temperature, t is the time, x, y and z are the coordinates, Φ is the internal heat generation, which represents laser heating. Ma and Bin [128] states that the thermal exchange of the newly solidified part with the surroundings is mainly due to convection heat transfer, which is described by the following equation

$$-k\frac{\partial T}{\partial n} = h(T^{inf} - T) \tag{3.10}$$

where h is the thermal exchange coefficient between the part and the environment, T^{inf} is the temperature of the environment, and T is the temperature.

2007: Gusarov et al. [136] use the following heat conduction equation to define their model

$$\frac{\partial H}{\partial t} - v\frac{\partial H}{\partial x} = \frac{\partial}{\partial x}\left(k\frac{\partial T}{\partial x}\right) + \frac{\partial}{\partial y}\left(k\frac{\partial T}{\partial y}\right) + \frac{\partial}{\partial z}\left(k\frac{\partial T}{\partial z}\right) + U \tag{3.11}$$

where H is the volumetric enthalpy, v is the scanning velocity of the laser, k is the thermal conductivity, and U is the heat source due to volumetric absorption of the laser radiation. Gusarov et al. focused on the laser radiation in the powder and the conduction heat losses. Convection was not considered for their model.

2010: Zhang et al. [129] utilised the following equations to model the heat transfer mechanisms during the SLM process

$$\rho C\frac{\partial T}{\partial t} = \lambda\left(\frac{\partial^2 T}{\partial x^2} + \frac{\partial^2 T}{\partial y^2} + \frac{\partial^2 T}{\partial z^2}\right) + q_e + q_c \tag{3.12}$$

and

$$\lambda_e\frac{\partial T}{\partial n} + h(T - T_0) + \sigma\varepsilon\left(T^4 - T_0^4\right) - q = 0 \tag{3.13}$$

where q_c is the heat dissipation from the material to the fluid, q_e is the energy density of the fibre laser, T_0 is the ambient temperature, n is the normal vector of the surface, h is the heat transfer coefficient, ε is the emissivity, σ is the Stefan-Boltzmann constant. This approach was very similar to Dai and Shaw [133] but the energy density of the fibre laser has been added and the formula can be observed below.

$$q_e = \frac{2AP}{\pi\omega^2}\, exp\left(-\frac{2r^2}{\omega^2}\right) \tag{3.14}$$

where ω is the equivalent radius of the laser beam, A is the powder bed absorptivity to the laser beam, P is the laser power, and r^2 is the distance from the powder bed to the centre of the laser beam area and is derived with the following equation

$$r^2 = (x - x_0)^2 + (z - z_0 - vt)^2 \tag{3.15}$$

where v is the velocity of the laser and t is time.

2012: Zeng, Pal, and Stucker [61] use the same equation as Ma and Bin [128]. to describe the governing heat conduction in the moving medium however, two boundary conditions are used. The one boundary condition is for surface convection and radiation and the equation is as follows:

$$-\lambda\frac{\partial T}{\partial z} = \varepsilon_\theta \sigma(T^4 - T_e^4) + h(T - T_e) \quad (3.16)$$

where T is temperature, λ is the conductivity coefficient, T_e is the environment temperature, ε_θ is the thermal radiation coefficient, h is the convection heat transfer coefficient, and σ is the Stefan-Boltzmann constant. This equation is similar to the one employed by Dai and Shaw [133]in their model.

2015: Yuan and Gu [127] investigate the influence of the Marangoni effect on the melt pool. The Marangoni effect is caused by the temperature gradient, heat and mass transfer as well as the melt pool configuration. The equations used to define the model are the same as those used by Zeng, Pal, and Stucker [61]. It was concluded that heat and mass transfer are mainly dominated by Marangoni convection.

3.1.3.2. Isolated single layer system

From all the sources [61], [105], [127]–[133] in the section above, three heat transfer mechanisms were identified. These heat transfer mechanisms are laser radiation, convection, and conduction. The largest heat loss mechanism is through convection with the ambient atmosphere of the SLM system [127], [128].

The author proposed that the heat loss mechanisms in the SLM process be isolated to a single layer. If this is performed, then there will be no melting of a layer onto a substrate or previous layer. Instead the layer will be free to move and warp during the cooling process. Since most of the heat loss in the system is due to convection at the top surface of the layer. The top surface of the exposed layer experiences a faster cooling rate through convection than the bottom of the layer, which experiences a slower cooling rate through conduction. This results in the top surface contracting at a faster rate than the bottom surface as displayed in Figure 3.2 below. This thermal mechanism introduces a Type II residual stress into the part. The grains at the top surface of the part experience a cold zone while the lower grains experience hot zones. The contraction of the cold zone at the top surface causes the hot zone to yield, which in turn, results in the part warping upwards in the positive z direction.

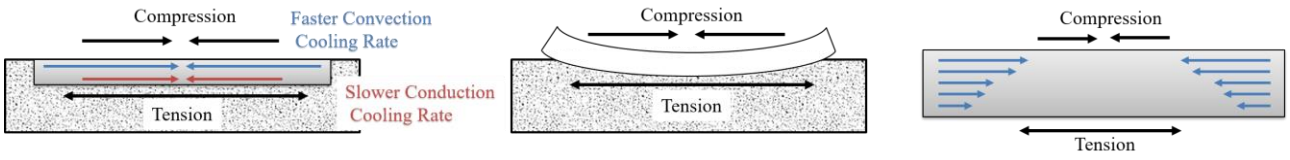

Figure 3.2: (Left) Warping mechanism caused by convection and conduction differences in heat loss (Centre) Warping of a layer due to convection heat loss at the top surface (Right) Visual representation of the contraction rates due to higher cooling rates at top surface of the part

Dadbakhsh et al. [86] found that the temperature distribution and cooling rates caused by the flow of gas in the chamber significantly influences the deformation and mechanical properties in the final parts. Therefore, one could state that the cooling rate due to convection plays a significant role in the part warping/deformation. Although the differences in cooling rates does influence the warping of the part, this is not the only warping mechanism. The induction of residual stress due to the expansion and contraction of the layers is discussed in the next section.

3.1.3.3. Multi-layer system with a base plate

With SLM, residual thermal stresses may be induced in a part with a base plate by the following two mechanisms:

1. The stresses are induced in the solid substrate under the present layer that is being melted, and
2. The stresses are induced due to the rapid cool down phase of the melted top layers.

Phenomenon 1 is referred to as the Temperature Gradient Mechanism (TGM), and it is the result of large thermal gradients in the solid substrate just underneath the laser spot as displayed in Figure 3.3. The expansion of the upper layer due to the high temperature gradient is restricted by the underlying colder solidified layers. This induces a compressive stress in the upper layers of the substrate, which may rise above the yield strength of the material and cause plastic deformation in those layers. When the top layers cool down their compressive state is converted into residual tensile stresses thus warping the part. With regards to the second phenomenon, the melted top layers shrink due to the thermal contraction of the material and this movement is prohibited by the lower layers, thus resulting in a tensile stress in the most upper layer, and compressive stresses below [49].

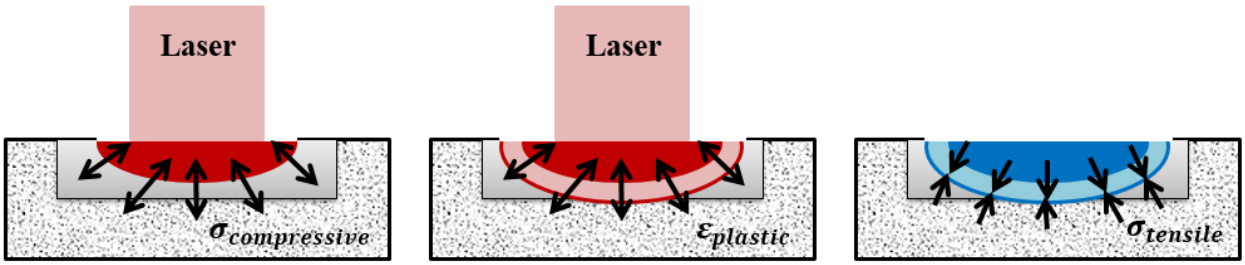

Figure 3.3: Temperature Gradient Mechanism in SLM adapted from [49]

In order to understand the residual stress profiles in SLM parts, Mercelis and Kruth [54] developed a simplified theoretical model. The assumptions that are made for this model are as follows:

- The part is being built on a base plate and both the part and base plate are at room temperature.

- The upper layer induces stress due to the shrinkage (αΔT), the tensile stress is equal to the material's yield strength σ.
- The stress σ_{xx} is independent of the y coordinate. (The variation of the normal stress along the y axis of the part is ignored).
- The general beam theory is valid.
- No external forces are applied to the base plate and part combination.

The strain profile that is assumed over the base plate and part combination is described by the following equation [54]:

$$\boldsymbol{\epsilon_{xx} = az + b} \tag{3.17}$$

where the coefficients a and b are given by the following equations:

$$\boldsymbol{a = -6\bar{\sigma}t\frac{(2mh_bh_p+mh_bh_pt+h_p^2+h_pt+mh_b^2)}{(4mh_b^3h_p+h_p^4+m^2h_b^4+6mh_b^2h_s^2+4mh_bh_p^3)}} \tag{3.18}$$

and

$$\boldsymbol{b = \bar{\sigma}t\frac{(2mh_b^3+6mh_ph_b^2+3mh_b^2t+6h_bh_p^2+6h_bh_pt+2h_p^3+3h_p^2t)}{(4mh_b^3h_p+h_p^4+m^2h_b^4+6mh_b^2h_s^2+4mh_bh_p^3)}} \tag{3.19}$$

where

$$\boldsymbol{m = \frac{E_{base}\omega_{base}}{E_{part}\omega_{part}}} \tag{3.20}$$

The other variables can be observed in Figure 3.4 below.

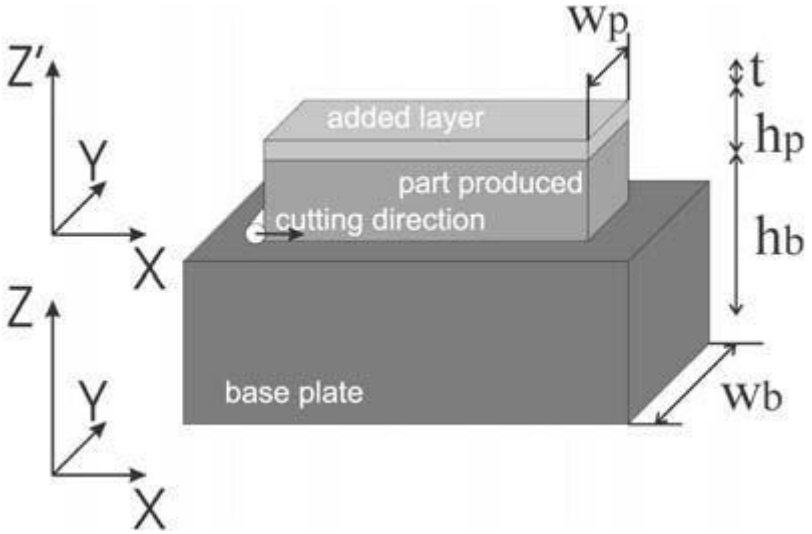

Figure 3.4: Simplified theoretical model of the SLM process [54]

The model attempted to quantify the phenomenon displayed in Figure 3.5.

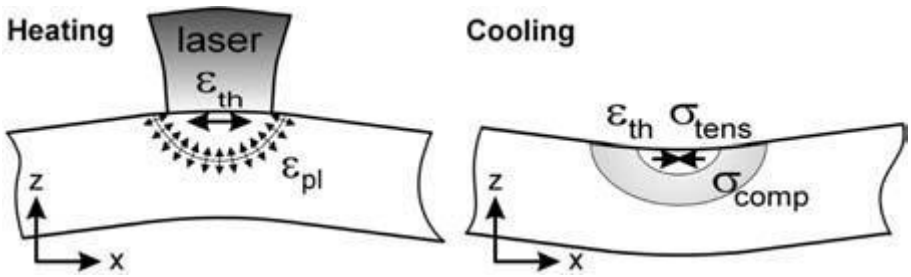

Figure 3.5: Temperature Gradient Mechanism inducing residual stress [54]

Mercelis and Kruth [54] derived several conclusions from their model such as:

- The stress profiles before the part is removed from the base plate, consist of a large zone of tensile stress at the top layers of the part. The lower part of the base plate is under tensile stress and the upper part of the base plate is under compressive stress as shown on the right in Figure 3.5.
- The more layers there are in the part, the larger the final residual stress will be. Also, shrinkage along the x axis reduces as the number of layers increases. Therefore, the residual stress is directly proportional to the height of the part.
- The thicker the base plate the smaller the resulting residual stress will be. With a thick base plate, the bending deformation becomes smaller. A thin base plate results in a high bending deformation and high residual stress.

3.2. SLM Strategies

There are many different SLM strategies that are currently being applied to improve the SLM process. Each strategy has a different effect on the mechanical properties of the final component. These mechanical properties include density, porosity, surface finish, residual stress and even geometry of the component. Some of the strategies that are being studied or have been developed are the:

- Skin-core build strategy [12], [137],[138]
- Dual laser scanning strategy [12], [37]
- Laser surface remelting strategy [84], [139]
- Vector and Layer scan strategies [43], [52], [140], [141]
- Feedback control [142]
- Base-plate heating [40], [54]

In this study a strategy will be defined as any scan pattern, exposure method, monitoring method, or heating method that is strategically used to influence a factor during the SLM process.

3.2.1. Skin-Core Build Strategy (Shell and Core Strategy)

In order to increase the productivity of the SLM process a multi laser scanning method has been developed called the skin-core method. The skin-core method makes use of two Nd:YAG lasers, both having different beam diameters. The one laser, which focuses on the outer edges (skin) of the part has a small beam diameter (d_s = 70-200 μm). The other laser, which focuses on the inner core (core) of the part has a large beam diameter (d_s = 400-1000 μm). These two lasers work in unison to produce parts in a fraction of the time without sacrificing part accuracy [12], [137]. The skin-core setup can be observed in Figure 3.6.

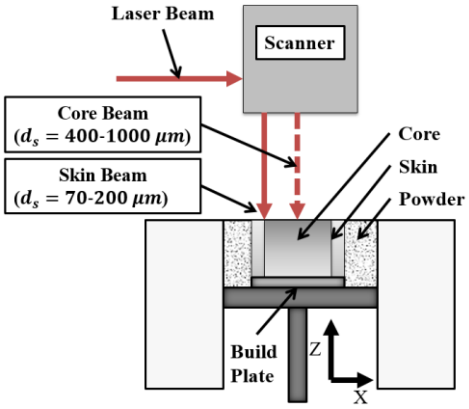

Figure 3.6: Schematic representation of the Skin-Core strategy adapted from [138]

The skin-core strategy was developed by a company called SLM Solutions and has been implemented in one of their latest machines the SLM500HL, which can be equipped with up to 4 laser beam sources to speed up build times [12]. Machines with these capabilities have a greater advantage over conventional manufacturing processes as the production lead times for small flexible batches are far less.

The skin-core strategy affects the following properties of the SLM process:

- The build lead time
- The part accuracy
- The surface roughness

3.2.2. Dual Laser Scanning

Deflection, cracking, and a rough surface finish are some of the problems often experienced with AM processes. Deflection and cracking are caused by the thermal stresses and inappropriate metallic structure from the rapid heating and quenching during the building process. In order to reduce these problems a dual laser scanning system has been proposed [12], [37]. A dual laser scanning system utilises two lasers within the SLM machine. One laser is used for the melting and bonding of the powder, and the other is used for either reheating or preheating the powder. A

possible setup utilises an Nd:YAG laser to melt the powder and a CO2 laser to heat the powder. The different setups can be observed in Figure 3.7.

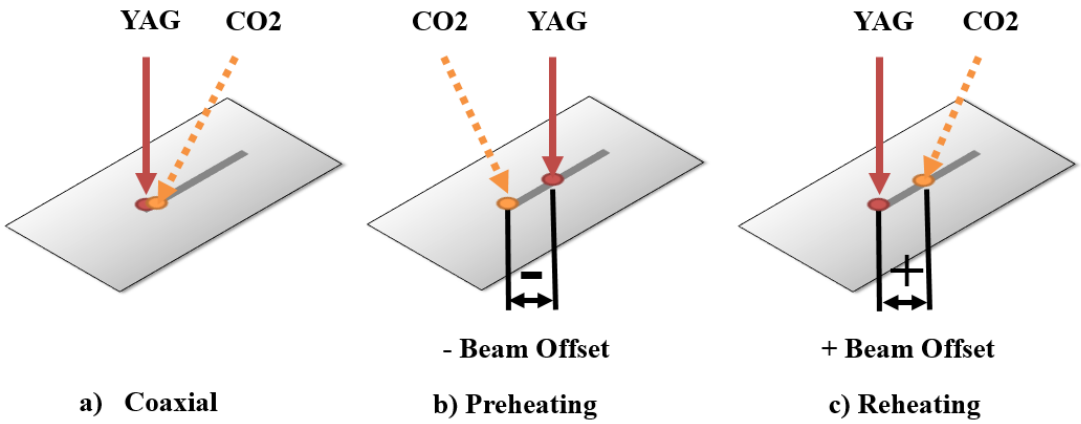

Figure 3.7: Possible laser beam configurations adapted from [37]

Another possible setup is utilising two Nd:YAG lasers [137] and reducing the power on the heating laser so that melting does not take place. A proven strategy with the reheating procedure is setting the CO2 laser at a 2 mm offset from the melting beam [37]. When the part is reheated by the heating laser beam with a 2 mm offset the maximum bending strength is at its largest. The Vickers hardness is at a minimum at this offset due to the increase in ductility, this in turn causes a larger fracture strain [37].

The dual laser scanning strategy affects the following properties of the part:

- The hardness
- The bending strength
- The ductility of the part

3.2.3. Laser Surface Remelting

Once a layer of powder has been scanned by the laser and the powder has been melted, the same slice can be rescanned by the laser before applying the next layer of powder. This strategy is called Laser Surface Remelting (LSR) [84], [139]. The surface remelting strategy has many different advantages but it is primarily used to decrease the porosity and improve the surface quality of the part. Due to the fact that the strategy involves scanning each layer twice or more, the downfall is that the production time of the part is increased. The LSR strategy can make use of different vector and layer scan strategies to achieve the best possible results. With regards to titanium alloys there are two methods used to improve the surface quality without inducing deformations in the part. Method one is to remelt the molten layers of the part three times before applying the next layer of powder. Method two utilises a large spot size to remelt the molten layer. Other methods include using the alternating scan strategy (zig-zag scan strategy) or the orthogonal scan strategy when

remelting the surfaces [139]. A combination of different scan strategies needs to be tested in order to achieve the best possible mechanical properties for a part printed out of Ti-6Al-4V.
The laser surface remelting strategy affects the following properties of the part:

- The microhardness [143][144]
- The friction and wear behaviour [143], [145], [146]
- The corrosion resistance [147], [148]
- The bio-integration of the part [149]
- The wettability [150]
- The surface quality [151]
- Prevention of surface cracks [151], [152]

Using very low power values and positioning the scan lines far away from each other result in a poor surface quality when performing LSR. However, if the opposite is performed, the melt pool will push towards the substrate and a smooth surface will result [84].

3.2.4. Vector and Layer Scan Strategies

There are many different vector and layer scan strategies, each is used for different features and each has their own advantages and disadvantages. This section lists and describes some of the developed vector and layer scan strategies that can be used in SLM processes. Scan strategies affect the material properties of the final part. The orientation of the material's grains is highly dependent on the scan strategy that is used. The scanning strategy can be used to control the grain orientation as well as the microstructural texture [83]. Due to the fact that there is no standard terminology for strategies, some strategies may be known by different terms. Most authors also tend to explain or label the strategy by using their own analogies. The different scan strategies along with the different terms and diagrams are listed in the following sections.

3.2.4.1. Vector strategies

Unidirectional Scan Strategy (Single Direction Scan Strategy)
The unidirectional scan strategy is a simple strategy where the scan vectors all face the same direction [48], [140]. The laser scans one vector from the starting point (tail) to the finish point (head) and then jumps back to the starting point of the next vector. High residual stresses result when using this scan strategy due to the high thermal stresses induced by the laser when melting the powder in a single direction. The unidirectional strategy is not commonly used, as the density of the part tends to be lower than the density of a part produced with another strategy [83]. The strategy can be observed in Figure 3.8.

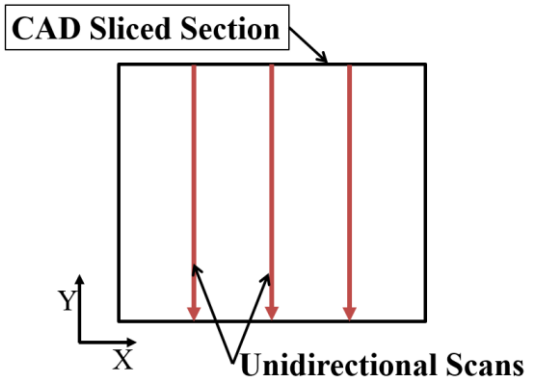

Figure 3.8: Unidirectional scan strategy adapted from [140]

Alternating Scan Vector (Zig-Zag/Raster Scan Strategy)

The alternating scan strategy alternates the vector direction after each scan [140]. The laser scans the one vector from the start point to the end point and then starts with the next vector. The starting point of the next vector is in close proximity to the end point of the previously scanned vector. The alternating scan strategy is displayed in Figure 3.9 below. Note the different directions of the scan vectors.

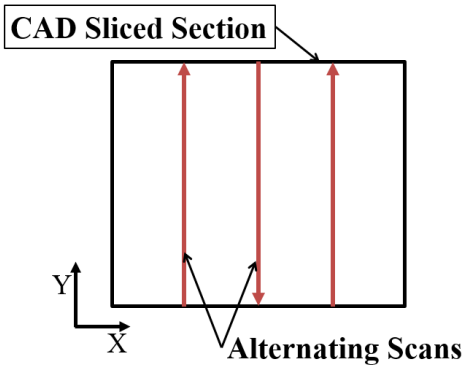

Figure 3.9: Alternating scan strategy adapted from [140]

The alternating scan strategy affects the following properties of the part:

- Residual stress is altered slightly along the scan direction

The Progressive Scan Strategy (Multi-Track Scan Strategy)

The progressive scan strategy is similar to the alternating scan strategy except the scan vectors are continuous and the laser scanner flows from one vector to the next without any delays or jumps [107], [127]. This scan strategy can be used for all types of model shapes. The strategy is displayed in Figure 3.10.

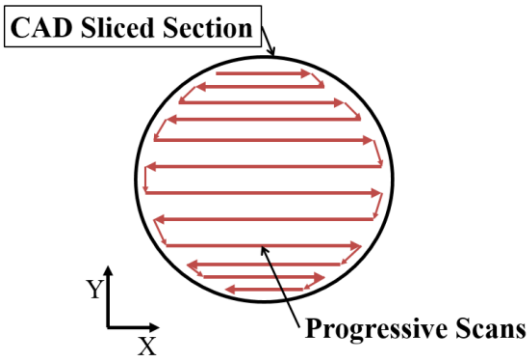

Figure 3.10: Progressive scan strategy adapted from [107]

The Progressive scanning strategy affects the following properties of the part:

- Residual stress is altered slightly

Contour Scan

The contour scan is a scan that is performed around the contour of the desired CAD sliced section [140]. The contour scan is used to create a distinct melt pool around the boarder of the CAD slice. The strategy can be observed below in Figure 3.11.

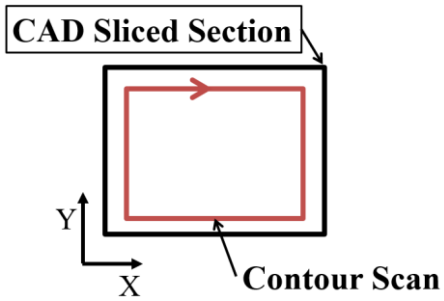

Figure 3.11: Contour scan strategy adapted from [140]

The contour scan strategy affects the following properties of the part:

- Surface finish is altered [140]
- Increases edge (edge-effect) height [141]

Helix Scan Strategy

The helix scan strategy was developed in order to reduce the deformation in the melted layer caused by steep thermal gradients [107]. The helix scan strategy is most suited for the production of complex parts. However, the strategy is not suited for the production of cylindrical parts or ring parts. This is due to the fact that the scan path would be constant along the entire cylindrical model and this would cause a weak bond between the build layers. The helix strategy requires the use of a Voronoi diagram of each build layer, a toolpath algorithm is then used to generate recursive helix scan paths for each layer [153], [154]. Due to the fact that the scan paths are different for each layer the bonding strength is increased. Figure 3.12 is an illustration of the helix scan strategy. There are many different ways in which one could expose the helix scan strategy. The vectors could change

direction after each exposure or one could expose the vectors from the outside to the inside and vice versa [43].

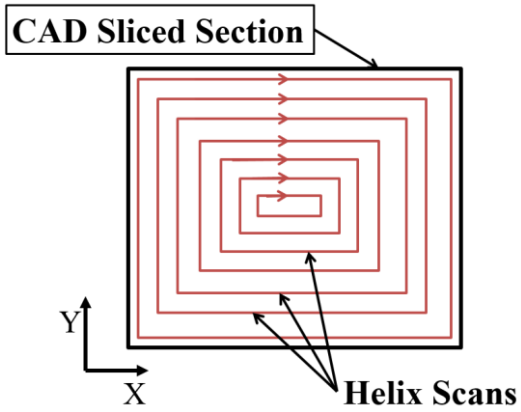

Figure 3.12: Helix scan strategy adapted from [107]

The helix scanning strategy affects the following properties of the part:

- Residual stresses and deformation in the part are altered
- Surface finish of the part is rough

Spiral Scan Strategy

The spiral scan strategy is similar to the helix scan strategy but the scan is continuous and does not jump from one vector to another. The scan vectors are arranged in a spiral manner around the sliced layer. The residual stress in the part is reduced when the spiral scan strategy is employed. The spiral vector orientation is illustrated in Figure 3.13 below.

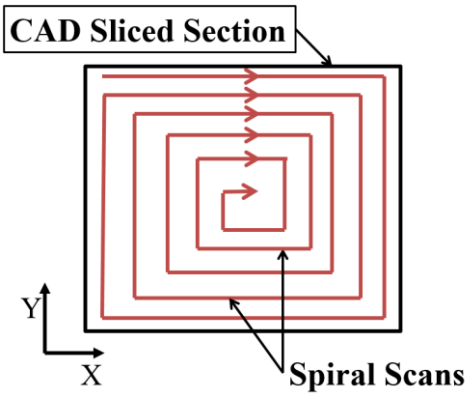

Figure 3.13: Spiral scan strategy adapted from [139]

The Spiral scanning strategy affects the following properties of the part:

- Residual stresses and deformation in the part are altered

Island Scanning Strategy

The “island” scanning strategy is a patented strategy that was developed by Concept Laser GmbH. In order to decrease the residual stresses in the part, caused by steep thermal gradients, the island strategy reduces the area to be scanned into smaller sections (roughly 5mm x 5mm). The islands are also scanned in a random order with shorter scan tracks, which means localised heating of large

sections does not take place [43], [141]. Other commercial machine manufacturers use a similar strategy called ‘striping’ where the part is subdivided into long stripes instead of square islands. The island strategy can be observed in Figure 3.14. Note that for the default strategy, each island is made up of alternating scan vectors; this further reduces the localised thermal stresses and also provides a smooth surface finish.

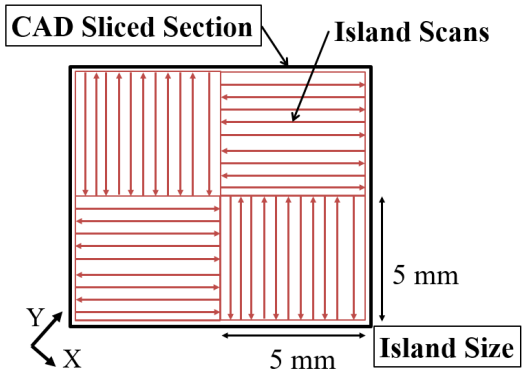

Figure 3.14: Island scan strategy adapted from [141]

The Island scanning strategy affects the following properties of the part:

- Residual stress is altered significantly

Concept Laser Scan Patterns

The M2 Cusing machine has a limited amount of scan patterns that can be chosen using the machine software. The software package that came with the M2 Cusing machine only allows contour scans as well as the scan patterns displayed in Figure 3.15. These patterns are the hatch vectors that will be used to solidify the islands. Once a layer is completed, the islands all shift by 1 mm in the x and y directions. Scan patterns 1 and 2 are the same but just are oriented through different axes. The same goes for patterns 3 and 4. Pattern 5 is the combination of pattern’s 3 and 4 and the laser would scan 3 and 4 consecutively on top of each other. Scan pattern 6 is also a combination of patterns 3 and 4 but they make up a 10 x 10 mm set of islands as displayed in the figure.

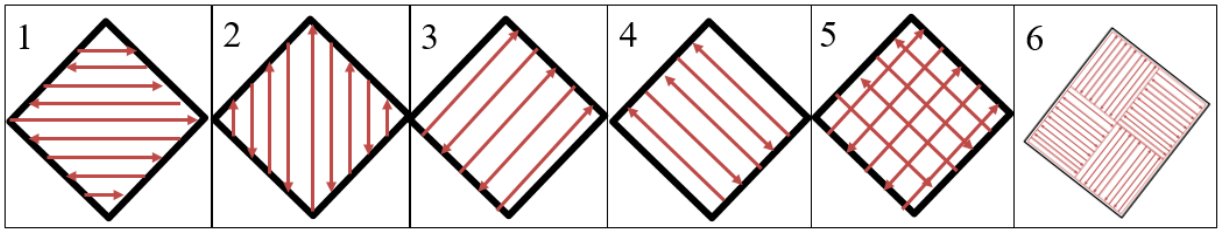

Figure 3.15: M2 Cusing scan pattern options

3.2.4.2. Layer scan strategies

The Inter-Layer Stagger Scanning Strategy (Knitting Strategy or Refill Strategy)

The inter-layer stagger strategy is used to repair defects in the previously scanned layers by scanning the next layer at an offset, so that the laser scans at the scan track overlapping zone [155], [156]. Often powder situated in the overlapping zone is not completely melted. The refill scanning strategy corrects this flaw by melting all of the powder situated in the overlapping zone, which results in stronger bonds between layers. The inter-layer stagger scan strategy is depicted in Figure 3.16 below.

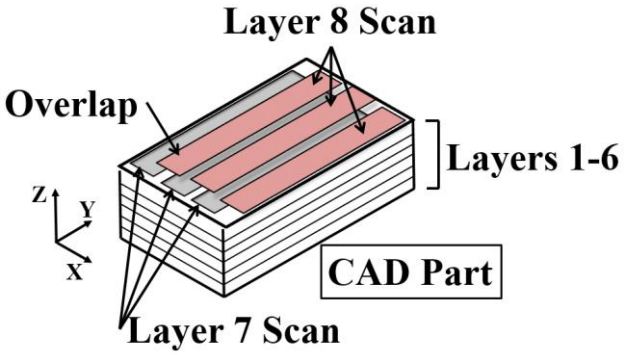

Figure 3.16: Inter-Layer stagger scan strategy adapted from [156]

The inter-layer stagger scan strategy affects the following properties of the part:

- Quality of end use part is improved
- Porosity of the part is reduced
- Improved bonding strength between layers

Orthogonal Scan Strategy (Cross-Hatching Strategy)

The orthogonal scan strategy is when successive layers are scanned orthogonally to each other [155]. This strategy is used to reduce the stress build up along the scans, by changing the direction of the scan after each layer [157]. Figure 3.17 displays four different layers. Layers 1 and 3 are scanned in the y-direction and layers 2 and 4 are scanned in the x-direction.

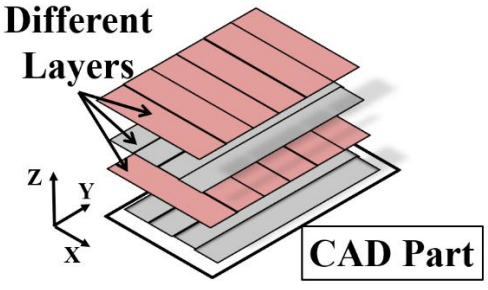

Figure 3.17: Orthogonal scan strategy adapted from [156]

The orthogonal scan strategy affects the following properties of the part:

- Residual stress is reduced
- Porosity of the part is reduced

- Surface finish is improved

Lattice Structure Strategies

Utilising lattice structures in a part is a cost and time saving method. Lattice structures reduce the volume of the part, which saves on material costs and processing time. Investigations [11], [158] on lattice structures have been performed regarding the potential of utilising them for applications in lightweight structures, energy absorbers, vibration control, medical implants, and heat exchangers.

Contour-Hatch Scan Strategy

The contour-hatch scan strategy is the most commonly used scan strategy for the fabrication of lattice structures. This strategy involves taking each build layer and creating many scan vectors for the lattice structure. The laser beam then switches between scan vectors in order to produce a high number of scanner delays [12]. A contour scan is also scanned around the edge of the part before or after the hatch scans are performed to achieve the desired strut diameter. The contour-hatch scan strategy is depicted in Figure 3.18 below. The CAD sliced section in the figure is a cross-section of a lattice strut.

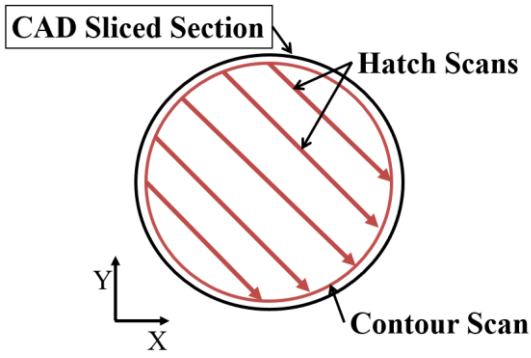

Figure 3.18: Contour-Hatch scan strategy [12]

Although the scan strategy depicted above has five hatch scan vectors, the number of hatch scans is dependent on the scan spacing, beam diameter (spot diameter), and diameter of the strut. These parameters are generally predefined.

The contour-hatch scanning strategy affects the following properties of the part [12]:

- The build-up errors are reduced
- Struts in the lattice structure are more accurate
- Struts have better surface roughness [158]
- The lattice structure density is accurate in comparison to CAD Model

Pointlike Exposure Scan Strategy

The pointlike exposure strategy is also commonly used for the fabrication of lattice structures. Rehme recommends the use of the pointlike strategy over the contour-hatch strategy [11]. Unlike the contour-hatch strategy the pointlike exposure strategy reduces the complex geometry to a set of points of exposure, which results in less jumps and scanner delays [12]. A Matlab tool can be used to determine the intersection points of the lattice structure for each build layer. The layers are scanned using infinitely small scan tracks and the strut diameter is controlled by the exposure time of the laser [158]. Due to the melting process being time dependent, the pointlike strategy is less accurate than the contour-hatch strategy. However, unlike the contour-hatch strategy, the pointlike strategy can be used for strut diameters less than 150 µm [158]. The pointlike strategy is depicted in Figure 3.19 below.

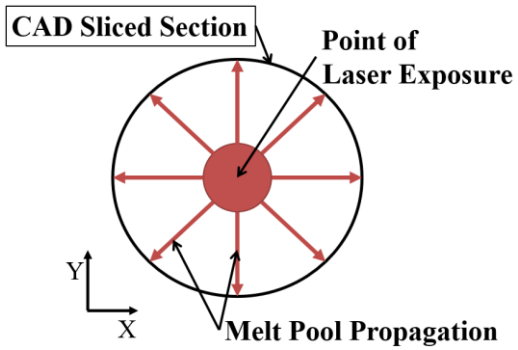

Figure 3.19: Pointlike exposure scan strategy [12]

It can be observed that the laser is exposed in the centre of the strut and the melt pool propagates until the desired diameter is achieved then the laser is shifted to the next point of the build.

The pointlike exposure scanning strategy affects the following properties of the part [12]:

- Slight deviations are introduced in the struts of the lattice structure
- The lattice structure density is greater than designed
- Struts have a rough surface finish

Due to the different mechanisms used for bonding of the layers, parts developed using the contour-hatch strategy display different mechanical properties to parts developed using the pointlike exposure strategy [99].

3.2.5. Feedback Control

K.U. Leuven has developed an in-process monitoring feedback system for an SLM machine, which utilises a high speed CMOS Camera and photodiode [142]. The system is used to observe the laser spot and melt pool throughout the entire part building process. The melt pool size can directly affect over-hangs, holes, and sharp corners where the supporting powder bonds with the melt pool and

causes a deformation (known as Dross) in the part. This deformation affects the accuracy of the part and would require post processing operations in order to remove the bonded powder.

In conventional SLM machines, the laser power and scanning velocity are kept constant during the entire building process. However, some parts have complex geometries and some features cannot be accurately produced using fixed scanning parameters. The melt pool size is related to the laser power and the scanning velocity of the laser. The size of the melt pool has a maximum for a certain scanning velocity and it starts having a decaying effect after the maxima has been reached [142]. With the feedback system, the melt pool can be carefully monitored using the CMOS camera and the photodiode. The machine power and scan velocity can be adjusted accordingly in order to achieve the greatest accuracy from the SLM machine.

The feedback control strategy affects the following properties of the part:

- Part accuracy by sharp corners and overhangs
- The surface roughness

3.2.6. Base-Plate Heating or Preheating

One strategy that can be utilised to drastically reduce the residual stress in the part is to heat the build plate or the powder bed before and during the SLM process [40], [54]. This strategy is difficult to achieve because extreme alterations to the machine have to be performed. The build plate would have to be altered to include a heating element within the plate. This strategy cannot be used on hybrid parts because heating the part could alter the mechanical properties. The relationship between the residual stress in the part and the temperature of the build plate is an inversely proportional one [159]. In order to achieve a minimum residual stress in the part, the build plate would have to be heated (roughly 150-600°C) and some machines are not designed to withstand high temperatures within the build chamber. Also the Argon or Nitrogen gas inside the build chamber would also be heated, which could lead to problems with the gas handling systems of the machine. When heating the powder bed, care should be taken to not overheat the powder. If the powder is overheated it could melt and the particles could bond together in the powder bed.

The heating of the base plate strategy affects the following properties of the part:

- Reduces the residual stress in the part and the base plate

3.3. Concept Laser Patent

The following is the relevant section of the Concept Laser GmbH Patent, which has been translated from German. The patent is for the selective laser sintering or melting of metals using a stochastic island scanning method in order to reduce thermal stresses.

Patent Document Number: DE10042134A1 28.03.2002
Title: Process for manufacturing three-dimensional sintered workpieces
Applicant: Concept Laser GmbH, 96215 Lichtenfels, DE
Inventor: Herzog, Frank Carsten, 96215 Lichtenfels, DE

As is apparent from the plan view of a workpiece **1** according to **Fig.** 1 (Note the figures are not available on the patent), have temporally successively irradiated individual portions **2** separated by a distance greater than or at least equal to the average diameter of these individual sections **2.** The individual sections **2** are provided with numbers, which illustrate the sequence of irradiation. The individual sections **2** are thereby stochastically distributed in succession. By the individual sections **2** are irradiated in the manner described, voltages which result from the changes in the material, uniformly distributed over the workpiece **1** and a distortion of the workpiece **1** is prevented. In particular, the temporal succession irradiated individual portions have such a distance from each other **2,** that which occurs in consequence of the radiation of heat is effected substantially uniformly into the layer to be sintered **8, 8** '. Due to the uniform heat input thermal stresses can be prevented, which can lead to distortion of the workpiece **1** or even cracking [160].

DE 43 09 524 C1 is also already known to divide documents into individual sections and the individual sections, such as squares, to solidify succession. The joints are left between the individual areas or individual irradiation cells to ensure that the workpiece interior prevents warping as a result of tension [160].

Claims:

1. Process for manufacturing three-dimensional sintered workpieces, in particular Stereolithography for use in a laser-sintering machine, where in layers sintered material, in particular liquid, pasty, powdery or granular sintered material is applied from a storage device on a substrate and is heated by irradiation of partially defined individual sections such that the components of the sintered material by irradiation range dependent on the workpiece, connect with partial melting, characterized in that temporally successively irradiated individual portions have a distance from one another, which is greater than or at least equal to the mean diameter of said individual portions.

2. The method according to claim 1, characterized in that the individual portions are successively irradiated in a stochastic distribution.
3. The method according to any one of the preceding claims, characterized in that the consecutively irradiated individual portions have such a distance from each other that the irradiation occurs in consequence of the heat input is effected substantially uniformly into the layer to be sintered.
4. The method according to any one of the preceding claims, characterized in that adjacent individual portions overlap opposite edges.
5. The method with the features of the preamble of claim 1, characterized in that a grid structure is sintered in the layers, the density of which differs from the lattice structure lying within the surface regions [160].

The patent is discussed and evaluated in further sections.

3.4. Influence of Scan Parameters on Integrity

There are as many as 130 factors which have an effect on a parts integrity during the SLM process [155]. The laser power, scan speed, hatch spacing, and layer thickness should not be varied independently when attempting to optimise parameters for density. It is difficult to determine the effects of different process parameters on the residual stress and porosity of a part. The following section summarises from literature the influence of laser power, scan speed, hatch spacing, and layer thickness on residual stress.

3.4.1. Laser power

The maximum temperature of the melt pool is reduced with a reduction in laser power [161], [162]. The reduction in power also reduces the melt pool size but increases the cooling rates [161]. According to Wu et al. [163] a higher laser power leads to a lower deformation.

High porosity in parts is mainly attributed to high energy inputs into the substrate [84]. A high laser power has been found to reduce the porosity in parts, however, the hatch spacing and scan speed also have a significant effect on the porosity [56].

3.4.2. Scan speed

According to Brückner et al. [164] a reduction in scan speed leads to reduced residual stresses in a one track model. Vasinonta et al. [165] states that the reduced scan speed decreases the temperature gradients and Manvatkar et al. [161] claims that the cooling rate is also reduced. So the residual stresses are inversely proportional to the scan speed.

To achieve a low porosity in an SLM component, a low scanning speed should be used. Once the scanning speed is set too high, the melt pool gets smaller and this causes large holes in the layer where unsolidified powder could be present. This problem can be counteracted with a reduction in hatch spacing or an increase in laser power.

3.4.3. Hatch spacing

The increase in hatch spacing results in less geometric deviation in terms of warping. This is due to the fact that, with increased hatch spacing, the localised heating of the laser decreases. The porosity of laser sintered parts linearly increases with layer thickness and hatching distance [58]. The hatch spacing should be varied with the laser powder and scan speed in order to determine the optimal hatch spacing. In the interest of time saving a large hatch spacing is desirable but the scan speed and laser power would then need to be decreased and increased respectively. Therefore, since the scan speed has the largest influence on time, the hatch spacing should be selected first and then the laser power and scan speed accordingly. Since reduction in deviation requires a large hatch spacing and reduction in porosity requires a small hatch spacing, a balance needs to be found through parameter optimisation.

3.4.4. Layer thickness

Thick powder layers are not desirable, as it leads to the formation of droplets and deteriorates the parts quality [155]. The increase in layer thickness however, leads to less residual stress and deviation in a component [166].

Density tests with SLM prove that the technology is able to produce near full dense (98–99%) objects with some rest porosity due to various reasons such as evaporation of elements (High laser power) with a high vapour pressure, trapped gas, bad surface quality (Poor parameter choices), reduction in the solubility of the dissolved elements in the melt pool during cooling and solidification [109].

3.5. Influence of Deposition Patterns

It has been established that the stresses in the direction of the scan tracks are larger than those developed perpendicular to it [48], [54]. One could use this knowledge to develop a scan pattern that mitigates the residual stress build-up. Several authors found that the deformation of a part (similar to a hybrid part) is larger in the direction of the scan tracks [43], [106], [126], [166]. The number of methods one can utilise to scan a layer is vast, as shown in Section 3.2. An important strategy that can be utilised to reduce residual stresses and geometric deviation, is to create a strategy that allows less time to pass between the scanning of two adjacent tracks. The heat input

from the first track, which has not fully dissipated, will act as a preheating mechanism for the next track that is scanned next to it. This should reduce the thermal gradient and also the yield stress of the material [48].

3.6. Chapter Summary

The residual stress and warping mechanisms that occur during AM processes such as SLM were discussed and defined. A new theory was suggested, which suggests reasons why warping occurs in single layer SLM parts. Next the different SLM strategies were researched and discussed along with the effects on certain part properties. Only scanning strategies were varied in this study. The influence of certain parameters on the residual stress of SLM parts were also discussed.

Chapter 4

Experimental Methodology

4.1. Research Methodology

The research methodology was broken up into various stages and experiments in order to develop the new strategy. Firstly, a background study was conducted to determine the effects of warping on tool steel hybrid parts when varying the height. Once a relation was shown the next phase could begin. Research then had to be conducted on all of the scan strategies that are currently in use and ones that were developed by other researchers. A few scan strategies were then suggested for further testing and analysis.

A major problem was identified which could have been detrimental to the study. Delamination of parts, from the base plate, was occurring on the M2 Cusing machine, which would negatively affect the results from this study. A solution was proposed and tested with different starting strategies. The solution was then validated.

Due to the machine software limiting the user and the ability to change the scanning strategy, a new method had to be established to expose the newly developed scan strategies. A new method was developed and tested and has been coined Hatch Pattern Design (HPD). The new scan strategies were suggested and were all scanned onto the powder bed to observe any deviation. This qualitative experiment revealed the most suitable strategy to use.

The newly developed scan strategy was then compared to the Concept Laser default strategy on a substrate, in order to closely inspect the strategies on a microscopic level. Once satisfied and some changes were made the validation experiments were performed. The newly developed strategy was compared to the default scan strategy in terms of porosity and deviation. The research methodology steps can be observed graphically in Figure 4.1.

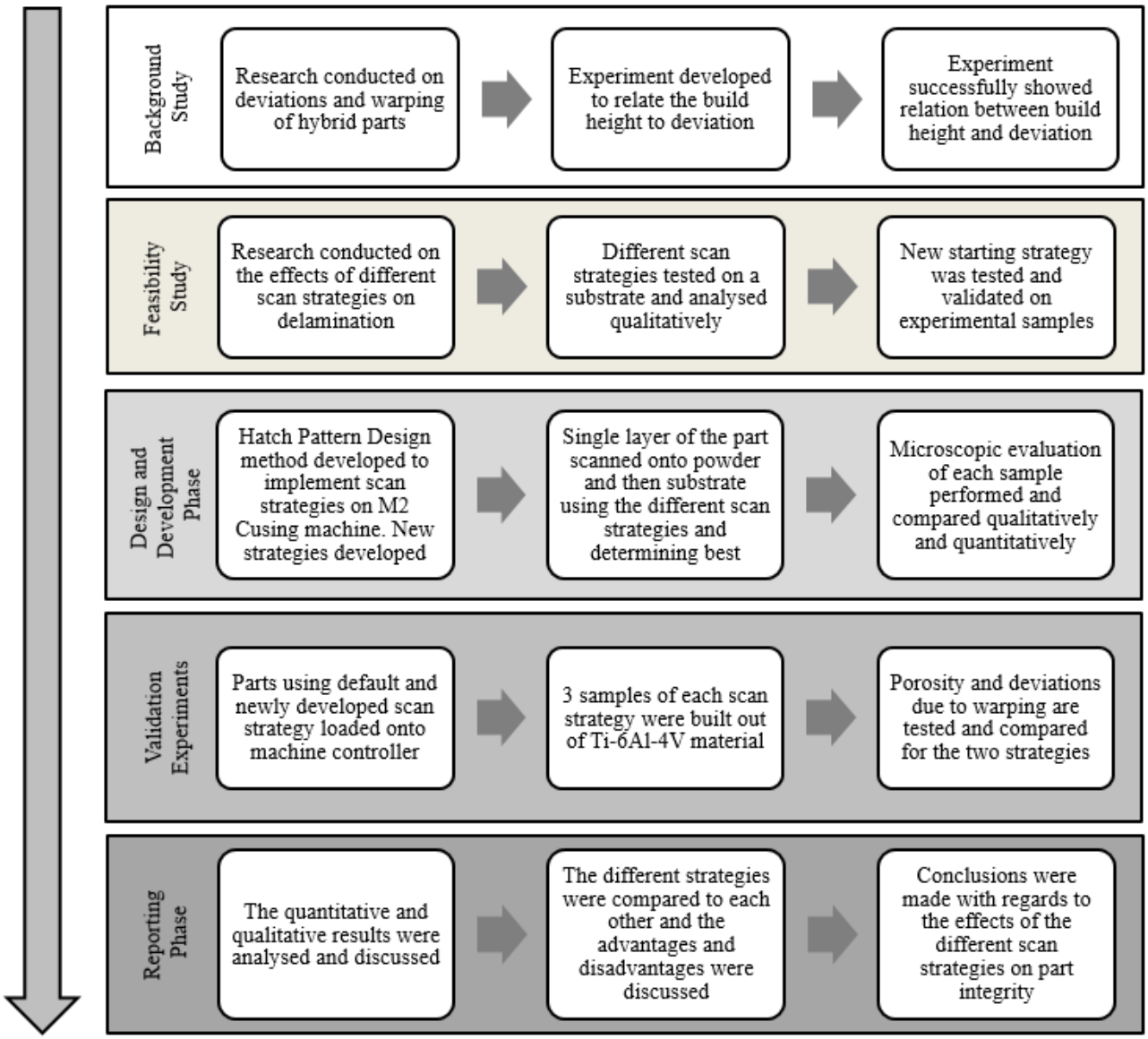

Figure 4.1: Research methodology process showing the different phases of this study

The layout of the experimental sections was done in such a way as to improve the reader's experience and to create a logical flow. The layout was also important so that each experiment could be extracted and added to a journal or conference paper with very little or no changes to layout. The layout was derived from the PhD thesis of B. Vrancken [48].

Chapter 5

Background and Feasibility Studies

5.1. Background Study

5.1.1. Experimental Setup and Design

Firstly, the effects of thermally induced residual stress on the geometrical deviation of hybrid parts manufactured by SLM on the Concept Laser M2 Cusing system had to be evaluated. Three tool steel test base plates of equal geometry were produced using high speed milling (on the Hermle C40U milling machine) onto which a hybrid section was built with the Concept Laser M2 Cusing machine. The base for each specimen was uniform with dimensions 120 mm x 120 mm x 20 mm. Three different heights (10 mm, 20 mm, and 30 mm) were built onto the bases respectively. Since residual stress occurs between successive layers, increasing the height of the hybrid section should increase the residual stresses. Therefore, it was expected to see more deformation as the amount of built up layers increased.

5.1.1.1. Machine setup and machine parameters

The samples were measured using a Mitutoyo A710 Coordinate Measuring Machine (CMM). Measurements were post processed and deviations to the original CAD models analysed in Delcam PowerShape. The experimental setup can be observed in Figure 5.1.

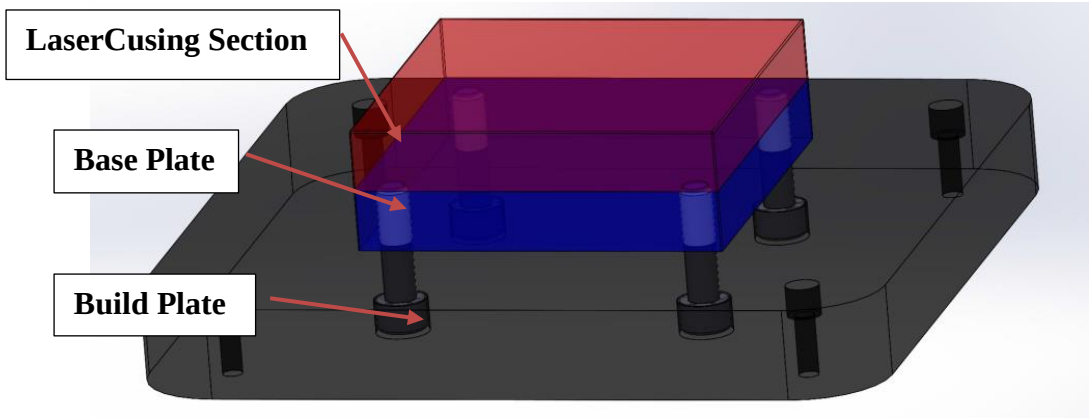

Figure 5.1: Background study experimental setup on Concept Laser M2 Cusing base plate

The Concept Laser default parameters were specified for the processing of the SLM section of the hybrid part. The default laser parameters can be observed in Table 5.1.

Table 5.1: Laser parameters for background study

Parameter	Contour	Skin
Power [Watts]	30	185
Speed (sp) [mm/s]	140	600
Focus Diameter (d) [mm]	0.15	0.15
Operation Mode	Continuous	Continuous
Hatch Spacing (a1) [mm]	0.2	0.105

The scanning strategy chosen was the Island scan strategy. The islands and laser scan vectors are demonstrated in Figure 5.2.

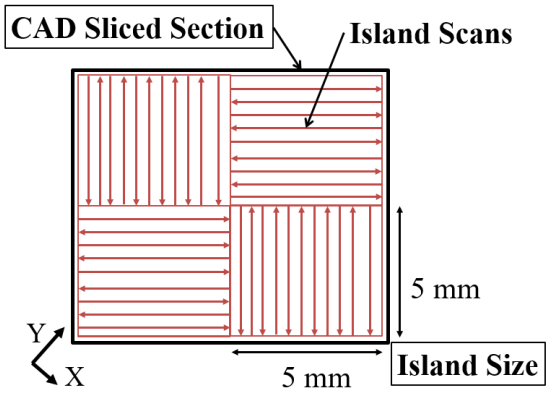

Figure 5.2: Island scan strategy from Concept Laser GmbH [141]

The parameters were kept constant for all three specimens. The layer thickness/resolution was set to 30 µm and the island size was set to 25 mm² with an edge length of 5 mm. The power and focus diameter of the laser were also kept constant for all three specimens.

5.1.1.2. Material used

The material used for the hybrid base plates was tool steel (1.2316) and the material used for the SLM process was CL 50WS powder (1.2709). The plate material 1.2316 is commonly used for mould applications and the SLM material is commonly used for powder bed fusion processes as it is easily heat treatable. The material properties of these two materials are presented in Table 5.2.

Table 5.2: Material properties of 1.2316 and 1.2709 [167], [168]

Properties	1.2316 (Base plate)	1.2709 (SLM Powder)
Tensile Strength, Yield	950 MPa	900-1100 MPa
Modulus of Elasticity	207 GPa	160-200 GPa
Coefficient of Thermal Expansion (Linear)	11.0 µm/m-°C	10.3 µm/m-°C
Specific Heat Capacity	0.460 J/g-°C	0.430-0.470 J/g-°C
Thermal Conductivity	24.3 W/m-K	14.2-15.8 W/m-K

5.1.1.3. Coordinate Measuring process

The measuring specimens were glued directly to the granite table of the Mitutoyo A710 coordinate measuring machine. Specimens were mounted with the SLM section face downwards because the top surfaces of the specimens were flat in comparison to the base plate. The CMM machine, as well as the setup of the hybrid sample can be observed in Figure 5.3.

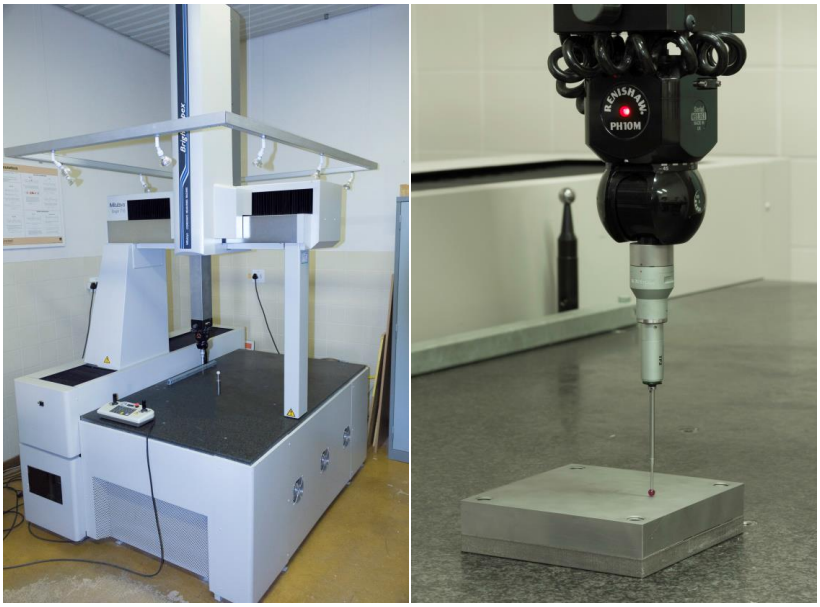

Figure 5.3: Mitutoyo A710 CMM (Left) with hybrid sample setup (Right)

The hybrid samples were measured along the centres of the top surface as well as diagonally across. The side profiles of the hybrid sample were also measured to determine if there was any angular deviation. The chosen measuring paths are displayed in Figure 5.4.

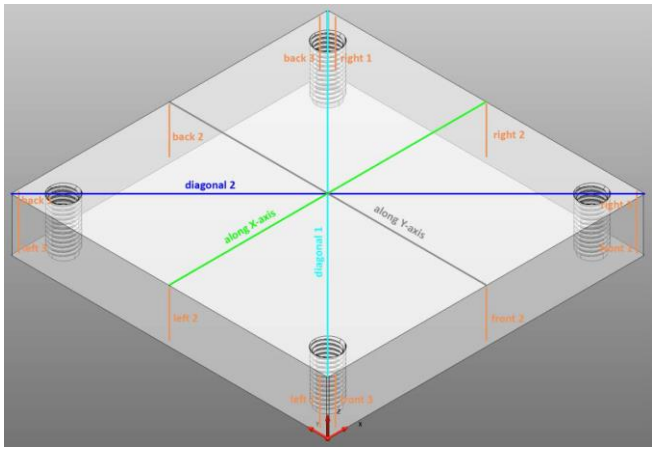

Figure 5.4: Measuring paths of each specimen

5.1.2. Results and Discussion

Once the samples were produced the deviation was measured using the CMM machine. All three specimens were measured using the same measurement program along the same measuring paths.

The following results were published in the RAPDASA 2015 Conference proceedings the paper is referenced in Appendix F.

5.1.2.1. Surface deviation

The measured surface point clouds were imported into the Delcam PowerShape program and the points were used to fit solid surfaces for the creation of models that have the geometry of the measured warped hybrid plates. The warped plates were compared to the original CAD models and the deviation was computed and can be observed in Table 5.3.

Table 5.3: Shape deviation from CMM scans

Scale [mm]	10 mm Specimen	20 mm Specimen	30 mm Specimen
MAX 0,80 0,60 0,40 0,20 0.00 -0,20 -0,40 -0,60 -0,80 -MAX	**Shape Deviation – Bottom Surface**		
	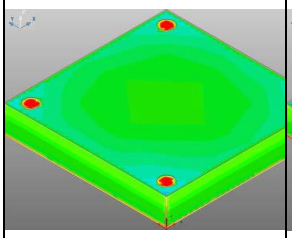	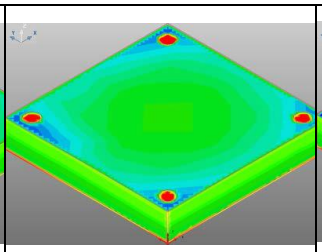	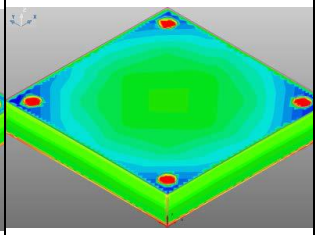
	Shape Deviation – Top Surface		
	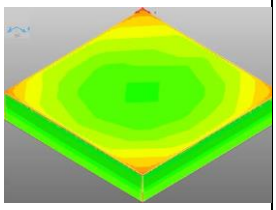	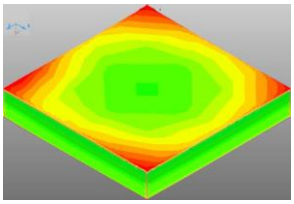	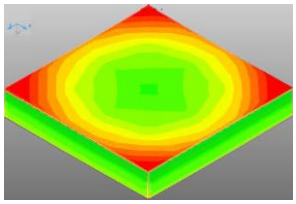
MAX 0,16 0,12 0,08 0,04 0.00 -0,04 -0,08 -0,12 -0,16 -MAX	**Shape Deviation – Side Surface**		
	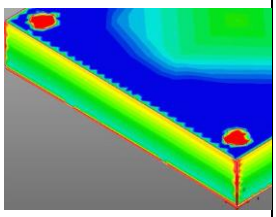	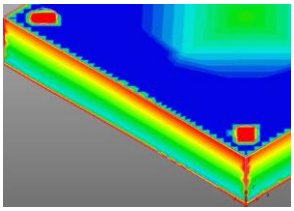	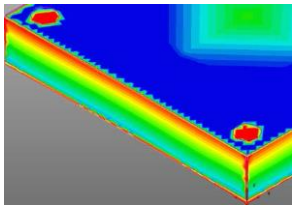
	Maximum Deviation		
	0.570 mm	0.834 mm	1.005 mm

The shape deviation of the bottom surface shows that the edges are warped in the direction of the SLM top section. This indicates that the corners of the entire hybrid part are thinner than the centre of the part. The results were deduced by using a 20 mm parallel translation of the bottom surface in

the positive Z direction under the assumption that the hybrid plate's thickness did not change during the build process. The side surface deviation shows the angular deviation along the surface.

5.1.2.2. Angular deviation

The angular deviation is the deviation of the side surfaces with the SLM top surface as reference. This is due to the fact that the powder scraper of the SLM machine is fixed in position and should always scrape a flat layer of powder, eventually compensating for any warping during previous build layers. However, irregularities on the surface can still arise from imperfect coating layers due to degradation and wear of the rubber coater blade, during the period of the build. This was witnessed on the parts, but did not influence the surface significantly. The angular deviation concept, α, is graphically described in Figure 5.5 below.

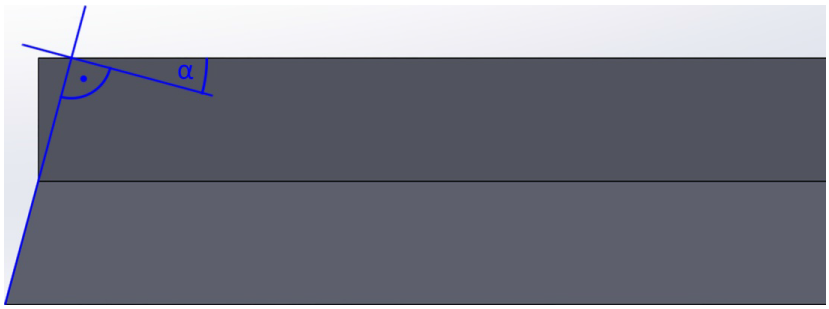

Figure 5.5: Angular side surface deviation

On each side of the specimens, three angles were measured. The CMM measurements of the angles in both decimal degree values and minutes and seconds are listed in Table 5.4.

Table 5.4: Angular deviation

Position	α (10 mm) [°]		α (20 mm) [°]		α (30 mm) [°]	
Left 1	0.630	37' 48"	0.677	40' 37"	0.780	46' 48"
Left 2	0.484	29' 02"	0.735	44' 06"	0.770	46' 12"
Left 3	0.474	28' 26"	0.696	41' 46"	0.850	51' 00"
Back 1	0.408	24' 29"	0.725	43' 30"	0.801	48' 04"
Back 2	0.417	25' 01"	0.755	45' 18"	0.790	47' 24"
Back 3	0.251	15' 04"	0.768	46' 05"	0.785	47' 06"
Right 1	0.371	22' 16"	0.698	41' 53"	0.881	52' 52"
Right 2	0.471	28' 16"	0.847	50' 49"	0.953	57' 11"
Right 3	0.506	30' 22"	0.843	50' 35"	0.870	52' 12"
Front 1	0.332	19' 55"	0.636	38' 10"	0.797	47' 49"
Front 2	0.25	15' 00"	0.687	41' 13"	0.841	50' 28"
Front 3	0.316	18' 58"	0.733	43' 59"	0.773	46' 23"
$\bar{x}_{\alpha}$	0.409	24' 32"	0.733	43' 59"	0.824	49' 26"

The average deviation angle $\bar{x}_\alpha$ can be calculated for each specimen due to the fact that each specimen is symmetric in geometry. A proportional correlation between the building thickness and the angular side deviation was identified and can be observed in Figure 5.6.

Figure 5.6: Correlation between the building thickness and the angular side deviation

5.1.2.3. Contour scan

In Figure 5.7 the measurements taken along the diagonal contour lines along the top surface are presented. It shows the deviation trend curve along the diagonal line "Diagonal 1" for each of the specimens.

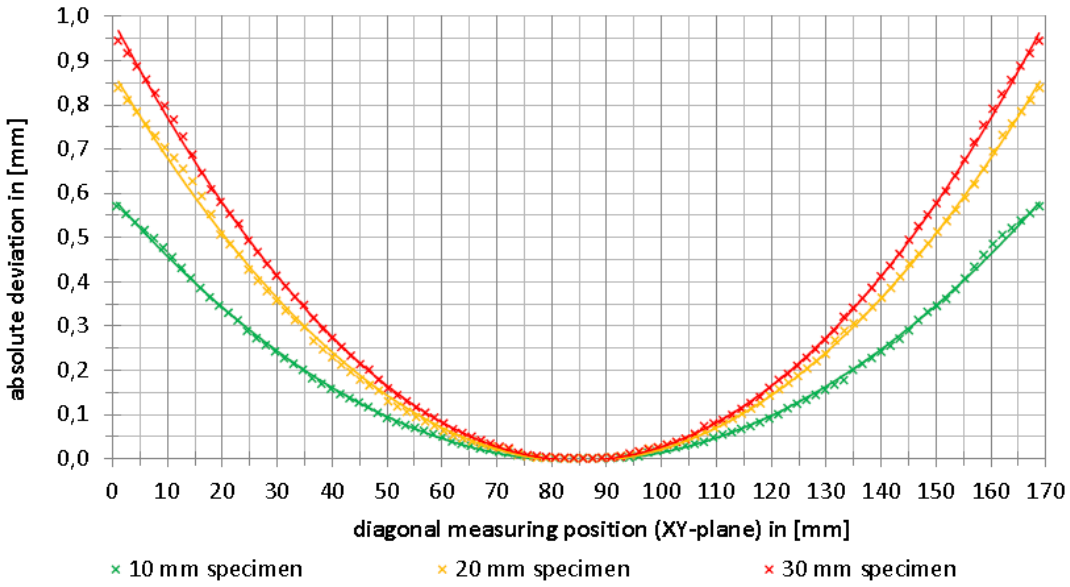

Figure 5.7: Deviation trend curve along diagonal

The exponential shape of the graphs suggests a quadratic relationship between the shape deviation and the measuring position on the specimen. "Diagonal 2" was left out because the differences between diagonal 1 and diagonal 2 are marginal. The maximum shape deviations as well as the mean deviation per specimen and contour lines are listed in

Table 5.5.

Table 5.5: Maximum and mean deviation

Section	10 mm specimen		20 mm specimen		30 mm specimen	
	Maximum	Mean	Maximum	Mean	Maximum	Mean
	[mm]		[mm]		[mm]	
Along X-axis	0.316	0.104	0.411	0.141	0.494	0.173
Along Y-axis	0.275	0.093	0.440	0.149	0.531	0.183
Diagonal 1	0.570	0.193	0.838	0.286	0.944	0.325
Diagonal 2	0.566	0.185	0.829	0.284	1.043	0.367
$\bar{x}$ axial direction	0.296	0.099	0.426	0.145	0.513	0.178
$\bar{x}$ diagonal direction	0.568	0.189	0.834	0.285	0.994	0.346
Surface	0.570	0.177	0.834	0.279	1.005	0.319

The average values $\bar{x}$ for axial and diagonal direction are used to identify the correlation between the building thickness and the maximum as well as the mean deviation in these directions. This correlation is valid for the building setup with a tool steel hybrid plate with an area of 120 mm x 120 mm and a thickness of 20 mm.

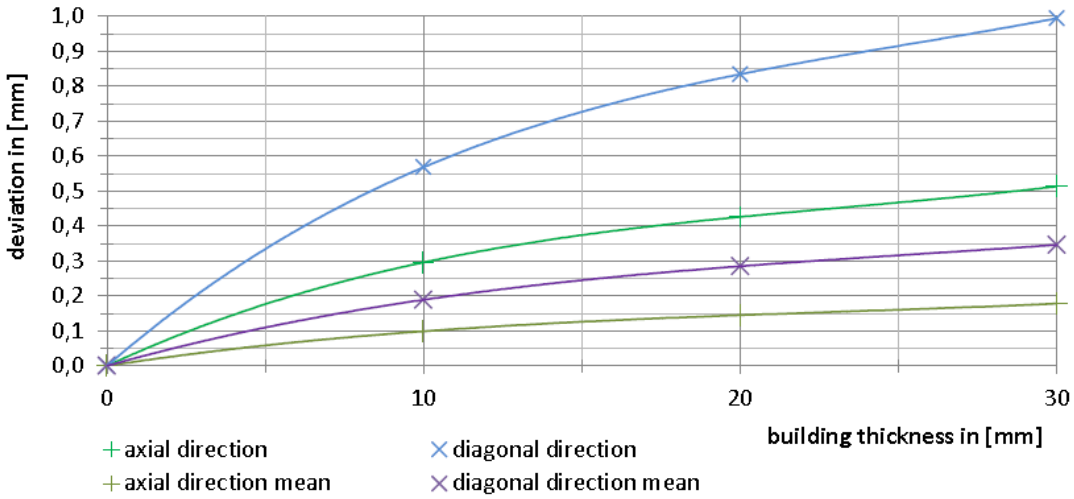

Figure 5.8: Deviation correlation in axial and diagonal direction

The evaluation of the measured data showed that there is nearly no difference between the measurements along the X and Y-axes, as well as the two diagonal directions respectively.

5.1.3. Summary and Recommendations

The background study suggests that geometric deviation does occur during the SLM process. The shape deviation/warping in a SLM hybrid part seems to be proportional to the building thickness.

Since the residual stress in a part is a consequence of the high temperature gradients, the greater deformation of thicker parts suggests that residual stresses in this particular part increases proportional to the build thickness. Also, the angular deviation of the hybrid part seems to be proportional to the building thickness of the part, which further supports the suspicion. These findings seem to support the findings of Mercelis and Kruth [54] where they state that the magnitude of the residual stresses depends on the part height as well as the height and stiffness of the base plate.

5.2. Feasibility Study

One of the problems that occur when producing hybrid parts is delamination of the SLM section from the base part. In Figure 5.9 one can observe a set of fracture test samples that have delaminated from the base plate due to residual stress build up. The default island scan strategy was used to expose the starting slices to the base plate.

Figure 5.9: Delamination of a Ti-6Al-4V fracture test sample from the base plate before new starting strategy was applied

Delamination during the production of hybrid parts could be very costly and could result in a high scrap rate of parts. The challenges with delamination had to be overcome first in order to continue with this study. It was revealed in Section 2.5.3.2 that with the M2 Cusing machine, the base plate and the coater blade are aligned by eye and set by the machine operator. There is no electronic or mechanical method to align these two vital instruments to the low tolerance that is required. So, when a build is started there is a good chance that the first coated layer will be more or less than the defined layer thickness (Usually 30 µm). This problem would lead to inaccuracies in the hybrid parts and could also lead to delamination of the SLM part from the base part.

5.2.1. Experimental Setup and Design

In order to ensure the SLM part does not delaminate from the SM part (Base plate), a new starting strategy had to be developed. Several different starting scan strategies were tested and a suitable strategy to ensure the SLM part is correctly bonded to the SM part, was revealed.

5.2.1.1. Machine setup and parameters

Firstly, the different scanning strategies had to be compared to each other by exposing them on a 1.2 mm thick sheet of titanium. The M2 Cusing machine from Concept Laser GmbH was used to expose the 8 scan strategies. The titanium base plate was sufficiently taped to the machine's build plate and aligned with the coater blade (Figure 5.10). A layer of powder, roughly 80 µm thick, was evenly distributed onto the plate by the coater blade. 8 single layer parts were then loaded onto the Concept Laser software and a different scanning strategy was chosen for each. Each strategy was exposed by the laser onto the base plate with the following laser parameters: the laser power was set to 100 W, the scan speed was 600 mm/s, and the hatch spacing was 105 µm. Once all 8 strategies

were exposed on the plate, the plate was removed. The different exposed layers were analysed and a mechanical method was employed to attempt to remove each layer. A steel scraper was used to try and remove the exposed layer from the plate. An allocation of 1 minute per scan strategy was given to attempt to remove as much of the exposed slice as possible. The experimenter was not to change their technique during this process and had to stick to the time allocated. This was only a qualitative way of determining which strategy bonded the best to the base plate.

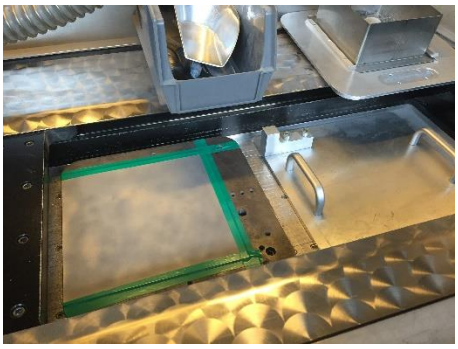

Figure 5.10: 1.2 mm base plate set up in the SLM machine

The 8 scan strategies can be observed in Figure 5.11 where the numbering convention has been kept constant throughout this study. The first 6 strategies are the Concept Laser M2 Cusing machines pre-set strategies. Strategy 7 and 9 are the newly developed strategies. Note how 7 and 9 are not the same, as the order in which the vectors are scanned, is different.

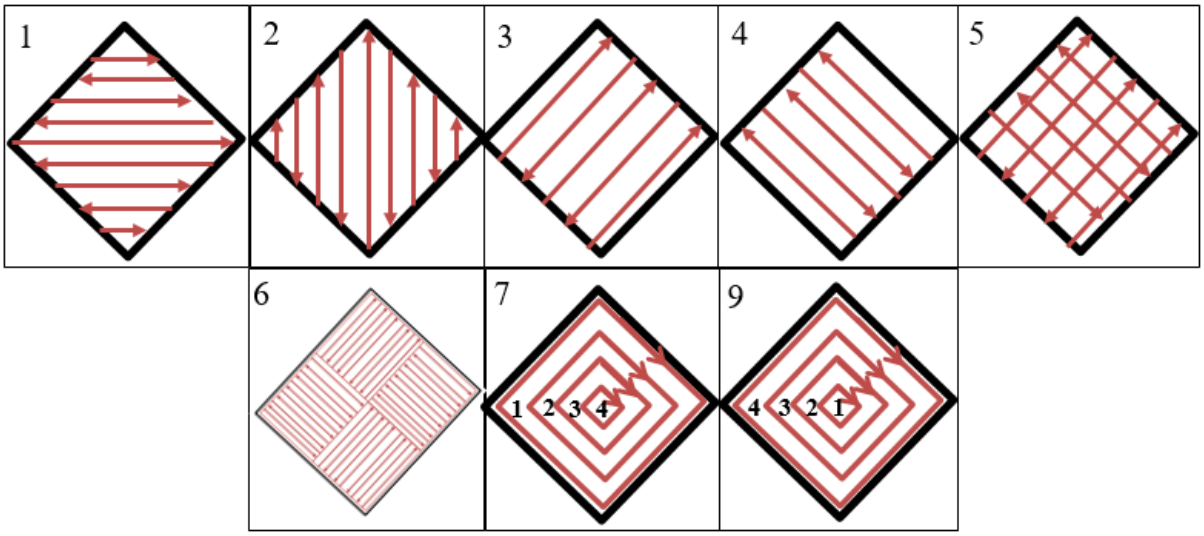

Figure 5.11: The 8 different scan strategies used for delamination strategy experiment

5.2.2. Results and Discussion

Once the single layer parts were exposed onto the base plate, the plate was removed from the machine and inspected. Only scan strategy 5 appeared to have properly bonded with the plate. Scan strategy 5 is an island scan strategy that uses two consecutive raster scans to solidify the powder.

The first raster scan is performed in one orientation and then the second raster scan is performed directly after the first but is rotated through 90 degrees to the first. Burn residue was found on the underside of the plate where strategy 5 was bonded to the plate. This indicated that a large thermal gradient was induced in the part and that the heat generated from the laser can penetrate many more layers than the other scan strategies. This makes scanning strategy 5 ideal to correctly bond the SLM section to a machined section or base plate. Figure 5.12 shows the base plate after the mechanical method was used to remove the exposed slices.

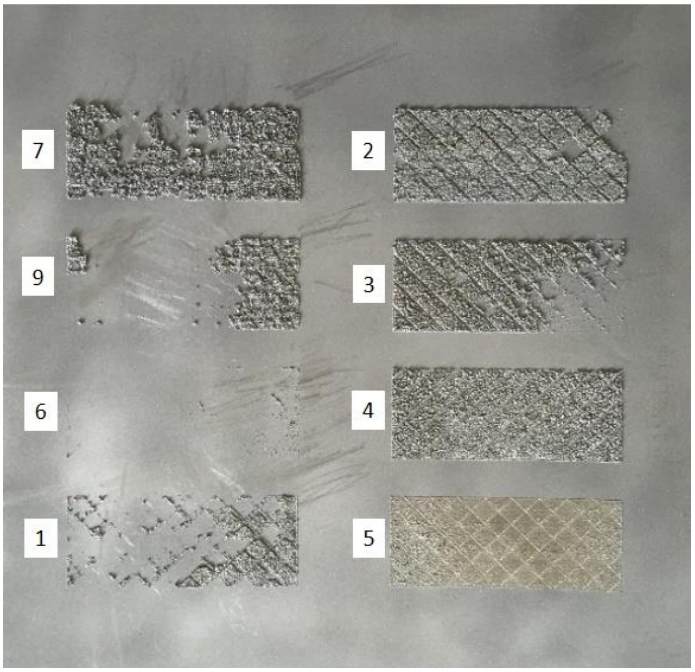

Figure 5.12: Base plate with scan patterns after a tool was used to attempt to remove the scanned layer

One could notice that the machine's default scan strategy, strategy 6 has been completely removed. Strategies 1 and 9 also did not fare well. The other patterns bonded acceptably but failed to fully penetrate the 1.2 mm base plate. It was decided that in order to ensure a satisfactory bond between the SLM part and the base plate, scan strategy 5 would be used when performing the initial exposure slices. The new starting strategy would require that slice 0 and slice 1 of the part would need to be exposed using pattern 5 before starting the building process. This should ensure that the chances of delamination are either reduced significantly or completely removed.

5.2.2.1. Validation experiment

To verify the results, the new starting strategy was used in the SLM process of the original fracture test samples that were originally delaminating off the base plate. The parts were built using the same default parameters that were used on the first samples. Three of these parts were produced and the bond between the base plate and the SLM part can be observed in Figure 5.13 below.

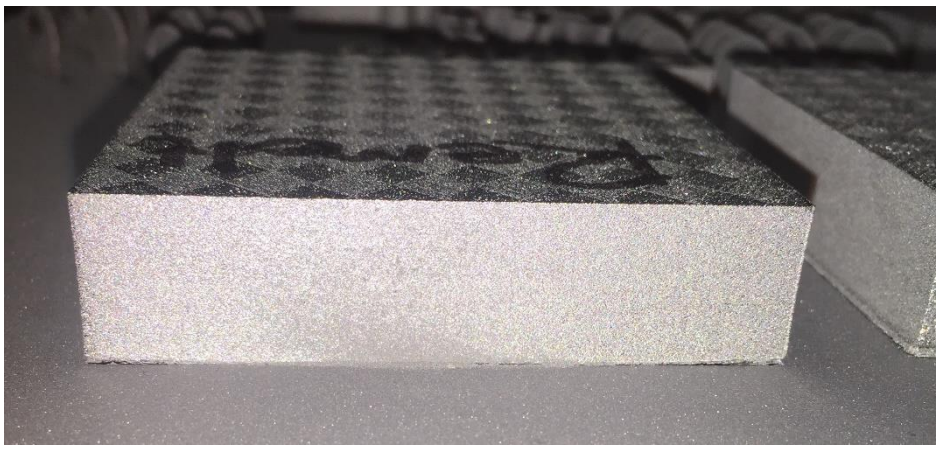

Figure 5.13: Verification parts of newly developed starting strategy

One can observe from the figure above that there is slight delamination from the base plate on the left and right of the part. The delamination is considerably less than that shown in Figure 5.9. Further reduction of residual stress in the parts will also result in less delamination.

5.2.3. Summary and Recommendations

A new strategy to bond the part to the base plate was successfully developed. Negligible delamination was present in the validation experiment. The part's geometry was not visually affected by the slight delamination that was experienced. The new strategy can be utilised to bond the SLM and SM parts together during the hybrid production process. Using this strategy could result in less parts being scrapped due to delamination during the SLM process.

5.3. Chapter Conclusion

The background study revealed that geometric deviation does occur during the SLM process when producing hybrid parts. The geometric deviation seems to be proportional to the height or number of layers of the build and this was confirmed by a study performed by Mercelis and Kruth [54]. Therefore, in order to effectively limit the variables when comparing the default and newly developed scan strategy, the height should not be varied for the samples.

A new starting strategy that can be utilised to bond the SLM part to the base plate was successfully developed. Upon inspection of the current process chain for the Concept Laser M2 Cusing machine, several problems were identified. The major problem that was unfavourable for hybrid part production was the delamination of the SLM section from the SM section. This problem was solved using a double melt scan pattern that melts the island consecutively. This resulted in a better bond of the SLM section to the base plate.

Chapter 6

Scanning Strategy Development

6.1. Hatch Pattern Design Method

In order to develop a new scan strategy using the M2 Cusing machine, a new method had to be established to override the machine's standard scan strategies. The largest hurdle for this study was the machine's software limitations. In pursuit of finding a solution, the Concept Laser Slice (CLS) files were thought to be the answer, as they contained all the vector and parameter information for the machine. Once opened, it was found that the CLS files were partially encrypted. All of the relevant vector and laser information had been encrypted using some sort of encryption method. After spending hours trying to determine and decode the encryption language a new approach was suggested.

The new approach made use of a CAD program to design the required hatch pattern, this method has been labelled Hatch Pattern Design (HPD). The M2 Cusing machine has a limited number of hatching patterns that the user can choose from on the machine software. The machine software only allows the user to choose from part contour scans as well as the 6 hatch scan patterns displayed in Figure 6.1 below. Scan strategy 6 is Concept Laser's Default strategy that is used when selecting default parameters.

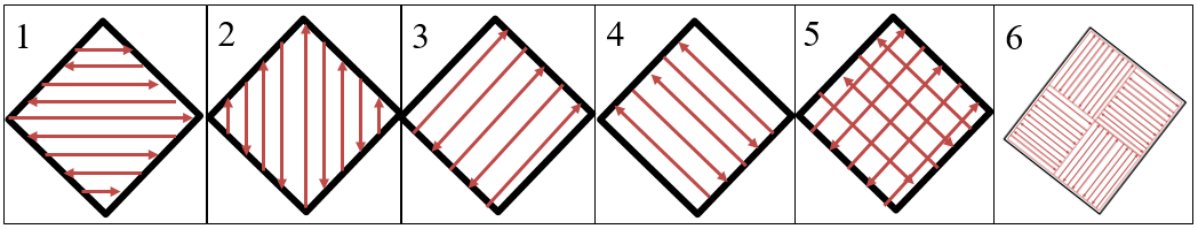

Figure 6.1: Concept Laser M2 Cusing 6 scan pattern options that are programmed on the machine's software.

With the HPD method, the user will utilise a CAD software of their choice, to design the required hatching scan lines as separate parts. The required hatching pattern is designed by creating a part that represents the hatch line (hatch vector). Since the laser determines the direction in which it will scan the designed part, the term vector cannot be used, as the magnitude is user defined but the direction relies on the laser scanning algorithm. Hereafter, the hatch vectors will be referred to as hatch lines for this method. The width of the hatch line should be equal to the width of the spot diameter of the laser. In this study, CAD software such as Solidworks and Delcam PowerShape were used to create the hatch lines. The STL files were then imported into the Concept Laser slicing software, Magics.

Magics is used to position parts on a virtual machine base plate and then slice the parts using a user defined parameter set. Once the parts are sliced they are exported as Concept Laser Slice files. Each part will have their own CLS file. The CLS files are then imported onto the M2 Cusing machine's computer and opened using the Concept Laser software. The user must import the files in the order that they would like the pattern line sets to be scanned by the laser. The software can then be used to set the machine and laser parameters for the newly imported parts. When selecting laser scanning parameters, it is important that the user not use any fill vectors for the hatching but rather use only the contour scan option. The laser will then only scan the contours of the parts that were imported. The summary of the process chain of the HPD method is displayed in Figure 6.2.

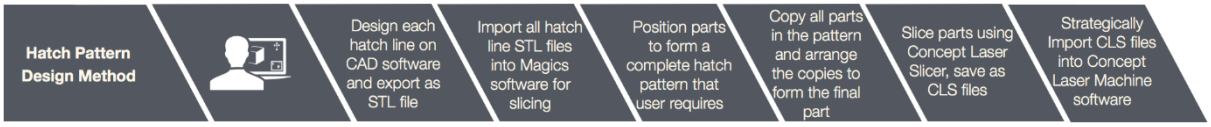

Figure 6.2: Hatch Pattern Design Process Chain that the user can follow to design hatch patterns that can be executed on the Concept Laser M2 Cusing machine

The Hatch Pattern Design method development process went through five different iterations; each iteration was optimised until the method was sufficient. An example of a hatch part is displayed in Figure 6.3. The part is 10 mm high and consists of 4 lines which represent the scan tracks. The part is 1 of 24 other parts that make up a 5 mm by 5 mm island using the helix scan pattern, defined in Section 3.2.4.1. The final part that needs to be the end product of the SLM process is the standard part that was used for all the iterations. The final part has the following dimensions: 120 x 25 x 10 mm as this was the size required for the samples for further experimentation. The final part is made up of 120, 5 mm x 5 mm islands.

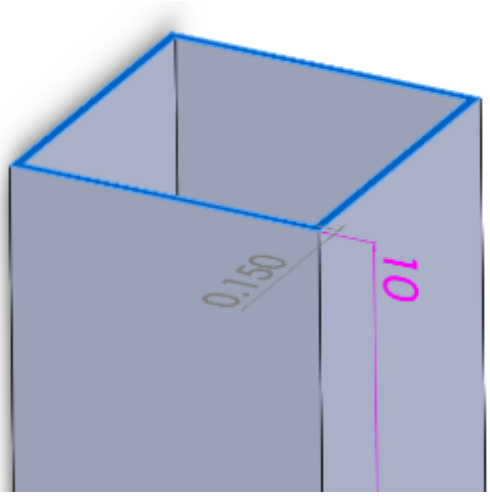

Figure 6.3: 1 of 24 helix scan pattern parts for a 10 mm high final part that is made up with 5 x 5 mm islands

One should note that the part in Figure 6.3 above, is from the first iteration of the HPD method and the islands did not shift or rotate after each layer. Not shifting the part would result in very poor porosity and accuracy of the final part [50]. The first iteration was used as a test to see if the

machine would perform as expected. The different iterations that the design went through are discussed in more detail in the following sections.

6.1.1.1. First iteration

The first iteration used 24 different parts for 1 island and when the component/part consisted of 120 islands per layer there would be 2880 parts, which would need to be uploaded onto the machine's software. This resulted in the machine's computer becoming very slow and often freezing. So, to counter this problem, the hardware of the M2 Cusing and Rofin laser computers needed to be upgraded, to cope with the high processing demands. The Random-Access Memory (RAM) was upgraded to 3 GB DDR3 on the laser and the SLM machine computers. The first iteration was simplified by using the copy function in Magics. As discussed above, the first iteration was merely to test if the method worked correctly.

6.1.1.2. Second iteration

The next iteration of the HPD method required the hatch line parts to be sliced into 30 µm layers (Depends on what layer thickness the user requires). This was performed to vary the position of the hatch lines after each layer. This method was derived from literature [155], [156], [169] in order to reduce porosity and increase bonding strength. Two inter-layer stagger hatch lines can be observed in Figure 6.4 below. With this strategy, the number of parts grew to 5880 parts for a 120 mm x 25 mm x 10 mm part.

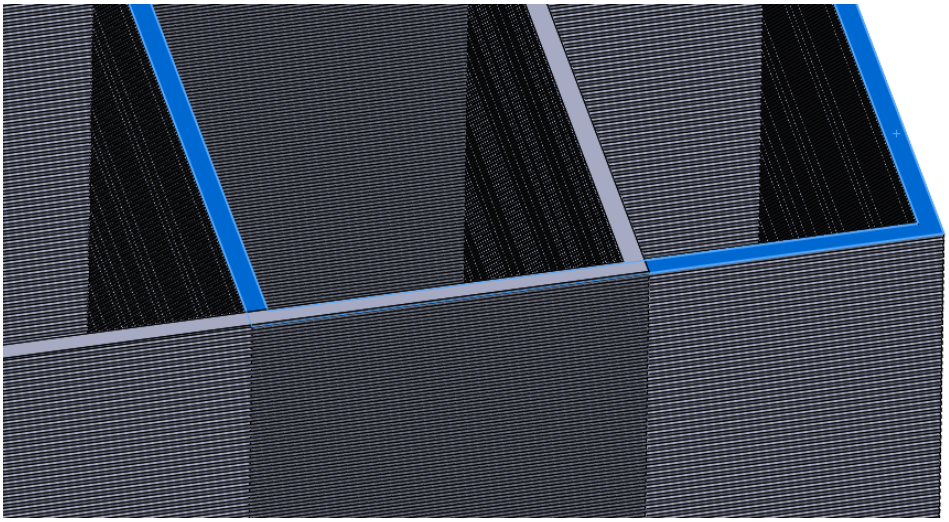

Figure 6.4: Hatch Pattern Design method with inter-layer stagger scanning strategy. Two parts are stacked together like a deck of cards where each layer of the one part is stacked in between each layer of the other part

6.1.1.3. Third iteration

The third iteration drastically decreased the number of parts required to 480 parts for a 120 mm x 25 mm x 10 mm part. The hatch lines were designed as long parts in order to reduce the number from 2880 hatch parts per final part to only 120 hatch parts per final part. This value excludes the

alternating layer, which uses another 120 hatch parts. It was discovered that if one melts all of the 5 x 5 mm hatch lines together without leaving gaps between them, a significant amount of warping occurs as all the islands are joined together in this moment. This was discovered during the scanning strategy deformation experiment in Section 6.1. The solution to this problem is discussed in Section 6.2.2.2. The long parts that make up the hatch lines can be observed in Figure 6.5. The inter-layer part is displayed on the right.

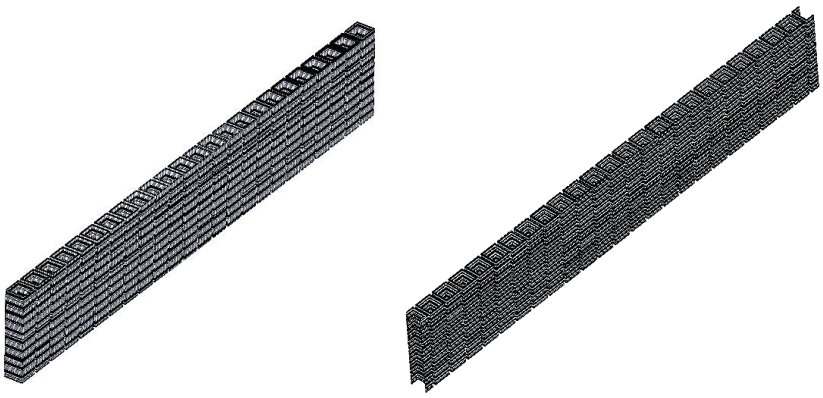

Figure 6.5: Hatch Pattern Design method with long parts to reduce the number of overall parts. The layers of each part are stacked in between each other. The right part stacks into the left part.

6.1.1.4. Forth iteration

The forth iteration was also derived from literature [155] and required the scan vectors to be orthogonal and offset between layers. The scan vectors now had to shift by 2.5 mm in the x and y directions for alternating layers. This is performed to improve the porosity and improve surface quality [155]. For this iteration Delcam PowerShape was used. PowerShape allows the user to copy and move parts easily. Users can then create parts and hide certain sections of those parts. PowerShape then allows the user to save the unhidden parts as STL files. This was advantageous as the parts could then be imported directly into the Magics software. This new process drastically reduced the number of parts to only 72 parts but this resulted in the loss of control over the way in which the laser scans the vscan tracks. When one part with 120 contour scans is exposed by the laser, the laser scans the hatch lines in an arbitrary manner.

6.1.1.5. Final iteration

The number of parts required increased again in the final iteration to 1220 parts. Since there were less parts being imported into the machine software with each iteration a certain degree of control was lost and the order in which the islands were scanned was now done randomly by the laser. This is because an entire set of hatch lines were being imported as one part and the laser would scan these vectors according to a certain preprogramed algorithm. In pursuit of optimising the STL importing and copying process for the HPD method, a model was developed in Excel. The model helps the user correctly design and place the designed hatch lines in the Magics software so that a

complete experimental sample can be produced. The model can be observed in Appendix A. For the purpose of this study the final iteration was not optimised further as it sufficed in terms of performing the experiments.

The Hatch Pattern Design method had to be tested on the M2 Cusing machine. The machine was set up and every iteration was used to expose or engrave onto a substrate on the machine and observations were made. Any problems that were identified were then corrected in the subsequent iteration.

6.1.2. Results and Discussion

The Hatch Pattern Design method improved after each iteration. Several changes and observations were made during each iteration and are discussed further. The summary of the iteration stages can be observed in Figure 6.6.

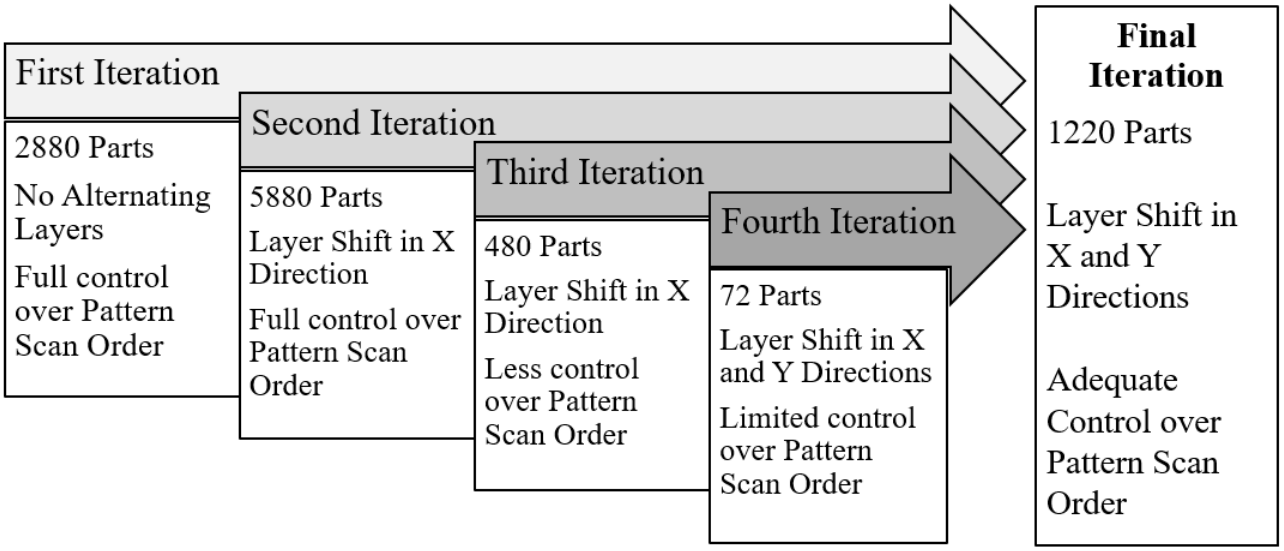

Figure 6.6: Summary of the five iteration steps taken to develop the Hatch Pattern Design method

Once each iteration had been finalised and the parts were all exported as CLS files, they had to be tested on the SLM machine. The machine was set up with just a dulled base plate so that the slices could be engraved on the plate rather than using powder and other costly resources. An example of the engraved slice on the base plate is presented in Figure 6.7.

Figure 6.7: The results of the Hatch Pattern Design method scanned with the M2 Cusing machine onto a dulled titanium base plate

The following lessons were learnt from the five iterations:

- The machine's computer was incredibly slow when a large amount of parts were loaded onto the software. This caused the machine's computer to freeze and unexpectedly end the programs. The computers needed to be upgraded in order to cope with the high processing demands. Fortunately, only the RAM on the computers needed to be upgraded, which was not a costly venture.
- The parts were exposed by the laser in the order they were uploaded onto the machine's software. This means that the user has full control over which hatch line sets, the laser scans first and in what order they should be scanned.
- One problem that was identified is the user has no control over the direction that the hatch lines are scanned. Since the contour scan is performed counter clockwise, all the hatch lines are scanned in a counter clockwise direction.
- It is of vital importance that the user set every part's laser parameters to contour scan only. If this operation is not performed the machine's software will try and create islands in each hatch part and this is a very lengthy, processor intensive task, which leads to the computer freezing.

6.1.3. Summary and Recommendations

The Hatch Pattern Design method was successfully utilised to override the machines limiting software. The scan pattern could now be changed to a user defined pattern and the user also could control how the pattern was scanned. One should note that the HPD method was not intended for complex parts or shapes but rather as a tool for research purposes, so that users can research the effects of different scan strategies when the machine limits the user.

A few limiting factors were identified and these factors are:

- The number of parts needed to be imported are directly proportional to the size of the final part, problems could occur when the part is very large, as the computers would need to process many parts.
- Rotation of the islands could prove to be very difficult with this method. It is suggested that one create the final part by copying a large array of hatch patterns and then simply cutting out the required shape in Magics. This method is labelled the Cookie Cutter method and has not been tested in this study.

6.2. Scanning Strategy Design and Development

A challenge was faced to develop a strategy that does not fall under the scope of the Concept Laser Patent [160]. If one analyses the portion of the patent that is provided in Section 3.3, they would note several defining characteristics of the Concept Laser Patent. These characteristics are:

- The layers of sintered material are melted in individual partially defined portions or Islands.
- The portions or islands are melted according to an algorithm that will only allow successive melting of a portion or island that is at a distance greater than or equal to the mean diameter of the predefined portion, from the previously melted portion. In laymen's terms the algorithm will not allow a portion or island to be melted directly next to a portion or island that was just melted.
- The melting of the portions or islands is performed in a stochastic (random) manner with the algorithm constraints.
- The melting of portions or islands is performed in such a way that the input of heat is done so in a uniform manner along the entire layer.

Mercelis and Kruth [54] found that the exposure strategy that is used to fuse the powder layers and to create the part, has a large influence on the residual stress levels in the part. It was concluded that the stresses are larger when perpendicular to the scan direction than along the scan direction. It is suggested that a subdivision of the layer into smaller sections results in a lower maximum stress value. The Concept Laser strategy helps to drastically reduce the thermal stresses in a part.

With the purpose of developing a scan strategy that reduces the residual stress in a part, several studies and the results had to be compared and the results are as follows:

- A long scan vector leads to high residual stress within the melt track and subsequently, distortion of the structure [170].
- Orientating the scan vectors, every layer reduces the residual stress [44], [157].
- Subdivision of the layer into smaller parts results in lower maximum stress values [54].
- Alternating the vector direction results in a higher density due to less un-melted zones [44].
- The helix scan strategy significantly reduces the residual stress in a part [107].
- The alternating layers should be offset and orthogonal to each other [155].
- Exposing the islands in sectors along the layer reduces the residual stress in the part [54].

The reader should take note that the above research only played a small role in the development of the scanning strategy. The design of the new scan strategy is explained in the following section.

6.2.1. Scan Strategy Design

The newly developed scan strategy has been labelled the Varying-Helix Island Scan Strategy. The helix scan strategy is a combination of the Island scan strategy, the contour scan strategy, the helix strategy and the inter layer stagger scanning strategy. Therefore, the following advantages could be expected:

The island scanning strategy affects the following properties of the part [44], [54]:

- Residual stress is reduced significantly
- Surface finish is improved

The contour scan strategy affects the following properties of the part:

- Surface finish is improved [140]
- Increases edge (edge-effect) height [141]

The helix scanning strategy affects the following properties of the part [43], [107]:

- Residual stresses and deformation in the part are reduced
- Surface finish of the part is rough

The inter-layer stagger scan strategy affects the following properties of the part [169]:

- Quality of end use part is improved
- Porosity of the part is reduced
- Improved bonding strength between layers

The newly developed scan strategy is discussed in more detail in the following sections and can be observed in Figure 6.8. Further improvement to a scanning strategy can be achieved through parameter optimisation. Residual stresses, deformation, temperature gradients and/or cooling rates are reduced by [48]:

- A high laser power
- Low scan speed
- Thicker layers
- Shorter scan vectors
- Use of preheating

In the following sections the different key strategies were developed to reduce the deviation of hybrid parts. Three strategies were suggested, two vector exposure strategies and one part exposure strategy. The vector exposure strategies encompass the style in which the vectors of the hatch and

contours are scanned. The part exposure strategy involves the manner in which the sections in a part layer are scanned.

6.2.2. Vector Exposure Strategy

6.2.2.1. Hatch fill vector scanning strategy

The first suggested strategy proposes how the vectors should be scanned and melted by the laser in order to fill or solidify the islands. There are many ways to expose the hatch vectors of an island or section in a part. Concept Laser's strategy relies on melting a complete island before moving over to another island. It is suggested by the author that the vectors be melted in a strategic way to reduce the amount of heat induced in a section. The newly developed scan strategy is displayed in Figure 6.8. The order in which the strategy is scanned was determined in the Scanning Strategy Deformation Experiment in Section 6.3.

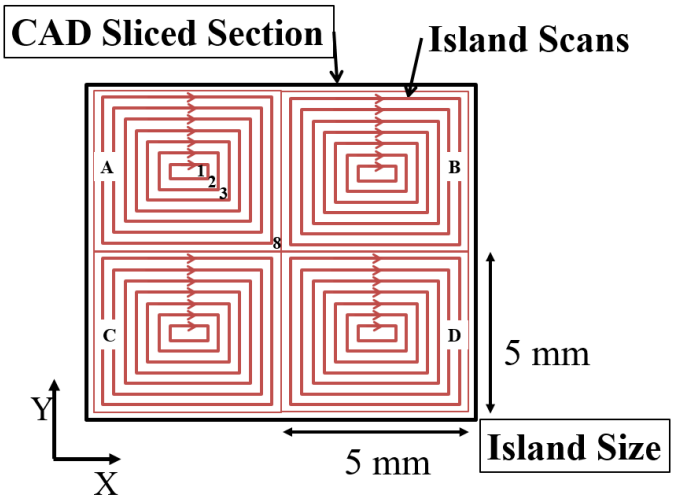

Figure 6.8: Newly developed scan strategy, which utilises the island scan strategy, the contour scan strategy, the helix scan strategy, and the inter-layer stagger strategy

With reference to the figure above, the laser will begin in island A and scan vector set 1. Once vector set 1 is scanned the laser will move to island B and scan vector set 1 and so on until all the vector 1 sets, in all of the islands have been scanned. The laser will then move over to vector set 2 and will repeat the same process as before. The laser will repeat this process until all of the vector sets in all of the islands have been scanned. This should reduce the thermal gradient and also the yield stress of the material [48]. Since the heat input from the scanned vector, which has not fully dissipated, will act as a preheating mechanism for the next scan vector that is scanned next to it. The Concept Laser island strategy melts a 5 mm x 5 mm island in roughly 0.4 s, so this results in a high thermal load over a 25 mm² area, in a short amount of time. This thermal load will be distributed amongst several islands, with the new scanning strategy. The suggested strategy will result in a lower thermal load with the largest melted area being 3 mm² and the time taken to melt this area would be 0.033 seconds.

The vector magnitudes and times are displayed in Table 6.1 below. All the vector calculations can be observed in Appendix B. The following assumptions were made for the calculations:

- The default island scan strategy is controlled by an algorithm that won't melt any islands near a previously melted island. Therefore, it was assumed that the distance of the next island would be 5 to 10 mm for a 5x5 mm island parameter. An average value of 7.5 mm was chosen for the vector length for shifting from one island to the next.
- The sum of the magnitudes of the vectors for the default strategy were calculated with the given parameters and not provided from the machine manufacturers. There could, therefore be a small discrepancy between actual and calculated.
- The scan speed is assumed to be kept constant even when the laser is off.
- The waiting times of the laser are not taken into consideration.

Table 6.1: Vector Calculations of the Default and New Scan Strategies where the vector lengths and scan times are compared.

	Units	Default	New	Percentage Difference
Magnitude of Vectors for 1 Island	mm	234.895	238.080	1.36%
Scan Speed	mm/s	600	600	0.00%
Exposure Time for 1 Island	s	0.391	0.397	1.36%
Magnitude of Vectors for 5 Islands	mm	1174.475	2152.920	83.31%
Exposure Time for 5 Islands	s	1.957	3.588	83.31%
Amount of Sections to Melt	-	24	24	0.00%
Exposure Time for 1 Layer	s	46.979	88.417	88.20%
Amount of Layers	-	333	333	0.00%
Whole Part				
Exposure Time Theoretical	s	15644.007	29442.794	88.20%
Exposure Time Theoretical	H	4.346	8.179	88.20%
Actual Exposure Time	H	4.633	9.633	107.91%

The vector magnitudes and scan times, of the default Concept Laser strategy, were compared to that of the newly developed scan strategy. One could observe that if the patterns were just scanned and no other scanning strategies were present then the percentage difference in time to scan one 5x5 mm island is 1.36% in favour of the default strategy. This time difference is not significant enough to make a substantial difference to the overall fabrication time. However, if the times for the new scanning strategy are compared to the default scanning strategy over the whole layer, the difference in time is considerable. The time for the new strategy is almost double that of the default strategy. This is due to the fact that the new strategy scans all the vectors in sections and moves from vector

to island rather than island to island. The distance covered by the laser, with the new strategy is 83.31% more than the distance of the default strategy.

Although the difference in total vector magnitudes is large, the scan speed is the deciding factor for the fabrication time. If the scan speed is doubled for the new scan strategy, the times will be the same. However, one might argue that the scan speed could then also be doubled for the default strategy. This argument would be valid, though, laser parameters have different effects with different scan strategies. Doubling the scan speed for both scan strategies could have a detrimental effect on a part's mechanical properties of one strategy, but not the other. There also could be no change in properties for one strategy whilst the change in the parameters could benefit or detriment the other.

The required properties of the part should be listed and then the applicable strategies should be decided on first, and the parameters should then be optimised accordingly. Some of the parameters that influence the time of a build are:

- Scan speed
- Scan pattern vector magnitudes
- Hatch spacing
- Layer melting strategies
- Vector scanning strategies
- Layer thickness
- Laser surface remelting

Each parameter and strategy has its advantages and disadvantages. In order to achieve a rapid fabrication time, the parameters and strategies should be optimised for time. This however, could have its disadvantages and have negative effects on the final part's mechanical properties. More time could also be spent on post processing if the incorrect parameters and strategies result in an undesirable mechanical property or the part needs to be scrapped and reworked.

6.2.2.2. Island contour scanning strategy

The next strategy is a method of joining all the islands together so that the porosity is reduced. Concept Laser uses beam compensation to connect the islands together. Beam compensation cannot be performed with the helix scan pattern. Instead it is suggested that the space between islands be zero and the space between the island vectors would be equal to the hatch spacing parameter. This strategy presented one problem, when all of the islands are joined together with the laser, the 5x5 mm scan lines now become the length and width of the part as it is scanned. All the islands now act as one part and as the part cools the islands contract and start to curl. This phenomenon was

observed in the Scanning Strategy Deformation Experiment in Section 6.3. The following strategy has been proposed to eliminate this problem. It was suggested that the outer most vector sets of the islands be scanned in a strategic manner.

From Figure 6.8 one could observe that the vector sets have been labelled from 1 to 8 and the islands have been labelled A, B, C, and D. The old method of scanning was to scan vector set 8 in all the islands one after another. This caused the islands to fuse together and act as one long melt pool, which led to a large stress build up in those vector sets. In order to counter this, the new strategy allows the laser to only scan the outer vector sets (8) that are not neighbouring each other. For example, the laser will not scan A and B at the same time but would rather scan islands A and D at the same time and after a predefined period of time the laser will then scan islands B and C. This allows the islands enough time to cool and set before they are fused together with other islands, which in turn reduced the warping of the vectors.

6.2.3. Sector Exposure Strategy

The 120 mm x 25 mm x 10 mm final part was now made up of part sectors consisting of 5 islands per sector as depicted in Figure 6.9. This sector is a set of 5 hatch line sets and this is 1 of 24 island fill vector sets.

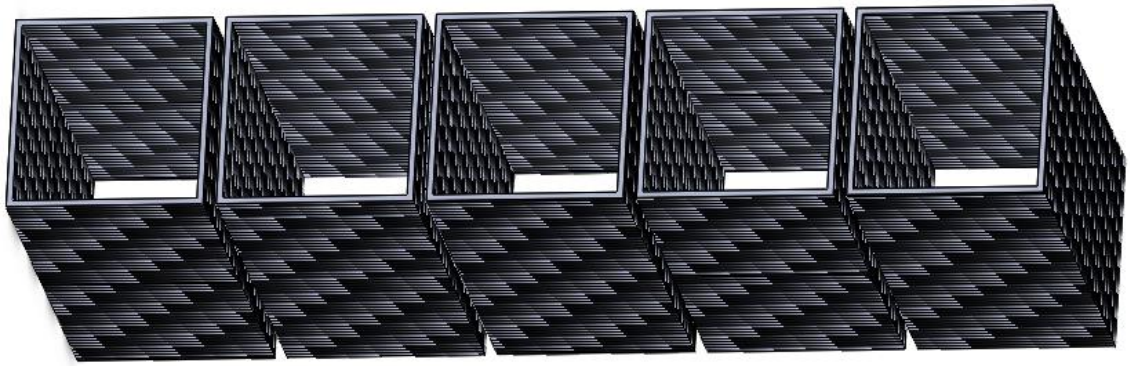

Figure 6.9: Hatch Part for Final Iteration

In order to evenly distribute the high thermal gradients during the melting process the following strategy was designed to expose sectors of the final part in a structured, incremental way. The way in which the scan strategy is exposed is shown in Figure 6.10.

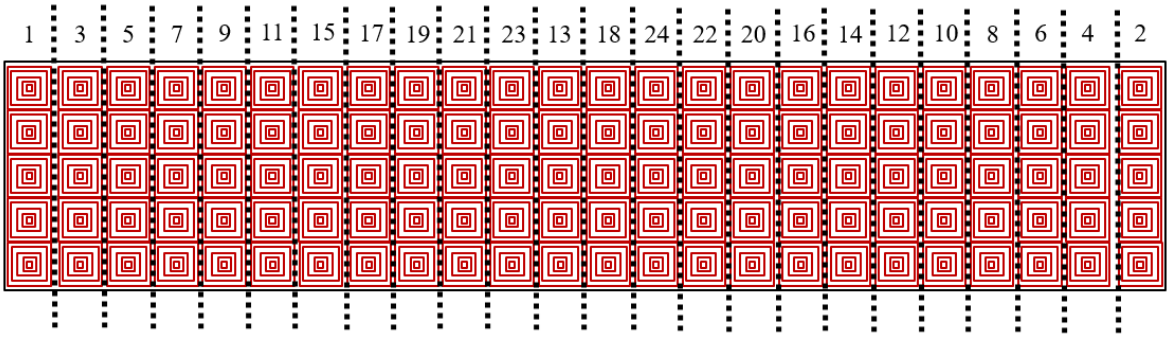

Figure 6.10: Newly developed scan strategy exposure order

One can observe from the figure that the whole part is broken up into 24, 25 mm x 5 mm sectors. The sectors are scanned by the laser in numerical order until the entire sector is completely melted before moving over to the next sector. So, the laser will scan sector 1 until the entire sector is solidified and the laser will then move to sector 2 and so on. This then allows symmetrical heat input into the layer.

6.2.4. Summary and Recommendations

A hatch scan pattern and three new scan strategies were developed, which move the newly developed scanning strategy, out of the scope of the Concept Laser Patent. Two hatch fill vector strategies were developed to reduce the geometrical deviations in a component caused by thermal stress build-up. An island contour scan strategy was also developed in order to fuse the islands together in an efficient way.

6.3. Scanning Strategy Deformation Experiment

Once the scanning pattern was decided on the scanning strategies needed to be tested. The hatch fill vector strategy, discussed in Section 6.2.2.1, was established using the following qualitative experiment.

6.3.1. Experimental Setup and Design

To test the different scan strategies, and to get a broad indication of deformation and porosity, a simple experiment was designed. Samples with the size 120 mm x 25 mm were loaded onto the machine software. An exposure slice of each of the 10 scan patterns (displayed in Figure 6.11 below) was performed on the top surface of the powder bed. Once the laser scans the top layer of the powder, the solidified layer is free to deform and move. Any warping can then be visually inspected and the island connectivity can also be determined when removing the solidified layer from the powder bed. Each pattern in Figure 6.11 is a 5 mm x 5 mm island except for pattern 6, which is a 10 mm x 10 mm pattern as the islands shift the vector orientation by 90 degrees.

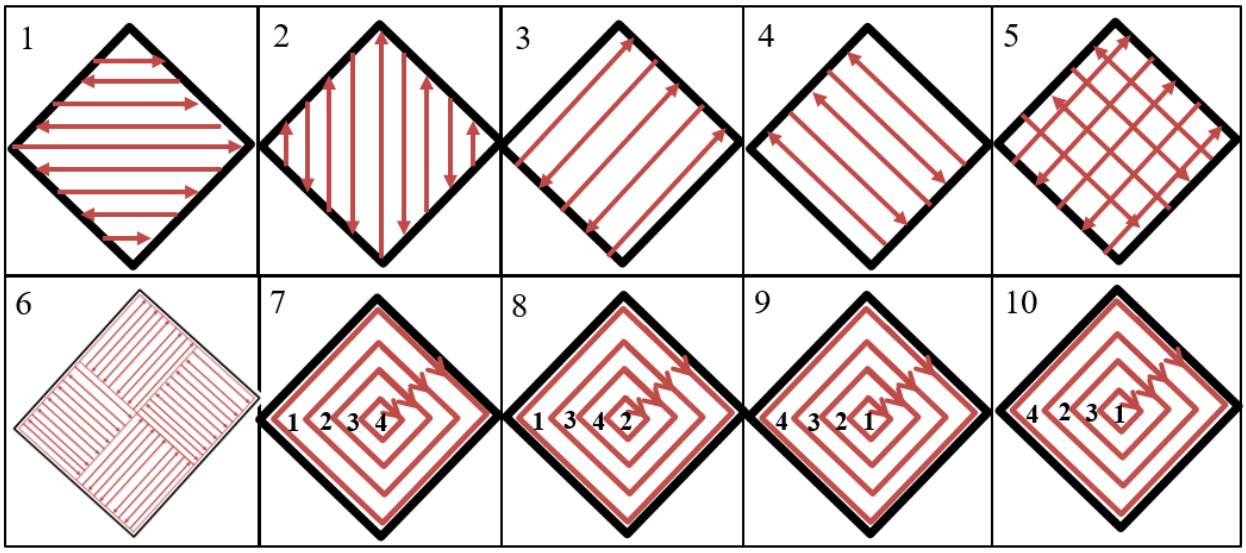

Figure 6.11: The 10 different island scan patterns used for the deformation experiment. Islands 1 to 6 are the M2 Cusing machine standard selection and islands 7 to 10 are the newly developed helix scan strategies.

One might suggest that scan patterns 1 and 2 as well as 3 and 4 are the same and that they should not all be included as variables in this experiment. However, this is not the case for two reasons, reason one being, the laser works with a galvanometric scanning system, which consists of two mirrors driven by limited-rotation motors. One mirror controls movement in the x direction and the other controls movement in the y direction. In the perfect world, there would be no difference between the two motors and thus the mirrors would rotate without error. However, errors do exist, which are caused by the movement of the mirrors and this effects the different scan strategies depending on which axis the vectors are oriented. The second reason is the scan strategy orientation

is also dependent on the part orientation. Scan strategy 1 performed on a long part oriented in the direction of the x axis is identical to performing scan strategy 2 on the same long part oriented in the direction of the y axis. However, this again is only true if the motors moving the mirrors were exactly the same.

Since the core feature of the island scan strategy is that the part is divided into small islands, these islands are connected by using a beam compensation. For the scan strategies 1 to 6, beam compensation is the length that the vector extends over the island boundary. Beam compensation can be observed graphically in Figure 6.12.

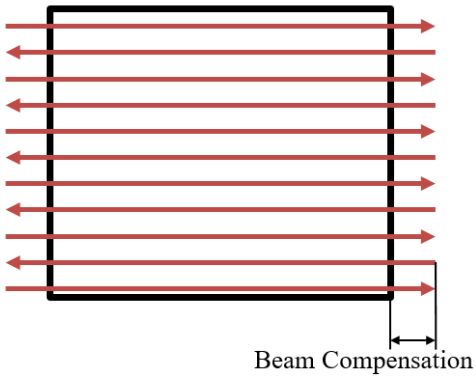

Figure 6.12: Beam compensation strategy on an Island employed by Concept Laser for scan strategies 1 to 6

In this study the beam compensation was set to a value of 0.15 mm, which is nearly 7 times greater than the default of 0.0225 mm. This was performed in order to achieve the best possible bond between islands. For the helix scan strategy the beam compensation strategy is not used, but rather the hatch fill vectors are bonded to each other. The helix scan strategy island fusing method is to be compared to the Concept Laser beam compensation method.

The terms ‘pattern’ and ‘strategy’ are cautiously used by the author throughout the paper, this is because the machine uses a strategy to melt the patterns but according to research [54], [101], [107] the hatch pattern is also referred to as a strategy. The order in which the vectors of patterns 7 to 10 are scanned varied and the vectors were scanned in the numerical order shown in Figure 6.11. Scan patterns 1 to 6 are the standard hatch fill patterns that can be selected on the M2 Cusing machine. Scan strategy 6 is the Concept Laser default strategy and is depicted as 4 islands in Figure 6.11. In order to build the single layer experimental samples on titanium alloy powder, the Concept Laser M2 Cusing machine was utilised without a base plate, using only the powder as support to allow for free movement of the melted parts. Powder was obtained from TLS Technik GmbH (Sachsen-Anhalt, Germany) and has a rated particle size distribution of 25-55 µm. The physical setup of the machine is schematically presented in Figure 6.13.

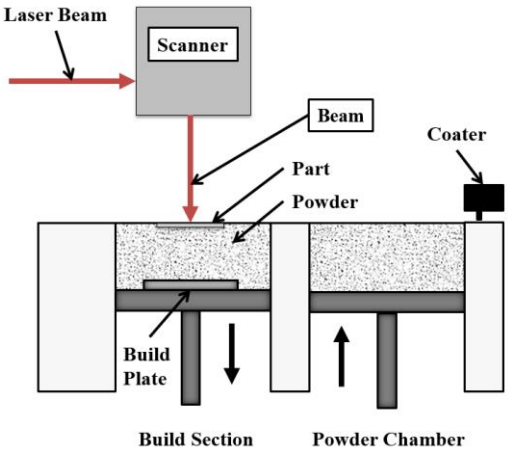

Figure 6.13: Concept Laser M2 Cusing machine setup for deformation experiment where the part is exposed onto the powder bed and not a base plate or substrate

The laser power was set to 100 Watts with a scan speed of 600 mm/s and a focus diameter of 0.15 mm. The hatch spacing was set to 0.105 mm and the fan speed was kept constant for each sample run at 65%. An exposure slice of each scan strategy was performed on the top surface of the powder bed. Once the laser scans the powder, a melt pool is created with the exposed powder. The powder melts as the material's melting temperature is reached. The heat is then dissipated with conduction through the powder below and with convection through the gas in the build chamber. If the temperature of the conducted heat is above the melting temperature of the powder, the powder particles will melt into the originally scanned melt pool and form a thick layer of melted powder on the bottom surface.

The material in the melt pool is expanded to a certain degree (depending on the material's coefficient of thermal expansion) due to the high temperature. Once conduction and convection take place the material slowly cools and contracts. The top surface of the exposed layer, which undergoes a convection process to the gas in the chamber, contracts at a much faster rate than the bottom surface, which is insulated by the powder/previous layer and only loses heat through conduction and minimal convection. It is during this occurrence that the scanned layers tend to curl and warp upwards.

The exposed scans were visually inspected for warping and different deviation problems. A qualitative approach was taken. The following criteria was used when analysing the scans on the powder bed. A decision matrix (Table 6.2) was used with a rating scale of 1 to 3. The scan strategies with highest scores were the most desirable. The criteria are:

1. There is warping of the part out of the powder bed. Rating scale (1 = warping, 3 = no warping out of the powder)

2. There is warping of an island out of the powder bed. Rating scale (1= more than the corner warped out of the powder, 2 = the corners of the island warped out of the powder but the island shape was still intact, 3 = there was no warping of the islands)
3. The interconnectivity between the islands is not sufficient. Rating Scale (1 = The whole part broke up into its individual islands, 2 = One or more islands stayed connected to each other, 3 = the whole part stayed together when being removed)
4. The interconnectivity between the island hatch vectors is not sufficient. Rating Scale (1 = The islands broke up when being removed, 2 = the islands remained intact when being removed with one or more exceptions, 3 = all of the islands remained intact when being removed)

Table 6.2: Decision Matrix used to rank the scan strategies according to set criteria

	Scan Strategy Number									
Criteria	**1**	**2**	**3**	**4**	**5**	**6**	**7**	**8**	**9**	**10**
1										
2										
3										
4										
Total										

Criteria 1 gives an indication of the melting of the islands and the solidification and cooling effects on the warping of the sample. If warping is present in the sample, this would give an indication that there is a larger residual stress built up in the sample than a sample that has not warped. Criteria 2 similarly to Criteria 1 gives an indication of the residual stress build up but rather in the individual islands. Criteria 3 gives an indication of the bond strength between the islands of the sample. If the islands separate, then a weak bond is indicated. However, if the sample remains intact during the removal process, then a strong bond between the islands is indicated. Criteria 4 gives an indication of the bonds between the hatch vectors of each island. If the islands fall apart when removed, then a weak bond is present between the hatch vectors.

6.3.2. Results and Discussion

The images in Figure 6.14 display the samples created in the experimental runs. Each scan strategy was scanned onto the powder bed in a random manner. The experiment was repeated three times to ensure that the results were accurate. Once the scans were performed, two experimenters made observations on the deviation of the layers and islands. The results were compared and tabulated. The removal of the layers was also observed. A pair of pliers were used to gently shift the parts onto a platform without damaging them. Some parts were not joined at all and had to be removed island

by island and others could be removed without disintegrating. The selection of scan strategies on the M2 Cusing machine from Concept Laser GmbH can be observed in Figure 6.14 below.

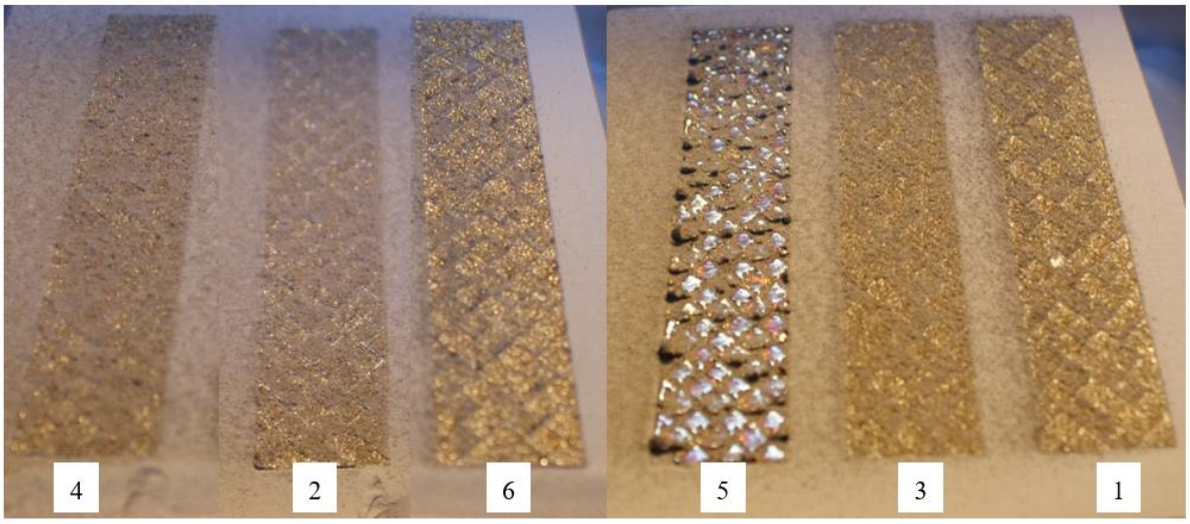

Figure 6.14: Selection of 6 scan strategies on M2 Cusing machine exposed as a single layer onto powder without a base plate

From the figure above the samples from the standard selection of scan strategies on the M2 Cusing machine can be observed. One should take note that the islands from scan strategy 5 are curling out of the powder bed. This is because the laser exposes each island, twice, consecutively. This induces high thermal stresses in the island, which causes it to curl upwards. When attempting to remove the 6 Concept Laser standard samples all the samples broke up into individual islands. Some islands were still bonded to each other but the whole layer could not be removed intact. This could be an indication that the beam compensation strategy employed by Concept Laser is not optimal. An example of how the layers broke up is depicted in Figure 6.15.

Figure 6.15: Island Scan Strategy 6 attempt at removing the sample from powder bed

The individual islands of Scan Strategy 6 can be observed in Figure 6.15. This is an indication that the bonds between the islands are not adequate. These results were observed for all the standard Concept Laser scan strategies. Different results were observed for the four helix scan strategies and are discussed below. The experimental samples from the newly developed scan strategies experimental runs can be observed in Figure 6.16.

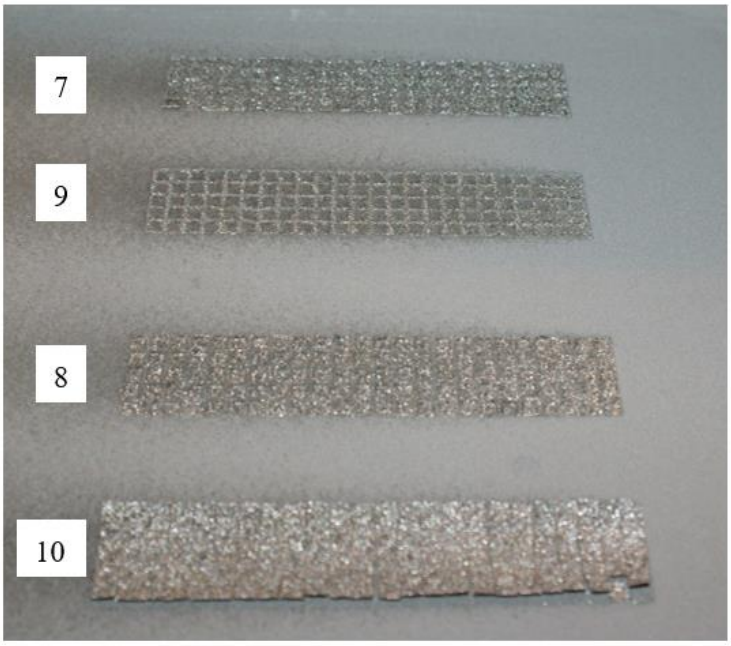

Figure 6.16: Newly developed helix scan strategies exposed as a single layer onto powder without a base plate (Photo taken from a different angle to show warping)

The samples from the newly developed scan strategy all varied depending on the melting sequence that was used. One can observe how each helix scan strategy differs visually from the next. This indicates that the order in which the vectors of a scan pattern are melted, could have a significant effect on the mechanical properties of a part. This suspicion would still need to be proven statistically with quantitative results and will not be done in this study. If one inspects Figure 6.16 by scan strategy 10 they would note that the islands have all warped from the powder bed. Scan strategies 7 and 8 also displayed some warping of the individual islands. The results from the experiments are tabulated in Table 6.3.

Table 6.3: Decision Matrix of the different Scan Strategies used to analyse each strategy against the set criteria discussed in Section 6.3.1

	Scan Strategy Number									
Criteria	**1**	**2**	**3**	**4**	**5**	**6**	**7**	**8**	**9**	**10**
1	3	3	3	3	3	3	3	3	3	1
2	3	3	3	3	1	3	2	2	3	1
3	2	2	1	1	2	2	3	2	3	2
4	2	2	2	2	3	2	2	2	2	2
Total	10	10	9	9	9	10	10	9	11	6

From Table 6.3 it can be noted that scan strategy 9 had the best results followed closely by scan strategies 1, 2, 6, and 7. The deciding factors were the interconnectivity between the islands and vectors, where scan strategy 9 faired best. This is because when removing sample 9 from the machine, the sample remained intact. While using the same level of caution when removing the other samples, they would all tend to fall apart as shown in Figure 6.15.

6.3.3. Summary and Recommendations

A qualitative comparison of 10 different scan strategies was performed on the Concept Laser M2 Cusing machine. Newly developed scan strategy 9 faired best with scan strategies 1, 2, 6, and 7 in close second. Since scan strategy 6 is the M2 Cusing machine's default strategy, for the remainder of this study scan strategy 6 and newly developed strategy 9 were compared to each other with regards to different properties and shortfalls.

The beam compensation strategy employed by Concept Laser to fuse islands together has certain downfalls in terms of porosity and bonding strength. A new method where the hatch vectors fuse the islands together was proposed and tested. The helix scan strategy 9 showed the most promising results. The entire sample remained intact when removed, indicating strong bonds between the islands. Even though the scanning pattern of strategies 7, 8, 9, and 10 are the same, the way in which the vectors were melted affected the final part.

6.4. Substrate Experiment

To get a closer inspection of each island scan pattern an experiment had to be designed. Beneficial to proper inspection of the islands it was proposed that the islands be scanned on a substrate with a single layer of powder.

6.4.1. Experimental Setup and Design

The aim of this experiment was to determine if the quality of the hatch scan melt pools for the newly developed scan strategy was acceptable. The hatch scan melt pools and islands were analysed on a microscopic level and the default and newly developed strategies were compared to each other in terms of gaps between islands and island appearance.

6.4.1.1. Machine setup

A 1.2 mm thick Ti-6Al-4V plate had to be cut into smaller plates with dimensions 70 mm (L) x 35 mm (W) x 1.2 mm (H). These plates were attached to the Concept Laser M2 Cusing machine's base plate with insulation tape as depicted in Figure 6.17. This experiment did not require the scans to be correctly positioned on the substrates as only the island's qualities were to be inspected and not the warping of the substrate.

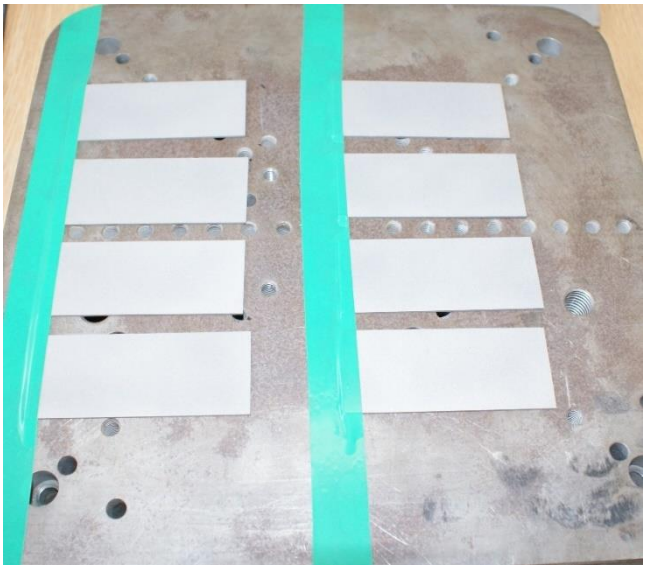

Figure 6.17: Ti-6Al-4V plates attached to the SLM machines build plate with insulation tape

The base plate was then placed in the M2 Cusing machine and was tightly screwed to the machine's build plate. The coater blade was aligned to the base plate and the base plate was referenced to zero. The Ti-6Al-4V ELI powder from TLS Technik was sieved into the powder chamber and the base plate was then coated with a layer (approximately 30 µm thick) of powder. The powder bed was then moved to the process chamber and the chamber was filled with Argon gas.

6.4.1.2. Process parameters

The recommended default process parameters by Concept Laser were used for this experiment. These parameters (Table 6.4) are not the optimal parameters, since changing different parameters, lead to different material properties. Subsequently the scan strategies were the only variable, these parameters were kept constant throughout the duration of the experiment.

Table 6.4: Default process parameters for the M2 Cusing machine recommended by Concept Laser GmbH

Machine Parameters			
Parameter	**Value**		
Coater Blade Type	Flexible Rubber Blade		
Layer thickness	30 µm		
Fan Speed	65%		
Cusing Process Parameters			
Exposure Sequence	Vectors then Contours		
Powder delivering height correction factor	180%		
Laser Parameters			
Parameter	**Units**	**Skin**	**Contours**
Power	Watts	100	100
Speed (sp)	mm/s	600	600
Focus/Spot Diameter (d)	mm	0.15	0.15
Operation Mode	-	Continuous	Continuous
Hatch Spacing (a1)	mm	0.105	0.105

6.4.1.3. Scan strategies

The two scan strategies that were utilised for the experiment were the default island strategy 6 and the newly developed scan strategy 9 from the deformation experiment in Section 6.1. Scan strategy 9 was chosen as the results indicated that it was the most suited strategy in comparison to the other newly developed helix scan strategies. The two scanning strategies are displayed in Figure 6.18.

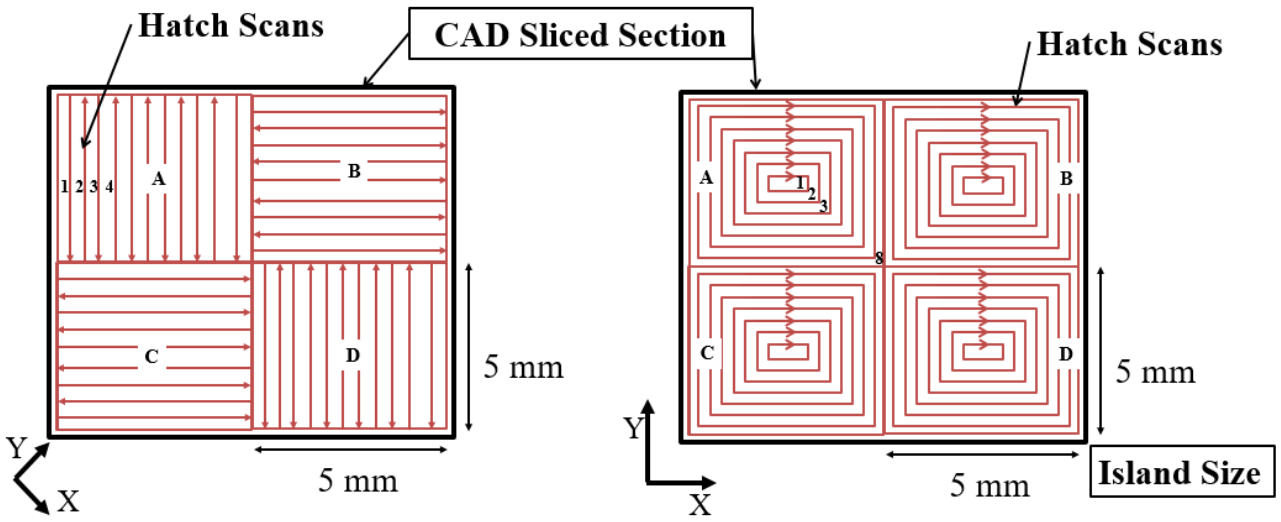

Figure 6.18: (Left) Default island scan strategy (Right) Newly developed scan strategy

The scanning methods used to expose the default and newly developed scan strategies are discussed in Table 6.5

Table 6.5: Concept Laser default and newly developed scan strategies explained

	Concept Laser Scan Strategy	**Newly Developed Scan Strategy**
Vector Scan Pattern	Alternating Scans	Helix Scans
Vector Scan Strategy	Scans each vector of the island until the island is completely scanned	Scans one vector set of one island then moves to another island and scans one vector set and so on, for 5 islands
Islands Bonding Method	Beam Compensation	Hatch Spacing Fusing
Layer Scanning Method	Stochastic Scanning of Islands so that the heat is evenly distributed along the layer	Structured scanning of islands in order to evenly distribute heat along the layer

6.4.1.4. Microscopic evaluation

A program called Stream Essentials was utilised together with an Olympus SZX7 stereo microscope. The view from the microscope was replicated on the computer screen and the Stream Essentials computer software allows the user to measure the item displayed on the screen. Each island was observed using the Stereomicroscope and the GX 51 inverted microscope and were qualitatively analysed. The hatch scans of the newly developed strategy were measured using the Olympus GX51 inverted microscope and these results were quantitively analysed.

A sample set of 3 islands were analysed from each sample. These islands were randomly selected and the entire island was inspected under the Stereomicroscope. The joint between four islands was also inspected and comments were made. The hatch scan quality of the newly developed scan strategy was inspected by measuring the hatch spacing of six hatch melt pools for each of the three

samples. The hatch melt pools were selected randomly and measured twice in order to get an average for each hatch spacing. The actual hatch spacing achieved was compared to the theoretical hatch spacing of 105 µm.

6.4.2. Experimental Results and Discussion

The experimental samples that were produced on the Concept Laser M2 Cusing machine can be observed in Figure 6.19 below.

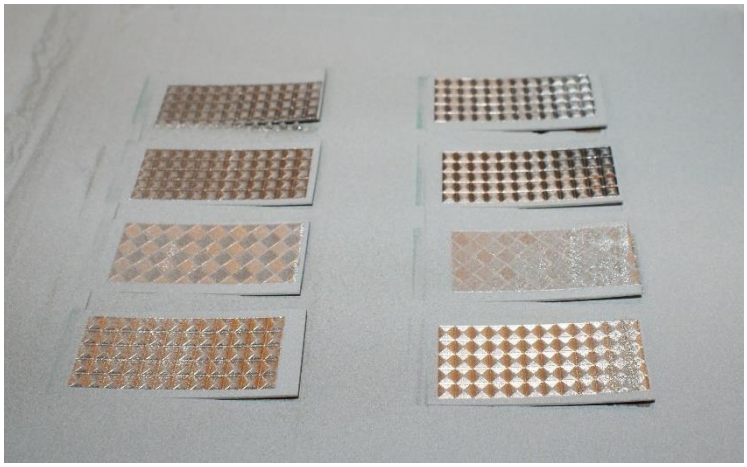

Figure 6.19: Substrate experimental samples produced on the Concept Laser M2 Cusing machine

One could note that the samples all curled out of the powder bed. This is a clear indication of the deviation that is caused by residual stress build-up.

6.4.2.1. Analysis of island appearance

The island appearance was analysed using the Olympus SZX 7 Stereomicroscope. An example of the islands from the two different scanning strategies can be observed in Figure 6.20.

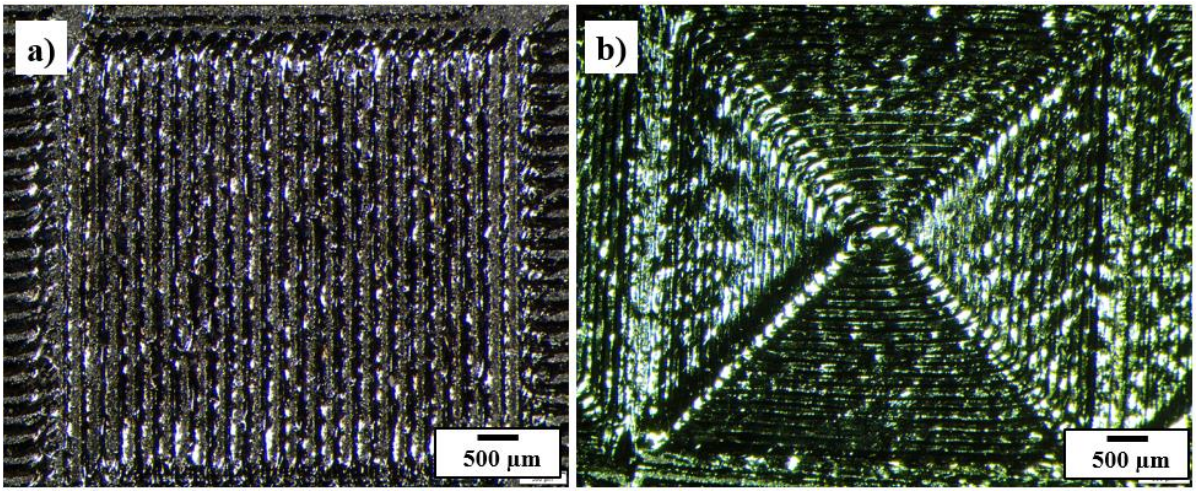

Figure 6.20: Pictures of (a) Default Scan Strategy Island and (b) Newly Developed Scan Strategy Island taken with the Olympus Stereo Microscope

From the figure above the user can observe that, in both scan strategy samples, the islands are not adequately fused together. There is a clear gap around each island which indicates that the island

bonding strategies are not adequate. One of the changes that can be recommended for the newly developed scan strategy is to optimise the distances between the islands so that the distance is equal to the hatch spacing. The joint of four islands on the samples were then compared visually using the Olympus GX 51 inverted microscope. An example of these islands can be observed in Figure 6.21.

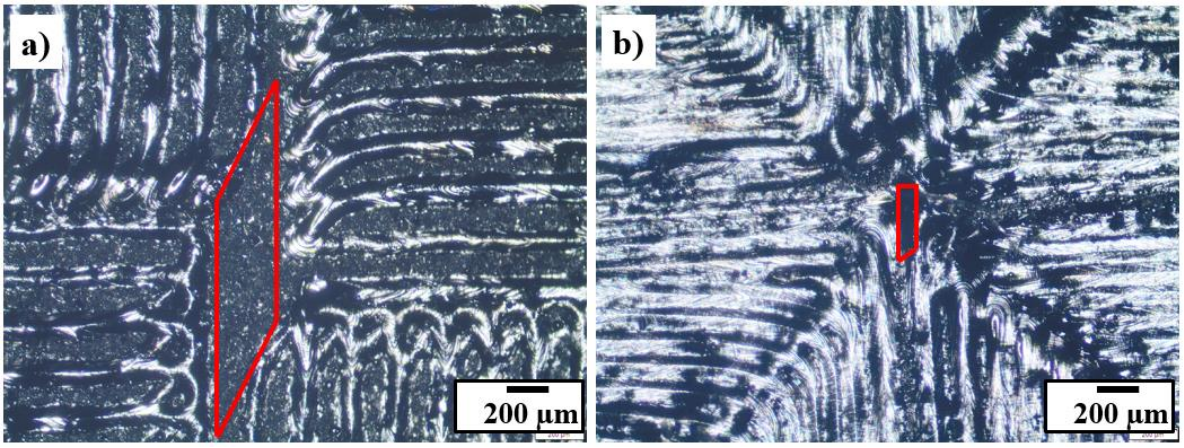

Figure 6.21: Pictures of the joint between four islands for (a) Default Scan Strategy and (b) Newly Developed Scan Strategy taken with the Olympus Inverted Microscope, Size difference highlighted with red lines

From the figures above one could observe the large gap present between the four islands on the default strategy samples. The gap between the islands on the new strategy samples is visually smaller. Large gaps in the layers could lead to porosity problems which will be analysed in the porosity experiment in Section 7.1. One should also take note of the hatch lines which loop at the boundaries of the islands in the default strategy islands. This could also lead to the introduction of keyhole pores which would also increase the porosity. All of the images from this experiment can be observed in Appendix C.

6.4.2.2. Analysis of hatch quality

The quality of the hatch scans of the newly developed strategy was inspected using the Olympus GX51 Microscope. A picture taken using the Stream Essentials software with 2 measurements can be observed in Figure 6.22 below:

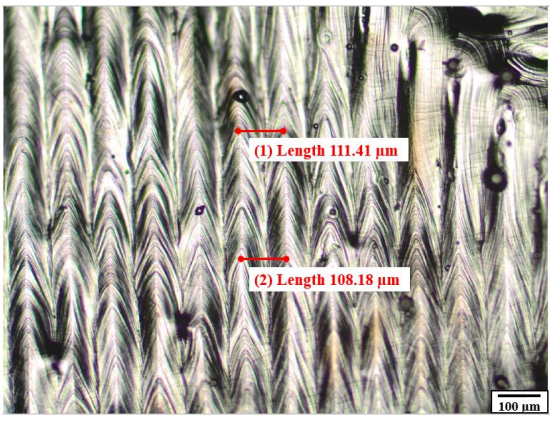

Figure 6.22: Newly developed scan strategy hatch scans observed and measured using an Olympus GX51 Microscope and Stream Essentials software

The measurements were only tabulated after all of the readings were taken in order to discourage any experimenter bias. The readings were taken at random and different islands were also chosen at random. The results from the measurements are shown in Table 6.6.

Table 6.6: Results of the Hatch Scan measurements of the newly developed scan strategy

	Island Number	Reading 1 [µm]	Reading 2 [µm]	Average [µm]
Sample 1	**1**	108.19	101.83	105.01
	2	105.69	102.50	104.10
	3	99.22	111.41	105.32
	4	111.41	108.18	109.80
	5	105.69	115.24	110.47
	6	116.52	118.42	117.47
	Average	107.79	109.60	108.69
	Std. Dev.	5.86	6.72	5.05
Sample 2	**1**	88.14	87.32	87.73
	2	89.24	91.20	90.22
	3	106.40	105.15	105.78
	4	124.44	114.27	119.36
	5	100.68	98.33	99.51
	6	97.92	84.52	91.22
	Average	101.14	96.80	98.97
	Std. Dev.	13.35	11.40	12.04
Sample 3	**1**	118.41	116.51	117.46
	2	119.80	129.48	124.64
	3	106.69	111.54	109.12
	4	90.75	89.55	90.15
	5	104.70	105.52	105.11
	6	108.07	111.89	109.98
	Average	108.07	110.75	109.41
	Std. Dev.	10.56	13.14	11.72
Total Average		105.66±10.31	105.71±12.02	105.69±10.70

From Table 6.6 above one can observe that the total averages for all of the readings is equal to the designed hatch spacing of 105 µm. This is a clear indication of the laser accuracy when scanning the helix scan strategy. The graph of the average of the hatch spacing readings per sample is displayed in Figure 6.23.

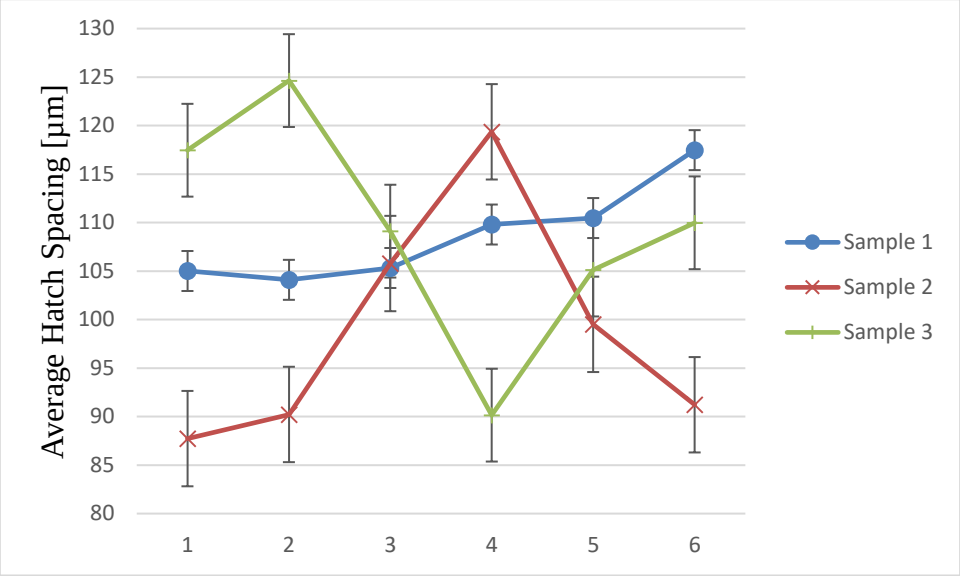

Figure 6.23: Graph of average hatch spacing for each sample with random islands

One could observe from the graph that the hatch spacing measurements all deviate around the theoretical hatch spacing of 105 µm. Some of the outliers fall below the theoretical value which could lead to porosity problems. It is therefore suggested that the hatch spacing be decreased, which could reduce the residual porosity in the samples. This however, will not be performed in this study as it falls outside of the scope. This will be included in future work.

6.4.3. Summary and Recommendations

The islands of the two scan strategies were compared and the appearance of each were analysed. The hatch spacing of the newly developed scan strategy was measured and compared to the theoretical value that was selected as a parameter. Recommendations were made on how to improve the island quality of the newly developed scan strategy going forward.

With the Raster scan, on the default scan strategy, it was noted that the laser continues to melt outside of the 5 mm x 5 mm island to connect the islands with the beam compensation. The problem that was noted is that when the laser turns around to melt the next vector, a keyhole pore is formed. This leads to a porosity on the outside of the island and could be detrimental to the part's mechanical properties. It is suggested that a turnaround strategy be used where the laser is turned off before moving to the next vector. This strategy is referred to as working with ghost vectors or skywriting [48].

6.5. Chapter Conclusion

A method to override the Concept Laser M2 Cusing machine's software was developed. The Hatch Pattern Design method makes use of CAD software in order to design a specific scan pattern. The

designed parts that make up the pattern, can then be imported into the M2 Cusing machine's software, in the order the user requires the vectors to be scanned.

A scan strategy was designed through the use of thorough research. The strategy was a combination of many different strategies that resulted in less residual stress build-up. All of the strategies used have certain advantages and disadvantages. The newly developed scan strategies were then tested.

Several strategies were then compared to each other through exposing the strategy onto the powder bed without a substrate. The parts on the powder bed were free to warp and deviate, as there was no interference from a substrate. Observations were made about the deviation and bonding strengths between the vectors and islands.

The default scan strategy and the best strategy from the deformation experiment were then compared. Both strategies were exposed onto a substrate and the quality of the hatch was inspected. The newly developed strategy visually had better features than the default strategy.

Chapter 7
Validation of Scan Strategy

7.1. Porosity Experiment

One of the challenges faced by the SLM technology is that the parts produced are not 100 % dense and contain a fraction of porosity. Most studies utilise parameter optimisation to reduce the porosity during the process [56]–[60]. It is suggested by the author that scan strategy optimisation should be utilised first in order reduce the porosity of parts.

7.1.1. Experimental Design

The porosity experiment can be divided into three steps. The first is the manufacturing of the samples on the Concept Laser M2 Cusing machine. The second step is the measuring of the porosity on a microCT scanner. The third and final step is the statistical analysis of the results. The summary of the experimental steps are displayed in Figure 7.1. The detailed setup can be observed in Appendix E.

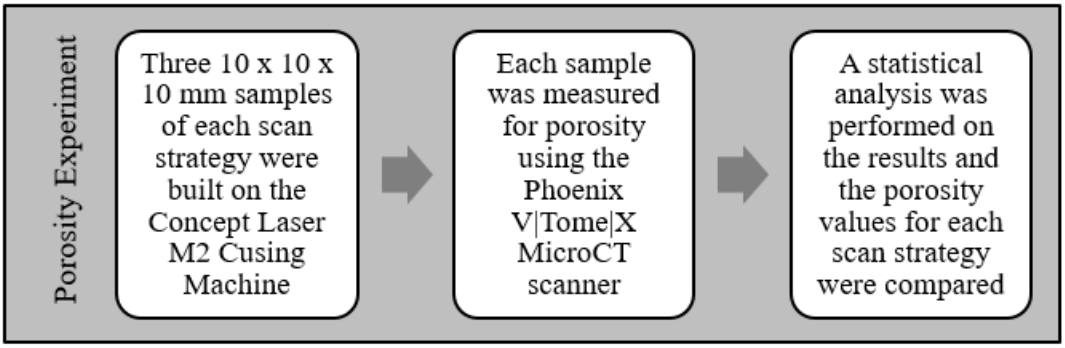

Figure 7.1: Experimental Design summary for the porosity experiment

7.1.1.1. CT scanning of samples

A CT scanner was used to determine the porosity of the samples produced with SLM. A General Electric Phoenix V|Tome|X L240/NF180 X-ray micro computed tomography (microCT) machine was utilised. The X-ray settings were 160 kV and 100 microA, 2000 images were acquired in a full rotation at image acquisition time of 500 ms per image, with no averaging and no skipping of images. The detector shift was activated to minimize ring artefacts. Background calibration was performed and the scan time was approximately 40 minutes per scan. Reconstruction was done with the system-supplied Datos reconstruction software. Analysis was performed with Volume Graphics VGStudio Max 2.1 or Visualization Sciences Group Avizo Fire 8.0 commercial 3D analysis software packages. The analysis of the CT scans was performed by the Central Analytical Facilities at Stellenbosch University.

7.1.1.2. Statistical analysis

A two-tailed Student t-Test with assumed equal variances, for independent samples, was performed (alpha = 0.05) to determine if a significant difference exists between the obtained porosity values from the different strategies. Therefore, the null hypothesis was set that all specimens are from the same population, this means $H_0: \mu_1 = \mu_2$ and the alternative hypothesis $H_1: \mu_1 \neq \mu_2$. Thus, rejection of the null hypothesis would imply a significant difference between the strategies.

7.1.2. Results and Discussion

Once the samples were built and analysed in the CT scanner. The results were compared and tabulated. The 3D renderings and porosities from the CT scans can be observed in

Table 7.1.

Table 7.1: CT Scan results and comparison between the two scanning strategies

Default Control Scan Strategy	Helix Island Scan Strategy
Sample 4 – 0.68% Porosity	Sample 1 – 0.42% Porosity
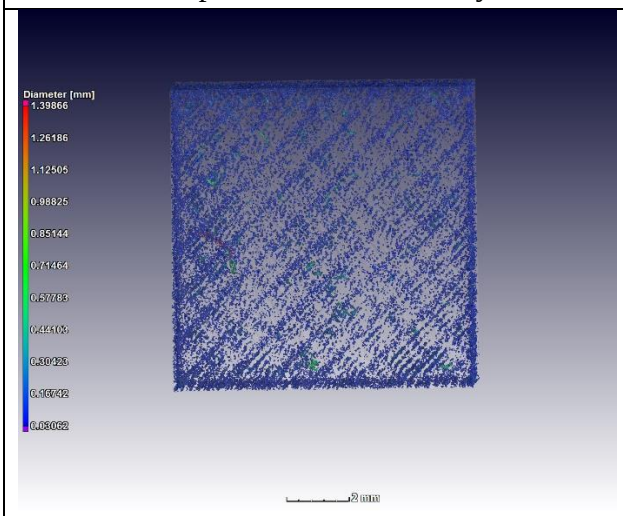	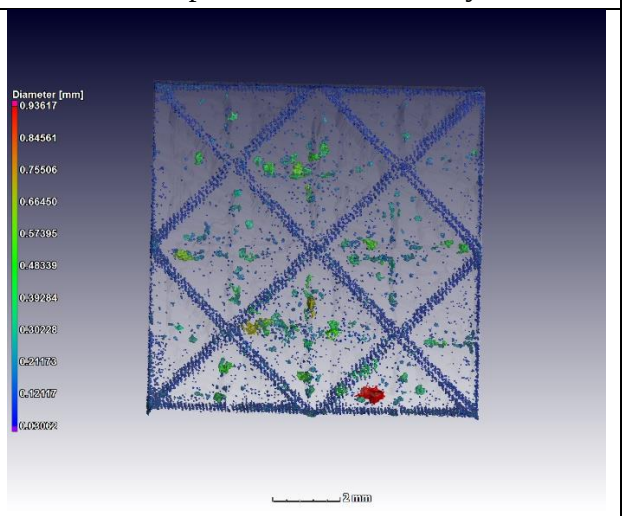
Sample 5 – 0.71% Porosity	Sample 2 – 0.39% Porosity

<table>
<tr><td> 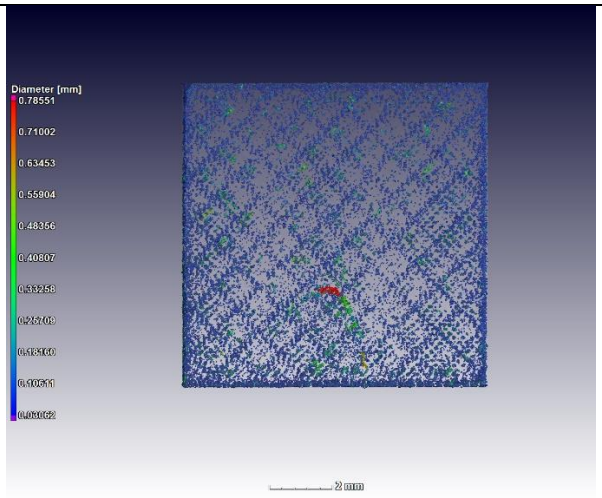
</td><td> 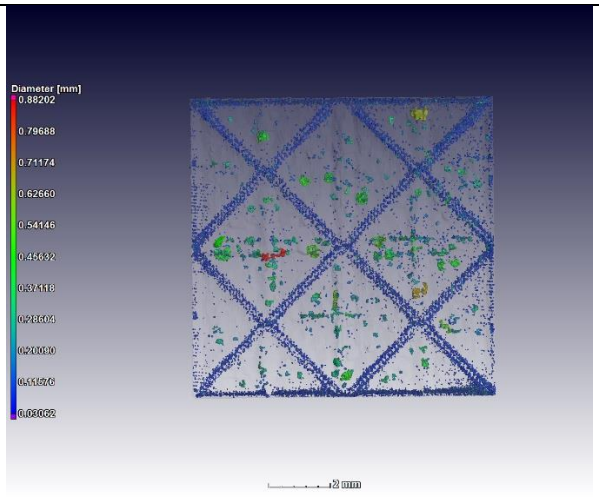
</td></tr>
<tr><td>Sample 6 – 0.83% Porosity</td><td>Sample 3 – 0.43% Porosity</td></tr>
<tr><td> 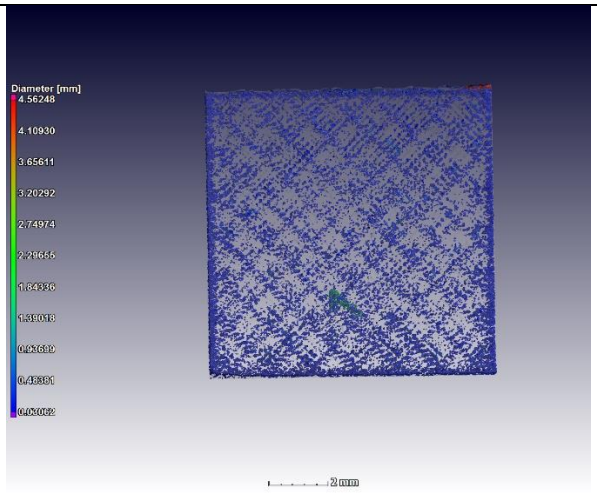
</td><td> 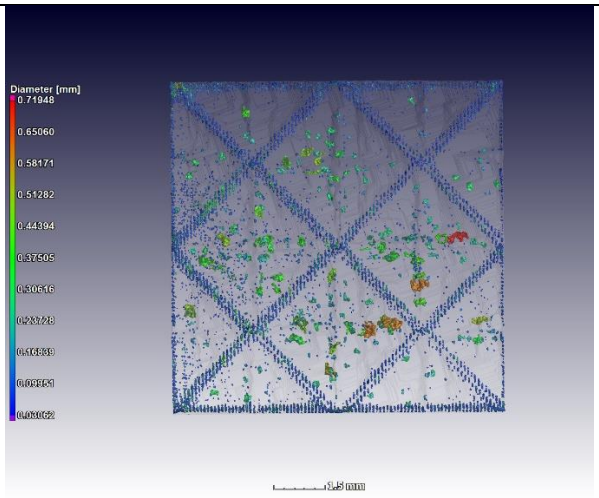
</td></tr>
<tr><td>Average</td><td>0.740%</td><td>Average</td><td>0.413%</td></tr>
<tr><td>Standard Deviation</td><td>0.079%</td><td>Standard Deviation</td><td>0.021%</td></tr>
</table>

One can observe from the table above that the porosity in the default strategy samples is larger than the new strategy samples. One can note an average decrease in porosity of 44.19% between the default strategy samples and the new strategy samples. A graph showing the porosity for each sample can be observed in Figure 7.2.

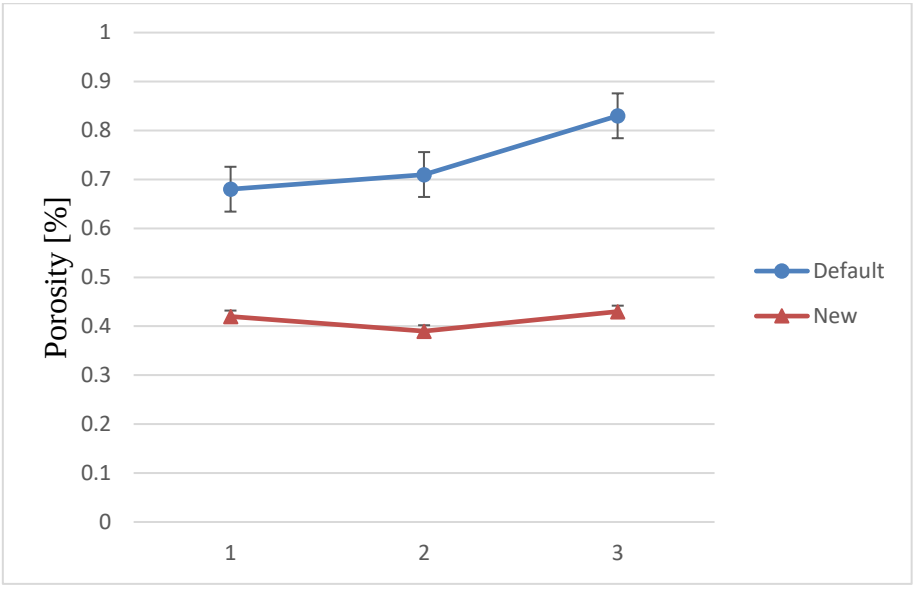

Figure 7.2: Graph of porosity percentage of the 6 samples which compares the new and default strategies on the Concept Laser M2 Cusing machine

From the figure above one should take note of the error bars. The default strategy results varied substantially for each sample. This could be attributed to the stochastic method of melting the islands which the strategy employs. The porosity values of the new strategy samples do not vary noticeably. A two-tailed Student t-Test (Appendix D) was conducted. The null hypothesis was rejected and there is a significant difference ($p = 0.0023$) between the default and new strategy with regards to porosity. The difference in standard deviation could be attributed to the fact that the newly developed strategy is structured and each part was scanned with the exact same hatch pattern and strategy therefore the standard deviation is small. However, the default scan strategy is a stochastic process and thus no two parts will have the same layers, so the standard deviation is larger.

Considering that the only factor that was varied was the scan strategy, this implies that the newly developed strategy yields a more consistent porosity volume per specimen. It could be attributed to the fact that the newly developed strategy has a different island bonding method, which utilises the entire length of the vector to bond with another vector, rather than just overlapping the islands with a beam compensation.

7.1.3. Summary and Recommendations

A comparison of the porosity of samples produced using the default and new scan strategies was performed. The use of the newly developed scan strategy resulted in samples with significantly less porosity than the samples produced using the Concept Laser default scan strategy. The porosity can be further improved by performing a parameter optimisation experiment using the Helix island scan strategy, but this falls outside of the scope of this study and will form part of future work.

7.2. Deviation Experiment

7.2.1. Experimental Design

Warping or curling of parts produced by SLM is a challenge for the application of SLM to manufacture hybrid parts. Warping is caused by the high residual stresses that are induced during the melting and solidifying process [44], [54], [59], [86], [107]–[109]. To determine whether changing the scan strategies would affect the geometrical deviation of hybrid parts manufactured by SLM, on the Concept Laser M2 Cusing system, the following experiment was designed and the process steps can be observed in Figure 7.3 below. The experimental parameters can be viewed in Appendix F.

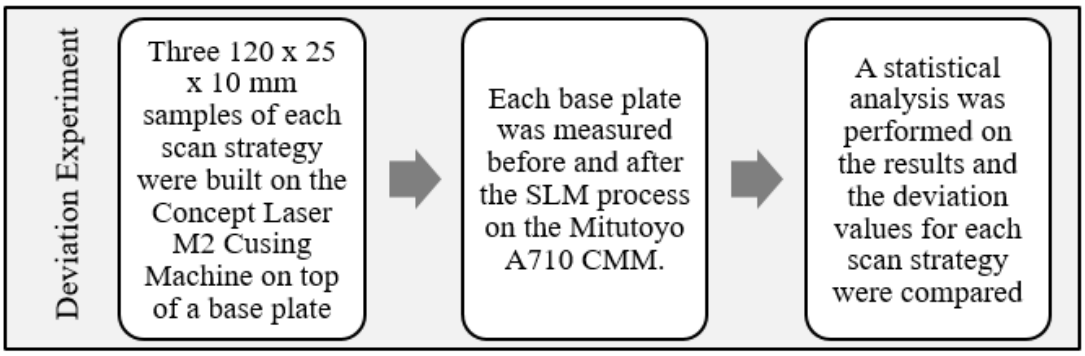

Figure 7.3: Experimental Design summary for the deviation experiment

The objective of this experiment was to determine whether using the newly developed scan strategy is in fact significantly better, in terms of geometrical deviation (warping), than the patented default strategy from Concept Laser GmbH.

7.2.1.1. Sample Preparation

To create a hybrid part there needs to be a section of the part that has been produced with a subtractive manufacturing process and a section that has been produced with an SLM process. Eight (2 spare) titanium alloy base plates of equal geometry were stress free and annealed before the SLM section was built on them with the Concept Laser M2 Cusing machine. The base plates were cut from an annealed billet of Ti-6Al-4V ELI with dimensions 120 mm (L) x 25 mm (W) x 20 mm (H). The billet was cut in half using an Agie Charmilles CA20 EDM wirecut machine to produce billets with dimensions 120 mm (L) x 25 mm (W) x 10 mm (H). To attach the Ti-6Al-4V billets to the Concept Laser SLM machine, an M8 hole had to be drilled and tapped into each one. The holes were drilled and tapped using the DMG Mori DMU 65 Monoblock 3-Axis Milling Machine with a 6.8 mm diameter Somta drill and M8 Somta Tap specified for titanium alloys. The hole was drilled in the centre of the billet in order to promote warping of the part during the SLM process. The M8 screw should not interfere with the warping of the material as it is expected that the bending

moment caused by the residual stress should act around the centre of the billet. Once machining was completed the billets were referred to as base plates for the SLM process. It is expected that the base plates experience compressive stresses along the top surfaces and tensile stress along the bottom surfaces.

7.2.1.2. Pre SLM base plate measurements

Before the SLM process took place, the Mitutoyo Bright A710 coordinate measuring machine (CMM) was used to measure each base plate, which were then marked from 1 to 8. This was done as the machining could have caused some error and the base plates are not perfectly flat to begin with. The CMM tool path was 5 lines each with 45 data points. The origin of the part was set to the centre of the hole and the deviation was measured. The CMM axis, origin, and tool path lines can be observed in Figure 7.4.

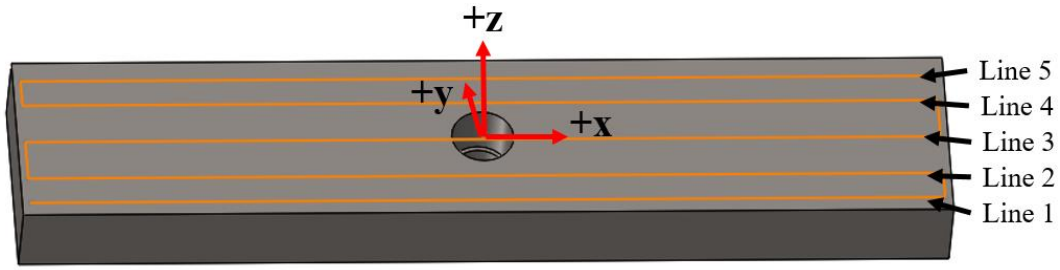

Figure 7.4: Coordinate measuring process of the base plates before use in the SLM process to accurately determine the warping after the SLM process

7.2.1.3. Machine setup

Once the measurement process was completed, the base plates were then sand blasted and demagnetised. The plates were all cleaned in an ultrasonic cleaner. The plates were cleaned in acetone, then 90% pure ethanol, then deionised water to remove any residue left on the base plates. The base plate was then screwed onto the building plate by using one M8 screw. New screws were used for each build and the screws were all tightened to the same torque using a torque wrench. The orientation and setup of the base plate on the build plate of the M2 Cusing machine can be observed in Figure 7.5.

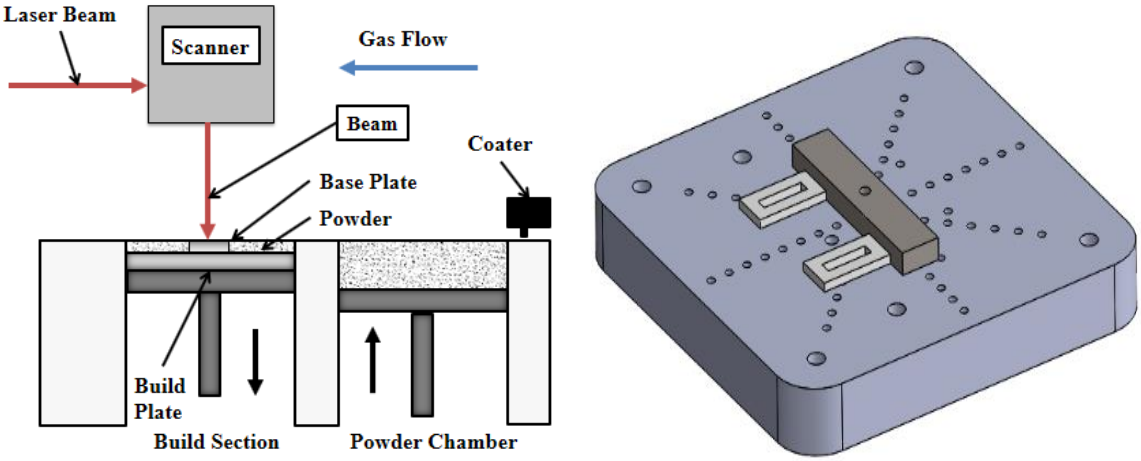

Figure 7.5: (Left) Setup of Concept Laser M2 Cusing machine and (Right) setup of the Ti-6Al-4V ELI base plate on the M2 Cusing machine's build plate

7.2.1.4. Building the samples

The M2 Cusing machine was set up to print. The Argon gas was connected to the machine. The filter was changed and the powder was changed to Ti-6Al-4V ELI. The powder was sieved using a 105 µm rated sieve. The parts were imported into the Concept Laser machine software and the parameters were set for the parts. The process parameters that were used are discussed in the following section.

7.2.1.5. Measurement of post SLM parts

The Mitutoyo Bright A710 coordinate measuring machine was used to measure the final deviation of the warping samples. A total of 222 data points were measured along the x axis on the bottom surface of the titanium base plates. These 222 data points were divided into 5 lines which were spread across the surface. The same program and probe was used as the one that was used to record the pre-SLM readings. The tool path of the probe and all the data collection points can be observed in Figure 7.6 below. The CMM results from the pre-SLM measurements and the post-SLM measurements were compared and the difference in the points was determined. The final deviation caused by the warping during the SLM process could then be revealed.

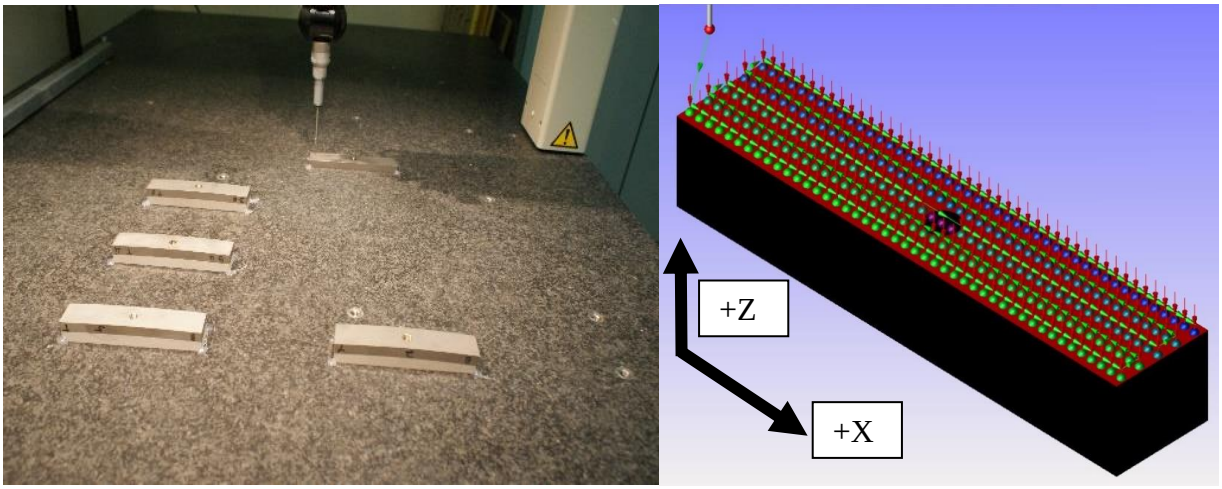

Figure 7.6: (Left) Hybrid parts on the CMM table with the bottom surface being measured for deviation. (Right) Tool path of CMM machine for titanium base plate measurements

A repeated measures analysis of varience (ANOVA) was performed on the CMM results. Therefore, the null hypothesis was set that all specimens are from the same population, this means $H_0: \mu_1 = \mu_2$ and the alternative hypothesis $H_1: \mu_1 \neq \mu_2$. Thus rejection of the null hypothesis would imply a significant difference between the deviation and hence the strategies. The independent variable was the scan strategy and the dependent variables are the deviation along the x axis before treatment and deviation along the x axis after treatment. The treatment is the SLM process.

7.2.2. Experimental Results and Discussion

In order to correctly compare the two scanning strategies, three samples of each strategy were built using the Concept Laser M2 Cusing machine. Each sample was built separately on days that had similar weather patterns, to reduce any temperature fluctuations in the machine's build chamber. Two samples, each produced using different scan strategies, can be observed in Figure 7.7 below.

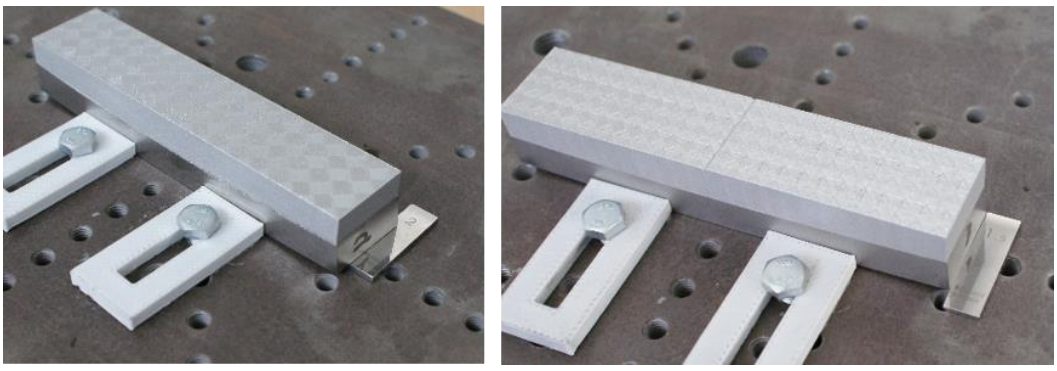

Figure 7.7: Isometric view: Comparison of two samples (Left) Default scan strategy sample with a 2 mm gauge block under side (Right) Newly developed scan strategy sample with 1.5 mm gauge block on side

One might observe from the figure above that there is a gauge block on the right-hand side of each sample. This gave an initial indication of the deviation. The sample on the left is the sample produced with the default scanning strategy. A 2 mm gauge block was placed under the deviated

section giving an initial indication of the deviation that occurred during the SLM process. On the right hand side, is the sample produced using the newly developed scan strategy. This sample was warped less than 1.5 mm as the gauge block could not fit under the deviated section. This gave an initial indication that the new scan strategy was successful and the aim was achieved. A side by side comparison of the side view of the samples can be observed in Figure 7.8 below.

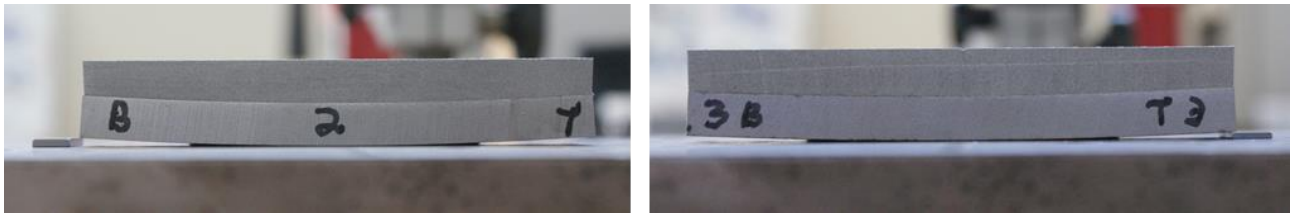

Figure 7.8: Side view: Comparison of two samples (Left) Default scan strategy sample with a 2 mm gauge block under side (Right) Newly developed scan strategy sample with 1.5 mm gauge block on side

It can be noted that the deviation in the default strategy sample on the left is noticeably larger than the new scan strategy sample on the right. Further measurements of the deviation were performed in order to confirm these initial observations.

Once the samples were produced the deviation was measured using the CMM machine. All six specimens were measured using the same measurement program along the same measuring paths. The samples were left on the CMM table for a day before the measurements were performed to reduce any deviation due to thermal expansion or contraction. The summarised results from the CMM readings can be observed in Table 7.2 below.

Table 7.2: Maximum and mean deviation from the CMM results of the difference of PreSLM and PostSLM

Scan Strategy	CMM Tool Path	Sample 1		Sample 2		Sample 3	
		Mean	Maximum	Mean	Maximum	Mean	Maximum
		[mm]		[mm]		[mm]	
Default Scan Strategy	Line 1	-0.6102	-1.671	-0.6907	-1.996	-0.5851	-1.812
	Line 2	-0.6422	-1.793	-0.6984	-1.989	-0.6357	-1.925
	Line 3	-0.6286	-1.789	-0.7230	-2.012	-0.6378	-1.911
	Line 4	-0.6585	-1.942	-0.7787	-2.079	-0.7391	-1.925
	Line 5	-0.5978	-1.805	-0.7188	-2.192	-0.7209	-1.95
	Average	-0.6274	-1.800	-0.7219	-2.054	-0.6637	-1.905
	Std. Dev.	0.024	0.096	0.035	0.085	0.064	0.054
Newly Developed Scan Strategy	Line 1	-0.5336	-1.508	-0.4758	-1.366	-0.4825	-1.368
	Line 2	-0.4745	-1.506	-0.4498	-1.361	-0.4434	-1.311
	Line 3	-0.5305	-1.496	-0.4992	-1.393	-0.4082	-1.272
	Line 4	-0.5967	-1.566	-0.5867	-1.458	-0.3666	-1.246
	Line 5	-0.6286	-1.598	-0.6579	-1.567	-0.3493	-1.147

	Average	-0.5528	-1.535	-0.5339	-1.429	-0.4100	-1.269
	Std. Dev.	0.061	0.045	0.086	0.086	0.055	0.082

From the results above one could observe that the deviation of the samples produced using the default scan strategy is in fact larger than the deviation of the samples produced using the newly developed scan strategies. The results from all of the data points from the CMM machine were plotted in Figure 7.9. The deformation was derived by determining the difference between the pre-SLM measurements and the post SLM measurements.

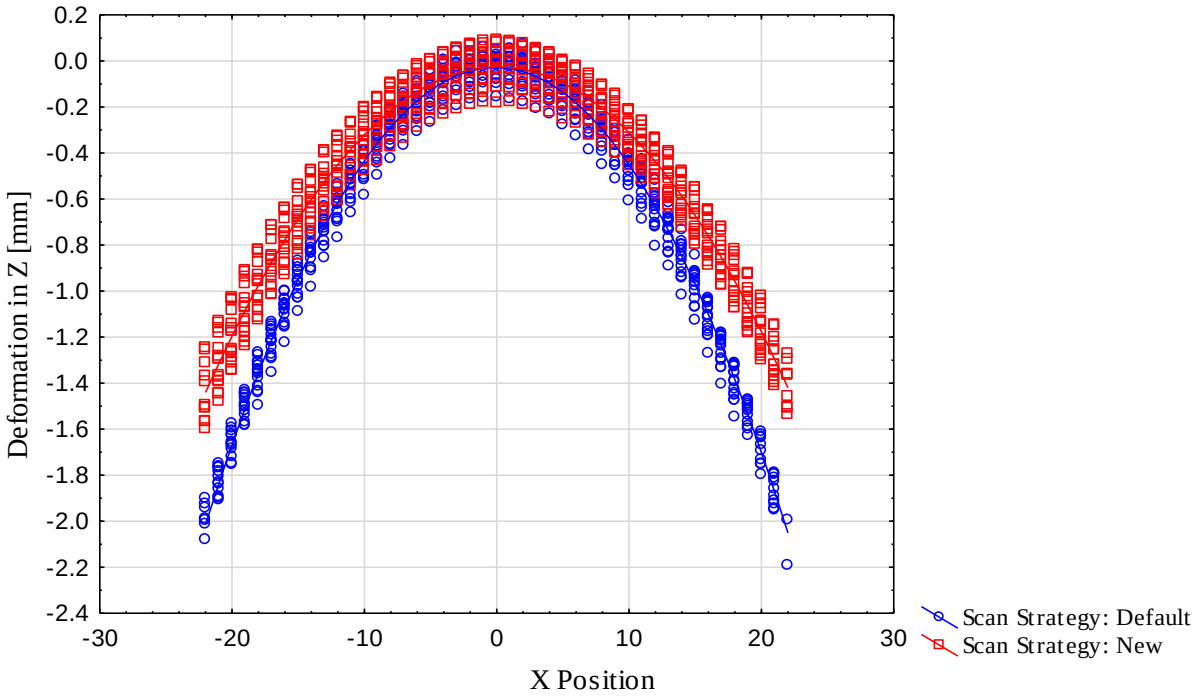

Figure 7.9: Scatterplot of Deformation in Z against the X position, categorised by the scan strategy on the same graph

The quadratic functions which define the parabolic trend lines for the two scan strategies in the figure above are:

Scan Strategy: Default Scan Strategy = $-0.029 - 0.0008x - 0.0041x^2$

Scan Strategy: Newly Developed Scan Strategy = $-0.0262 + 0.0005x - 0.0029x^2$

One might observe that the gradient coefficients for the default strategy are greater than those of the new strategy. This indicates that the deviation of the samples produced with the newly developed strategy increased at a slower rate than those produced with the default strategy.

A Repeated Measures Analysis of Variance was performed on all of the results from the CMM readings. The Standard Error of Estimate was 0.0684 and sigma-restricted parameterisation was used. The results can be observed in Table 7.3.

Table 7.3: Results from the Repeated measures ANOVA with sigma-restricted parameterisation and a standard Error of Estimate of 0.0684

Effect	SS	Degrees of Freedom	Mean Square	F	p
Intercept	42.87193	1	42.87193	9166.144	0.000000
Position	0.01253	4	0.00313	0.670	0.619161
Scan Strategy	1.20247	1	1.20247	257.091	0.000000
Error	0.11225	24	0.00468	-	-
Repeat	40.73526	1	40.73526	4338.560	0.000000
Repeat*Position	0.03145	4	0.00786	0.837	0.514918
Repeat*Scan Strategy	1.00725	1	1.00725	107.279	0.000000
Error	0.22534	24	0.00939	-	-

From the table above one could detect that all of the scan strategy results are highly significant with a p value very close to 0. The least squares mean results from the ANOVA were plotted on the graph in Figure 7.10 below. The samples pre-SLM and post SLM were tested for a significant difference with regards to the scan strategy.

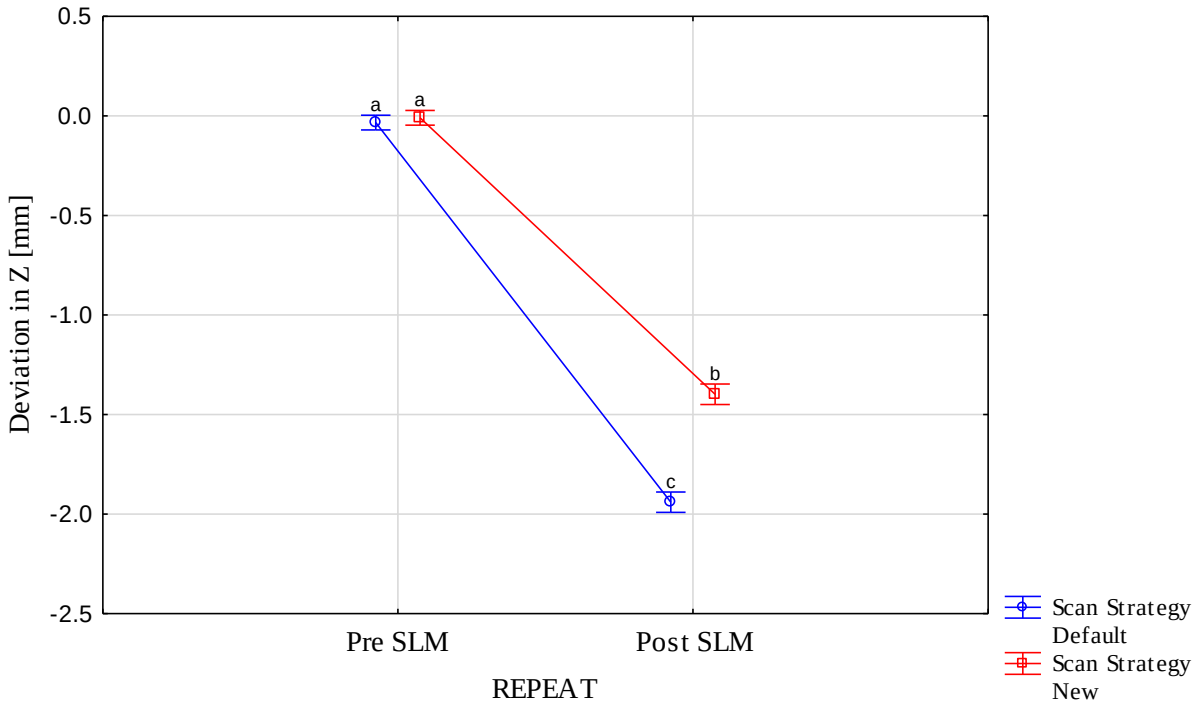

Figure 7.10: Least Squares Means Repeated Measures ANOVA results. Current Effect: F(1, 24) = 107.28, p = 0.00000. The error bars denote the 95% confidence intervals

One can observe from the graph above that the difference in the readings of the base plates before the SLM process was not significant. It can also be observed that the two scan strategies differ significantly with regards to the deviation in the z direction post SLM. The two conditions differed significantly on scan strategy, F(1,24) = 107.28 with p less than 0.05. Therefore, the null hypothesis can be rejected.

Table 7.4: Least Square means from the repeated measures ANOVA with current effect F(1, 24) = 107.28, where p = 0.00000

Scan Strategy	Repeat	Deviation Mean	Deviation Std. Err.	Deviation -95%	Deviation +95%	N
Default	PreSLM	-0.03333	0.017884	-0.07024	0.00358	15
Default	Post SLM	-1.94040	0.024858	-1.99170	-1.88910	15
New	PreSLM	-0.00933	0.017884	-0.04624	0.02758	15
New	Post SLM	-1.39813	0.024858	-1.44944	-1.34683	15

In support of the significant difference in the means, one can observe by looking at the 95% confident intervals, that the worst deviation of the new strategy is less than the best deviation of the default strategy. An average decrease in deviation of 27.95% was observed between the two scanning strategies, in favour of the newly developed scan strategy. The residuals from the ANOVA were plotted (Appendix E) and are normally distributed, which shows the assumptions that were made, were accurate.

7.2.3. Summary

The effects of selective laser melting strategies on the geometry of hybrid parts were analysed. The results showed a significant difference in deviation for the different scan strategies. The newly developed scan strategy significantly improved the warping of the hybrid parts, compared to the patented default strategy from Concept Laser GmbH. One could conclude that in this case the Concept Laser scan strategy was not the optimal strategy and further improvements can be suggested for the newly developed scan strategy in the following section.

7.3. Chapter Conclusion

It was determined that varying the SLM scan strategies does in fact have a significant effect on the porosity and geometrical deviation of hybrid parts. A scan strategy that does not fall under the scope of the Concept Laser Patent was successfully designed and developed. Applying the newly developed scan strategy over the default scan strategy, resulted in a decrease in part porosity for a set sample size as well as part deviations due to warping for specific part dimensions.

The newly developed scan strategy is in fact significantly better, in terms of warping, than the patented default strategy from Concept Laser GmbH for the production of hybrid parts. Only a specific sized hybrid part was tested and more experiments would need to be performed in order to determine if the conclusions can be applied to all hybrid parts.

Chapter 8

Conclusions and Recommendations

8.1. Conclusion

The effects of selective laser melting on the geometry of hybrid parts were analysed in the background study. It was determined that the shape deviation of an SLM hybrid part seems to be proportional to the building thickness (number of layers) of the SLM section. Since the residual stress in a part is a consequence of the high temperature gradients, the greater deformation of thicker parts suggests that residual stresses in this particular part (120 mm x 120 mm x 20 mm) increases proportionally to the build thickness. These findings seem to support the findings of Mercelis and Kruth [54] where they state that the magnitude of the residual stresses is dependent on the part height.

The current SLM process chain for the Concept Laser M2 Cusing machine was studied and several problem areas in the current process were identified for hybrid part manufacturing. The most detrimental factor was identified as delamination of the SLM section from the SM section. Several starting strategies were suggested and tested and only one was identified to correct the problem. The strategy was tested and validated and was used throughout the study.

A method was developed in order to change the standard scan strategy on the Concept Laser M2 Cusing machine. The machine's software is very limiting and does not allow the user to vary from the scan strategies that come standard on the software. The Hatch Pattern Design method was created and tested through various iterations. The HPD can be used by researchers to create and scan their own scan strategies on the Concept Laser M2 Cusing machine.

A scan strategy that does not fall under the scope of the Concept Laser Patent was successfully designed and developed. Applying the newly developed scan strategy over the default scan strategy, resulted in a decrease in part deviations due to warping for specific part dimensions. The porosity in samples produced using the new strategy was significantly less than the porosity in samples produced using the default strategy. This is an indication that the patented island scan strategy by Concept Laser GmbH might not be the optimal scan strategy for hybrid parts. This is also an indication that changing the scan strategy rather than performing parameter optimisation could lead to better results.

8.2. Contributions to Practice

In this study a new method to override machine scan strategies was developed. Researchers could use the Hatch Pattern Design method in order to further the study of the effects of scan strategies on SLM and hybrid parts.

The product design specification (PDS) is an important aspect of any design and should be used to determine what strategies, parameters, and post processing should be utilised to achieve the required mechanical properties. The author proposes a new outlook on SLM process optimisation. It is suggested that the scan strategies be selected according to the product design specifications for the final part. Once the applicable strategies have been selected according to certain criteria, the process optimisation can take place. It is proposed that the parameter optimisation be performed only after the optimal strategies have been identified and optimised.

8.3. Recommendations and Future Work

8.3.1. Recommendations

In order to improve the newly developed scan strategy several suggestions could be made:

1. The hatch spacing could be decreased from 105 µm to improve the porosity and surface finish. As with most x and y coordinate systems where a circle is scanned by using circular interpolation, the mirrors of the laser scanning system do not circular interpolate x and y coordinates to scan a circular path [89]. So, with a helix scan strategy, the square corners of the vector intersection are not scanned by the laser but rather a rounded corner is scanned. This is the result of distortion caused by the laser scanning system as the scan speed is too high for the laser to turn in a sharp 90 degree corner.

2. The islands of the newly developed scan strategy should be orientated by a set angle range with regards to the part shape. When a vector of 5 mm is scanned with the laser in only the x direction then the largest forces, induced in the melt pool due to contraction of the melt pool when cooling, will result in the x direction. The deviations due to warping can be decreased further by varying the orientation angle for each layer [166].

3. The islands can be shifted in the x and y direction by a predetermined value after each layer.

4. The time between each vector scan, should be optimised so that the second scan performed acts as a remelting operation, which relieves stress while scanning the next vector set.

5. The part should be orientated so that the flow of gas is perpendicular to the part rather than parallel.

6. The helix scan strategy can be scanned from outside to the inside. Nickel et al. [43] found that scanning the vectors from the outside to the inside, results in a low and uniform deflection. The hatch spacing would also need to be optimised for this case, as the remelt or reheat of the previous scan relies on the overlap of the melt pools.

7. The helix vectors should start from a single vector in the centre and develop outwards to a justified size. This will decrease the chance of having a local hotspot in the centre of the pattern, which in turn will stop the formation of keyhole pores in the centre [171].

8. The effects of changing the directions of the vectors in the helix strategy should be studied in order to determine what benefits or detriment there is to the warping. Alternating the vector direction results in a higher density due to less un-melted zones [44].

9. Mercelis and Kruth [54] found that the stresses are larger perpendicular to the scan direction than along the scan direction. The author suggests that a strategy be developed, which monitors the shape of the part. If the part is rectangular, such as the samples in this study, and the greater length is in the x direction. Then the majority of the scan lines should be in the x direction. This would ensure that the larger stresses act in the y direction, which has a smaller size and thus the stress build up will not be as large as if it were acting in the x direction.

10. Ideally the optimal scan strategy should be calculated on a layer by layer approach, taking into account the part geometry and adjusting the fundamental process parameters. This allows the microstructure and quality to be tailored to the final application of the component, this would require significant research into the thermal modelling of the SLM process [172].

8.3.2. Future Work

- Since the newly developed strategy was made up of 3 different strategies, the effects of each strategy should be investigated. A duplication of the deviation experiment is proposed but only the strategies that make up the newly developed strategy should be varied.

- A porosity optimisation experiment should be performed on the newly developed strategy in order to determine if the porosity could be reduced further to produce a near 100% dense part.

- It is recommended that the effects of different scan strategies on different part properties be mapped. This should be performed in a similar manner to the work completed by Kruth et al. [101].

- The recommendations made should be tested to refine the newly developed scan strategy further.

References

[1] R. I. Campbell and D. J. De Beer, “Rapid prototyping in South Africa: past, present and future,” *Rapid Prototyp. J.*, vol. 11, no. 4, pp. 260–265, 2005.

[2] D. de Beer, R. I. Campbell, and E. Pei, “Additive Manufacturing in South Africa: Building on the Foundations,” *Rapid Prototyp. J.*, vol. 17, no. 2, pp. 156–162, 2011.

[3] T. Wohlers, “Rapid prototyping, tooling and manufacturing state of the industry annual worldwide progress report,” Fort Collins, 1999.

[4] L. Schutters, “South Africa: Maker Nation,” *Popular Mechanics*, Johannesburg, pp. 34–39, Jun-2015.

[5] F. T. Piller, C. Weller, and R. Kleer, “Business Models with Additive Manufacturing—Opportunities and Challenges from the Perspective of Economics and Management,” in *Advances in Production Technology*, New York: Springer Online, 2014, pp. 39–48.

[6] K. P. Karunakaran, S. Suryakumar, V. Pushpa, and S. Akula, “Low cost integration of additive and subtractive processes for hybrid layered manufacturing,” *Robot. Comput. Integr. Manuf.*, vol. 26, no. 5, pp. 490–499, 2010.

[7] “Aerosud,” 2014. [Online]. Available: http://www.aerosud.co.za/tech. [Accessed: 18-Apr-2016].

[8] K. Campbell, “SA taking global lead in powder bed 3D printing technology,” *Creamer Media’s Engineering News*, 2015. [Online]. Available: http://www.engineeringnews.co.za/print-version/sa-taking-global-lead-in-powder-bed-3d-printing-technology-2015-11-05. [Accessed: 18-Apr-2016].

[9] J. Fernández and M. Arizmendi, “Machines for the Aeronautical Industry,” in *Machine Tools for High Performance Machining*, New York: Springer, 2009, pp. 399–420.

[10] W. Cole, “Boeing engineers and technologists are constantly developing better ways to design and make products.,” *Boeing Frontiers*, 2004.

[11] O. Rehme, “Cellular Design for Laser Freeform Fabrication,” Laser Zentrum Nord, 2009.

[12] R. Poprawe, C. Hinke, W. Meiners, J. Schrage, S. Bremen, and S. Merkt, “SLM Production Systems: Recent Developments in Process Development, Machine Concepts and Component Design,” in *Advances in Production Technology*, New York: Springer Online, 2014, pp. 49–65.

[13] S. Das, M. Wohlert, J. J. Beaman, and D. L. Bourell, “Processing of titanium net shapes by SLS/HIP,” *Mater. Des.*, vol. 20, no. 2–3, pp. 115–121, 1999.

[14] E. O. Ezugwu, J. Bonney, and Y. Yamane, “An overview of the machinability of aeroengine alloys.,” *J. Mater. Process. Technol.*, vol. 134, pp. 233–253, 2003.

[15] J. C. Williams and E. A. Starke, “Progress in structural materials for aerospace systems.,” *Acta Mater.*, vol. 51, pp. 5775–5799, 2003.

[16] Airbus, “Printing the future: Airbus expands its applications of the revolutionary additive layer manufacturing process,” 2014. [Online]. Available: http://www.airbus.com/presscentre/pressreleases/press-release-detail/detail/printing-the-future-airbus-expands-its-applications-of-the-revolutionary-additive-layer-manufacturi/. [Accessed: 20-Apr-2016].

[17] D. J. De Beer, M. Truscott, G. J. Booysen, L. J. Barnard, and J. G. Van Der Walt, “Rapid manufacturing of patient-specific shielding masks, using RP in parallel with metal spraying,” *Rapid Prototyp. J.*, vol. 11, no. 5, pp. 298–303, 2005.

[18] B. Vandenbroucke and J.-P. Kruth, “Direct Digital Manufacturing of Complex Dental Prostheses,” in *Bio-Materials and Prototyping Applications in Medicine*, New York: Springer, 2008, pp. 109–124.

[19] F. J. C. Braga, R. F. C. Marques, E. D. A. Filho, and A. C. Guastaldi, “Surface modification of Ti dental implants by Nd:YVO4 laser irradiation,” *Appl. Surf. Sci.*, vol. 253, no. 23, pp. 9203–9208, 2007.

[20] L. E. Murr, S. A. Quinones, S. M. Gaytan, M. I. Lopez, A. Rodela, E. Y. Martinez, D. H. Hernandez, E. Martinez, F. Medina, and R. B. Wicker, “Microstructure and mechanical behavior of Ti-6Al-4V produced by rapid-layer manufacturing, for biomedical applications,” *J. Mech. Behav. Biomed. Mater.*, vol. 2, no. 1, pp. 20–32, 2009.

[21] E. C. Santos, M. Shiomi, K. Osakada, and T. Laoui, “Rapid manufacturing of metal components by laser forming,” *Int. J. Mach. Tools Manuf.*, vol. 46, no. 12–13, pp. 1459–1468, 2006.

[22] D. Hagedorn-Hansen, G. A. Oosthuizen, and T. Gerhold, “Resource-Efficient Process Chains To Manufacture Patient-Specific Prosthetic Fingers,” *South African J. Ind. Eng.*, vol. 27, no. May, pp. 75–87, 2016.

[23] G. A. Oosthuizen, D. Hagedorn-Hansen, and T. Gerhold, “Evaluation of Rapid Product Development Technologies for Production of Prosthesis in Developing Communities,” in *SAIIE25 Proceedings*, 2013, no. July, p. 590.1-590.14.

[24] D. Hagedorn-Hansen, L. P. Steenkamp, M. M. Jansen van Rhensburg, and G. A. Oosthuizen, “Resource Efficient Process Chains to Manufacture Patient Specific Prosthetic Hands Using Open Ssource Devices,” in *SAIIE 27 Proceedings*, 2016, pp. 1–9.

[25] L. Nickels, “World’s first patient-specific jaw implant,” Elsevier Ltd, 2012.

[26] M. B. Bezuidenhout, A. D. Van Staden, G. A. Oosthuizen, D. M. Dimitrov, and L. M. T. Dicks, “Delivery of Antibiotics from Cementless Titanium-Alloy Cubes May Be a Novel

Way to Control Postoperative Infections," *Hindawi Publ. Corp. BioMed Res. Int.*, 2015.

[27] D. Dimitrov, K. Schreve, N. De Beer, and P. Christiane, "Three Dimensional Printing in the South African Industrial Environment," *South African J. Ind. Eng.*, vol. 19, pp. 195–213, 2008.

[28] L. C. Hieu, N. Zlatov, J. Vander Sloten, E. Bohez, L. Khanh, P. H. Binh, P. Oris, and Y. Toshev, "Medical rapid prototyping applications and methods," *Assem. Autom.*, vol. 25, no. 4, pp. 284–292, 2005.

[29] B. Muller, T. Toppel, C. Rotsch, A. Bohm, J. Braunig, and R. Neugebauer, "Functional Integration in Implants through Additive Manufacturing Technology and Smart Materials," in *European Forum on Rapid Prototyping*, 2012.

[30] J. M. Schierholz and J. Beuth, "Implant infections: A haven for opportunistic bacteria," *J. Hosp. Infect.*, vol. 49, no. 2, pp. 87–93, 2001.

[31] C. N. Elias, J. H. C. Lima, R. Valiev, and M. a Meyers, "Biomedical Applications of Titanium and its Alloys," *J. Miner. Met. Mater. Soc.*, no. March, pp. 46–49, 2008.

[32] B. Derby, "Materials opportunities in layered manufacturing technology," *J. Mater. Sci.*, vol. 37, no. 15, pp. 3091–3092, 2002.

[33] A. Fukuda, M. Takemoto, T. Saito, S. Fujibayashi, M. Neo, D. K. Pattanayak, T. Matsushita, K. Sasaki, N. Nishida, T. Kokubo, and T. Nakamura, "Osteoinduction of porous Ti implants with a channel structure fabricated by selective laser melting," *Acta Biomater.*, vol. 7, no. 5, pp. 2327–2336, 2011.

[34] S. Fujibayashi, M. Neo, H. M. Kim, T. Kokubo, and T. Nakamura, "Osteoinduction of porous bioactive titanium metal," *Biomaterials*, vol. 25, no. 1, pp. 443–450, 2004.

[35] S. J. Hollister and T. L. Bergman, "Additive/Subtractive Manufacturing Research and Development in Europe," *Evaluation*, no. July, pp. 1–150, 2010.

[36] D. Dimitrov, W. van Wijck, N. de Beer, and J. Dietrich, "Development, evaluation, and selection of rapid tooling process chains for sand casting of functional prototypes," *Proc. Inst. Mech. Eng. Part B J. Eng. Manuf.*, vol. 221, no. B9, pp. 1441–1450, 2007.

[37] F. Abe, K. Osakada, M. Shiomi, K. Uematsu, and M. Matsumoto, "The manufacturing of hard tools from metallic powders by selective laser melting," *J. Mater. Process. Technol.*, vol. 111, no. 1–3, pp. 210–213, 2001.

[38] S. S. Dimov, D. T. Pham, F. A. Lacan, and K. D. Dotchev, "Rapid tooling applications of the selective laser sintering process," *Assem. Autom.*, vol. 21, no. 4, pp. 296–302, 2001.

[39] G. N. Levy, R. Schindel, and J. P. Kruth, "Rapid Manufacturing and Rapid Tooling With Layer Manufacturing (Lm) Technologies, State of the Art and Future Perspectives," *CIRP Ann. - Manuf. Technol.*, vol. 52, no. 2, pp. 589–609, 2003.

[40] K. Osakada and M. Shiomi, “Flexible manufacturing of metallic products by selective laser melting of powder,” *Int. J. Mach. Tools Manuf.*, vol. 46, no. 11 SPEC. ISS., pp. 1188–1193, 2006.

[41] C. Laser, “Datasheet: X line 1000R Metal laser melting system,” 2014.

[42] P. Aggarangsi and J. Beuth, “Localized preheating approaches for reducing residual stress in additive manufacturing,” *Proc. SFF Symp., Austin*, pp. 709–720, 2006.

[43] A. H. Nickel, D. M. Barnett, and F. B. Prinz, “Thermal stresses and deposition patterns in layered manufacturing,” *Mater. Sci. Eng. A*, vol. 317, no. 1–2, pp. 59–64, 2001.

[44] J. P. Kruth and M. Badrossamay, “Part and Material Properties in Selective Laser Melting of Metals,” in *Proceedings of the 16th International Symposium on Electromachining*, 2010.

[45] W. Michaeli and M. Schönfeld, “Komplexe Formteile kühlen,” *Kunststoffe 96*, vol. 8, pp. 37–41, 2006.

[46] S. Bremen, W. Meiners, and A. Diatlov, “Selective Laser Melting. A manufacturing technology for the future?,” *Laser Tech. J.*, vol. 9, no. 2, pp. 33–38, 2012.

[47] A. Moammer, “Thermal Management of Moulds and Dies: A Contribution to Improved Design and Manufacture of Tooling for Injection Moulding,” PhD Thesis, Stellenbosch University, 2011.

[48] B. Vrancken, “Study of Residual Stresses in Selective Laser Melting,” KU Leuven, 2016.

[49] K. Kempen, L. Thijs, B. Vrancken, J. Van Humbeeck, and J.-P. Kruth, “Producing Crack-Free, High Density M2 Hss Parts By Selective Laser Melting: Pre-Heating the Baseplate,” *Proc. 24th Int. Solid Free. Fabr. Symp.*, pp. 131–139, 2013.

[50] D. Vanbuel, “Vermoeiingsgedrag van Ti6Al4V componenten geproduceerd door het Selectief Laser Smelten Proces.,” University of Leuven, 2011.

[51] I. Gibson, D. W. Rosen, and B. Stucker, *Additive Manufacturing Technologies: Rapid Prototyping to Direct Digital Manufacturing*. New York: Springer, 2010.

[52] M. Fateri, J.-S. Hötter, and A. Gebhardt, “Experimental and Theoretical Investigation of Buckling Deformation of Fabricated Objects by Selective Laser Melting,” *Phys. Procedia*, vol. 39, pp. 464–470, 2012.

[53] N. Guo and M. C. Leu, “Additive manufacturing: Technology, applications and research needs,” *Front. Mech. Eng.*, vol. 8, no. 3, pp. 215–243, 2013.

[54] P. Mercelis and J.-P. Kruth, “Residual stresses in selective laser sintering and selective laser melting,” *Rapid Prototyp. J.*, vol. 12, no. 5, pp. 254–265, 2006.

[55] P. J. T. Conradie, D. M. Dimitrov, G. A. Oosthuizen, and P. Hugo, “Resource efficiency assessment of combining selective laser melting and five axis milling for titanium components,” in *Proceedings of Rapid Product Development Association of South Africa*

Conference, 2014, pp. 1–8.

[56] H. Hassanin, F. Modica, M. A. El-Sayed, J. Liu, and K. Essa, "Manufacturing of Ti–6Al–4V Micro-Implantable Parts Using Hybrid Selective Laser Melting and Micro-Electrical Discharge Machining," vol. 18, no. 9, pp. 1544–1549, 2016.

[57] E. Santos, F. Abe, Y. Kitamura, K. Osakada, and M. Shiomi, "Mechanical properties of pure titanium models processed by selective laser melting," in *Proceedings of the Solid Freeform Fabrication Symposium*, 2002, pp. 180–186.

[58] A. N. Chatterjee, S. Kumar, P. Saha, P. K. Mishra, and A. Roy Choudhury, "An experimental design approach to selective laser sintering of low carbon steel," *J. Mater. Process. Technol.*, vol. 136, no. 1–3, pp. 151–157, 2003.

[59] C. Qiu, N. J. E. Adkins, and M. M. Attallah, "Microstructure and tensile properties of selectively laser-melted and of HIPed laser-melted Ti-6Al-4V," *Mater. Sci. Eng. A*, vol. 578, pp. 230–239, 2013.

[60] F. Abe, E. Costa Santos, Y. Kitamura, K. Osakada, and M. Shiomi, "Influence of forming conditions on the titanium model in rapid prototyping with the selective laser melting process," *Proc. Inst. Mech. Eng. Part C J. Mech. Eng. Sci.*, vol. 217, no. 1, pp. 119–126, 2003.

[61] K. Zeng, D. Pal, and B. E. Stucker, "A Review of Thermal Analysis Methods in Laser Sintering and Selective Laser Melting," in *Proceedings of the Solid Freeform Fabrication Symposium*, 2012, pp. 796–814.

[62] J.-P. Kruth, "Material incress manufacturing by Rapid Prototyping Techniques," in *Annals of the CIRP 40(2)*, 1991, pp. 603–614.

[63] Z. Zhu, V. G. Dhokia, A. Nassehi, and S. T. Newman, "A review of hybrid manufactured processes - state of the art and future perspectives.," *Int. J. Comput. Integr. Manuf.*, vol. 26, no. 7, pp. 596–615, 2013.

[64] A. Gleadall, N. Vladov, J. Segal, S. Ratchev, M. Plasch, D. Kimmig, and M. Dickerhof, "A decision support methodology for embodiment design and process chain selection for hybrid manufacturing platforms," *Int. J. Adv. Manuf. Technol.*, 2016.

[65] A. Gleadall, N. Vladov, J. Segal, S. Ratchev, M. Plasch, D. Kimmig, and M. Dickerhof, "A decision support methodology for embodiment design and process chain selection for hybrid manufacturing platforms," *Int. J. Adv. Manuf. Technol.*, 2016.

[66] K. Karunakaran, S. Suryakumar, V. Pushpa, and S. Akula, "Low cost integration of additive and subtractive processes for hybrid layered manufacturing," *Robot. Comput. Integr. Manuf.*, vol. 26, pp. 490–499, 2010.

[67] *Mitsubishi Tooling Technology*, 1st ed. Tokyo: Mitsubishi Material Corporation, 2005.

[68] J. W. Roe, *English and American Tool Builders*. New York: Yale University Press, 1916.

[69] M. Saxer, N. de Beer, and D. M. Dimitrov, "High-Speed 5-Axis Machining for Tooling Applications," *South African J. Ind. Eng.*, vol. 23, no. 3, pp. 144–153, 2012.

[70] M. Cotteleer, M. Mahto, and J. Holdowsky, "The 3D opportunity primer," 2013.

[71] M. J. Cotteleer, "3D opportunity: Additive manufacturing paths to performance, innovation, and growth," in *SIMT Additive Manufacturirng Symposium*, 2014, p. 23.

[72] M. Królikowski and K. Filipowicz, "Verification of Geometrical Accuracy of Selective Laser Melting (SLM) Built Model," *VERSITA Adv. Manuf. Sci. Technol.*, vol. 37, no. 3, pp. 85–91, 2013.

[73] D. T. Pham and R. S. Gault, "A comparison of rapid prototyping technologies," *Int. J. Mach. Tools Manuf.*, vol. 38, no. 10–11, pp. 1257–1287, 1998.

[74] *ASTM F2792–10 standard terminology for additive manufacturing technologies*, Annual Boo. ASTM.

[75] A. C. van Staden, "A Fundamental Analysis on Additive Manufacturing of a Cemented Tungsten Carbide," Stellenbosch University, 2015.

[76] J. P. Kruth, "Material Incress Manufacturing by Rapid Prototyping Techniques," *CIRP Ann. - Manuf. Technol.*, vol. 40, no. 2, pp. 603–614, 1991.

[77] J.-P. Kruth, M. C. Leu, and T. Nakagawa, "Progress in Additive Manufacturing and Rapid Prototyping," *CIRP Ann. - Manuf. Technol.*, vol. 47, no. 2, pp. 525–540, 1998.

[78] C. K. Chua and K. F. Leong, *Rapid prototyping: principles and applications*. Singapore: World Scientific, 2003.

[79] B. Evans, *Practical 3D Printers: The Science and Art of 3D Printing*. New York: Apress, 2012.

[80] R. R. Dehoff and S. S. Babu, "Characterization of interfacial microstructures in 3003 aluminum alloy blocks fabricated by ultrasonic additive manufacturing," *Acta Mater.*, vol. 58, no. 13, pp. 4305–4315, 2010.

[81] H. K. Rafi, N. V Karthik, H. Gong, T. L. Starr, and B. E. Stucker, "Microstructures and Mechanical Properties of Ti6Al4V Parts Fabricated by Selective Laser Melting and Electron Beam Melting," vol. 22, no. December, pp. 3872–3883, 2013.

[82] T. Wohlers, "Wohler's Report 2013," Colorado, USA, 2013.

[83] L. Thijs, F. Verhaeghe, T. Craeghs, J. Van Humbeeck, and J.-P. Kruth, "A study of the microstructural evolution during selective laser melting of Ti-6Al-4V," *Acta Mater.*, vol. 58, no. 9, pp. 3303–3312, 2010.

[84] E. Yasa and J. P. Kruth, "Application of Laser Re-Melting on Selective Laser Melting Parts," *Adv. Prod. Eng. Manag.*, vol. 6, no. 4, pp. 259–270, 2011.

[85] S. Dadbakhsh, L. Hao, P. G. E. Jerrard, and D. Z. Zhang, “Experimental investigation on selective laser melting behaviour and processing windows of in situ reacted Al/Fe 2O 3 powder mixture,” *Powder Technol.*, vol. 231, pp. 112–121, 2012.

[86] S. Dadbakhsh, L. Hao, and N. Sewell, “Effect of selective laser melting layout on the quality of stainless steel parts,” *Rapid Prototyp. J.*, vol. 18, no. 3, pp. 241–249, 2012.

[87] I. Yadroitsev, I. Yadroitsava, P. Bertrand, and I. Smurov, “Factor analysis of selective laser melting process parameters and geometrical characteristics of synthesized single tracks,” *Rapid Prototyp. J.*, vol. 18, no. 3, pp. 201–208, 2012.

[88] I. Yadroitsev, P. Krakhmalev, I. Yadroitsava, S. Johansson, and I. Smurov, “Energy input effect on morphology and microstructure of selective laser melting single track from metallic powder,” *J. Mater. Process. Technol.*, vol. 213, no. 4, pp. 606–613, 2013.

[89] A. Manakov and H. S. Ivo, “A Mathematical Model and Calibration Procedure for Galvanometric Laser Scanning Systems,” *Vision, Model. Vis.*, pp. 207–214, 2011.

[90] Concept Laser GmbH, “M2 Cusing Operation Manual,” Germany, 2010.

[91] Hofmann, “Material Data CL 41TI ELI Titanium Alloy,” Lichtenfels, 2014.

[92] F. Liou, K. Slattery, M. Kinsella, J. Newkirk, H.-N. Chou, and R. Landers, “Applications of a hybrid manufacturing process for fabrication of metallic structures,” *Rapid Prototyp. J.*, vol. 13, no. 4, pp. 236–244, 2007.

[93] K. a. Mumtaz and N. Hopkinson, “Selective Laser Melting of thin wall parts using pulse shaping,” *J. Mater. Process. Technol.*, vol. 210, no. 2, pp. 279–287, 2010.

[94] M. Thöne and S. Leuders, “Influence of heat-treatment on Selective Laser Melting products – e.g. Ti6Al4V,” in *SFF*, 2012, pp. 492–498.

[95] T. Sercombe, N. Jones, R. Day, and A. Kop, “Heat treatment of Ti-6Al-7Nb components produced by selective laser melting,” *Rapid Prototyp. J.*, vol. 14, no. 5, pp. 300–304, 2008.

[96] B. Vrancken, L. Thijs, J.-P. Kruth, and J. Van Humbeeck, “Heat treatment of Ti6Al4V produced by Selective Laser Melting: Microstructure and mechanical properties,” *J. Alloys Compd.*, vol. 541, pp. 177–185, 2012.

[97] S. Dadbakhsh and L. Hao, “Effect of hot isostatic pressing (HIP) on Al composite parts made from laser consolidated Al/Fe2O3 powder mixtures,” *J. Mater. Process. Technol.*, vol. 212, no. 11, pp. 2474–2483, 2012.

[98] F. Wang, “Mechanical property study on rapid additive layer manufacture Hastelloy X alloy by selective laser melting technology,” *Int. J. Adv. Manuf. Technol.*, vol. 58, no. 5–8, pp. 545–551, 2012.

[99] J. Bültmann, S. Merkt, C. Hammer, C. Hinke, and U. Prahl, “Scalability of the mechanical properties of selective laser melting produced micro-struts,” *J. Laser Appl.*, vol. 27, 2015.

[100] K. A. Ghany and S. F. Moustafa, “Comparison between the products of four RPM systems for metals,” *Rapid Prototyp. J.*, vol. 12, no. 2, pp. 86–94, 2006.

[101] J. P. Kruth, L. Froyen, J. Van Vaerenbergh, P. Mercelis, M. Rombouts, and B. Lauwers, “Selective laser melting of iron-based powder,” *J. Mater. Process. Technol.*, vol. 149, no. 1–3, pp. 616–622, 2004.

[102] J. P. Kruth, B. Vandenbroucke, J. Van Vaerenbergh, and I. Naert, “Digital manufacturing of biocompatible metal frameworks for complex dental prostheses by means of SLS/SLM,” *Virtual Model. Rapid Manuf. Adv. Res. VIRTUAL RAPID Prototyp.*, pp. 139–145, 2005.

[103] G. Ziolkowski, E. Chlebus, P. Szymczyk, and J. Kurzac, “Application of X-ray CT method for discontinuity and porosity detection in 316L stainless steel parts produced with SLM technology,” *Arch. Civ. Mech. Eng.*, vol. 14, no. 4, pp. 608–614, 2014.

[104] D. Hagedorn-Hansen, R. Cichon, M. B. Bezuidenhout, P. A. Hugo, and G. A. Oosthuizen, “Geometric Deviation of Hybrid Parts Produced by Selective Laser Melting,” in *Rapid Product Development Association of South Africa*, 2015, pp. 1–9.

[105] M. Matsumoto, M. Shiomi, K. Osakada, and F. Abe, “Finite element analysis of single layer forming on metallic powder bed in rapid prototyping by selective laser processing,” *Int. J. Mach. Tools Manuf.*, vol. 42, no. 1, pp. 61–67, 2002.

[106] H. Pohl, A. Simchi, M. Issa, and H. C. Dias, “Thermal Stresses in Direct Metal Laser Sintering,” in *Proc. of the Solid Freeform Fabrication Symp*, 2001, pp. 366–372.

[107] B. Qian, Y. S. Shi, Q. S. Wei, and H. B. Wang, “The helix scan strategy applied to the selective laser melting,” *Int. J. Adv. Manuf. Technol.*, vol. 63, no. 5–8, pp. 631–640, 2012.

[108] C. R. Knowles, T. H. Becker, and R. B. Tait, “Residual Stress Measurements and Structural Integrity Implications for Selective Laser Melted Ti-6AL-4V,” *South African J. Ind. Eng.*, vol. 23, no. 2, pp. 119–129, 2012.

[109] E. Yasa, J. P. Kruth, and J. Deckers, “Manufacturing by combining Selective Laser Melting and Selective Laser Erosion/laser re-melting,” *CIRP Ann. - Manuf. Technol.*, vol. 60, no. 1, pp. 263–266, 2011.

[110] S. O. Onuh and Y. Y. Yusuf, “Rapid prototyping technology : applications and benefits for rapid product development,” *J. Intell. Manuf.*, vol. 10, pp. 301–311, 1999.

[111] E. Brinksmeier, G. Levy, D. Meyer, and A. B. Spierings, “Surface integrity of selective-laser-melted components,” *CIRP Ann. - Manuf. Technol.*, vol. 59, no. 1, pp. 601–606, 2010.

[112] M. B. Bauza, S. P. Moylan, R. M. Panas, S. C. Burke, E. Martz, J. S. Taylor, R. H. Knebel, R. Bhogaraju, and M. Grove, “Study of accuracy of parts produced using additive manufacturing,” in *2014 ASPE Spring Topical Meeting: Dimensional Accuracy and Surface Finish in Additive Manufacturing*, 2014, pp. 1–8.

[113] C. Laser, “Materials for laser melting with metals.” [Online]. Available: http://www.concept-laser.de/en/technology/materials.html. [Accessed: 13-Oct-2016].

[114] A. C. Van Staden, D. Hagedorn-Hansen, G. A. Oosthuizen, and N. Sacks, “Characteristics of single layer Selective Laser Melted tool grade cemented tungsten carbide,” in *International Conference on Competitive Manufacturing, COMA ’16*, 2016, pp. 141–146.

[115] M. Peters and C. Leyens, *Titanium and Titanium Alloys, Fundamentals and Applications*. Weinheim: Wiley, 2003.

[116] G. Lutjering, J. Williams, and A. Gysler, “Microstructure and mechanical properties of titanium alloys,” *Microstruct. Prop. Mater.*, vol. 2, pp. 1–74, 2000.

[117] S. M. Kelly and S. L. Kampe, “Microstructural evolution in laser-deposited multilayer Ti-6Al-4V builds: Part I. Microstructural characterization.,” *Metall. Mater. Trans.*, vol. 35, no. 6, pp. 1861–1867, 2004.

[118] L. L. Parimi, G. Ravi, D. Clark, and M. M. Attallah, “Microstructural and texture development in direct laser fabricated IN718,” *Mater. Charact.*, vol. 89, pp. 102–111, 2014.

[119] R. Boyer, G. Welsch, and E. W. Collings, *Materials Properties Handbook: Titanium Alloys*. OH: ASM International, 1994.

[120] J. M. Holt and C. Y. Ho, *Structural Alloys Handbook*. IN: CINDAS/Purdue University, 1996.

[121] *Metals Handbook, Vol. 3, Properties and Selection: Stainless Steels, Tool Materials and Special-Purpose Metals*, 9th ed. OH: American Society for Metals, 1980.

[122] ASM, “Titanium Ti-6Al-4V (Grade 5), Annealed,” 2015. [Online]. Available: http://asm.matweb.com/search/SpecificMaterial.asp?bassnum=MTP641. [Accessed: 19-Jun-2015].

[123] C. Amon, J. Beuth, H. Kirchner, R. Merz, F. Prinz, K. Schmaltz, and L. Weiss, “Material Issues in Layered Forming,” in *Solid Freeform Fabrication Conference Proceedings*, 1993, pp. 1–10.

[124] P. J. Withers and H. K. D. H. Bhadeshia, “Residual stress : Part 1--measurement techniques,” *Mater. Sci. Technol.*, vol. 17, no. 4, pp. 355–365, 2001.

[125] P. J. Withers, “Residual stress and its role in failure.,” *Reports Prog. Phys.*, vol. 70, no. 12, pp. 2211–2264, 2007.

[126] M. F. Zaeh and G. Branner, “Investigations on residual stresses and deformations in selective laser melting,” *Prod. Eng. Res. Dev.*, vol. 4, no. 1, pp. 35–45, 2010.

[127] P. Yuan and D. Gu, “Molten pool behaviour and its physical mechanism during selective laser melting of TiC/AlSi10Mg nanocomposites: simulation and experiments,” *J. Phys. D. Appl. Phys.*, vol. 48, no. 3, 2015.

[128] L. Ma and H. Bin, “Temperature and stress analysis and simulation in fractal scanning-based

laser sintering," *Int. J. Adv. Manuf. Technol.*, vol. 34, no. 9–10, pp. 898–903, 2006.

[129] D. Q. Zhang, Q. Z. Cai, J. H. Liu, L. Zhang, and R. D. Li, "Select laser melting of W-Ni-Fe powders: Simulation and experimental study," *Int. J. Adv. Manuf. Technol.*, vol. 51, no. 5–8, pp. 649–658, 2010.

[130] T. Childs, C. Hauser, and M. Badrossamay, "Selective laser sintering (melting) of stainless and tool steel powders: experiments and modelling," *Proc. Inst. Mech. Eng.*, vol. 219, no. 4, pp. 339–357, 2005.

[131] J. P. Kruth, G. Levy, F. Klocke, and T. H. C. Childs, "Consolidation phenomena in laser and powder-bed based layered manufacturing," *CIRP Ann. - Manuf. Technol.*, vol. 56, no. 2, pp. 730–759, 2007.

[132] I. A. Roberts, C. J. Wang, R. Esterlein, M. Stanford, and D. J. Mynors, "A three-dimensional finite element analysis of the temperature field during laser melting of metal powders in additive layer manufacturing," *Int. J. Mach. Tools Manuf.*, vol. 49, no. 12–13, pp. 916–923, 2009.

[133] K. Dai and L. Shaw, "Finite element analysis of the effect of volume shrinkage during laser densification," *Acta Mater.*, vol. 53, no. 18, pp. 4743–4754, 2005.

[134] J. P. Holman, *Heat Transfer*, Tenth Edit. New York: McGraw-Hill, 2010.

[135] K. Dai, X. Li, and L. Shaw, "Thermal Analysis of Laser-Densified Dental Porcelain Bodies: Modeling and Experiments," *J. Heat Transfer*, vol. 126, no. 5, p. 818, 2004.

[136] A. V. Gusarov, I. Yadroitsev, P. Bertrand, and I. Smurov, "Heat transfer modelling and stability analysis of selective laser melting," *Appl. Surf. Sci.*, vol. 254, no. 4, pp. 975–979, 2007.

[137] L. Der Schritt, "SLM ® 500 HL Laser Beam Melting System," 2014.

[138] H. Schleifenbaum, W. Meiners, K. Wissenbach, and C. Hinke, "Individualized production by means of high power Selective Laser Melting," *CIRP J. Manuf. Sci. Technol.*, vol. 2, no. 3, pp. 161–169, 2010.

[139] J.-P. Kruth, E. Yasa, and J. Deckers, "Roughness Improvement in Selective Laser Melting," in *Proceedings of the 3rd International Conference on Polymers and Moulds Innovations*, 2008, pp. 170–183.

[140] R. Stamp, P. Fox, W. O'Neill, E. Jones, and C. Sutcliffe, "The development of a scanning strategy for the manufacture of porous biomaterials by selective laser melting," *J. Mater. Sci. Mater. Med.*, vol. 20, no. 9, pp. 1839–1848, 2009.

[141] E. Yasa and J. Deckers, "Investigation on occurrence of elevated edges in selective laser melting," in *International Solid Freeform Fabrication Symposium*, 2009, pp. 180–192.

[142] J. Kruth, P. Mercelis, J. Van Vaerenbergh, and T. Craeghs, "Feedback control of Selective

Laser Melting," in *Proceedings of the 3rd International Conference on Advanced Research in Virtual and Rapid Prototyping*, 2007, pp. 1–7.

[143] S. Kac and J. Kusinski, "SEM structure and properties of ASP2060 steel after laser melting," *Surf. Coatings Technol.*, vol. 180–181, pp. 611–615, 2004.

[144] Y. Xianqing, Z. Chengjun, S. Xuefeng, H. Manping, and M. Jianguo, "Microstructure evolution of WC/steel composite by laser surface re-melting," *Appl. Surf. Sci.*, vol. 253, no. 9, pp. 4409–4414, 2007.

[145] D. Felgueroso, R. Vijande, J. M. Cuetos, R. Tucho, and A. Hernandez, "Parallel laser melted tracks: Effects on the wear behaviour of plasma-sprayed Ni-based coatings," *Wear*, vol. 264, pp. 247–263, 2008.

[146] Y. Zhang, J. Chen, W. Lei, and R. Xv, "Effect of laser surface melting on friction and wear behavior of AM50 magnesium alloy," *Surf. Coatings Technol.*, vol. 202, no. 14, pp. 3175–3179, 2008.

[147] C. H. Tang, F. T. Cheng, and H. C. Man, "Improvement in cavitation erosion resistance of a copper based propeller alloy by laser surface melting.," *Surf. Coatings Technol.*, vol. 182, pp. 300–307, 2004.

[148] W. L. Xu, T. M. Yue, H. C. Man, and C. P. Chan, "Laser surface melting of aluminium alloy 6013 for improving pitting corrosion fatigue resistance," *Surf. Coat. Technol.*, vol. 200, pp. 5077–5086, 2006.

[149] M. Tritica, B. Gakovic, D. Batani, T. Desai, P. Panjan, and B. Radak, "Surface modifications of a titanium implant by a picosecond Nd :YAG laser operating at 1064 and 532 nm," *Appl. Surf. Sci.*, vol. 253, pp. 2551–2556, 2006.

[150] J. Lawrence and L. Li, "A laser based technique for the coating of mild steel with a vitreous enamel.," *Surf. Coatings Technol.*, vol. 140, pp. 238–243, 2001.

[151] F. Z. Henari and W. Blau, "Excimer-Laser Surface Treatment of Metals for Improved Adhesion," *Appl. Opt.*, vol. 34, pp. 581–584, 1995.

[152] J. Grum and J. M. Slabe, "Effect of laser re-melting of surface cracks on microstructure and residual stresses in 12Ni maraging steel.," *Appl. Surf. Sci.*, vol. 252, pp. 4486–4492, 2006.

[153] B. Qian, L. C. Zhang, Y. S. Shi, and B. Liu, "Voronoi approach to recursive generation of tool path for SLS.," *CADDM*, vol. 18, no. 2, pp. 13–30, 2008.

[154] B. Qian, L. C. Zhang, Y. S. Shi, and B. Liu, "Recursive polygon offset computing for rapid prototyping applications based on Voronoi diagrams," *Int. J. Adv. Manuf. Technol.*, vol. 49, pp. 1019–1028, 2009.

[155] W. Di, Y. Yongqiang, S. Xubin, and C. Yonghua, "Study on energy input and its influences on single-track,multi-track, and multi-layer in SLM," *Int. J. Adv. Manuf. Technol.*, vol. 58,

no. 9–12, pp. 1189–1199, 2012.

[156] R. H. Morgan, A. J. Papworth, C. Sutcliffe, P. Fox, and W. O'Neill, "High density net shape components by direct laser re-melting of single-phase powders," *J. Mater. Sci.*, vol. 37, no. 15, pp. 3093–3100, 2002.

[157] L. Thijs, M. L. Montero Sistiaga, R. Wauthle, Q. Xie, J. P. Kruth, and J. Van Humbeeck, "Strong morphological and crystallographic texture and resulting yield strength anisotropy in selective laser melted tantalum," *Acta Mater.*, vol. 61, no. 12, pp. 4657–4668, 2013.

[158] S. Merkt, C. Hinke, J. Bultmann, M. Brandt, and M. Xie, "The mechanical response of TiAl6V4 lattice structures manufactured by SLM in quasi static and dynamic compression tests," vol. 17006, pp. 3–10, 2015.

[159] M. Shiomi, K. Osakada, K. Nakamura, T. Yamashita, and F. Abe, "Residual Stress within Metallic Model Made by Selective Laser Melting Process," *Ann. CIRP*, vol. 53, no. 1, pp. 195–198, 2004.

[160] F. C. Herzog, "Production of sintered workpieces involves heating individual areas of material irradiation so that they fuse together, where individual areas are separated by distance at least their diameter," 10042134, 2002.

[161] V. Manvatkar, A. De, and T. DebRoy, "Spatial variation of melt pool geometry, peak temperature and solidification parameters during laser assisted additive manufacturing process," *Mater. Sci. Technol.*, vol. 31, no. 8, pp. 924–930, 2015.

[162] M. Alimardani, E. Toyserkani, J. P. Huissoon, and C. P. Paul, "On the delamination and crack formation in a thin wall fabricated using laser solid freeform fabrication process: An experimental-numerical investigation," *Opt. Lasers Eng.*, vol. 47, no. 11, pp. 1160–1168, 2009.

[163] A. S. Wu, D. W. Brown, M. Kumar, G. F. Gallegos, and W. E. King, "An Experimental Investigation into Additive Manufacturing Induced Residual Stresses in 316L Stainless Steel," *Metall. Mater. Trans. A*, vol. 45, no. 13, pp. 6260–6270, 2014.

[164] F. Brückner, D. Lepski, and E. Beyer, "Modeling the Influence of Process Parameters and Additional Heat Sources on Residual Stresses in Laser Cladding," *J. Therm. Spray Technol.*, vol. 16, no. 3, pp. 355–373, 2007.

[165] A. Vasinonta, J. L. Beuth, and M. Griffith, "Process Maps for Predicting Residual Stress and Melt Pool Size in the Laser-Based Fabrication of Thin-Walled Structures," *J. Manuf. Sci. Eng.*, vol. 129, no. 1, pp. 101–109, 2007.

[166] J.-P. Kruth, J. Deckers, E. Yasa, and R. Wauthle, "Assessing and comparing influencing factors of residual stresses in selective laser melting using a novel analysis method," *Proc. Inst. Mech. Eng. Part B J. Eng. Manuf.*, vol. 226, no. 6, pp. 980–991, 2012.

[167] "1.2316 Mold Steel," 2015. [Online]. Available: http://www.matweb.com/search/datasheet.aspx?matguid=d1d7a74c990240d9852cc3e846d2966c&ckck=1. [Accessed: 30-Jun-2015].

[168] "1.2709 Powder Steel," 2015. [Online]. Available: http://www.matweb.com/search/DataSheet.aspx?MatGUID=e9f7cb19eb81450d8f67966151bd1802. [Accessed: 30-Jun-2015].

[169] X. Su and Y. Yang, "Research on track overlapping during Selective Laser Melting of powders," *J. Mater. Process. Technol.*, vol. 212, no. 10, pp. 2074–2079, 2012.

[170] C. Klahn, F. Bechmann, S. Hofmann, M. Dinkel, and C. Emmelmann, "Laser additive manufacturing of gas permeable structures," *Phys. Procedia*, vol. 41, pp. 873–880, 2013.

[171] L. Thijs, B. Vrancken, J.-P. Kruth, and J. Van Humbeeck, "The Influence of Process Parameters and Scanning Strategy on the Texture in Ti6Al4V Parts Produced by Selective Laser Melting," in *Proceedings of the Materials Science and Technology (MS&T) Conference*, 2013, pp. 21–28.

[172] L. N. Carter, C. Martin, P. J. Withers, and M. M. Attallah, "The influence of the laser scan strategy on grain structure and cracking behaviour in SLM powder-bed fabricated nickel superalloy," *J. Alloys Compd.*, vol. 615, pp. 338–347, 2014.

[173] Rofin, "Rofin Starfiber." [Online]. Available: https://www.rofin.com/fileadmin/user_upload/content/5_produkte/3_faserlaser/Dat_StarFiber_100-600_V1_2015_E.pdf. [Accessed: 14-Oct-2016].

[174] "Calibration Report," Stellenbosch, 2012.

[175] "CT Scanner," *Stellenbosch University*, 2016. [Online]. Available: http://blogs.sun.ac.za/ctscanner/introduction/. [Accessed: 11-Aug-2016].

[176] A. Staude and J. Goebbels, "Determining the Spatial Resolution in Computed Tomography – Comparison of MTF and Line-Pair Structures," *Int. Symp. Digit. Ind. Radiol. Comput. Tomogr.*, pp. 1–9, 2006.

[177] "Consideration for a Specimen Micro-CT Scan," 2010.

[178] O. Corporation, "Olympus Stereomicroscope System SZX7." [Online]. Available: http://www.olympusamerica.com/files/seg_bio/szx7_brochure.pdf. [Accessed: 01-Nov-2016].

[179] O. Corporation, "GX 51 Inverted Microscope." [Online]. Available: http://www.olympus-ims.com/en/microscope/gx51/#!cms[tab]=%2Fmicroscope%2Fgx51%2Fspecifications. [Accessed: 01-Nov-2016].

[180] J. Antony, "Fundamentals of Designing Experiments.," in *Design of Experiments for Engineers and Scientists*, London: Elsevier Ltd., 2003, pp. 6–16.

[181] M. Cavazzuti, “Design of Experiments,” in *Optimization Methods: From Theory to Design*, Heidelberg: Springer-Verlag, 2013, pp. 13–42.

Appendix A: Equipment and DoE

Measurement and Experimental Instruments

An understanding of the instruments that will be used in a study is very important. The research outputs are limited by the capabilities of the research instruments. In order to complete the research, several machines were used. These machines are discussed in the following sections and a basic description is given for each machine.

M2 Cusing Machine

In order to produce the experimental parts a selective laser melting machine was used. The STC-LAM at the University of Stellenbosch has a Concept Laser M2 Laser Cusing machine shown in Figure A.1. The technical data of the machine can be observed below in Table A.1.

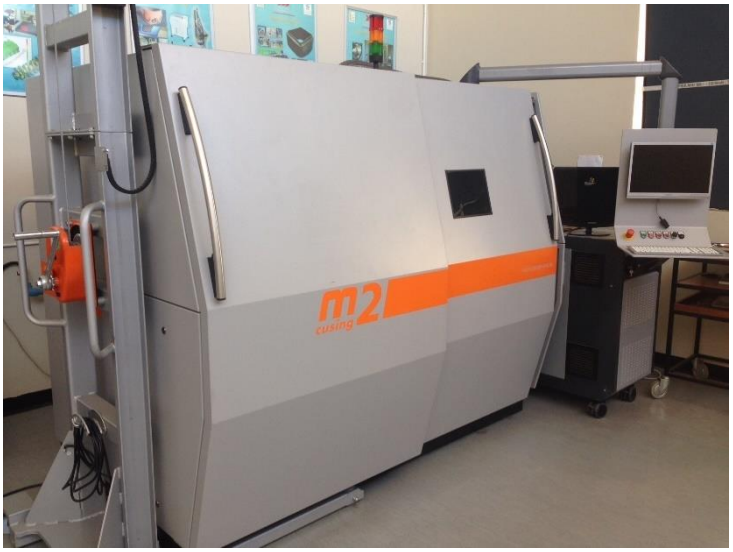

Figure A.1: Concept Laser M2 Cusing Machine at Stellenbosch University

Table A.1: M2 Laser Cusing machine specifications adapted from [91]

Specification Description	Values
Build Envelope LaserCUSING	250 mm x 250 mm x 280 mm (x, y, z)
Layer Thickness LaserCUSING	20 µm – 50 µm
Production Speed	2 – 20 cm^3/hour (material dependant)
Laser System	Fibre Laser 200 Watt
Maximum Scanning Speed	7 m/s
Zero Point Clamping System	EROWA, System 3R
Connected Loads	Power Consumption 7.0 kW
	Power Supply 3/N/PE AC 400V, 32A
	5 bar Compressed Air
Inert Gas Consumption	Approximately 2.5 m^3/hour
Operating Conditions	15 - 35°C

There are several factors that influence the running costs of the M2 Laser Cusing machine, such as, the cost of materials, the cost of gas, and the electricity costs. These factors must be taken into account when determining the overall cost of SLM technology over other commercial technologies.

Rofin StarFiber Laser

The SLM process requires a special laser in order perform the fast, accurate, scans which the AM process demands. The laser that came with the Concept Laser M2 Machine is the Rofin Starfiber 200W laser. The specifications of the laser are displayed in Table A.2.

Table A.2: Rofin Starfiber 200 laser specifications [173]

Specification Description	Units	Value
Wavelength	nm	1070
Max. average power	W	200
Pulse frequency	kHz	Single shot up to 170
Pulse width	µs	1 - cw
Beam diameter	mm	5
Beam divergence (86% level)	mrad	collimated

Coordinate Measuring Machine

In order to determine the deviation in the test samples a coordinate measuring machine (CMM) was used. The STC has a Mitutoyo Bright Apex-710 CMM, which has the following specifications:

Table A.3: Specifications of the Mitutoyo A710 CMM Machine [174]

Specification Description	Value
Measuring Range	705 mm x 1005 mm x 605 mm (x, y, z)
Accuracy	3 µm – 5 µm
Controller	Mitutoyo DCC Control
Probing	Renishaw PH10M Probe Head Renishaw TP2 Touch Probe
Software	Mitutoyo GeoMeasure Software

Computerised Tomography Scanning

A computerised tomography (CT) scanner was used to scan samples in order to investigate and analyse the inside of the sample in a non-destructive way with a high resolution and contrast. The sample is exposed to collimated x-rays and the absorbed radiation is measured on the other side of the sample with a sensor. Thus scanning method is performed around the sample in order to render a full 3D construction of the sample. CT scanning can be used to measure porosity of the sample and to identify cracks, transitions, or inclusions in the material [175]. The CT scanner at Stellenbosch University is displayed in Figure A.2.

Figure A.2: General Electric V|Tome|X L240 CT Scanner that can be found in the Forestry Department at Stellenbosch University [175]

The resolution of the scan is dependent on the voxel size. The voxel size is the size of a 3D pixel in the rendered CT image, this pixel size is termed the nominal or spatial resolution of a CT measurement. The smaller the voxel size, the more accurate a measurement will be and more defects can be detected in a sample. There are several factors that influence the spatial resolution namely, the X-ray source and detector (focal spot size, pixel size, scattering), the magnification in the cone-beam geometry, the measurement strategy (projections per full rotation, reconstruction process), and finally the type of material of the sample (diffracts or reflects X-rays) [176], [177].

When determining the special resolution of the sample before scanning there are two different methods. The first method is to calculate the modulation transfer function (MTF) from the measured edge of a cylinder, the second method is to measure the contrast of the material to the background with regards to the size of the structures of line pairs [176]. A graph has been developed using these methods and can be observed in Figure A.3 below.

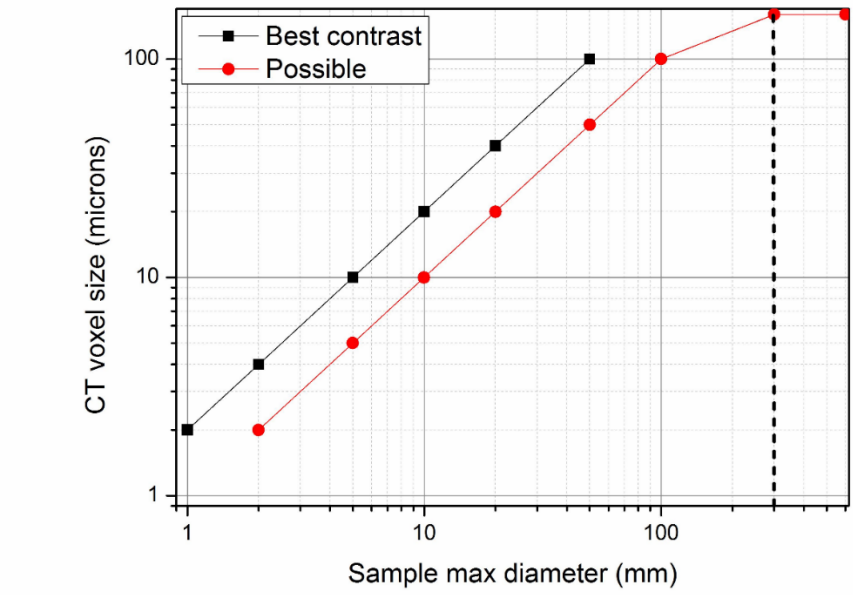

Figure A.3: Graph used to determine voxel size from sample size [175]

Using the graph above one can calculate the voxel size relative to the sample's maximum diameter. The smaller the diameter of the sample the better quality the CT scans will be. If the sample diameter is large, the voxel size will also be large and the CT scanner, then wont detect all of the inclusions smaller than the voxel size. The smallest voxel size with the microCT scanner is 2 microns meaning any inclusions or porosity that is smaller than 2 microns will not be detected.

Stereo and Inverted Microscopes

The Olympus SZX 7 stereomicroscope and GX 51 inverted microscope were used to inspect samples and hatch melt pools. The two microscopes located at Stellenbosch University's Mechanical Engineering laboratory can be observed in Figure A.4 below.

Figure A.4: (Left) Olympus SZX 7 Stereomicroscope and (Right) Olympus GX 51 Inverted Microscope

The specifications of the SZX7 and the GX 51 can be observed in Table A.4. The SC30 camera is used on both of the microscopes, to duplicate the image onto a computer. The Stream Essentials software is used for the camera control and to view the camera images in real time. Stream Essentials can also be utilised to measure the distance between pixels of microscope images. The zoom ratios of the microscopes as well as the important camera information is displayed in Table A.4.

Table A.4: Olympus SZX 7 Stereomicroscope, GX 51 Microscope and SC30 Camera Specifications [178], [179]

Specification Description	Value
Olympus SZX 7	
Zoom Ratio Values	7:1 (0.8x, 1x, 1.6x, 2x, 3.2x, 4.8x, 5.6x)
Light Source	White LED transmitted illumination stand
Olympus GX 51	
Zoom Ratio Values	5x, 10x, 20x, 50x, 100x
Light Source	100 W Halogen
SC30 Camera	
Total pixels	3.3 megapixel CMOS Sensor
Image Sensor	CMOS Sensor
Resolution	1024 x 768 pixels at 28 fps
Exposure Range	57 µs – 75 s
Software	Stream Essentials

Basic Principles of Statistical Methods

According to Antony and Cavazzuti [180], [181] there are three basic principles of experimental design, namely randomisation, replication, and blocking. These principles should be used to improve the efficiency and effectiveness of experimentation. The principles should be applied to avoid or completely remove mental bias of the experimenter. Experimental bias could have a detrimental effect on the statistical significance of certain factors [180]. The three principles are discussed in the following sections.

Randomisation

Randomisation is performed in order to reduce the effects that experimental bias can have on the outcome. Randomisation refers to the random order in which experimental runs are performed [180], [181]. This ensures that the conditions of an experimental run does not affect the conditions of another run. If noise factors are present, the effects will be averaged out when randomising the runs.

Replication

Replication is the process of repeating experimental trials in a random manner to obtain statistically accurate results and experimental error estimation [180], [181]. Replication can be performed on the entire experiment or just a portion of it. Experimental error, factor or interaction effects can be quite significant and replication would have to be performed in order to make these effects less significant. Note that repetition and replication are not the same thing.

Blocking

Blocking is the method of improving experimental design efficiency by removing the effects of peripheral variation caused by noise factors [180]. Cavazzuti [181] states that blocking is used to isolate known systematic bias effects in order to prevent them from concealing the main effects. To perform blocking, experiments are arranged in blocks (or groups) that are similar in nature. The variability is therefore reduced and the precision of the experiment is improved.

Appendix B: Development of Scan Strategies

Helix Scan Strategy 1:

Vector Pattern: Helix

Method: Structured scanning of each square vector set starting from the smallest square vector set moving in an outwards fashion to the largest vector set.

Proposed scanning strategy 1 can be observed in Figure B.1. The laser will begin in island A and scan vector set 1. Once vector set 1 is scanned the laser will move to island B and scan vector set 1 and so on until all of the vector 1 sets in all of the islands have been scanned. The laser will then move over to vector set 2 and will repeat the same process as before. The laser will repeat this process until all of the vector sets in all of the islands have been scanned.

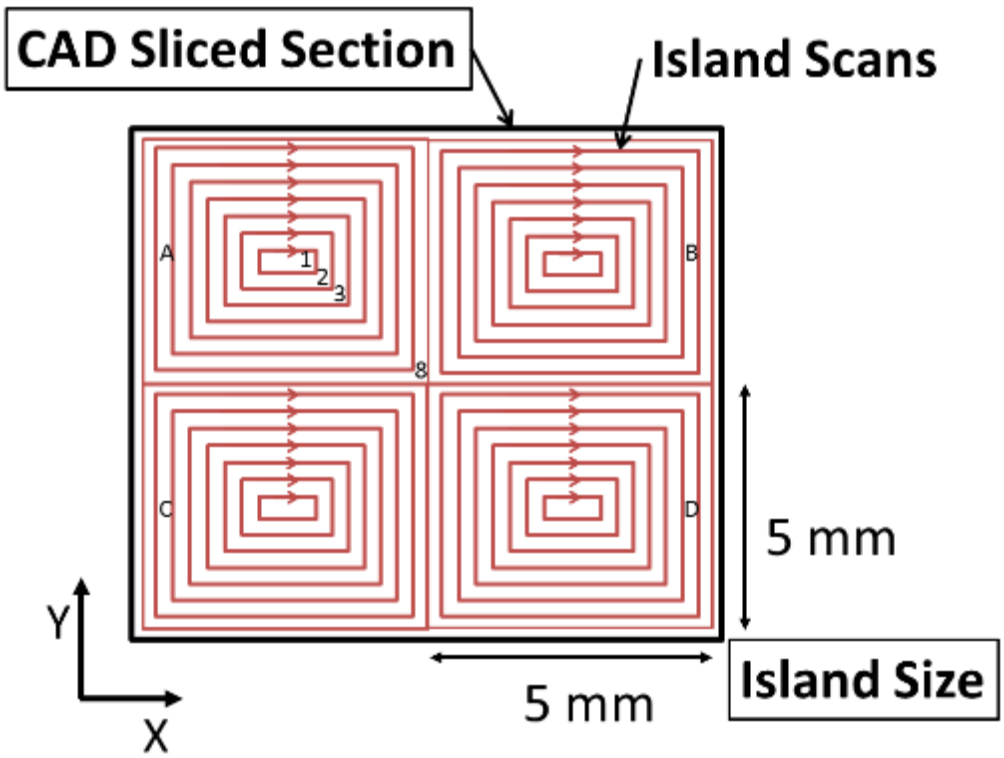

Figure B.1: Proposed Helix Scanning Strategy 1

Helix Scan Strategy 2:

Vector Pattern: Helix

Method: Structured scanning of each square vector set starting from the largest square vector set moving in an inwards fashion to the smallest vector set.

Proposed scanning strategy 2 can be observed in Figure B.2. The laser will begin in island A and scan the outer vector set 1. Once vector set 1 is scanned the laser will move to island B and scan

vector set 1 and so on until all of the vector 1 sets in all of the islands have been scanned. The laser will then move over to vector set 2 and will repeat the same process as before. The laser will repeat this process until all of the vector sets in all of the islands have been scanned.

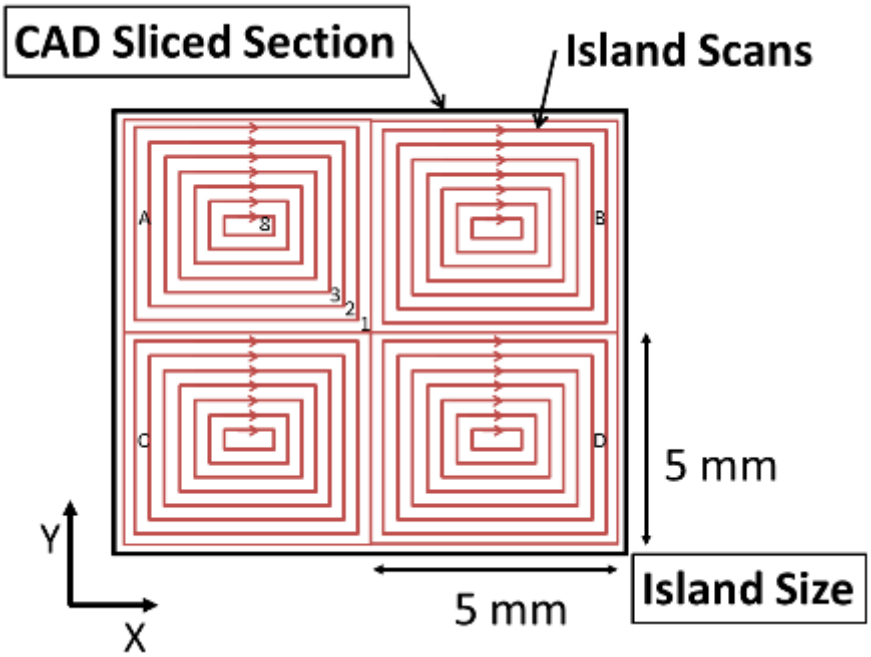

Figure B.2: Proposed Helix Scanning Strategy 2

Helix Scan Strategy 3:

Vector Pattern: Helix

Method: Structured scanning of each square vector set starting from the smallest square vector set moving to the largest vector set then to the second smallest vector set and so on.

Proposed scanning strategy 3 can be observed in Figure B.3. The laser will begin in island A and scan the inner vector set 1. Once vector set 1 is scanned the laser will move to island B and scan vector set 1 and so on until all of the vector 1 sets in all of the islands have been scanned. The laser will then move over to the outer vector set 2 and will repeat the same process as before. The laser will repeat this process until all of the vector sets in all of the islands have been scanned.

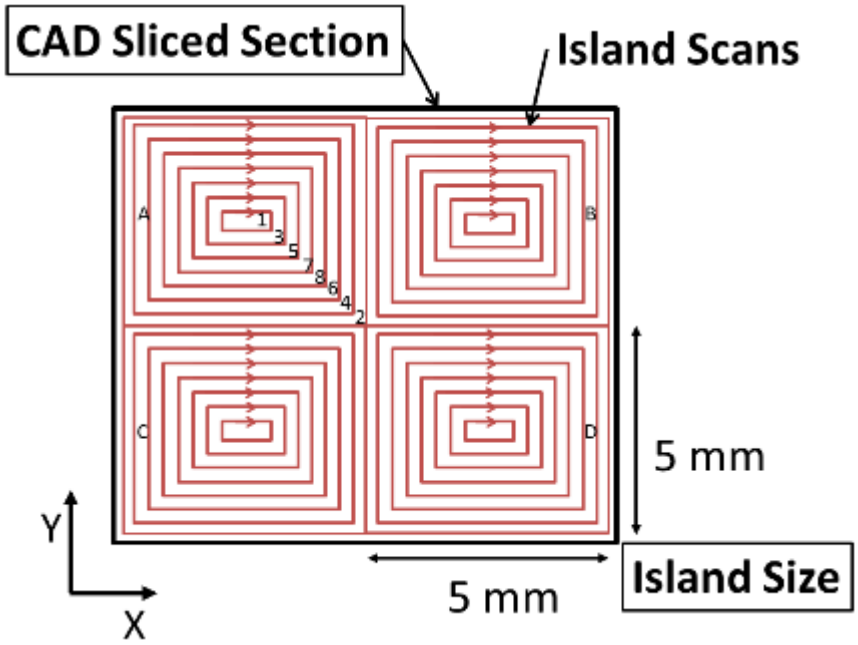

Figure B.3: Proposed Helix Scanning Strategy 3

The three proposed scan strategies are a combination of the Island scan strategy, the contour scan strategy, the helix strategy and the inter layer stagger scanning strategy.

Hatch Pattern Design Method

An Excel model was developed in order to assist users of the Hatch Pattern Design method in copying and designing the parts for Magics. The parts were imported into Magics one by one. Once a whole island was imported it could be copied until the entire part was formed. Two hatch parts are displayed in the figure below. The parts have been imported onto the Magics software and have been placed on the virtual machine bed on the origin.

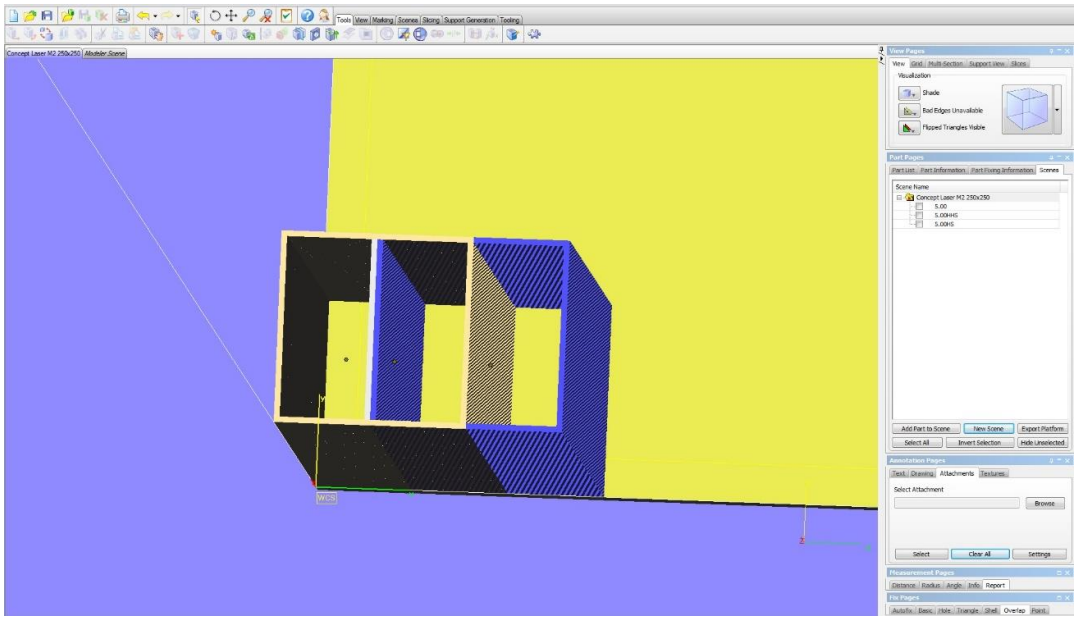

Figure B.4: Two hatch line parts imported into Magics software and stacked together

Excel Model

Excel model for Hatch Pattern Design method

	A	B	C	D	E	F	G	H
1		**Parameters**	Value	Units		**Part Parameters**	Value	Units
2		Beam Spot Diameter	0.15	mm		Size in the X direction	120	mm
3		Hatch Spacing Coef	0.7			Size in the Y direction	25	mm
4		Scanning Velocity	600	mm/s		Total Area per slice	=G2*G3	mm^2
5		Laser Power	100	Watts		Island area	=POWER(C6,2)	mm^2
6		Island Size	5	mm		Total Islands per slice	=G4/G5	
7		Actual Hatch Spacing	=C3*C2	mm				
8		Beam Compensation Coef	0.15					
9		Actual Beam Compensation	=C8*C2	mm		Total Time	=SUM(H16:H38	
10		Melt Pool Shrinkage Percentage	0.015			Total Time between outer scans	=G9/4	
11		Melt Pool Shrinkage	=C2*C10	mm				
12								
13			Helix Scan Vectors					
14		With Hatch Spacing	X	Y	Copy Space	Vector Length	Scan Time [s]	Scan Time per Slice
15	1	=$C$6	0	0	=2*C15	=B15*4	=F15/$C$4	=G15*$G$6
16	2	=IF(B15-(2*$C$7)>0, B15-(2*$C$7), " ")	=$C$7	=$C$7	=2*C16	=B16*4	=F16/$C$4	=G16*$G$6
17	3	=IF(B16-(2*$C$7)>0, B16-(2*$C$7), " ")	=C16+$C$7	=D16+$C$7	=2*C17	=B17*4	=F17/$C$4	=G17*$G$6
18	4	=IF(B17-(2*$C$7)>0, B17-(2*$C$7), " ")	=C17+$C$7	=D17+$C$7	=2*C18	=B18*4	=F18/$C$4	=G18*$G$6
19	5	=IF(B18-(2*$C$7)>0, B18-(2*$C$7), " ")	=C18+$C$7	=D18+$C$7	=2*C19	=B19*4	=F19/$C$4	=G19*$G$6
20	6	=IF(B19-(2*$C$7)>0, B19-(2*$C$7), " ")	=C19+$C$7	=D19+$C$7	=2*C20	=B20*4	=F20/$C$4	=G20*$G$6
21	7	=IF(B20-(2*$C$7)>0, B20-(2*$C$7), " ")	=C20+$C$7	=D20+$C$7	=2*C21	=B21*4	=F21/$C$4	=G21*$G$6
22	8	=IF(B21-(2*$C$7)>0, B21-(2*$C$7), " ")	=C21+$C$7	=D21+$C$7	=2*C22	=B22*4	=F22/$C$4	=G22*$G$6
23	9	=IF(B22-(2*$C$7)>0, B22-(2*$C$7), " ")	=C22+$C$7	=D22+$C$7	=2*C23	=B23*4	=F23/$C$4	=G23*$G$6
24	10	=IF(B23-(2*$C$7)>0, B23-(2*$C$7), " ")	=C23+$C$7	=D23+$C$7	=2*C24	=B24*4	=F24/$C$4	=G24*$G$6
25	11	=IF(B24-(2*$C$7)>0, B24-(2*$C$7), " ")	=C24+$C$7	=D24+$C$7	=2*C25	=B25*4	=F25/$C$4	=G25*$G$6
26	12	=IF(B25-(2*$C$7)>0, B25-(2*$C$7), " ")	=C25+$C$7	=D25+$C$7	=2*C26	=B26*4	=F26/$C$4	=G26*$G$6
27	13	=IF(B26-(2*$C$7)>0, B26-(2*$C$7), " ")	=C26+$C$7	=D26+$C$7	=2*C27	=B27*4	=F27/$C$4	=G27*$G$6
28	14	=IF(B27-(2*$C$7)>0, B27-(2*$C$7), " ")	=C27+$C$7	=D27+$C$7	=2*C28	=B28*4	=F28/$C$4	=G28*$G$6
29	15	=IF(B28-(2*$C$7)>0, B28-(2*$C$7), " ")	=C28+$C$7	=D28+$C$7	=2*C29	=B29*4	=F29/$C$4	=G29*$G$6
30	16	=IF(B29-(2*$C$7)>0, B29-(2*$C$7), " ")	=C29+$C$7	=D29+$C$7	=2*C30	=B30*4	=F30/$C$4	=G30*$G$6

Figure B.5: Excel model as shown on Microsoft Excel

The Model Results when using the default laser parameters can be observed in Table B.1.

Table B.1: Model Results when using the default laser parameters

	Hatch Spacing	X	Y	Copy Space	Vector Length	Scan Time [s]	Scan Time per Slice
1	5.000	0.000	0.000	0.000	20.000	0.0333	4.0000
2	4.790	0.105	0.105	0.210	19.160	0.0319	3.8320
3	4.580	0.210	0.210	0.420	18.320	0.0305	3.6640
4	4.370	0.315	0.315	0.630	17.480	0.0291	3.4960
5	4.160	0.420	0.420	0.840	16.640	0.0277	3.3280
6	3.950	0.525	0.525	1.050	15.800	0.0263	3.1600
7	3.740	0.630	0.630	1.260	14.960	0.0249	2.9920
8	3.530	0.735	0.735	1.470	14.120	0.0235	2.8240
9	3.320	0.840	0.840	1.680	13.280	0.0221	2.6560
10	3.110	0.945	0.945	1.890	12.440	0.0207	2.4880
11	2.900	1.050	1.050	2.100	11.600	0.0193	2.3200
12	2.690	1.155	1.155	2.310	10.760	0.0179	2.1520
13	2.480	1.260	1.260	2.520	9.920	0.0165	1.9840
14	2.270	1.365	1.365	2.730	9.080	0.0151	1.8160
15	2.060	1.470	1.470	2.940	8.240	0.0137	1.6480
16	1.850	1.575	1.575	3.150	7.400	0.0123	1.4800
17	1.640	1.680	1.680	3.360	6.560	0.0109	1.3120
18	1.430	1.785	1.785	3.570	5.720	0.0095	1.1440
19	1.220	1.890	1.890	3.780	4.880	0.0081	0.9760
20	1.010	1.995	1.995	3.990	4.040	0.0067	0.8080
21	0.800	2.100	2.100	4.200	3.200	0.0053	0.6400
22	0.590	2.205	2.205	4.410	2.360	0.0039	0.4720
23	0.380	2.310	2.310	4.620	1.520	0.0025	0.3040
24	0.170	2.415	2.415	4.830	0.680	0.0011	0.1360

The excel model can be used to copy the parts into Magics. Once the entire part is copied in the parts can be sliced using the Concept Laser Slicer. An example of how the slicer looks is displayed in Figure B.6.

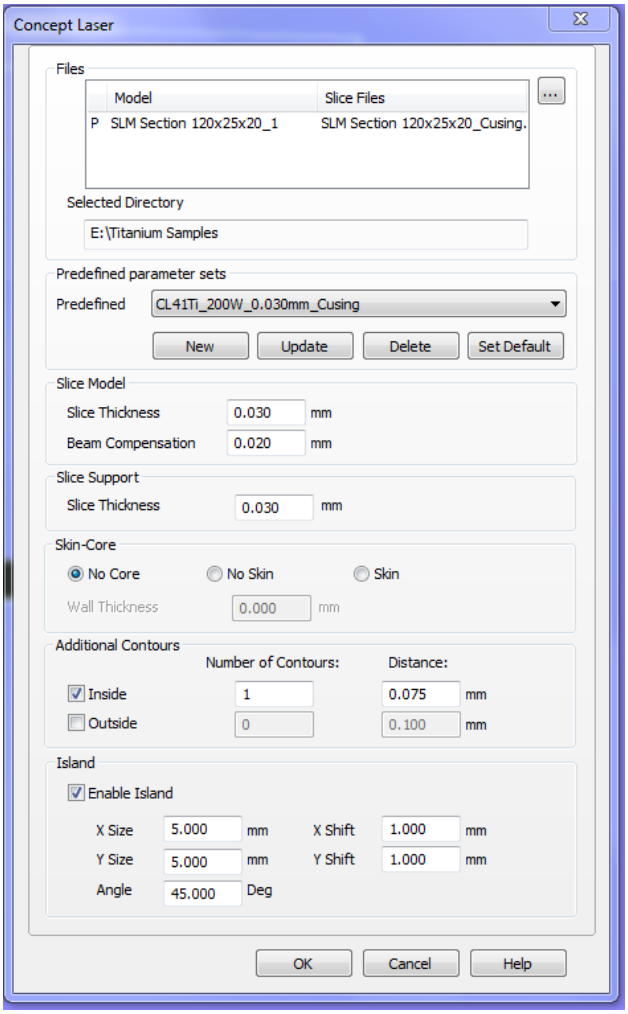

Figure B.6: Concept Laser Slicer used to slice parts in Magics and create a CLS file for the M2 Cusing machine

Concept Laser Machine Software

The machines software allows you to import the CLS files, which were output by Magics. These files are the hatch line parts. It was discovered that the order in which the parts are imported is the order in which the laser will scan them. An example of the Concept Laser machine software can be observed in Figure B.7.

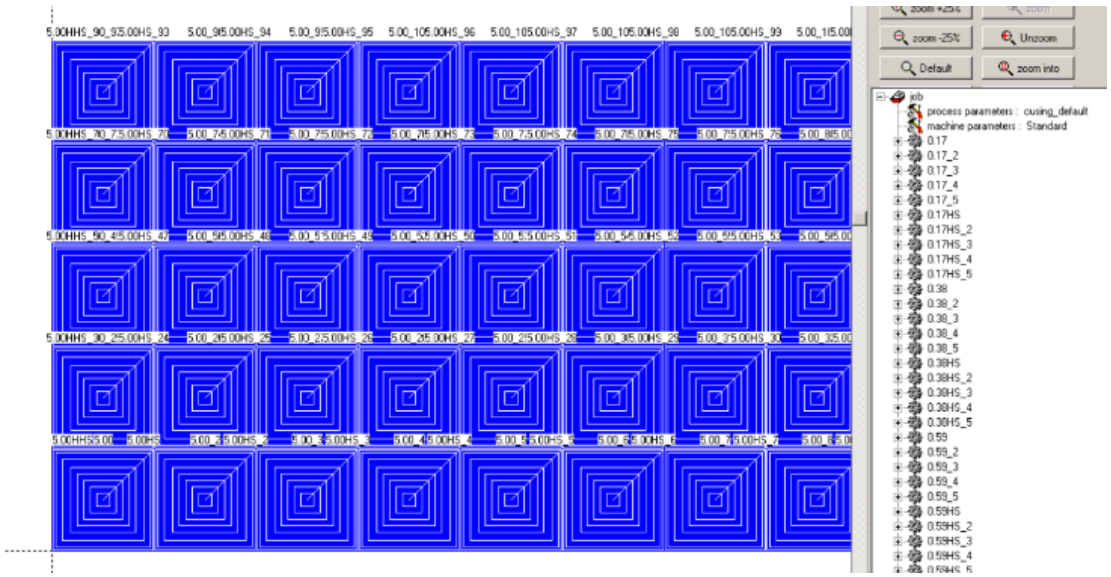

Figure B.7: Concept Laser machine software with the Newly Developed Scan Strategy Parts imported in a specific order

Appendix C: Initial Vector Calculations

Vector Calculations

The hatch vector spacing is
a = 0.7 x d where d is the spot/focus diameter of the laser

The spot diameter is set to 0.15 mm and cannot be changed without a technician
Therefore the hatch vector spacing is 0.7 x 0.15 = 0.105 mm

Vector lengths:
Raster Scan Vector Lengths

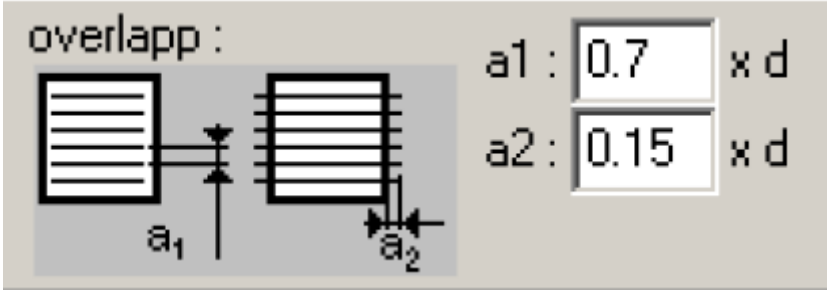

Figure C.1: Concept Laser default parameters as set on the M2 Cusing machine

a1 = 0.7 x d
The spot diameter is 0.15
Therefore the hatch vector spacing a1 is 0.7 x 0.15 = 0.105 mm

5/0.105= 47.62

Overlap:
a2 = 0.15 x d where d is the spot/focus diameter of the laser
The spot diameter is 0.15
Therefore the vector overlap a2 is 0.15 x 0.15 = 0.0225 mm
Therefore each vector is 5 mm = 5.0 mm

Vector Calculations for the different Scanning Strategies can be observed in Tables C.1 and C.2

Table C.1: Default Island Scan Strategy vector calculations

Raster Scan		
	Length of Vectors [mm]	Cumulative length [mm]
Scan 1	5	5
Scan 2	5	10
Scan 3	5	15
Scan 4	5	20
Scan 5 - 42	5	+200
Scan 44	5	220
Scan 45	5	225
Scan 46	5	230
Scan 47	4.895	234.895

The calculations for helix scanning can be observed in Table C.2

Table C.2: Newly Developed Helix Scan Strategy vector calculations

	Helix Scan		
	Vector Lengths of 1 side [mm]	Total length of 4 Sides [mm]	Cumulative length [mm]
Scan 1	4.895	19.58	19.58
Scan 2	4.685	18.74	38.32
Scan 3	4.475	17.9	56.22
Scan 4	4.265	17.06	73.28
Scan 5	4.055	16.22	89.5
Scan 6	3.845	15.38	104.88
Scan 7	3.635	14.54	119.42
Scan 8	3.425	13.7	133.12
Scan 9	3.215	12.86	145.98
Scan 10	3.005	12.02	158
Scan 11	2.795	11.18	169.18
Scan 12	2.585	10.34	179.52
Scan 13	2.375	9.5	189.02
Scan 14	2.165	8.66	197.68
Scan 15	1.955	7.82	205.5
Scan 16	1.745	6.98	212.48
Scan 17	1.535	6.14	218.62
Scan 18	1.325	5.3	223.92
Scan 19	1.115	4.46	228.38
Scan 20	0.905	3.62	232
Scan 21	0.695	2.78	234.78
Scan 22	0.485	1.94	236.72
Scan 23	0.275	1.1	237.82
Scan 24	0.065	0.26	238.08

Because the scan speed is 600 mm/s

Therefore:

Total time for Island with Raster Scan = 0.3915 seconds per island

Total time for Island with Helix Scan = 0.3968 seconds per island

Total Difference between Raster and Helix. Helix is 0.005308333 s slower than raster per island

The vectors for the Default Island Scan Strategy and Newly Developed Helix Strategy can be observed in Figure C.2 and Figure C.3 respectively.

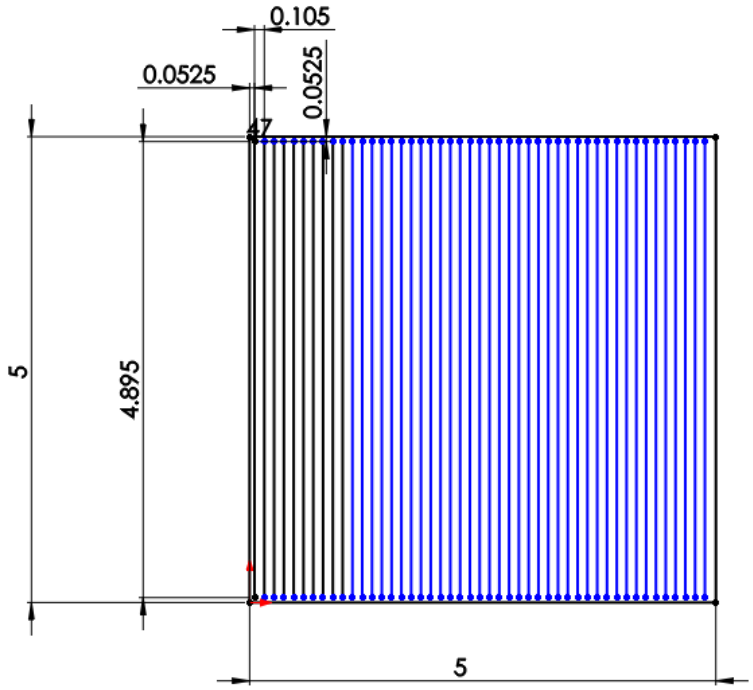

Figure C.2: Vector diagram of Default Island Scan Strategy created on Solidworks

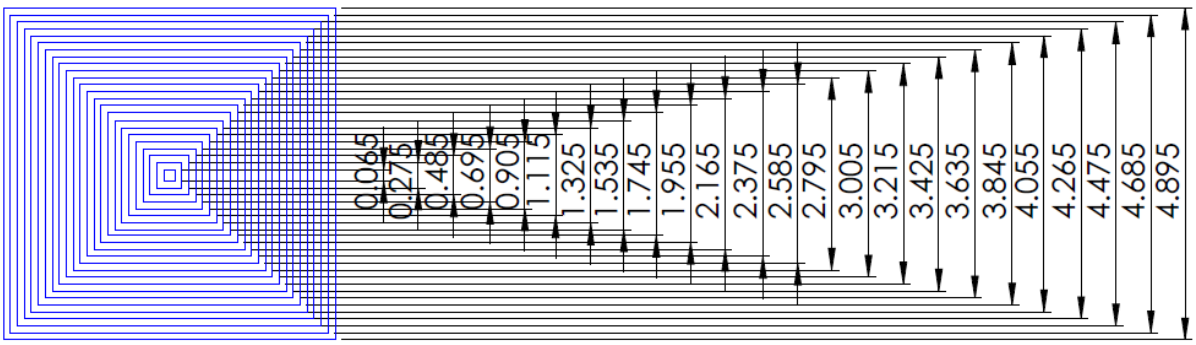

Figure C.3: Vector diagram of Newly Developed Helix Scan Strategy created on Solidworks

Since the vector melting strategy melts 5 islands at a time instead of completing 1 island and moving to another. The laser must travel a lot further and the vector calculations for the laser distance can be observed in Table C.3.

Table C.3: Vector calculations for 5 Islands with the helix scan pattern

Length of 5 Island Vectors	Cumulative Length of 5 island scan vectors	Distance from vectors	Distance Traveled to Melt 5	Distance Back to Start	Length of all Vectors	Cumulative Length
97.9	97.9	5	20	20.105	138.005	138.005
93.7	191.6	5	20	20.105	133.805	271.81
89.5	281.1	5	20	20.105	129.605	401.415
85.3	366.4	5	20	20.105	125.405	526.82
81.1	447.5	5	20	20.105	121.205	648.025
76.9	524.4	5	20	20.105	117.005	765.03
72.7	597.1	5	20	20.105	112.805	877.835
68.5	665.6	5	20	20.105	108.605	986.44
64.3	729.9	5	20	20.105	104.405	1090.845
60.1	790	5	20	20.105	100.205	1191.05
55.9	845.9	5	20	20.105	96.005	1287.055
51.7	897.6	5	20	20.105	91.805	1378.86
47.5	945.1	5	20	20.105	87.605	1466.465
43.3	988.4	5	20	20.105	83.405	1549.87
39.1	1027.5	5	20	20.105	79.205	1629.075
34.9	1062.4	5	20	20.105	75.005	1704.08
30.7	1093.1	5	20	20.105	70.805	1774.885
26.5	1119.6	5	20	20.105	66.605	1841.49
22.3	1141.9	5	20	20.105	62.405	1903.895
18.1	1160	5	20	20.105	58.205	1962.1
13.9	1173.9	5	20	20.105	54.005	2016.105
9.7	1183.6	5	20	20.105	49.805	2065.91
5.5	1189.1	5	20	20.105	45.605	2111.515
1.3	1190.4	5	20	20.105	41.405	2152.92

The time to melt 5 islands using this strategy is therefore 2152.92/scan speed

Therefore, 2152.92/600 = 3.5882 seconds for 5 islands. One could note that the scan speed is the limiting factor on time.

The vector diagram for the calculations above can be observed in Figure C.4.

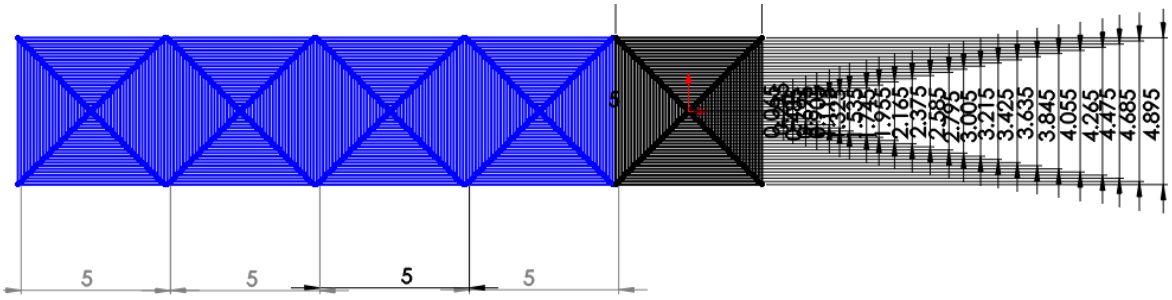

Figure C.4: Vector diagram for 5 Islands of Newly Developed Helix Scan Strategy created on Solidworks

Appendix D: Substrate Experiment Pictures

The pictures taken on the two microscopes are arranged in the tables below. First the Default Island Scan Strategy is displayed in Table D.1, Table D.2, and Table D.3

Table D.1: Default Scan Strategy Sample 1 pictures from Substrate Experiment

Default Island Scan Strategy Sample 1	
Island	**Joint Between Four Islands**
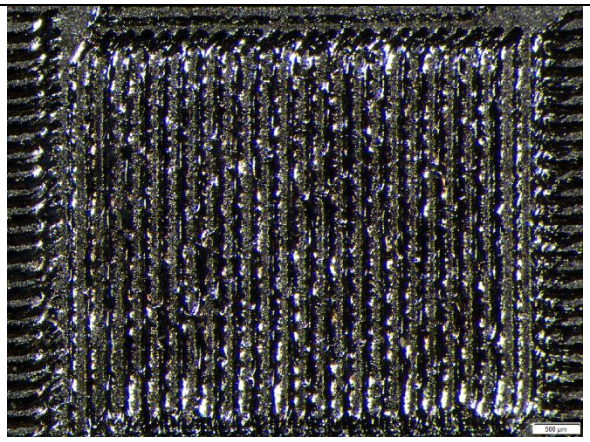	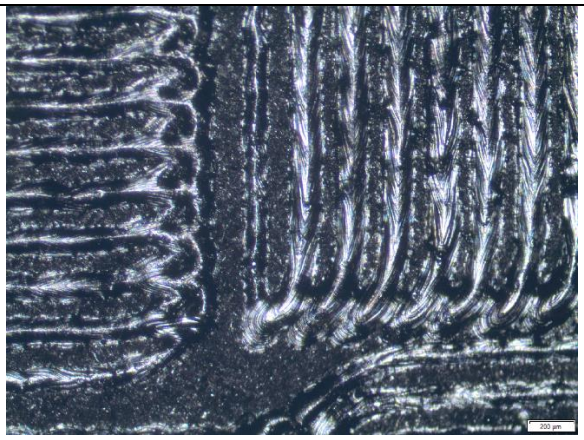
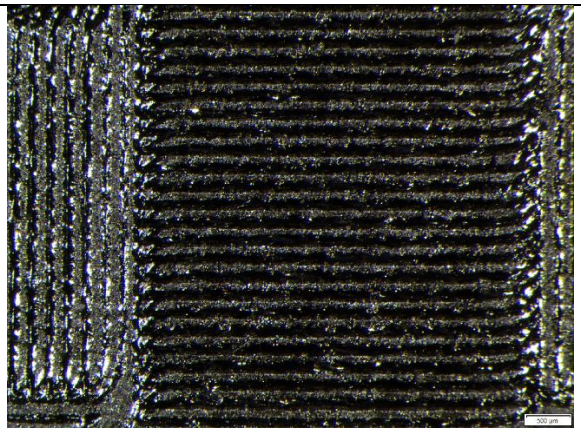	
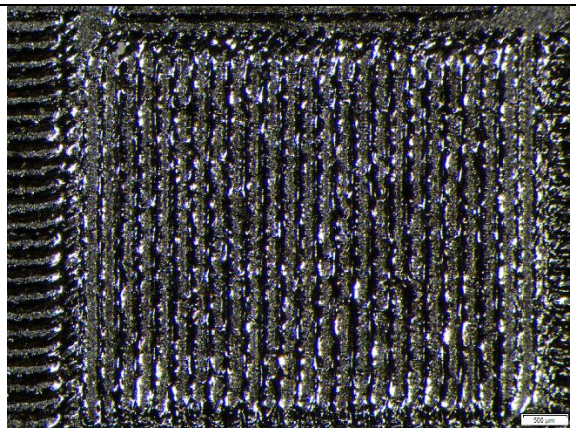	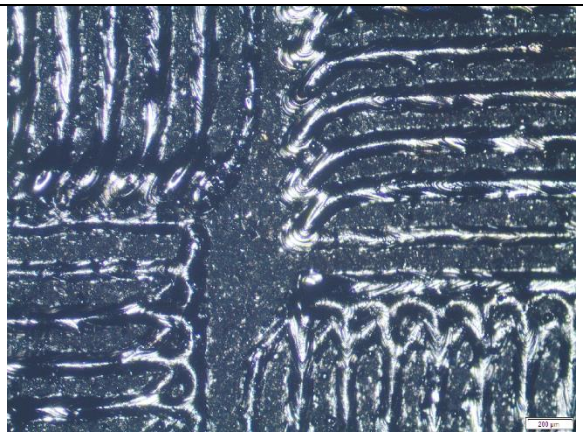

Table D.2: Default Scan Strategy Sample 2 pictures from Substrate Experiment

Default Island Scan Strategy Sample 2	
Island	**Joint Between Four Islands**
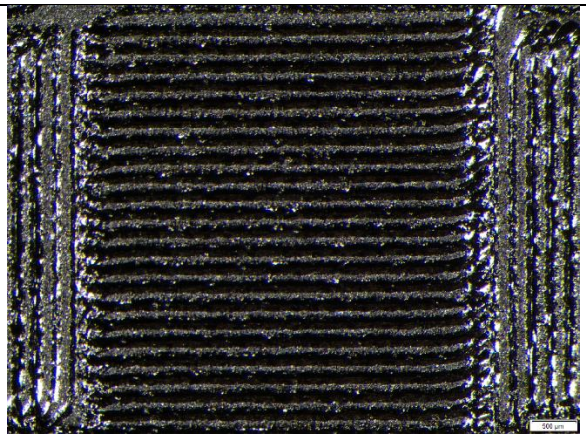	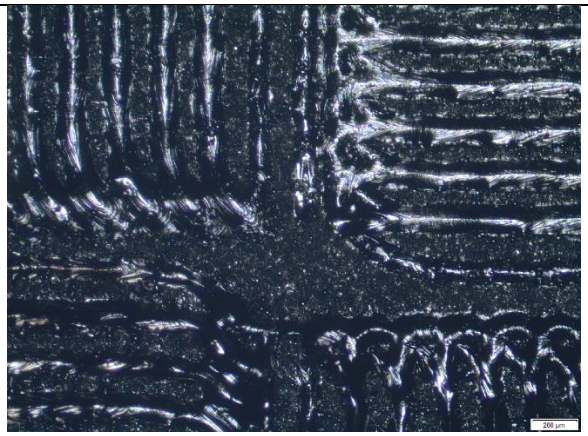
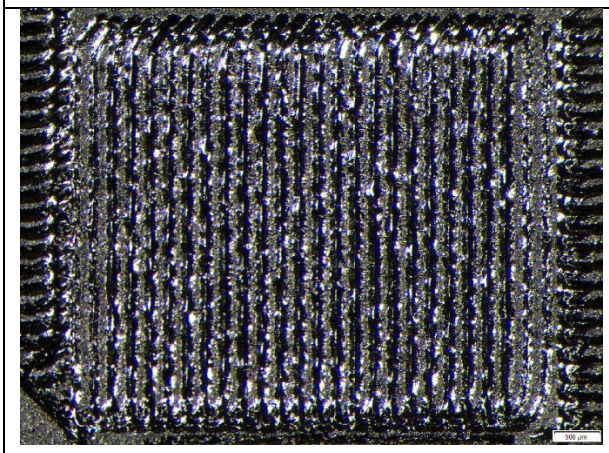	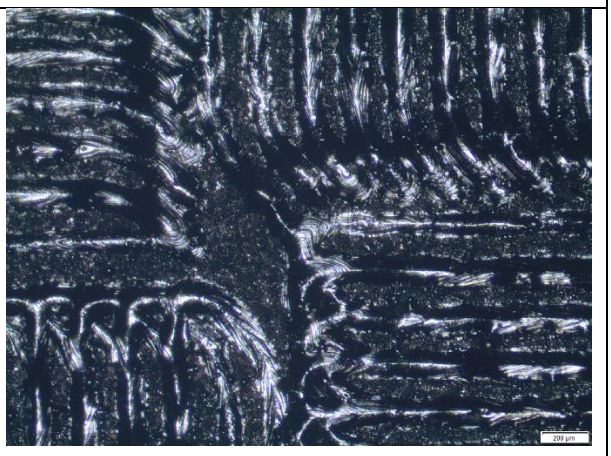
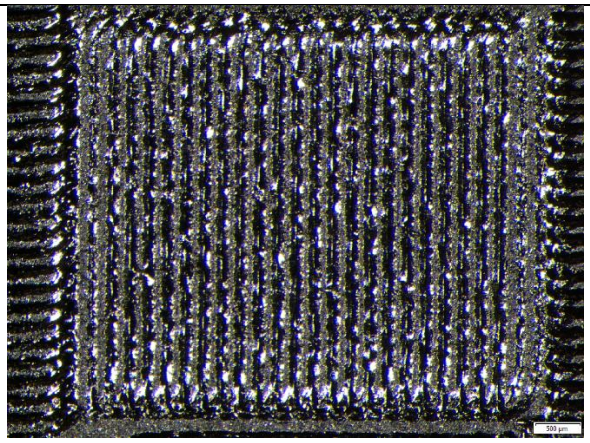	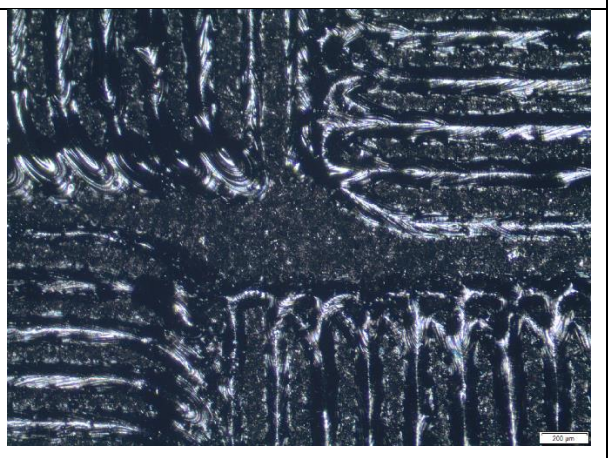

Table D.3: Default Scan Strategy Sample 3 pictures from Substrate Experiment

Default Island Scan Strategy Sample 3	
Island	**Joint Between Four Islands**
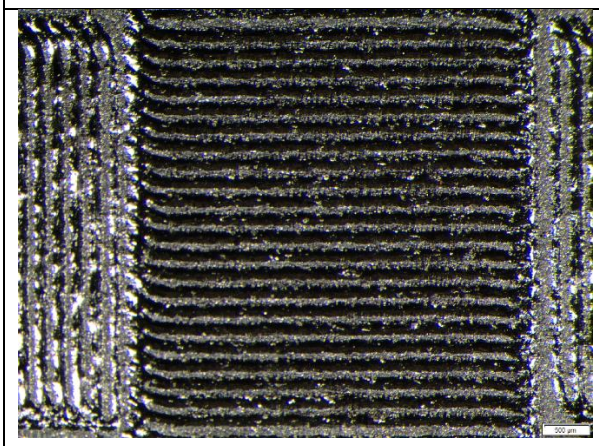	
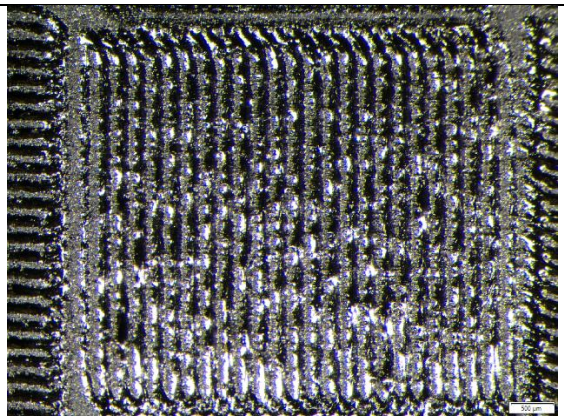	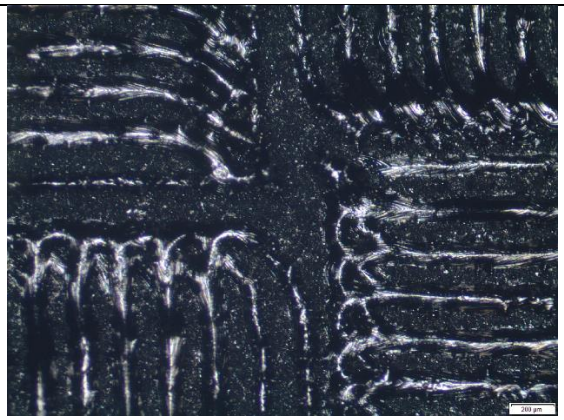
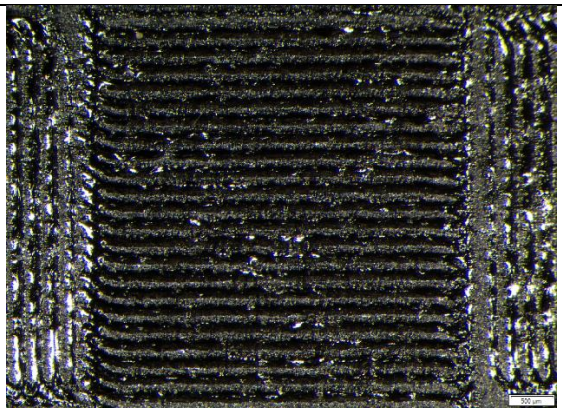	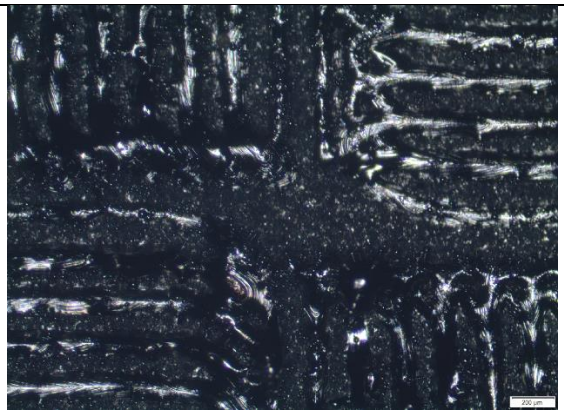

The pictures for the Newly Developed Helix Scan Strategy can be observed in Table D.4, Table D.5, and Table D.6 below.

Table D.4: Newly Developed Scan Strategy Sample 1 pictures from Substrate Experiment

Newly Developed Scan Strategy Sample 1	
Island	**Joint Between Four Islands**
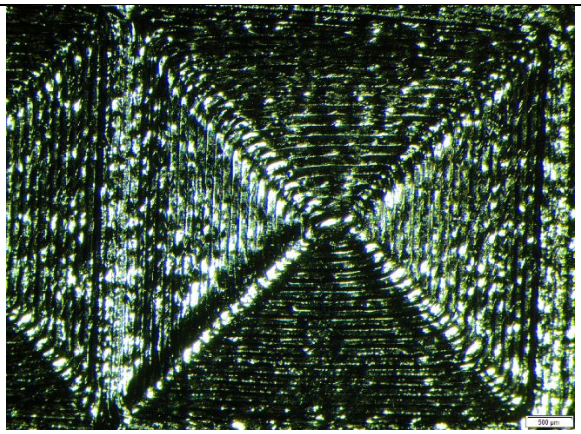	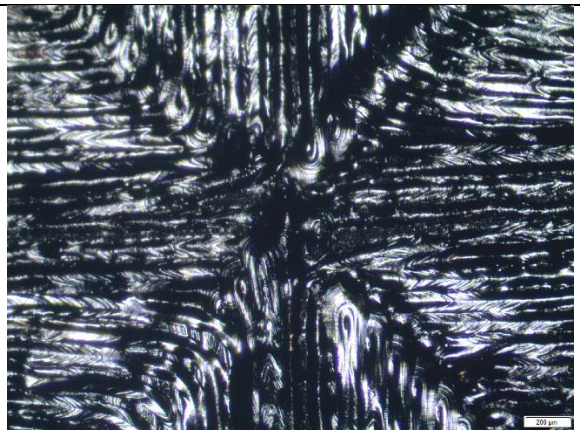
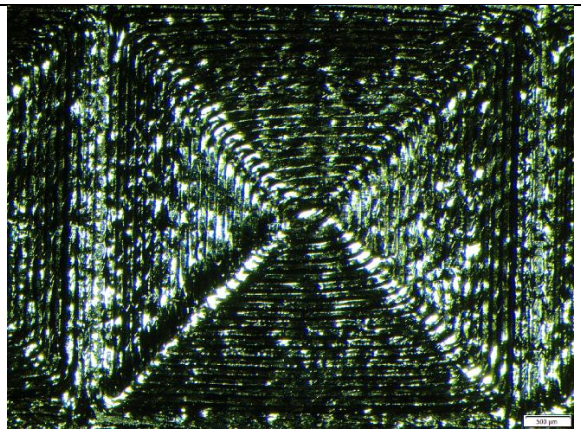	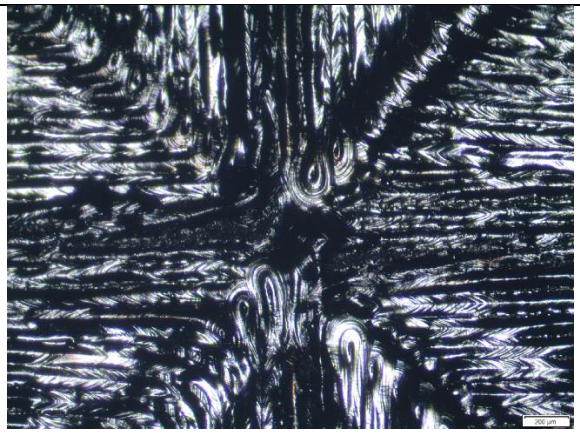
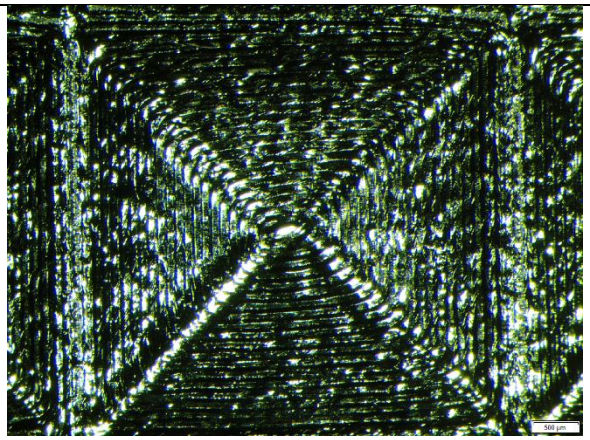	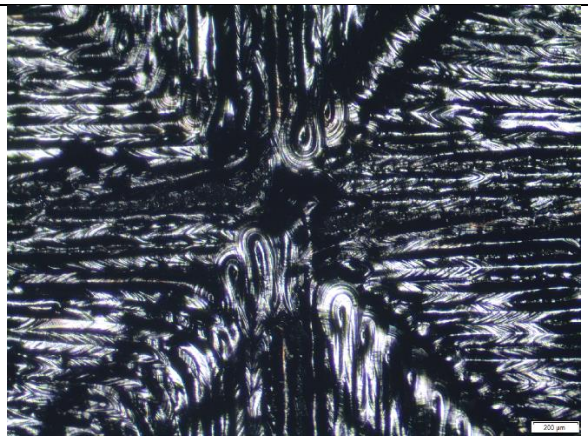

Table D.5: Newly Developed Scan Strategy Sample 2 pictures from Substrate Experiment

Newly Developed Scan Strategy Sample 2	
Island	**Joint Between Four Islands**
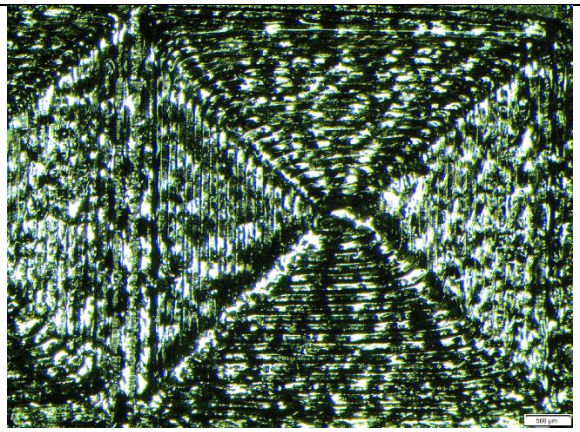	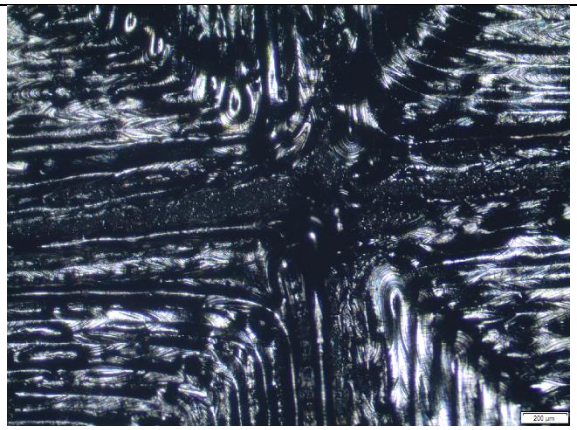
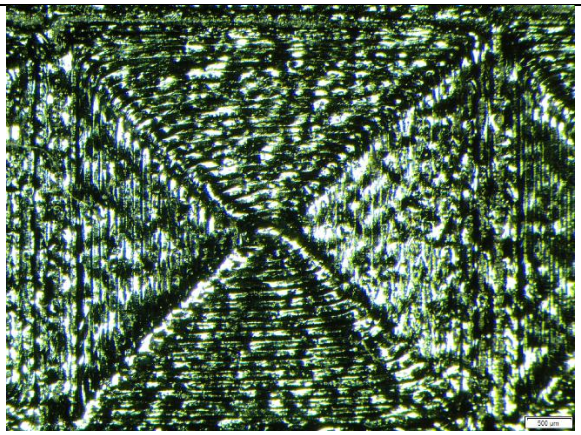	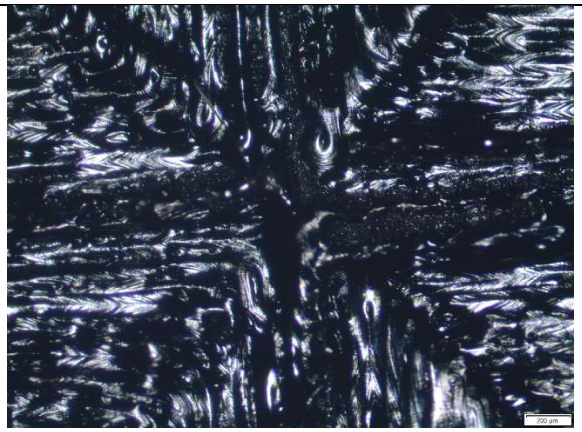
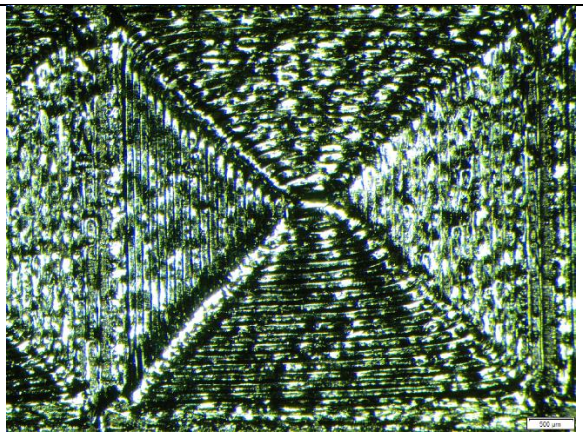	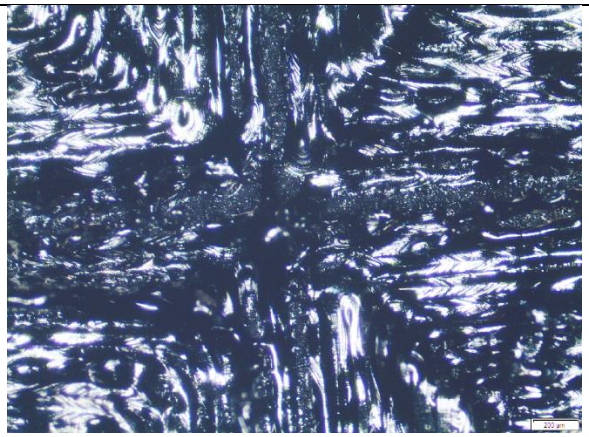

Table D.6: Newly Developed Scan Strategy Sample 3 pictures from Substrate Experiment

Newly Developed Scan Strategy Sample 3	
Island	**Joint Between Four Islands**
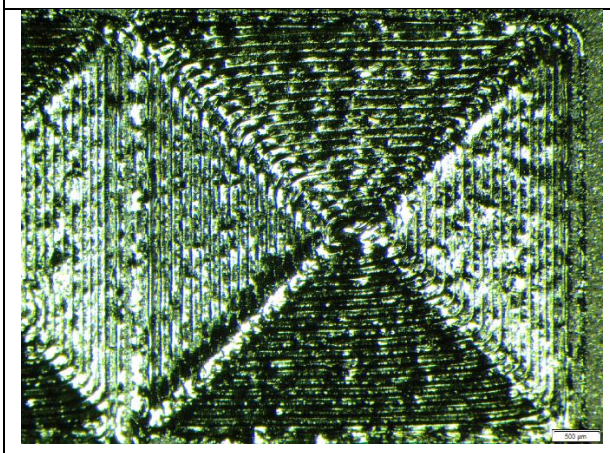	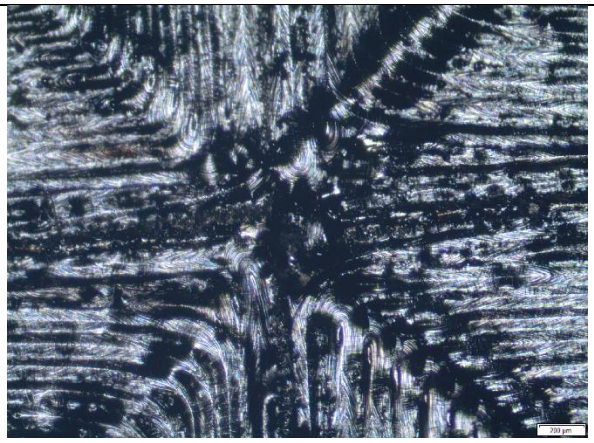
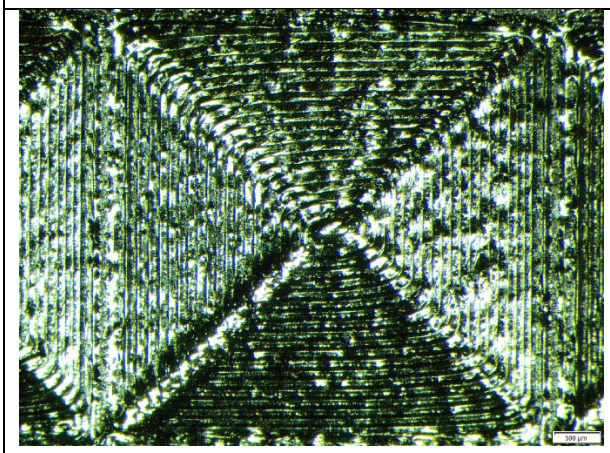	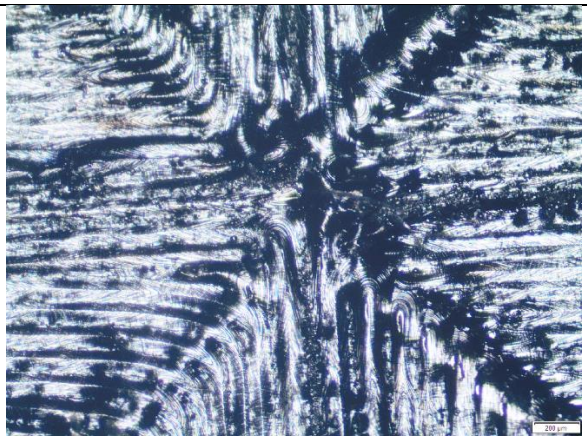
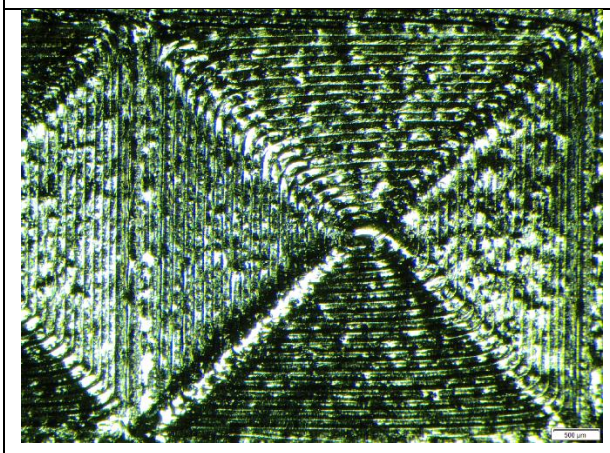	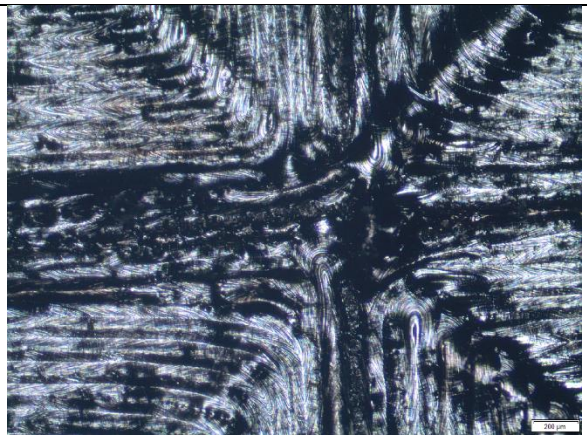

Appendix E: Porosity Experiment

Machine setup

The M2 Cusing machine was set up to build the samples. The Argon gas was connected to the machine. The filter was changed and the powder was changed to Ti-6Al-4V ELI. The powder was sieved using a 105 µm rated sieve. Six, 10 mm x 10 mm x 10 mm samples were designed for this experiment. The parts were imported into the Concept Laser machine software and were laid out and oriented as shown in Figure E.1. The parameters were set for the parts. The process parameters that were used are discussed in the following section.

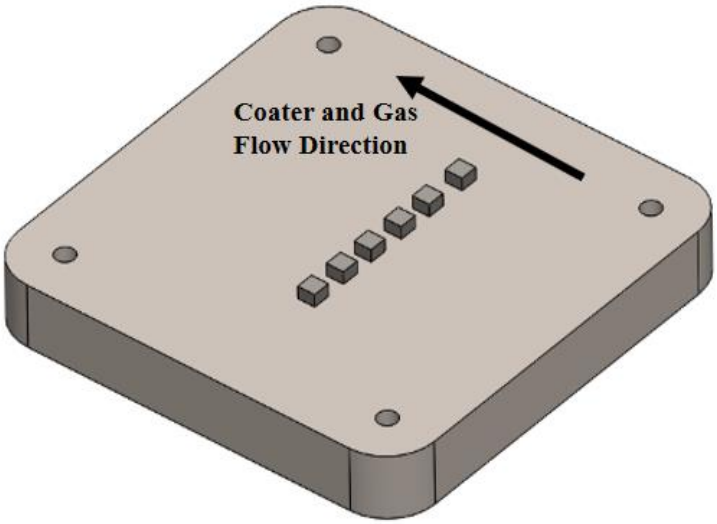

Figure E.1: Porosity sample orientation on the Concept Laser M2 Cusing machine

The reason for the layout and orientation shown in Figure E.1 is because the gas flow and the coater blade come from the right to the left. If one sample is in the front of another with reference to coating and gas flow, then that sample could interfere with the other. Residue could flow from one sample to the other from the gas flow or the coater. So the current setup prevents residue from contaminating the other samples.

Process parameters

The following parameters in Table E.1 were used as they are the recommended parameters by Concept Laser. These parameters are not the optimal parameters as changing different parameters, changes different material properties. Since the scan strategies were the only variable, these parameters were kept constant throughout the duration of the experiment.

Table E.1: Default process parameters for the M2 Cusing machine recommended by Concept Laser GmbH

Machine Parameters			
Parameter	**Value**		
Coater Blade Type	Flexible Rubber Blade		
Layer thickness	30 µm		
Fan Speed	65%		
Cusing Process Parameters			
Exposure Sequence	Vectors then Contours		
Powder delivering height correction factor	180%		
Number of additional slices	0		
Laser Parameters			
Parameter	**Units**	**Skin**	**Contours**
Power	Watts	100	100
Speed (sp)	mm/s	600	600
Focus/Spot Diameter (d)	mm	0.15	0.15
Operation Mode	-	Continuous	Continuous
Hatch Spacing (a1)	mm	0.105	0.105

Scanning strategies

The scanning strategy was the independent variable for this experiment as it was the only factor that was varied. The Concept Laser Default strategy was the benchmark in this study. The newly developed strategy was used in order to compare the strategies in terms of porosity. The two scanning strategies are displayed in Figure E.2.

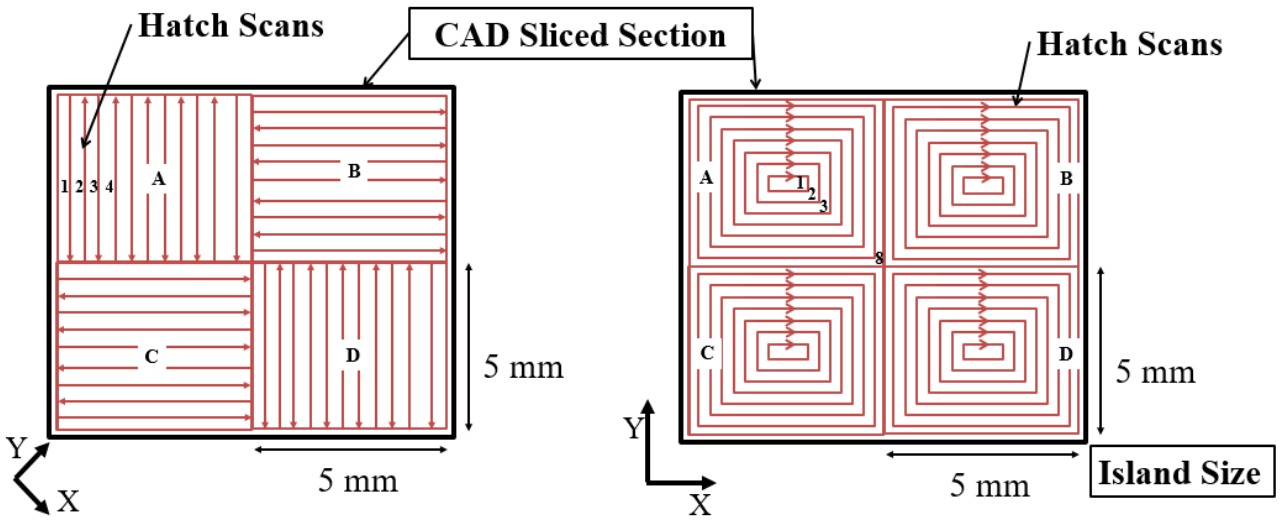

Figure E.2: (Left) Default island scan strategy (Right) Newly developed scan strategy

The way in which the vectors are exposed by the laser is very important. The default island scan strategy is exposed in the following manner, firstly, the slicing software creates random islands such as islands A, B, and C shown in Figure E.2. The laser will then begin to scan the vectors within the

selected island. In this case, the vectors are scanned in order from 1 to 4 and so on until the island is completely scanned. The order in which the island is chosen, is performed randomly by the computer. The newly developed scan strategy is scanned in a completely different manner. The laser will begin at island A and scan vector set 1. Once vector set 1 is scanned the laser will move to island B and scan vector set 1 and so on until all of the vector sets 1, in all of the islands, have been scanned. The laser will then move over to vector set 2 and will repeat the same process as before. The laser will repeat this process until all of the vector sets in all of the islands have been scanned.

Statistical Data

Sample	Default	New
1	0.68	0.42
2	0.71	0.39
3	0.83	0.43
Average		
Std. Dev.		

Two-tailed Student t-Test

Table E.2: Two-tailed Student t-Test used for porosity results

	Default	*New*
Mean	0.74	0.413333333
Variance	0.0063	0.000433333
Observations	3	3
Pooled Variance	0.003366667	
Hypothesized Mean Difference	0	
df	4	
t Stat	6.895255938	
P(T<=t) one-tail	0.001159714	
t Critical one-tail	2.131846786	
P(T<=t) two-tail	0.002319428	
t Critical two-tail	2.776445105	

Appendix F: Deviation Experiment

The following Machine and Cusing Process parameters were used for the production of the experimental samples. These parameters were not shown in the experimental setup.

Process parameters

The following parameters in Table F.1 were used as they are the recommended parameters by Concept Laser. These parameters are not the optimal parameters as changing different parameters, changes different material properties. Since the scan strategies were the only controlled variable, these parameters were kept constant throughout the duration of the experiment.

Table F.1: Default process parameters for the M2 Cusing machine recommended by Concept Laser GmbH

Machine Parameters			
Parameter	**Value**		
Coater Blade Type	Flexible Rubber Blade		
Layer thickness	30 µm		
Fan Speed	65%		
Cusing Process Parameters			
Exposure Sequence	Vectors then Contours		
Powder delivering height correction factor	180%		
Number of additional slices	0		
Laser Parameters			
Parameter	**Units**	**Skin**	**Contours**
Power	Watts	100	100
Speed (sp)	mm/s	600	600
Focus/Spot Diameter (d)	mm	0.15	0.15
Operation Mode	-	Continuous	Continuous
Hatch Spacing (a1)	mm	0.105	0.105

Scanning strategies

The scanning strategy was the independent variable for this experiment as it was the only factor that was varied. The Concept Laser Default strategy was the benchmark in this study. The newly developed strategy was used in order to compare the strategies in terms of deviation and warping. The two scanning strategies are displayed in Figure F.1.

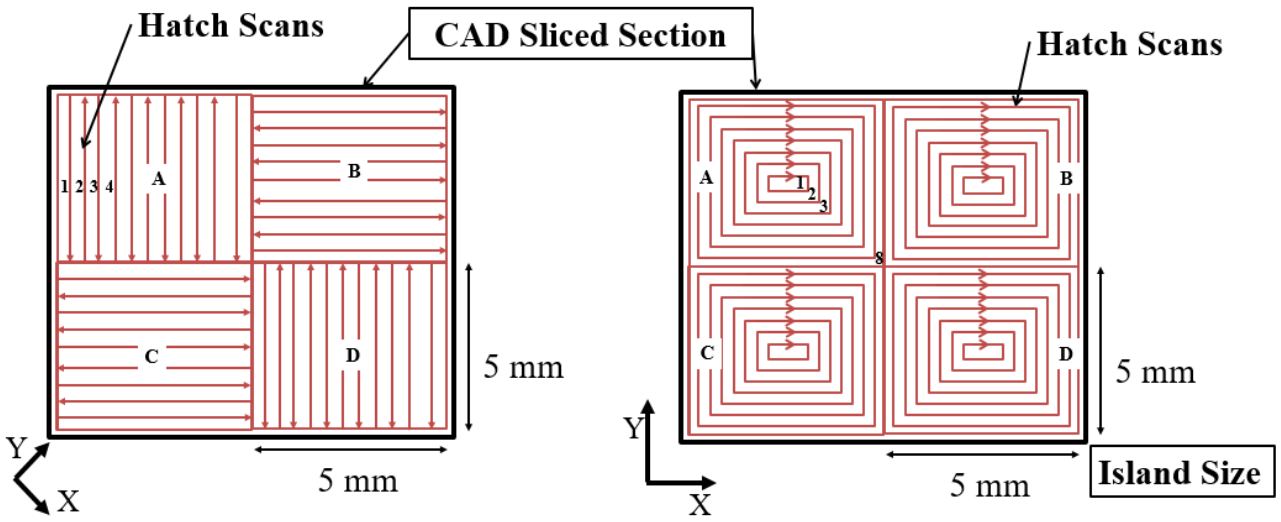

Figure F.1: (Left) Default island scan strategy (Right) Newly developed scan strategy

The way in which the vectors are exposed by the laser is very important. The default island scan strategy is exposed in the following manner, firstly, the slicing software creates random islands such as islands A, B, and C shown in Figure E.2. The laser will then begin to scan the vectors within the selected island. In this case the vectors are scanned in order from 1 to 4 and so on until the island is completely scanned. The order in which the island is chosen is performed randomly by the computer. The newly developed scan strategy is exposed in a completely different manner. The laser will begin in island A and scan vector set 1. Once vector set 1 is scanned the laser will move to island B and scan vector set 1 and so on until all of the vector sets 1 in all of the islands have been scanned. The laser will then move over to vector set 2 and will repeat the same process as before. The laser will repeat this process until all of the vector sets, in all of the islands have been scanned.

Machine parameters

Table F.2: Machine parameters that were not mentioned in the experimental setup

Coater blade type:	Flexible rubber blade
Speed	
Coater in process	100 mm/s
Coater manual	100 mm/s
Extra coating	300 mm/s

Cusing Process Parameters

Table F.3: Cusing Process parameters that were not mentioned in the experimental setup

Exposure sequence	Vectors then Contours
Powder delivering height:	180%
Scanning system	
Waiting time for beam off	0.3 ms
Waiting time for beam on	0.08 ms
Waiting time at edges	0 ms
Waiting time after laser jump max	1 ms
Waiting time after laser jump min	0.5 ms
Saturation after in mm	5 mm

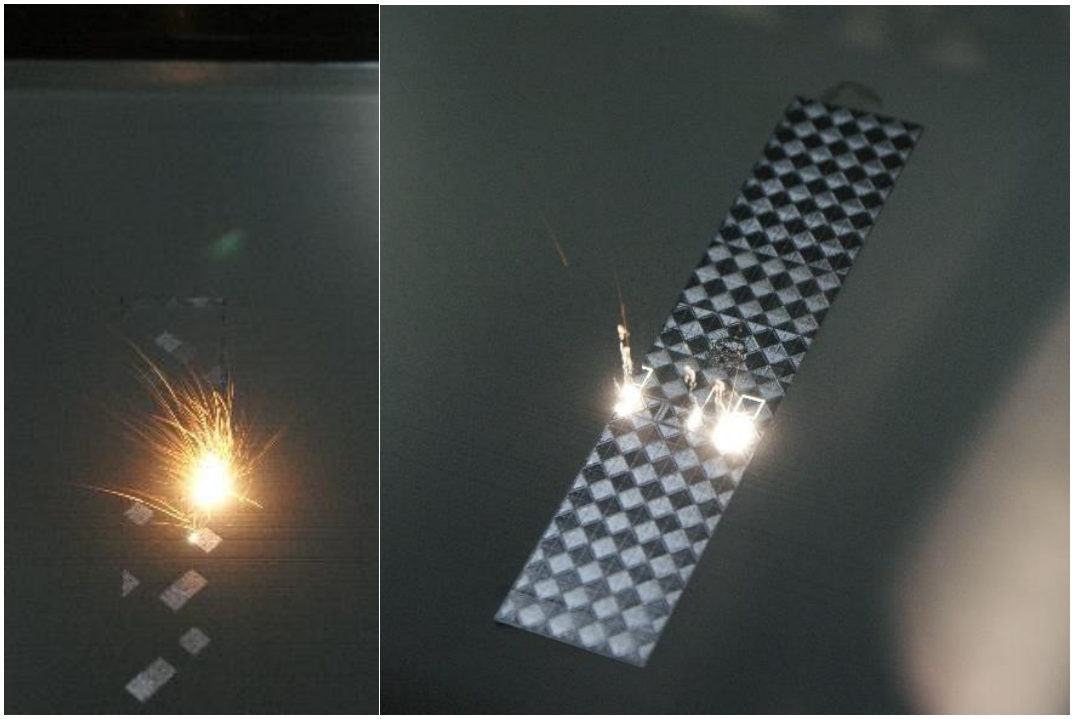

Figure F.2: Difference in scan strategies during production (Left) Default Strategy (Right) New startegy

Residual graphs for repeated measures ANOVA.

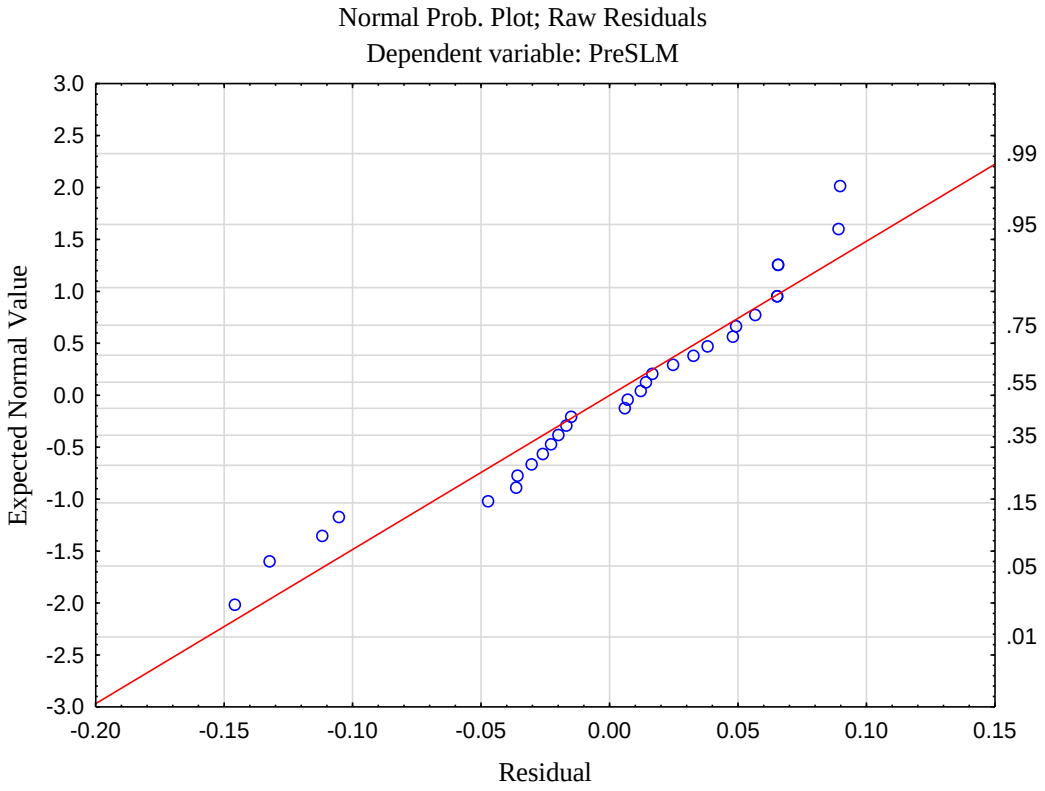

Figure F.3: Pre SLM normal probability plot, raw residuals

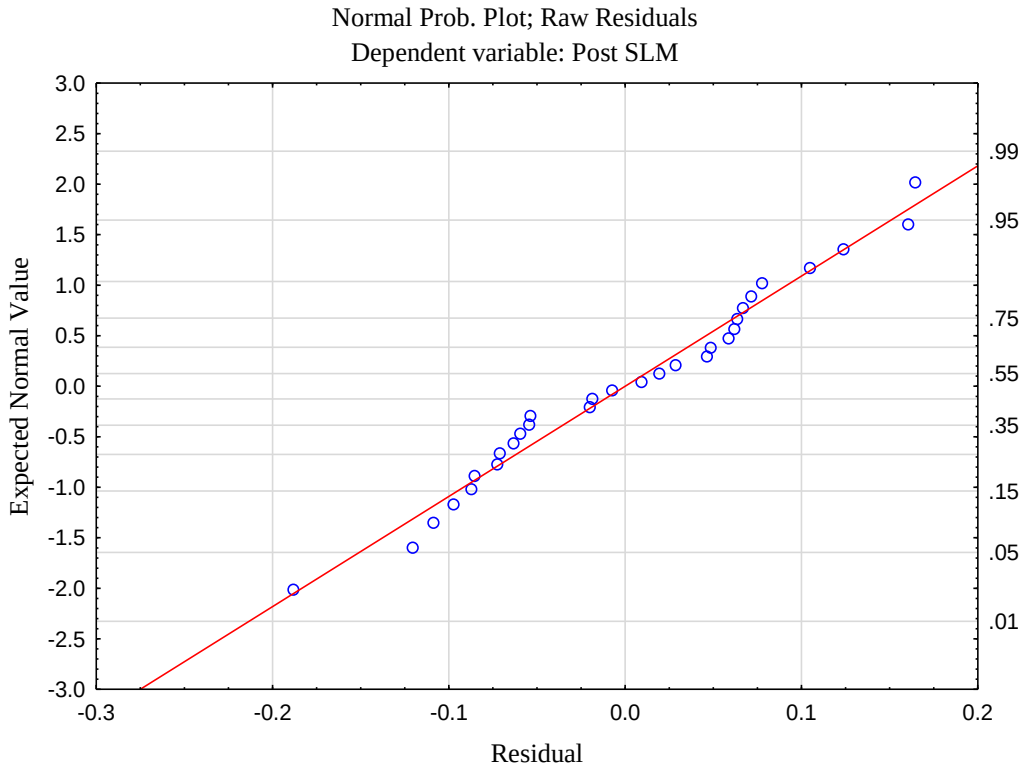

Figure F.4: Post SLM normal probability plot, raw residuals

Statistics

All CMM Points

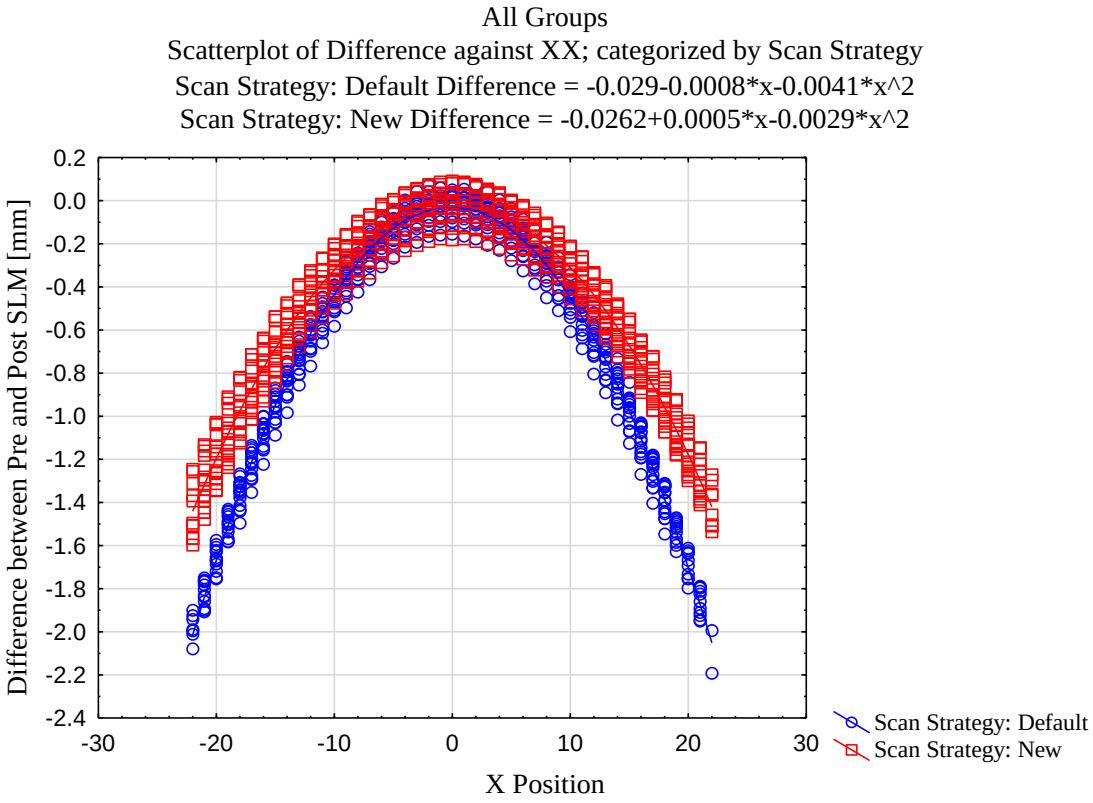

Figure F.5: Scatterplot of Deviation against X Position for all Lines

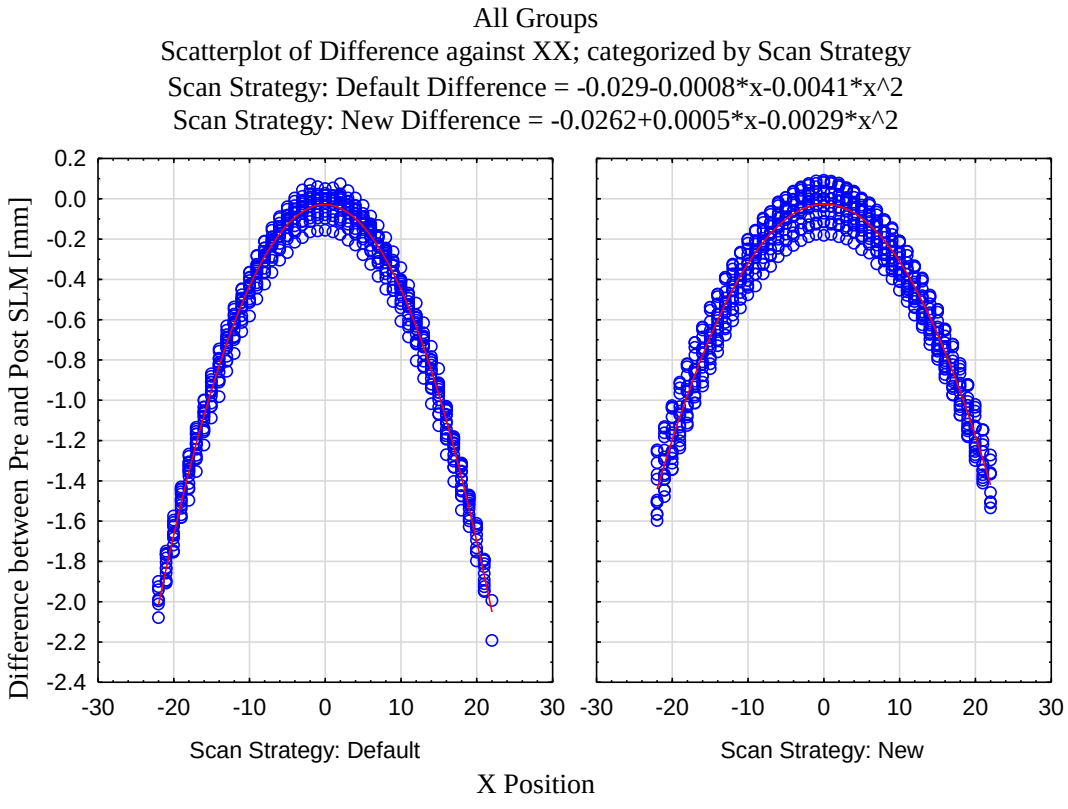

Figure F.6: Scatterplot of Deviation against X Position for all Lines on separate graphs

Line 1 Results

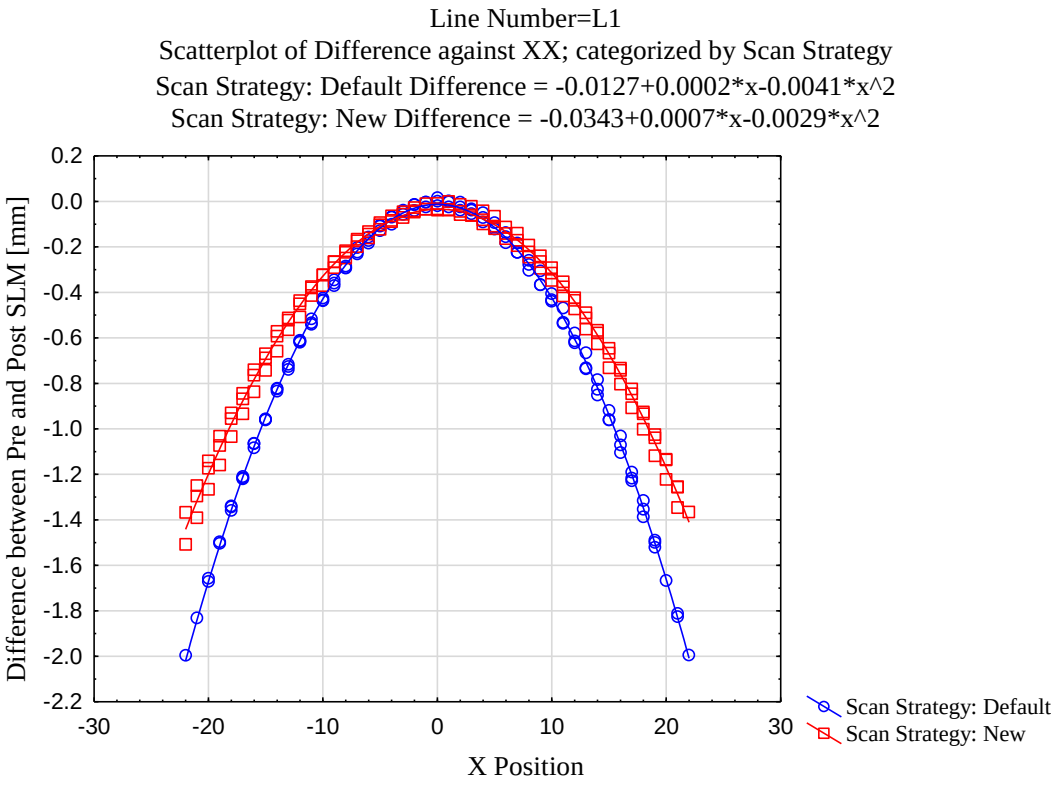

Figure F.7: Scatterplot of Deviation against X Position for Line 1

Line 2 Results

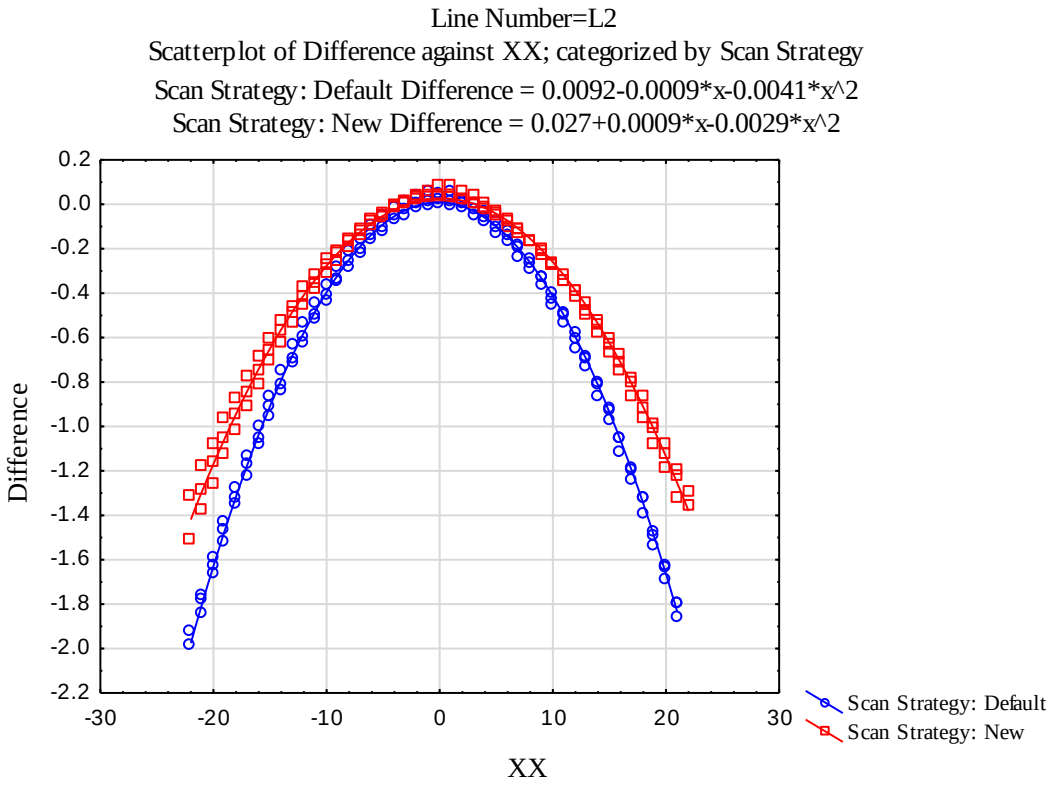

Figure F.8: Scatterplot of Deviation against X Position for Line 2

Line 3 Results

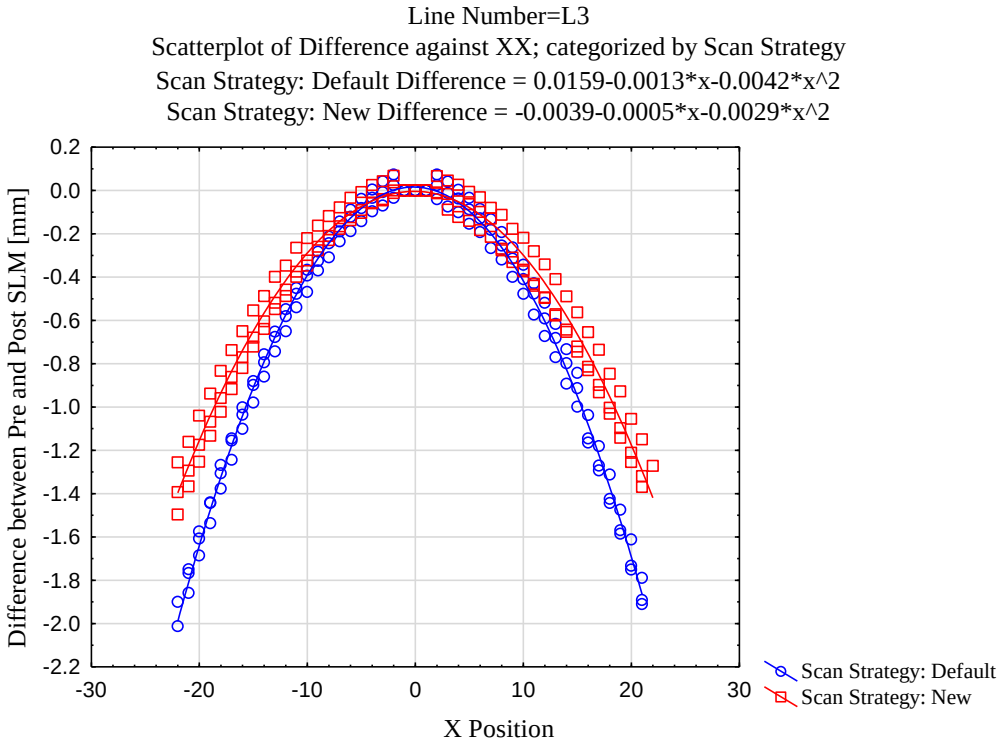

Figure F.9: Scatterplot of Deviation against X Position for Line 3

Line 4 Results

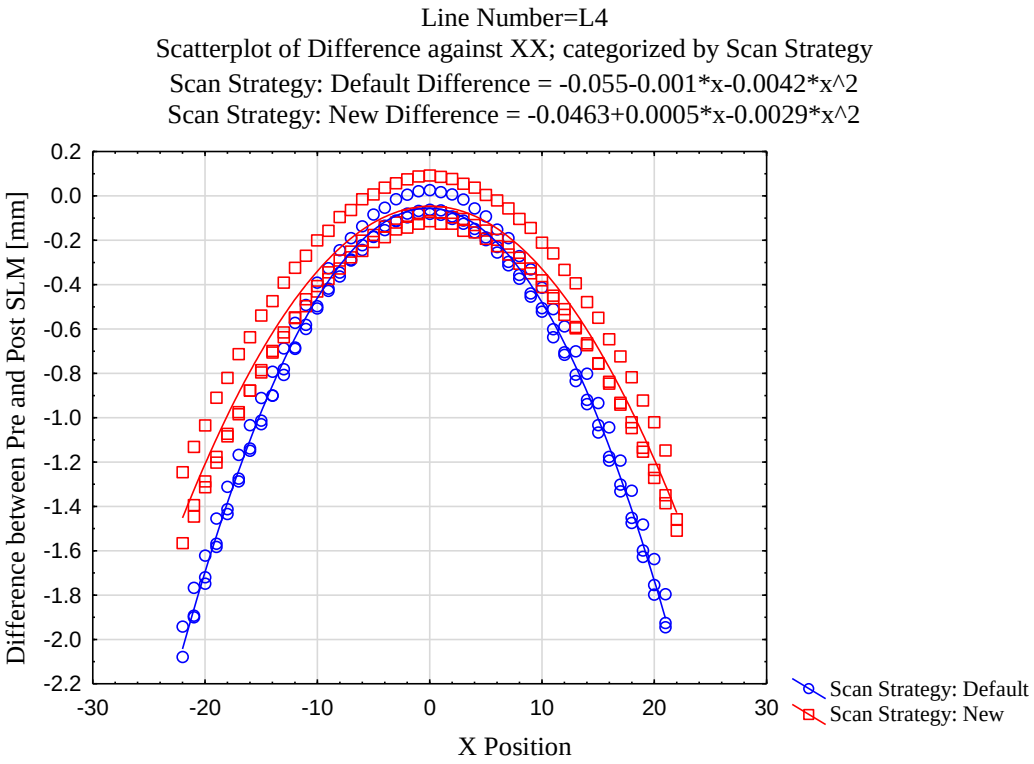

Figure F.10: Scatterplot of Deviation against X Position for Line 4

Line 5 Results

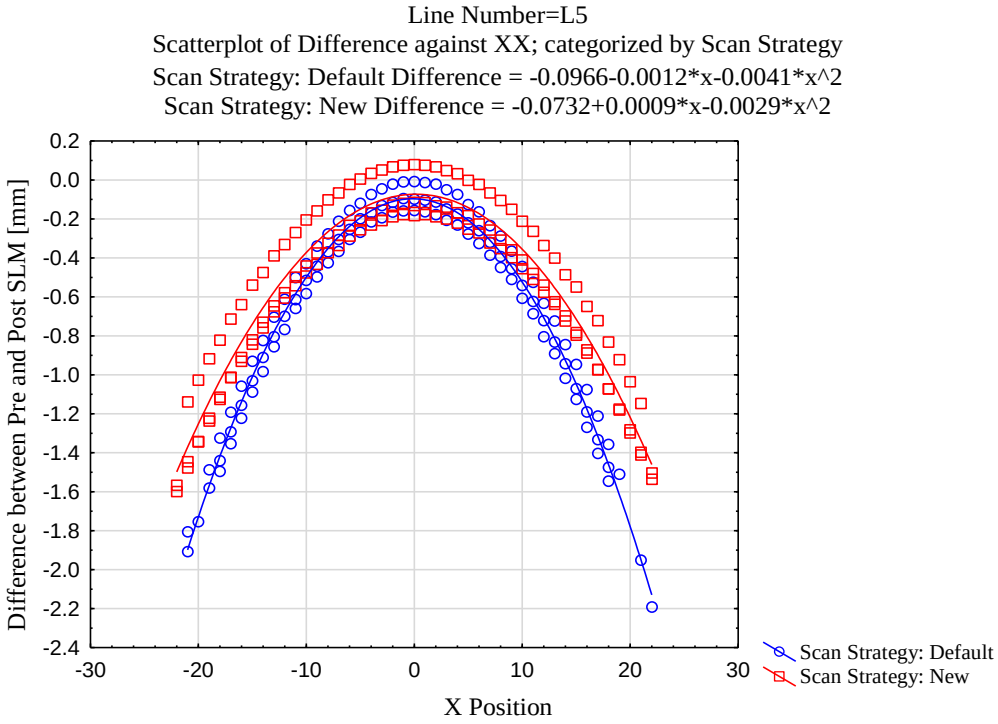

Figure F.11: Scatterplot of Deviation against X Position for Line 5

Appendix G: Conference Papers and Journal Articles

The following are conference and journal articles published by the author during the 2 year period of the Master's Degree.

- Resource Efficient Process Chains to Manufacture Patient-Specific Prosthetic Fingers, **D. Hagedorn-Hansen,** G.A. Oosthuizen, T. Gerhold. *South African Journal for Industrial Engineering*. May 2016, **Status:** Published

- Geometric Deviation of Hybrid Parts Produced by Selective Laser Melting, **D. Hagedorn-Hansen**, M.B. Bezuidenhout, P.A. Hugo & G.A. Oosthuizen, *RAPDASA Conference*. November 2015, **Status:** Published

- Characteristics of single layer Selective Laser Melted tool grade cemented tungsten carbide, A.C. Van Staden, **D. Hagedorn-Hansen**, N. Sacks, G.A. Oosthuizen, *COMA '16 Conference*, January 2016, **Status:** Published

- Resource Efficient Process Chain Strategies for Globally Competitive Manufacturers, **D. Hagedorn-Hansen**, E. Hagedorn-Hansen, G.A. Oosthuizen, *IAMOT Conference*, May 2016, **Status:** Published

- Visual Management Tool to Manage Manufacturing Resources, L.P. Steenkamp, **D. Hagedorn-Hansen**, G.A. Oosthuizen, *GCSM 14*, October 2016, **Status:** Published

- Waste to Resource Process Chain Strategies for Global Manufacturers, J.F.W. Durr, **D. Hagedorn-Hansen**, G.A. Oosthuizen, *GCSM 14*, October 2016, **Status:** Published

- Resource Efficient Process Chains to Manufacture Patient Specific Prosthetic Hands Using Open Source Devices, **D. Hagedorn-Hansen**, L.P. Steenkamp, M.M. Jansen van Rhensburg, G.A. Oosthuizen, *SAIIE 26 Conference Proceedings*, October 2017, **Status:** Published

- The Effects of Scan Strategies on Selective Laser Melted Parts, **D. Hagedorn-Hansen**, M.B. Bezuidenhout, P.A. Hugo & G.A. Oosthuizen, *RAPDASA 2016 Conference Proceedings*, November 2017, **Status:** Published

- Additive Manufacturing Based Resource Efficient Production of Surfboards, **D. Hagedorn-Hansen**, M.C. van Coller, A.C. Brent & G.A. Oosthuizen, *RAPDASA 2016 Conference Proceedings*, November 2017, **Status:** Published

- Investigating the effects of automating process chains towards sustainable manufacturing in South Africa, **D. Hagedorn-Hansen**, L.P. Steenkamp, E. Hagedorn-Hansen, G.A. Oosthuizen, *International Conference on Sustainable Materials Processing and Manufacturing, SMPM 2017*, January 2017, **Status:** Accepted